

# Spatiotemporal, Nonlinear Optics and the Quest for the Observation of Discrete Light Bullets

Dissertation  
zur Erlangung des akademischen Grades  
doctor rerum naturalium (Dr. rer. nat.)

vorgelegt dem Rat der Physikalisch-Astronomischen Fakultät  
der Friedrich-Schiller-Universität Jena

von Diplomphysiker Falk Eilenberger  
geboren am 20. Oktober 1981 in Schlema

Gutachter

1. ....
2. ....
3. ....

Tag der Disputation: .....

<b>1. Introduction.....</b>	<b>1</b>
<b>2. Spatiotemporal Pulse Generation and Forming .....</b>	<b>10</b>
2.1 Basic Pulses: Oscillators and Amplifiers.....	10
2.2 Advanced Pulses: Spectral Pulse Shaping.....	12
2.2.1 Calibration.....	14
2.2.2 Determination of the Initial Phase .....	14
2.2.3 Improved Optical Design .....	15
2.2.4 Coherent Spectral Broadening .....	16
2.3 Spatial Shaping: a Rotating Case Study .....	18
2.4 Outlook: Full Spatiotemporal Waveshaping with Metasurfaces .....	19
<b>3. Spatiotemporal Pulse Analysis Techniques.....</b>	<b>22</b>
3.1 Imaging Cross Correlator: Getting an Overview .....	22
3.2 Imaging Cross Correlating FROG: Seeing Details .....	25
3.3 1D Imaging Cross Correlating FROG: Fast and Accurate .....	30
3.4 Outlook: Analysis by Control.....	31
<b>4. Ultrafast Discrete Optics: Samples, Scales &amp; Models .....</b>	<b>34</b>
4.1 Nonlinear, Spatiotemporal, Discrete Optics: a Brief Introduction .....	34
4.2 A Qualitative Propagation Model.....	40
4.3 Propagation Environments .....	41
4.3.1 Femtosecond Written Waveguide Arrays .....	42
4.3.2 Fiber Arrays.....	43
4.4 A Quantitative Propagation Model.....	46
4.5 Scales and Dominating Effects.....	49
<b>5. Results of Experiments and Simulations .....</b>	<b>52</b>
5.1 Nonlinear Self-Limiting in Segmented Waveguide Arrays .....	53
5.2 Fundamental Light Bullets .....	58
5.3 Direct Spacetime Coupling .....	67
5.3.1 Spectral Symmetry Breaking of Light Bullets .....	70
5.3.2 Superluminally Decaying Light Bullets.....	74
5.4 Vortex Light Bullets .....	78
<b>6. Conclusions &amp; Outlook.....</b>	<b>89</b>
<b>7. Zusammenfassung.....</b>	<b>96</b>
<b>Appendix A: References .....</b>	<b>I</b>
<b>Appendix B: Bibliography .....</b>	<b>XX</b>
Peer Reviewed Journal Papers .....	XX
Invited Talks.....	XX
Conference Talks.....	XXI
Conference Poster .....	XXII
<b>Appendix C: Acknowledgements.....</b>	<b>XXIII</b>
<b>Appendix D: Curriculum Vitae .....</b>	<b>XXVI</b>
<b>Appendix E: Ehrenwörtliche Erklärung.....</b>	<b>XXVIII</b>
<b>Appendix F: Symbols .....</b>	<b>XXIX</b>
<b>Appendix G: Abbreviations .....</b>	<b>XXX</b>



# 1. Introduction

Electromagnetic waves are intrinsically spatiotemporal phenomena [Lan60, Lan75, Jac06]. Their propagation in space and time is a so-called 3+1 dimensional problem. An electromagnetic field, which is known on a three dimensional hyperplane of space-time, is defined in all of space-time, except for regions that are inaccessible for reasons of causality. This is due to the propagating nature of electromagnetic fields. Mathematically this propagation is described by Maxwell's equations. These differential equations relate the electromagnetic field on the hyperplane to an infinite series of neighboring planes, eventually filling space-time. The series of hyperplanes is parameterized by a single coordinate, the propagation coordinate, whereas the three coordinates, that span each hyperplane are called transverse coordinates. The propagation equations are in general nonlinear, due to the nonlinear response of optical materials to highly intensive electromagnetic fields.

One approach to describe electromagnetic fields in experiments is as follows. For each position  $z$  on an optical axis a field must be defined on the spatiotemporal subspace, consisting of the transverse spatial coordinates  $x$  and  $y$ , and along the time axis, with the coordinate  $t$ . This approach is useful if a directional flow of energy from a source, through an experiment, to a measurement point is defined. As all experiments in this thesis share this layout, we thus adopt this terminology.

Nevertheless, neither textbook optics [Sny83, Sal91, Bor99, Agr01, Boy03, Jac06], nor photonics research often deal with 3+1 dimensional nonlinear, spatiotemporal wave physics. Most areas of research are concerned with phenomena, which fall into either of the three classes of spatial optics, temporal optics, or nonlinear optics. Discounting of nonlinearity is common for moderately intense electromagnetic fields. The reduction of the spatial or temporal transverse coordinate is facilitated by the usage of sufficient boundary or initial conditions, wave confinement and/or symmetry. An example of the former is classical imaging optics [Bor99]. It largely ignores the temporal variation of the electromagnetic field, assuming either incoherent or monochromatic illumination. Guided wave photonics [Sny83] is an example of the latter technique. Here the field travels in a discrete set of transversally confined, linearly orthogonal modes. All dynamics can then be understood in terms of mode beating and mode perturbation.

The tremendous progress that photonics and its ubiquitous applications in science and technology have made in the last decades is often based on such subspace approaches. In this sense the advances that have lead researchers to proclaim the "century of the photon" [Goo11] have been derived from a just a small subset of photonics as a whole.

## 1. Introduction

If the limits of these classes of research are left behind new optical effects immediately arise. Research, which deals with either pair of the three main classes has led to the discovery of many new effects and concepts in photonics, as can be seen from Fig. 1. A straightforward consequence is that research in nonlinear, spatiotemporal photonics, i.e. in a combination of all three classes of research, will immediately bring forward new results. The endeavor of advancing nonlinear, spatiotemporal optics, pursued in this thesis, is therefore worth the effort, as it strives to “unleash” photonics from the restriction of reduced dimensionality.

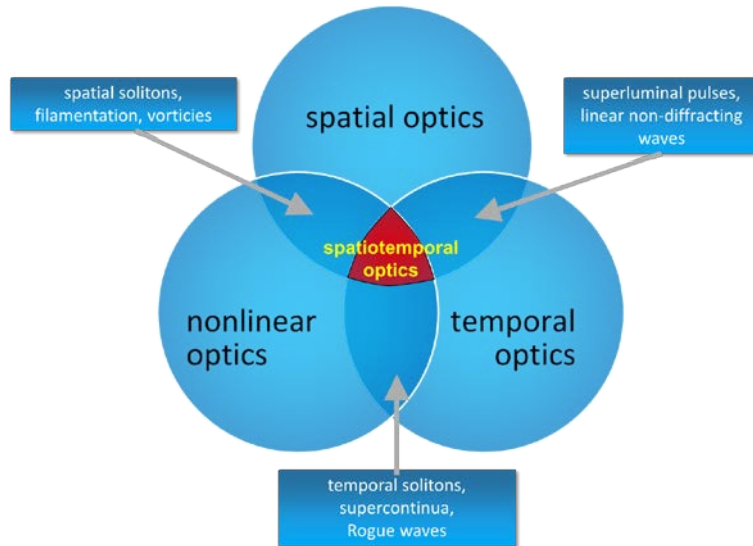


Fig. 1: The location of spatiotemporal, nonlinear optics, at the intersection of the important classes of photonics research: spatial, temporal and nonlinear optics. Effects and concepts that arise due to the interplay of either pair of the three are noted in their cross section areas. Spatiotemporal, nonlinear optics is linked to all three and thus particularly rich.

The generalization to spatiotemporal optics, however, comes for a prize. All steps required for a successful experiment, i.e. spatiotemporal pulse generation and analysis techniques as well as spatiotemporal numerical modelling and sample fabrication need to be carefully reviewed or newly developed. In this thesis we have made significant advances in the all fields related to spatiotemporal optical experiments, which allowed us to produce novel results in nonlinear, spatiotemporal optics. More specifically we have adopted and developed methods for spatiotemporal pulse generation and spatiotemporal pulse analysis. We also investigated various classes of propagation environments with respect to their suitability for nonlinear, spatiotemporal optics and introduced qualitative as well as quantitative modelling techniques.

As can be seen in Fig. 2 the development of these methods and samples, however, was not an end in itself. Instead it was driven by the quest for the experimental observation of a truly spatiotemporal, nonlinear entity – a solitary wavepacket, which is nonlinearly self-confined along all transverse dimensions simultaneously. This so-called Light Bullet had been the subject of intensive theoretical research since the seminal work by Silberberg [Sil90] but eluded clear

experimental observation prior to this thesis [Min10a].

In fact, the Light Bullet can, in some respect, be thought of as the “ultimate” optical, solitary wave. Solitary waves are among the most fascinating nonlinear wavepackets. Although they are subject to dispersion and/or diffraction they are marked by the absence of transverse broadening, which is otherwise an almost universal feature of linear wave propagation. The absence of linear broadening is facilitated by a balance with the nonlinearity. Solitary waves have been at the scope of science since their first observation in 1834 by Russell [Rus44] in a water channel and the first formulation of a nonlinear wave equation in 1894 by Korteweg and de Vries [Kor95] after work by Boussinesq [Bou71] and Rayleigh [Ray76]. Russell, in fact, already made systematic experiments in water tanks, i.e., he attempted to understand solitary waves from laboratory experiments.

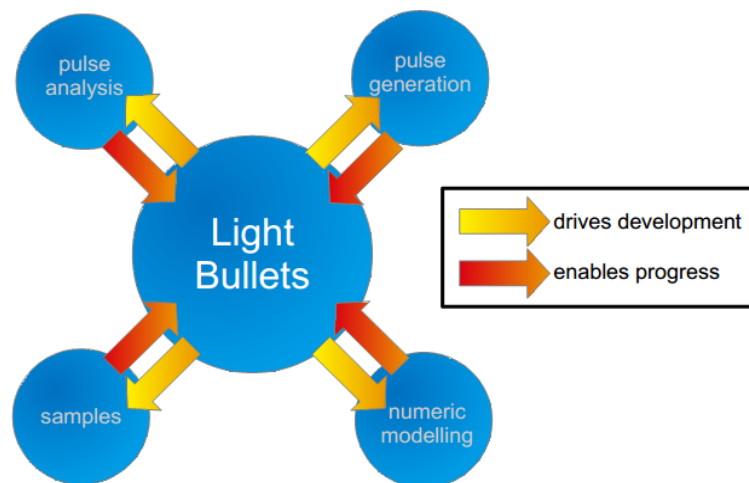


Fig. 2: Conceptual layout of this thesis and the areas of research it covers. The observation and characterization of discrete Light Bullets is the core topic. Activities in the field of pulse analysis, generation, numeric modeling, and sample description enable the understanding Light Bullets and are driven by it.

The significance and universality of Russell’s observation was not widely recognized until the second half of the 20<sup>th</sup> century, due to a lack of mathematical techniques, and the difficulty of exciting and observing nonlinear waves in an experiment. The first breakthrough in this respect was the development of the inverse scattering method [Gar67, Gar74, Abl91], which allows the construction of analytic solutions to a certain class of nonlinear wave equations, namely those that are integrable. This method itself is based on 19<sup>th</sup> century work on differential analysis, mainly by Bäcklund [Bäc73, Bäc75, Bäc80, Bäc81] and Lie [Lie74, Lie80a, Lie80b] and much younger findings by Gelfand, Levithan, and Marchenko [Gel51, Mar86]. This breakthrough is particularly interesting for two reasons. First it shows that there is a class of localized solutions, which propagate stationary without changing at all or which periodically reacquire their initial state in a breathing manner. Moreover, it can be shown that these wavepackets behave like particles, i.e., they scatter elastically off each other and remain asymptotically invariant under

## 1. Introduction

such scattering events. These wavepackets have therefore been termed “solitons” [Zab65]. A second fundamental finding is that solitons are not a feature of a particular nonlinear equation, but of a whole set, describing a large class of physical systems. Some examples are the Korteweg-de Vries equation, the nonlinear Schrödinger equation, and the Sine-Gordon equation. In this sense progress in the understanding of any of the physical systems improves the understanding of many other fields of science.

It must be noted that albeit only few real systems in nature are strictly integrable. Nevertheless, many non-integrable physical systems, which support nonlinear waves, also exhibit stationary wavepackets. These are termed “solitary waves”, although the term “solitons” is in the literature colloquially used, too, as will occasionally be done in this thesis. Being the solution of non-integrable systems solitary waves do not scatter elastically, which in fact means that their interaction properties are richer and more involved. Solitary waves have been predicted and observed in far too many systems to give a comprehensive overview [Abl91, Dau06] in this thesis. Just to name a few examples, solitons have been observed, e.g., in plasma waves [Zab65], deep water waves [Zak68, Bra96], weather phenomena [Cla81], in Bose-Einstein condensates [Bur99, Den00], and they play a central role in quantum field theory [Raj87]. Optical solitons are discussed below.

Two more key developments paved the way for nonlinear wave physics. The first milestone was reached when Pasta, Fermi, Ulam, and Tsingou published results of the first numerical study on nonlinear wave propagation [Fer55]. They investigated a series of nonlinearly coupled oscillators and found that the nonlinearity lead to the periodic recurrence of the initial state of the system. This work is also the first example of a discrete system, which supports solitary wave formation. The relation to continuous systems was found by Zabusky and Kruskal [Zab65], who first noted that the continuum limit of the Fermi-Pasta-Ulam-Tsingou chain is the Korteweg-de Vries equation. Again this behavior is not specific, instead one can think of the Fermi-Pasta-Ulam-Tsingou chain as the prototype for any chain of linked nonlinear, oscillating structures. Such chains, usually called discrete systems, are extremely abundant in natural and technical systems. Solitary waves have later been found in many discrete systems. They govern, e.g., the propagation of excitations in molecular systems [Dav91], such as in ionic crystals [Hol59a, Hol59b], in biomolecules [Dav73, Dav77], in acetylene [Su80, Su83], in DNA [Eng80], in molecular crystals [Fil89], in dielectric crystals [Swa99], or in phononic crystals [Sie88]. They also influence the propagation of excitations in the nervous system [Hod52, Hei05], the collective motion of nonlinear mechanical oscillators [Den92, Sat03], the development of localized structures in arrays of electric circuits [Mar95], the dynamics of coupled laser sources

[Gla98, Che01, Boc03], the development of traffic jams [Kur95, Kom95], the propagation of spin waves in antiferromagnets [Sch99, Sat04], the recurrence of discrete breathers in lattices of Josephson junctions [Bin00, Tri00], and the collective motion of atoms in arrays of Bose-Einstein condensates [Tro01], just to name a few.

The experimental observation of nonlinear wave propagation phenomena in general and solitary waves in particular in most of these systems is, however, difficult. Some of these systems are intrinsically hard to make experiments with, e.g., deep water oceanic waves and weather phenomena cannot be excited at will. In many other systems solitary waves exist on scales, e.g. time or length scales, where experimental analysis techniques are rare or do not exist at all. In a colloquial manner, nonlinear wave science was missing a sufficiently rich and accessible “playground,” in which nonlinear waves could be excited, observed and brought to interact with the environment under laboratory conditions.

The second key development was therefore the invention of the laser [Mai60] and the almost immediate realization that the high flux of photons per mode generated by this class of light sources could induce nonlinear polarization [Fra61, Arm62] into virtually any optical material. The dominating contribution to the nonlinear polarization for all non-centrosymmetric optical materials, e.g., for all optical glasses, is the  $\chi^{(3)}$ /Kerr-nonlinearity, which we consider in this thesis. Since its discovery nonlinear optics [Gar12] has established itself as the prototype environment for the understanding of nonlinear wave phenomena [Whi11] and has found widespread application [Gar13] in many fields of science and technology.

Particularly noteworthy within the scope of this thesis is the fact that the propagation of light under the influence of diffraction in the paraxial limit, second order dispersion, and the focusing Kerr nonlinearity can be described by the nonlinear Schrödinger equation [But90, Agr01, Boy03]. If only a single transverse coordinate is considered this equation is integrable and consequently one can exploit the similarity [Sha72] of dispersion and diffraction to excite spatial, as well as, temporal solitons, where nonlinearity balances diffraction or dispersion. Temporal solitons were first predicted [Has73] and observed [Mol80] in optical fibers. Spatial solitons were first observed in planar waveguides [Bar85, Ait90, Ait91a]. Discrete optical systems also support solitary waves. Infinitely extended waveguide couplers, so-called one-dimensional waveguide arrays, can be used to approximate chains of coupled oscillators, in the tight binding approximation [Kos54, Jon65]. Consequentially discrete optical solitons have been predicted [Chr88] and observed [Eis98]. Nonlinear optics has, however, developed into such a rich and many-faceted discipline that even a comprehensive overview over all kinds of optical solitons and solitary waves and their application is far beyond the scope of this thesis [Kiv03].

## 1. Introduction

The ability of the focusing Kerr effect to balance dispersion as well as diffraction along one transverse coordinate immediately leads to the question, if it can also balance linear broadening along a combination of two transverse coordinates or along all three simultaneously. In a homogeneous medium with local, nonlinear response this question can be answered from scaling arguments, using the Vakhitov-Kolokolov [Vak73] theorem. If applied onto the nonlinear Schrödinger equation one finds that only for the case of a single transverse coordinate solitary waves are stable. All solitary waves with more transverse degrees of freedom tend to diffract or collapse. Wave collapse [Akh68, She76, Ber98, Kiv00] was first observed in the context of unusual optical damage produced by Q-switched laser pulses in glass [Her64] and explained by the instability of the solitary wave of the two-dimensional nonlinear Schrödinger equation [Chi64]. This result was later generalized to more transverse dimensions [Sil90], where it was found that all high-dimensional solitary waves of the homogeneous nonlinear Schrödinger equation are unstable. The development of lasers with higher peak powers and shorter pulses meant that pulse collapse could eventually be studied in gases, too [Bra95]. It was found that the collapse of the optical wave onto smaller volumes is eventually balanced by the dielectric breakdown of the medium, limiting the peak intensity of the wave and generating a weakly ionized, defocussing plasma channel. Eventually a state of transient balance, called filament, is reached, which can extend over a few meters [LF99, Sku06]. In this filament the light co-propagates with a non-equilibrium plasma channel [Ber07, Cou07, Chi10, Bré12].

Although filaments are more or less stationary, spatiotemporal wavepackets, they are not Light Bullets in the strict sense. The generation of plasma is inherently related to loss and fundamentally limits the maximum propagation range. The stabilization of the wave collapse is also not externally tunable. Instead it relies on intrinsic material parameters, i.e. the molecule's ionization energy or the amount of higher order dispersion [Fib04].

Other approaches for the stabilization of Light Bullets have therefore been proposed [Wis02, Mal05]. Many of these are, however, currently hard to implement experimentally, such as those, which rely on the independent modulation of the linear and nonlinear refractive index [Tow02, Adh04, Tor09, Ye09], the diffraction strength [Zho11], or the longitudinal modification of the waveguide array [Bai03, Mih05, Bel08]. Other approaches considerably weaken the concept of solitariness, e.g., Light Bullets and Light Bullet trains based on non-instantaneous [Bur09, Gur09], saturable [Ska97], resonant [Leb10], or bi-valued [Edm92] nonlinearities or those where linear loss stops wave packet collapse [Bau98, Büt00] but no equilibrium is reached. Spatiotemporal two-color solitons in  $\chi^{(2)}$ -media [Liu99, Bur02] are inherently 2+1-dimensional, because they rely on the tilted pulse technique [Mar89, DT98] for group velocity matching and induction of

anomalous dispersion. Linear non-spreading spatiotemporal wavepackets [VL09, Cho10, Abd10, Pik12], albeit being called “linear Light Bullets”, are no solitary waves. They are also only weakly localized and their phase is non-stationary, although their amplitude is so.

However, discrete optical lattices, e.g., waveguide arrays, with Kerr nonlinearity have been predicted to support stable, two-dimensional, solitary waves [Efr02, Efr03], which inherit their stability from one-dimensional, discrete, spatial solitons [Chr88, Eis98], within certain limits [Eil10]. Experimental observation was successful in various implementations of waveguide arrays, such as in photo-induced waveguide arrays [Fle03b, Fle03a, Nes03], laser written waveguide arrays [Per04b, Sza06b], and fluid filled photonic crystal fibers [Vie12]. A more detailed overview over the development and achievements of nonlinear, discrete optics is given in Section 4.1.

In the core of this thesis we focus on the observation and characterization of discrete spatiotemporal solitary waves, so-called (discret) Light Bullets. Discrete Light Bullets have been predicted to be stable [Ace93, Tur93, Kiv94b, Led94, Mih04], as opposed to their homogeneous counterparts [Sil90]. However, experimental observation of stable, discrete Light Bullets, did lag behind the theoretical studies prior to this thesis. Attempts of observing discrete Light Bullets, even in one-dimensional waveguide arrays, remained inconclusive presumably due to a lack of spatiotemporal analysis techniques [Che03] and/or because of spurious, perturbative effects [Bab07, Ben08, Ben09, Gor10].

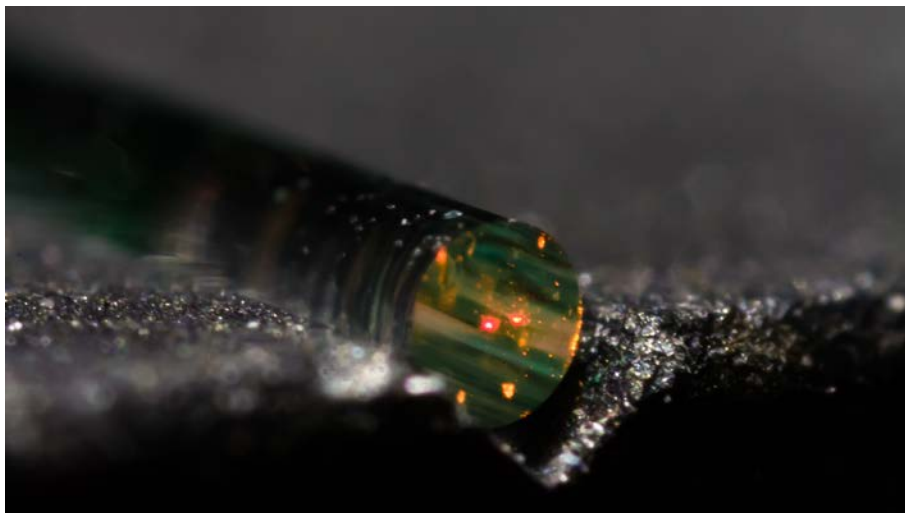


Fig. 3: Microphotographic image taken during a Light Bullet experiment. Depicted is the end facet of a fiber array. The red dot in the center is supercontinuum light generated in conjunction with the Light Bullets in the central core of the fiber array. Orange patches are dirt particles illuminated by supercontinuum light scattered into cladding modes.

As can be seen from Fig. 2 in this thesis we implement, improve and develop spatiotemporal pulse generation and pulse analysis techniques. We analyze various discrete optical environments for their suitability for spatiotemporal nonlinear optics and for their ability to sustain stable,

## 1. Introduction

discrete Light Bullets. We also investigate two different propagation models. With this experimental infrastructure we have been able to observe two different classes discrete Light Bullets in fiber arrays and carefully characterize their spatiotemporal properties and evolution dynamics. For an image of a fiber array during a Light Bullet experiment see Fig. 3.

We deal with issues related to the generation of spatiotemporal pulses. Forming of pulses with arbitrary temporal shape is an active topic in photonics [Sch05, Mon10, Cun10] and spatial beam shaping is routinely used in many experiments. However, the combination of both techniques, i.e. the generation of arbitrary spatiotemporal fields is currently not discussed much beyond the level of conceptual ideas. We first introduce basic pulse generation facilities, which had been available in this thesis. Then we focus on a spectral pulse shaping technique, which we have adapted for high power, high throughput, low aberration operation in collaboration with the Optical Systems Design and Microstructure Technology groups of the Institute of Applied Physics (IAP). Spatial shaping is discussed in the context the generation of discrete vortices in collaboration with the Microstructure Technology group of the IAP. An outlook onto a potential concept for spatiotemporal, arbitrary pulse generation based on dispersive metasurfaces is then given.

Spatiotemporal analysis techniques on the other hand have experienced substantial development in the last years. This development was mostly driven by temporal analysis techniques for ultrashort pulses [Kan93, Iac98, Tre02]. Many of these techniques are, in principle, compatible with spatial multiplexing, e.g., by combining them with imaging techniques [Akt10]. We present specific spatiotemporal pulse analysis techniques that we have implemented and developed in the course of this thesis. As the “workhorse” we set up an imaging cross correlator, a basic spatiotemporal pulse analyzer. It is also the basis for the imaging cross-correlator FROG, which we developed. It is one of the very few three dimensional spatiotemporal, phase resolving analysis techniques, that do not need a coherent reference. It measures the optical field on the largest number of independent points reported so far. Another product of this thesis is a simplified FROG, which only reconstructs signals along a single spatial dimension but does so orders of magnitude faster. We also demonstrated the feasibility of a concept for the unification of pulse generation and analysis, called Analysis-by-Control, which can be used for rapid prototyping of experiments.

Meaningful spatiotemporal experiments require samples with sufficiently interesting functionality. As the optical functionality of solid state samples is induced by their structure, a sophisticated three dimensional structuring technique is a prerequisite. This makes many highly developed structuring techniques, such as most lithography techniques [Lev05] unsuitable,

because they act on surfaces only. Three dimensional patterning of the sample, not only affects the spatial response but can also be used to tailor the local temporal response. This thesis focused on spatiotemporal, nonlinear optics in discrete structures [Chr03], i.e., in waveguide arrays. In particular we discuss femtosecond written waveguide arrays [Nol03, Per04b], produced by the Ultrafast Optics group of the IAP and drawn fiber arrays [Röp07, Röp11] produced by the Institute of Photonics Technologies. These classes of discrete optical samples are compatible with spatiotemporal, nonlinear experiments. Systematic comparison of the main effects that influence pulse propagation in fiber arrays reveals that the temporal scale of the Light Bullets is expected to a few femtoseconds only. We therefore introduce two propagation models that can be solved numerically. The first is the canonical model for spatiotemporal optics and is used to discuss characteristic parameters of the samples and the impact of geometry thereon. The second is also quantitatively correct and is used for numeric cross-validation of experimental data.

The core part of the thesis is devoted to the observation and characterization of nonlinear, spatiotemporal waves in waveguide arrays. As outlined in Fig. 2 it makes use of all peripheral developments of the prior chapters. We first investigate spatiotemporal wave propagation in a one-dimensional, segmented waveguide array in a parameter regime where Light Bullets cannot be observed and the dynamics is relatively simple and straightforward. Then we deal with the observation of fundamental Light Bullets, the characterization of some of their peculiar static and dynamic properties and the observation of Vortex Light Bullets. This ordering follows the direction of increasing complexity and decreasing symmetry. Special focus is put on understanding the influence of higher order effects, which limits the propagation length of Light Bullets but also induces an intriguing, intrinsically spatiotemporal evolution mechanism. This mechanism is related to the interdependence of the nonlinear, temporal, and spatial response of the system. We show that this interdependence also causes asymmetry in the spatiotemporal spectra of the Light Bullets and leads to superluminal decay. Later we excite the waveguide array with an asymmetric input pulse, exciting Vortex Light Bullets, which are, to the best of our knowledge, the most complex spatiotemporal solitary waves observed in an experiment, so far. All experimental results are backed up by rigorous numerical simulations and discussed in the context of simplified analytical models.

## 2. Spatiotemporal Pulse Generation and Forming

At the beginning of most experiments in nonlinear optics is the generation of a pulsed field  $E_0(x, y, t)$  with the properties that are desirable in this specific experiment. In this chapter we will present methods for the generation of ultrashort, high-power pulses, which will later be used in experiments to excite spatiotemporal fields with growing complexity. We will introduce the methods in the order of growing complexity and flexibility, starting with basic methods for fixed wavelength, fixed form pulse generation in Section 2.1 and then lift each of the restraints, eventually allowing us to generate pulses with arbitrary temporal shape using the spectral pulse shaping technique discussed in Section 2.2. A case study on the possibility and limits of spatial shaping of ultrashort pulses is presented in Section 2.3. Section 2.4 gives an outlook onto a possible future concept for spatiotemporal wave shaping, based on a generalization of multicolor metamaterial holograms.

Note that in this chapter, as in the rest of this thesis, we ignore polarization and implicitly assume linearly polarized light. Generalization to pulse generation and analysis techniques, which can handle arbitrarily polarized fields, is conceptually straightforward, albeit technically difficult to implement. Moreover it was unnecessary for the experiments discussed in Chapter 5, because the experimental environments introduced in Chapter 4 are polarization insensitive.

### 2.1 Basic Pulses: Oscillators and Amplifiers

Classically one aims for pulses  $E^{(0)}(x, y, t) = A^{(0)} \exp\left\{-2 \log(2) \left(\frac{x^2}{w^2} + \frac{y^2}{w^2} + \frac{t^2}{t^{(0)2}}\right)\right\} \exp\{i\omega_0 t\}$  with simple, smooth and well defined spatial and temporal properties, such as peak power  $P^{(0)} = |A^{(0)}|^2$ , beam diameter  $w$ , pulse duration  $t^{(0)}$ , and carrier wavelength  $\lambda_0 = 2\pi c_{ph}/\omega_0$ .

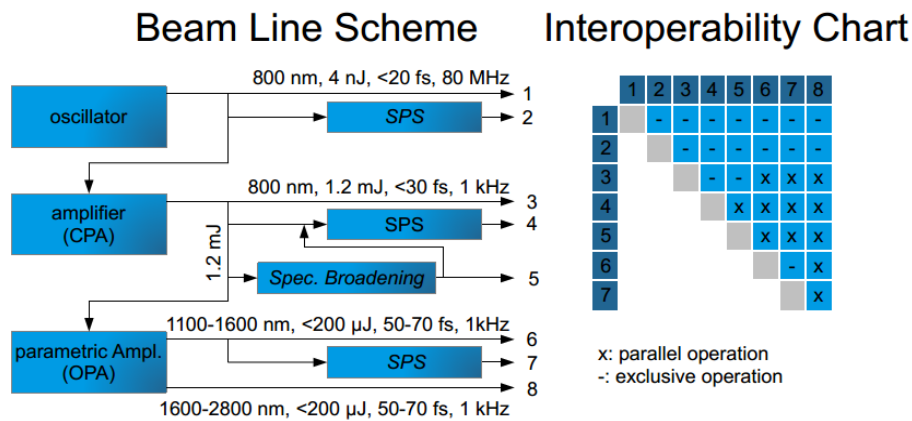


Fig. 4: Principle chart of available beam lines for the experiments described in this thesis. Italic labels denote unimplemented or unfinished devices. SPS: spectral pulse shaper. Interoperability chart denotes beam lines, that can be run in parallel.

Trains of such pulses, or at least approximations thereof, can be produced in modern short pulse

laser systems and chirped pulse amplifiers (CPAs). Arguably the most common lasers/CPA types used in contemporary, ultrafast optics labs, are based on lasing and amplification in Titanium-doped Sapphire (Ti:Sa) crystals. The Ti:Sa crystal offers broadband gain over almost a quarter octave centered around a peak gain wavelength of roughly  $\lambda = 800$  nm. Consequentially it is limited to generate pulses with a bandwidth of less than 200 nm and corresponding pulse durations of little less than 10 fs, with a carrier wave cycle duration of 2 fs. These specifications are rarely reached in real-world systems. In particular CPAs suffer from spectral narrowing due to spectrally uneven gain and pulse degradation due to non-compensated higher order dispersion.

Unless stated otherwise, in our experiments we used a Ti:Sa modelocked, femtosecond laser oscillator Micra from Coherent, which produces pulses with a repetition rate of 80 MHz, a pulse duration of  $t^{(0)} < 20$  fs, with 50 ... 100 nm bandwidth and a pulse energy of  $E = 4$  nJ. As depicted in Fig. 4 it can be used directly or pump a CPA. The CPA is a Legend Elite USP from Coherent, which reduces the repetition rate to 1 kHz and increases the pulse energy to 2.5 mJ. The pulse bandwidth is reduced to 50 nm, with a minimal pulse duration of 25 fs. This equates into a peak power of  $P^{(0)} \gg 10$  GW, which is larger than that of the Townes-soliton [Chi64], which is 6.3 GW in air. On the one hand this means that special care has to be taken when working with the beam to maintain its spatial and spectral quality, by reducing the beam path while maximizing its diameter, avoiding transmissive optics, and only using high-power compatible optical elements. On the other hand this means that the pulse power is more than sufficient to generate a plethora of nonlinear effects in solid state systems, which typically have nonlinearities that are at least three orders of magnitude larger than that of air [Boy03]. We are therefore in the advantageous position to be able to invest a part of the pulse energy into modifying the pulse's properties and changing its shape, envelope, and carrier wavelength.

Wavelength modification is achieved by routing half of the pulse through an optical parametric amplifier (OPA). The OPA uses multistage difference frequency generation (DFG) in  $\chi^{(2)}$ -crystals to turn the 1.2 mJ pump pulse from  $\lambda_0 = 800$  nm into a pair of pulses of longer wavelengths  $\lambda_{\text{OPASig}}$  and  $\lambda_{\text{OPAidl}}$ . They are related to the carrier wavelength  $\lambda_0$  of the pump pulse according to photon energy conservation  $\lambda_{\text{OPASig}}^{-1} + \lambda_{\text{OPAidl}}^{-1} = \lambda_0^{-1}$  and marked in Fig. 4. The remaining degree of freedom is determined by photon momentum conservation and is fixed by the adjustment of the angle of the  $\chi^{(2)}$ -crystals with respect to the pump beam. The wavelength of the signal pulse can be tuned in the range of  $\lambda_{\text{OPASig}} = 1100 \dots 1600$  nm. The conversion efficiency is in the range of 10 ... 40%. The signal pulse thus has an energy of  $E_{\text{OPASig}} = 50 \dots 300$   $\mu$ J. The energy of the idler pulse  $E_{\text{OPAidl}}$  is accordingly a bit lower because of its lower

## 2. Spatiotemporal Pulse Generation and Forming

photon energy. The pulse duration is increased with respect to the pump duration by the limited DFG gain bandwidth. Signal and idler have a duration of  $t_{\text{OPA}}^{(0)} \approx 50$  fs and a Gaussian spatial cross section.

In summary we have, at this point, the ability to generate nearly transform limited pulses with a duration of 25 fs at a fixed carrier wavelength of  $\lambda_0 = 800$  nm and a pulse energy of  $E = 1.2$  mJ. In a jitter-free, synchronized beam line we have pulses with tunable wavelength of  $\lambda_{\text{OPASig}} = 1100 \dots 1600$  nm, a duration of  $t_{\text{OPA}}^{(0)} = 50$  fs, and a pulse energy of  $E_{\text{OPA}} > 50$   $\mu$ J. Later we shall see that this combination is already very useful, as one beam can be used to excite spatiotemporal (ST) effects in an experiment. The other beam serves as a known reference which can be used to gate and measure the nonlinearly reshaped ST field. As all experiments discussed in this thesis have been carried out in fused silica, the two available wavelength ranges can be used to excite samples in the normal and the anomalous dispersion regime [Agr01], triggering very different nonlinear dynamics.

### 2.2 Advanced Pulses: Spectral Pulse Shaping

After having overcome the limitation of a fixed carrier wavelength we will now discuss the spectral pulse shaper (SPS), which we will use to obtain variable pulse shapes. SPS stages are being installed for the oscillator, the CPA and the OPA signal beam line, as shown in Fig. 4. Only the SPS in the CPA beam line is currently operable, however, the principles of operation and technical implementations are identical and are discussed in this chapter.

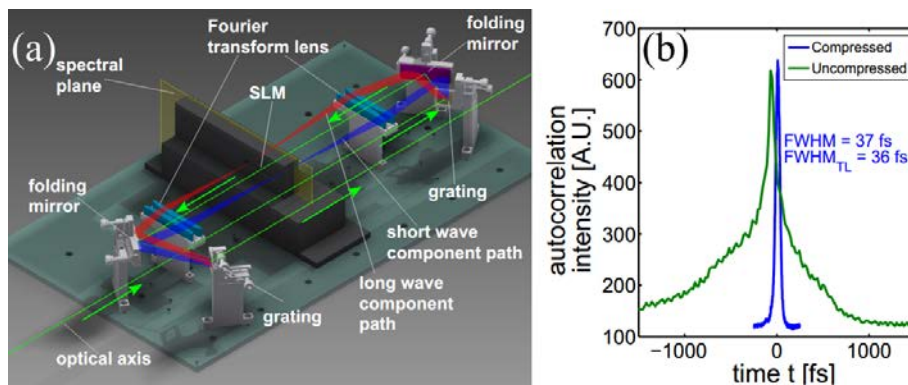


Fig. 5: (a) Physical layout of the optimized SPS setup, as discussed in Section 2.2.3. The polarizer, spectrometer, and SH stage are not displayed in this scheme. (b) Autocorrelation traces of pulses after the SPS setup, before (green) and after (blue) compensation of the unknown spectral phase  $\phi_0$  with the MIIPS algorithm. The compressed pulse has an autocorrelation FWHM duration of 37 fs whereas 36 fs would be the transform limit.

Pulse shaping in time domain is not an option for femtosecond pulses due to the unavailability of filters  $F(t)$  with sufficiently short response time (or bandwidth, in other words), which can transform in input pulse  $E^{(0)}(t)$  into an arbitrary output pulse  $E_{\text{out}}(t)$ . The output is related to

the input pulse with the transform equation  $E_{\text{out}}(t) = F(t) \otimes_t E^{(0)}(t)$  [Phi95], where  $\otimes_t$  denotes convolution in the time domain. However, we can exploit the fact that manipulation in the frequency domain becomes simpler for shorter pulses, as all spectral features grow with decreasing duration. In frequency domain the transform relation is a simple product:

$$E_{\text{out}}(\omega) = F(\omega) \cdot E^{(0)}(\omega). \quad (1)$$

This means that arbitrary output pulses can be generated if the input spectrum can be modulated by the complex Fourier transform of the filter  $F(\omega)$ , i.e., if each frequency (or wavelength) component can be manipulated in amplitude and phase. For practical reasons we are limited to lossy filters  $|F(\omega)| < 1$  and to a certain bandwidth  $\Delta\omega$  and spectral resolution  $\delta\omega$ . These quantities determine the maximum temporal window  $\Delta t = 2\pi/\delta\omega$  over which the filter can redistribute pulse energy and the minimal feature size that the filter can generate  $\delta t = \max(2\pi/\Delta\omega, t^{(0)})$ , where  $t^{(0)}$  is the transform limited input pulse duration.

The SPS implements such a spectral filter in the form of a 4f-setup [Wei95, Mes97], as depicted in Fig. 5(a). A diffraction grating disperses the wavelength components into beams with separate directions, which are focused by a cylindrical lens on the Fourier plane in the center of the setup. Here each wavelength component has a distinct location, by which it can be addressed and modulated. An inverted setup resynthesizes the pulse from the modulated spectrum. Common strategies for the spectral modulation [Wei00] are micromechanical adaptive arrays [Hac03, Tan12] or liquid crystal displays [Yel97]. Here we have used a liquid crystal spatial light modulator (SLM) with a one-dimensional (1D) display consisting of 640 pixels. In principle, an increase in spectral resolution by using a two-dimensional (2D) device is possible, up to the point, where line-by-line shaping is within reach [Cun10, Fer11]. The SLM used in this thesis consists of two back-to-back mounted transmissive displays with their extraordinary axis oriented perpendicular to the principal optical axis of the system and at  $\pm 45^\circ$  with respect to the pulse's polarization direction. By independent variation of the voltages applied to each pixel of both displays we can independently modulate each frequency component's phase and rotate its polarization state and thus, via a polarizer, modulate its amplitude. The amplitude  $|F(\omega)|$  and the phase  $\arg[F(\omega)]$  are given by the relations

$$|F(\omega)| = \cos\left(\frac{\Phi^{(A)}(\omega) - \Phi^{(B)}(\omega)}{2}\right) \quad \arg[F(\omega)] = \frac{\Phi^{(A)}(\omega) + \Phi^{(B)}(\omega)}{2}, \quad (2)$$

where  $\Phi^{(A/B)}(\omega)$  is the phase shift (modulus  $2\pi$ ) between the ordinary and extraordinary wave in display A/B for the frequency  $\omega$ . Given the design parameters of the system we can shape over a bandwidth  $\Delta\omega$ , with spectral resolution  $\delta\omega$  of

## 2. Spatiotemporal Pulse Generation and Forming

$$\Delta\omega = 600 \text{ THz} \quad \delta\omega = 0.9 \text{ THz}, \quad (3)$$

which equates into a temporal resolution  $\delta t$  and shaping range  $\Delta t$  of

$$\delta t = \max(10 \text{ fs}, t^{(0)}) \quad \Delta t = 6.7 \text{ ps}. \quad (4)$$

While the above presented concept of spectral pulse shaping is elegant, powerful, and conceptually simple, there are quite a few pitfalls that have to be overcome in order to make the device usable for practical purposes. Important obstacles and solutions are outlined in the sections below.

### 2.2.1 Calibration

To obtain a sought-after pulse we need to define a spectral filter  $F(\omega)$  and manipulate the spectral amplitude  $|F(\omega)|$  and phase  $\arg[F(\omega)]$  according to Eq. (2). The SLM, however, is only able to apply voltages  $U_i^{(A/B)}$  to pixels with index  $i$ . We therefore have to find a map  $\omega_i = \omega(i)$ , which translates pixel indices  $i$  into corresponding frequencies  $\omega_i$ . Then we have to map voltages onto applied phase shifts  $\Phi_i^{(A/B)}(U_i^{(A/B)})$ . We have to do so for both displays A and B, as well as, for each pixel index separately, because both displays act differently and are wavelength dependent.

The pulsed source itself is used for the calibration. In a first step the pulse is routed through the SPS and its spectrum is observed with a spectrometer after the pulse shaping device. Then a pixel  $i$  is selected and randomly manipulated. A spectrum for each realization is recorded and a computer algorithm determines the wavelength which has maximum variation. After all pixels have been treated in this manner,  $\omega_i = \omega(i)$  is determined. In a second step one display is set inactive, i.e., into a state of maximum voltage, where the extraordinary axis is nearly parallel to the direction of propagation and thus  $\Phi = 0$ . The other display's voltage is now varied systematically through all possible values, while the transmission of each wavelength is observed with the above mentioned spectrometer. Via inversion of Eq. (2)  $\Phi_i^{(A/B)}(U_i^{(A/B)})$  is then fully determined.

The SLM is now fully characterized and can be used to set the phase  $\Phi_i^{(A/B)}$  of each pixel with an accuracy of roughly 50 mrad. After the polarizer this translates into  $-16$  dB range for the filter amplitude  $|F(\omega)|$  and 50 mrad accuracy for the filter phase  $\arg[F(\omega)]$ .

### 2.2.2 Determination of the Initial Phase

At this point the output pulse  $E_{\text{out}}(\omega)$  is still not fully determined, although the action of the SPS and thus the shape of  $F(\omega)$  is. The exact shape of the input pulse  $E^{(0)}(\omega)$ , or more precisely, its

spectral phase  $\phi_0(\omega)$ , remains unknown. For the CPA there are four main sources for this uncertainty: (i) the CPA does not produce fully transform-limited pulses; during amplification in the CPA cavity a considerable amount of high order dispersion is acquired; (ii) the compressor must overcompensate the pulse chirp for the OPA to work perfectly, as some of the internal optics of the OPA introduce chirp; (iii) the pulse is reflected off dielectric mirrors and transmitted through a single thick beam splitter, all of which add additional chirp, (iv) slight misalignments of the SPS add additional chirp. All these accumulated phase variations, that considerably degrade the shape of an ultrashort pulse, can be compensated by the SPS, if they can be measured. Phase measurement for ultrafast pulses is a research subject in its own right and has seen the development of many methods over the last decades, such as FROG [Tre02] or SPIDER [Iac98]. Here we used MIIPS [Loz04], a method that retrieves the unknown spectral phase  $\phi_0(\omega)$  of a pulse, using the SPS itself. To do so a second harmonic (SH) crystal of sufficient bandwidth is placed after the setup and the spectrum of the SH is recorded, while the phase  $\arg[F(\omega)]$  of the SLM is varied systematically. An iterative retrieval algorithm then determines the local phase curvature  $d^2\phi_0/d\omega^2$  from the data and then the unknown phase  $\phi_0(\omega)$  via numerical integration. The algorithm needs less than one minute to converge onto a result and can compensate the unknown spectral phase  $\phi_0(\omega)$  to a degree, which allows us to get within 10% of a transform limited pulse, as shown in Fig. 5(b).

### 2.2.3 Improved Optical Design

While the SPS is now, in principle, fully operational this is not the case in reality. The naïve design from above has two major flaws that need to be rectified: low system throughput and imaging aberrations. The former is mainly determined by the diffraction efficiency of the diffraction gratings and can be mitigated by the use of efficient gratings and an appropriate choice of diffraction angles. In collaboration with the microstructure technology group of the IAP we designed and produced transmissive, electron beam lithographically written diffraction gratings, made from binary groove/ridge combinations in fused silica [Cla03]. They combine three important properties: (i) a high damage threshold, (ii)  $> 95\%$  diffraction efficiency for  $700 \text{ nm} < \lambda < 900 \text{ nm}$ , and (iii) high regularity, with no measurable ghosting. These gratings outperform all commercially available classic gratings designs, that either suffer from low efficiency, such as holographic gratings, or ghosting, such as ruled gratings. With the use of these gratings we can obtain a total system efficiency of more than 70%, limited mostly by the transmission of the SLM, which could be improved with anti-reflection coatings.

Imaging aberrations are, however, harder to mitigate. Highly efficient gratings necessarily have

## 2. Spatiotemporal Pulse Generation and Forming

small periods to make higher diffraction orders evanescent. This automatically introduces large diffraction angles of the various wavelength components, leading to a high numerical aperture (NA) of  $NA > 0.15$ . To make matters worse, high power operation necessitates large beam diameters in the order of 10 mm, such that phase front errors introduced by aberrations have a particularly strong impact. One further needs to consider chromatic aberrations, which arise from the large bandwidth of the system. In fact it was found that in the original design with singlet Fourier transform lenses, spectral components which are more than 10 nm away from the center wavelength, have considerable residual phase curvature. They converge onto a cylindrical focus a few meters after the SPS. In collaboration with the optical system design group of the IAP the SPS setup was thus systematically investigated with optical design software. It was found that replacement of the singlet Fourier transform lenses with doublet lenses reduces the phase front error from  $> 10 \lambda$  to  $0.2 \lambda$ , if the device positions can be set with tolerances  $< 0.1$  mm. Chromatic aberrations have been shown to be of little impact.

The SPS was consequentially computer-designed on a custom base plate to meet tolerances and to eliminate all unnecessary degrees of freedom in the adjustment process. A schematic of the resulting device is displayed in Fig. 5(a). In summary we have designed and characterized an SPS that surpasses, to the best of our knowledge, all commercially available devices in terms of efficiency, resolution, preservation of beam quality, and maximum power throughput.

### 2.2.4 Coherent Spectral Broadening

At this point the capabilities of the SPS can still not be fully exploited. The SPS is designed to work for wavelengths from 700 nm to 900 nm and thus shape pulses with features as small as 10 fs, as discussed in Eq. (3). In the current setup pulse features below 25 fs are, however, inaccessible due to the lack of bandwidth of the input pulse.

To exploit the full capabilities of the SPS the input pulse needs to be broadened spectrally. While nonlinear photonics offers a plethora of pulse broadening techniques most of these are unsuitable for our purpose. Self-phase modulation (SPM) based broadening in a bulk material cannot be used because the pulse power is not constant over the beam's cross section, which would lead to a radially dependent broadening. Classic waveguide (WG) broadening strategies [Sha82] are unsuitable because (i) solid state WGs [Hus01] are not able to handle multi-GW peak power pulses, nor are hollow-core bandgap fibers [Ouz05] and (ii) stimulated Raman scattering (SRS) redshifts the spectrum quickly and leads to strong pulse to pulse variation [Sol07] of the spectrum.

However a different class of WGs can be used to tackle these issues – the capillary WG [Mar64]

or its more advanced cousin, the Kagomé WG [Cou06]. Here light is guided in a fairly large low index void surrounded by a dielectric cladding. The guided field is not a mode in the classical sense but a smooth superposition of quasi-parallel plane waves with small propagation angles; similar to a paraxial, radial Gaussian beam in free space with many wavelengths in diameter. They interact with the refractive index step at the boundary by Fresnel reflection; the magnitude of which is near unity due to the grazing incidence angles. Moreover the phase relation here imposes zero-field at the boundary. Light is thus confined to the hollow core, with very little energy in the solid state cladding. For vacuum-“filled” Kagomé WGs propagation losses of less than 0.2 dB/m have been reported and guiding of multi-mJ femtosecond pulses has been demonstrated [Wan11]. The core can also be filled with gases of varying pressure, by simply placing the fiber in a gas-filled vacuum chamber.

Here the fiber has a 200  $\mu\text{m}$  core diameter and is filled with Argon. We exploit in the absence of SRS from SPM due to atomic nature of noble gases [Nol10, Jol11]. The SPM broadened spectrum is then fed into the SPS and recompressed [Nis96, Nis97, Hec11].

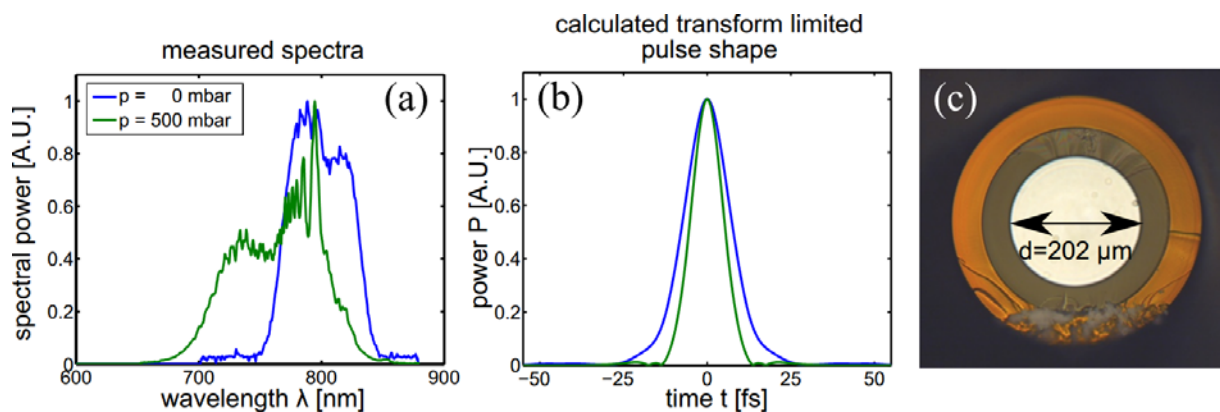


Fig. 6: (a) Spectrum after propagation in a capillary fiber with (blue) no Ar filling and FWHM = 58 nm and (green) 500 mbar Ar filling and FWHM = 94 nm. (b) Calculated transform limited pulses, belonging to spectra of (a). (c) White light microscopy image of the capillary.

At the current level of implementation we reach spectral broadening of a factor of less than 2 resulting in a spectral full-width at half maximum (FWHM) of 94 nm at a transmission efficiency of 40% with 500 mbar Argon pressure. Temporal recompression has not been tested at this point because the beam quality is seriously ill-affected by plasma generation and a further increase in pressure increases this detrimental effect. This could be mitigated by an increase of the diameter to 400  $\mu\text{m}$ , which would be the optimal value [Voz05, Rot11] with a broadening factor of up to 7 at an Argon pressure of 250 mbar, without considerable plasma formation. This value, together with pulse recompression, is planned to be demonstrated in the next iteration of the experiment.

## 2. Spatiotemporal Pulse Generation and Forming

### 2.3 Spatial Shaping: a Rotating Case Study

At this point we have overcome all limits that pertain to the temporal and spectral properties of the generated light and we have taken great care not to degrade the Gaussian cross section of the pulse. Nevertheless for some experiments a non-Gaussian spatial shape is desirable.

Similar to the strategy of indirectly shaping pulses in the spectral domain, discussed in Section 2.2, we here exploit a Fourier-space shaping technique to design the beam's focal pattern  $E_{\text{foc}}(x, y) = F(x, y) \otimes_{x,y} E^{(0)}(x, y)$ , which is in turn coupled into a sample. Here  $F(x, y)$  is a spatial filter, whereas  $E^{(0)}(x, y)$  is the focal plane distribution, without any filter. Such a filter can be implemented in the far field (e.g., in the collimated beam, before focusing with a lens of focal length  $f$ ) as

$$E_{\text{foc}}(\tilde{x}, \tilde{y}) = F(\tilde{x}, \tilde{y}) \cdot E^{(0)}(\tilde{x}, \tilde{y}), \quad (5)$$

where  $x = k_{\tilde{x}}f/k$ ,  $k = 2\pi/\lambda$ , and  $k_{\tilde{x}}$  is the spatial frequency that belongs to  $\tilde{x}$  and a similar relation holds for  $\tilde{y}$ .  $F(\tilde{x}, \tilde{y})$  is then nothing but a (partially) transmissive plate that modifies the local phase and amplitude to holographically generate a sought-after focal field distribution.

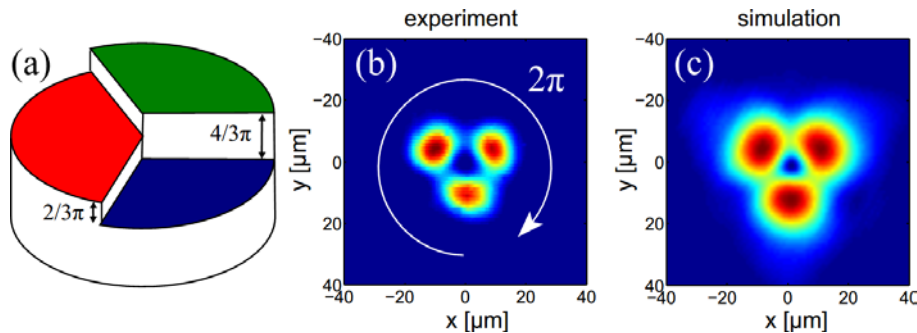


Fig. 7: (a) Phase plate design. (b) Experimental and (c) simulated image of the focal spot intensity produced by a Gaussian beam and the phase plate. Adjacent peaks have  $2/3\pi$  phase difference. Figure adapted from [Eil13c].

This strategy was used to excite Vortex Light Bullets (VLBs) in fiber arrays, which are discussed in detail in Section 5.4. To excite VLBs it was necessary to generate a compact triangular vortex and couple it into a waveguide array (WA), although excitation by a homogeneous vortex was predicted to be feasible [Fer05], it is inefficient. Generation of a discrete vortex field was achieved by modification of the well-known spiral phase plate technique [Sue04], in which a spiral phase ramp with a phase shift of  $2\pi M$  per revolution is imprinted on a collimated beam, where the integer  $M$  denotes the topological charge of the resulting beam. Upon Fourier transformation, carried out by insertion of a lens and observation in the lens' focal plane, a continuous optical vortex with topological charge  $M$  is generated. The phase shift is usually encoded in a transparent plate of refractive index  $n$ , where the thickness of the plate has an azimuthal gradient, such that it grows by  $M\lambda/(n-1)$  per revolution. We adopted the technique

## 2.4 Outlook: Full Spatiotemporal Waveshaping with Metasurfaces

for the generation of a discrete, triangular, compact Vortex, which by definition can only have an angular momentum of  $M = \pm 1$ , by replacing the smooth, azimuthal gradient by discrete height steps  $\delta$  in a silica wafer. The phase shift  $\phi$  is related to the step height  $\delta$  by

$$\phi = 2\pi(n(\lambda) - 1)\delta / \lambda_0. \quad (6)$$

Here  $\delta = \lambda/3 / (n(\lambda_0 = 1550 \text{ nm}) - 1)$  per  $120^\circ$  arc. The plate was fabricated in the Microstructure Technology Group of the IAP, using an etching technique.

As opposed to continuous vortices, the vortex-character of the focal plane pattern is directly confirmed by the spiraling motion of the three peaks before and after focal plane. Moreover, we find that the size, shape, and relative distance of the three peaks of the discrete vortex coincides very well with the arrangement of WGs in the fiber array (see Section 4.3.2). So a high coupling efficiency of  $> 60\%$  can be reached in simulations;  $> 40\%$  was achieved experimentally.

One must note, however, that this technique has some limitations, as it intrinsically introduces spatiotemporal distortions. This can be seen from the definition of the step height  $\delta$ , which only leads to a “correct”  $2\pi$  phase shift for one spectral component of the pulse at  $\lambda_0 = 1550 \text{ nm}$ . This distortion is, however, small because the pulse’s bandwidth of  $70 \text{ nm}$  is relatively small, compared to the carrier wavelength.

### **2.4 Outlook: Full Spatiotemporal Waveshaping with Metasurfaces**

While in the last section we have considered the wavelength-dependent nature of the spatial shaping process to be detrimental, albeit small, we now argue that it could be exploited to generate tailored spatiotemporal distributions of light. The idea is to combine the concepts put forward in Sections 2.2 and 2.3 into a common approach along the lines of a spatiotemporal (ST) generalization of Eqs. (1) and (5), such that

$$\begin{aligned} E_{\text{out}}(x, y, t) &= F(x, y, t) \otimes E^{(0)}(x, y, t) \\ E_{\text{out}}(\tilde{x}, \tilde{y}, \omega) &= F(\tilde{x}, \tilde{y}, \omega) \cdot E^{(0)}(\tilde{x}, \tilde{y}, \omega). \end{aligned} \quad (7)$$

This relation states that we could generate an arbitrary  $E_{\text{out}}(x, y, t)$ , if we were able to place a holographic plate in the far field, whose behavior was wavelength dependent in a controllable manner, i.e., that it would have arbitrary dispersion. It is clear that the ansatz from Section 2.3, using height variations in a dielectric material is unsuitable for this approach. None of the wavelength dependent terms in Eq. (6) is sufficient to generate the desired dispersion, neither in terms of the amount, nor in terms of flexibility. The approach is also hopeless because of its insufficient information content: the height variation  $\delta$  is the only degree of freedom per spatial pixel, with which we would have to try to shape a multi-valued, complex spectral response per

## 2. Spatiotemporal Pulse Generation and Forming

spatial pixel.

The number of degrees of freedom per pixel must therefore be increased. The optical response of each pixel and for each fixed wavelength must, however, remain close to that of a homogeneous material to avoid scattering into unwanted spatial frequencies. This could be achieved by the subwavelength structuring of each pixel with metallic subwavelength structures, that exhibit geometry-tunable plasmonic resonances [Pen99, Cai10] close the desired wavelength of operation. This approach would work entirely without a variation of the sample height; the resulting structures are thus referred to as meta-surfaces [Aie12a, Aie12b].

Of course, this approach would have its own difficulties, which cannot be guaranteed to be solvable for technical and fundamental reasons. Broadband operation close to a damped system resonance necessarily involves losses, because of the causality of the response function [Kro26, Kra27]. Furthermore, operation at optical frequencies is inevitably linked to broad resonance features due to the strong damping of electronic excitations near the plasma frequency of the metal structures [Joh72]. Nevertheless there has been recent, theoretical progress towards the creation of tailored spectral responses by the superposition of resonances [Dir13], albeit under simplifying assumptions.

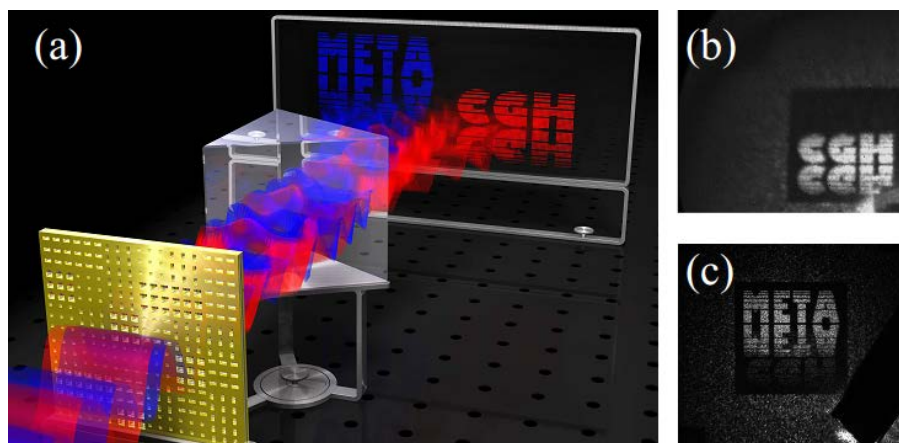


Fig. 8 (a) Schematic representation of a metasurface ST waveshaping device. (b) Experimental Fourier plane pattern at  $\lambda_1 = 1300$  nm and (c) at  $\lambda_2 = 905$  nm. Figure adapted from [Wal12].

A first step towards the experimental demonstration of full spatiotemporal waveshaping with metasurfaces was presented in [Wal12]. A two-color metamaterial hologram was designed, which produces two distinct images in the Fourier plane, if illuminated with two different wavelengths at  $\lambda_1 = 1300$  nm and  $\lambda_2 = 905$  nm. A schematic representation of the experimental layout and experimental Fourier plane images for both wavelengths are displayed in Fig. 8. This result was achieved by the fabrication of a computer generated hologram made of four different subwavelength pixel designs labeled A1, A2, B1, and B2. They have been designed such that at  $\lambda_1$  pairs with equal letters produce equal feedback, whereas at  $\lambda_2$  pairs with equal

## 2.4 Outlook: Full Spatiotemporal Waveshaping with Metasurfaces

numbers do so. Therefore at  $\lambda_1$  a binary hologram could be encoded independently of another one at  $\lambda_2$ . Extension towards an arbitrary number  $W$  of wavelengths, would, however, require an exponentially increasing number  $\mathcal{O}(\exp(W))$  of unit cell designs, such that the potential of this specific approach for ST waveshaping, although clearly visible, remains limited.

Furthermore challenges in modelling, design, and fabrication of spatially dispersive structures with an arbitrary temporal response are huge and at this point it remains unclear if any of these issues could be solved in a manner that makes metasurface wave shaping attractive for future application. However, the recent theoretical and experimental progress puts the “holy grail” of ST optics – full ST light field control – on the horizon of photonics, although it certainly is a vision at this stage.

## 3. Spatiotemporal Pulse Analysis Techniques

While the last chapter has been devoted to the generation of arbitrary ST pulse shapes, in this chapter we will discuss various techniques that are used for the analysis of unknown ST fields, mostly those that have been generated or modified by nonlinear ST experiments which will be reported in Chapter 5.

We will first present the imaging cross correlation technique (iXCorr) in Section 3.1, which is the workhorse for all ST experiments. It is a reasonable tradeoff between attainable resolution and depth of information on the one side and short measurement duration on the other side. This technique will then be generalized to the Imaging Cross Correlation Frequency Resolved Optical Gating technique (ImXFROG) in Section 3.2, which returns full ST information, with high temporal resolution at the price of extensive measurement times. Section 3.3 is devoted to OXFROG, a low dimensional version of ImXFROG that combines the advantageous properties of iXCorr and ImXFROG but is only applicable to a certain, albeit large class of experiments.

The chapter concludes by giving an outlook on the Analysis by Control (AbC) technique in Section 2.4, that was initially developed to investigate aberrations of the SPS setup discussed in Section 2.2. AbC is a novel approach towards the integration of pulse shaping and analysis into a single step. We envision AbC to allow for rapid prototyping of optical experiments and argue that its potential is just about to unfold.

### 3.1 Imaging Cross Correlator: Getting an Overview

Besides autocorrelation [Wei11] the arguably most basic and also most abundant class of techniques for the analysis of ultrashort pulses are cross correlation (XCorr) techniques. These evolved due to a lack of electronic sampling techniques with sufficient temporal resolution to resolve femtosecond features of optical signals. They are based on the interaction of the pulse to be characterized, called the signal, with a known pulse of similar or shorter duration, called the gate. The gate is delayed with respect to the signal pulse by a variable delay  $t$ . Often the interaction is of a sum-frequency (SF) type and takes place in a  $\chi^{(2)}$ -crystal of appropriate material, orientation, and thickness to guarantee phase matching of signal and gate photons over a sufficient bandwidth. Thus all photons present in the signal are up-converted with similar probability. Under these conditions a slow detector, which detects only the SF photons, records the following signal  $I_{\text{SF}}(t)$ :

$$I_{\text{SF}}(t) \propto \int I_{\text{Sig}}(\tau) I_{\text{Gate}}(\tau - t) d\tau, \quad (8)$$

i.e., the signal is sampled by the gate.

### 3.1 Imaging Cross Correlator: Getting an Overview

In nonlinear optical experiments well-defined gate pulses are often available as the excitation is almost always carried out with short, transform-limited laser pulses. These pulses can be split into multiple beam lines, one of which can bypass the experiment.

Depending on the concrete experimental setting Eq. (8) can be further approximated. If the gate pulse can be approximated by a  $\delta$ -function, i.e., it is extremely short and has a flat phase,  $I_{\text{SF}}(t) \sim I_{\text{Sig}}(t)$  holds and XCorr produces a scaled copy of the signal to be measured. The flatness of the phase is often given for laser pulses, or it can be enforced by pulse compression techniques, as discussed in Section 2.2. However, the signal pulse is often not sort enough for this approximation to hold. In particular in the anomalous dispersion regime [Agr01] pulses tend to contract into solitons [Has73, Mol80], such that the signal often has features that are shorter than the input pulse. In this situation the resulting XCorr still gives a good impression of the overall properties of the signal but all features are averaged over the duration of the gate.

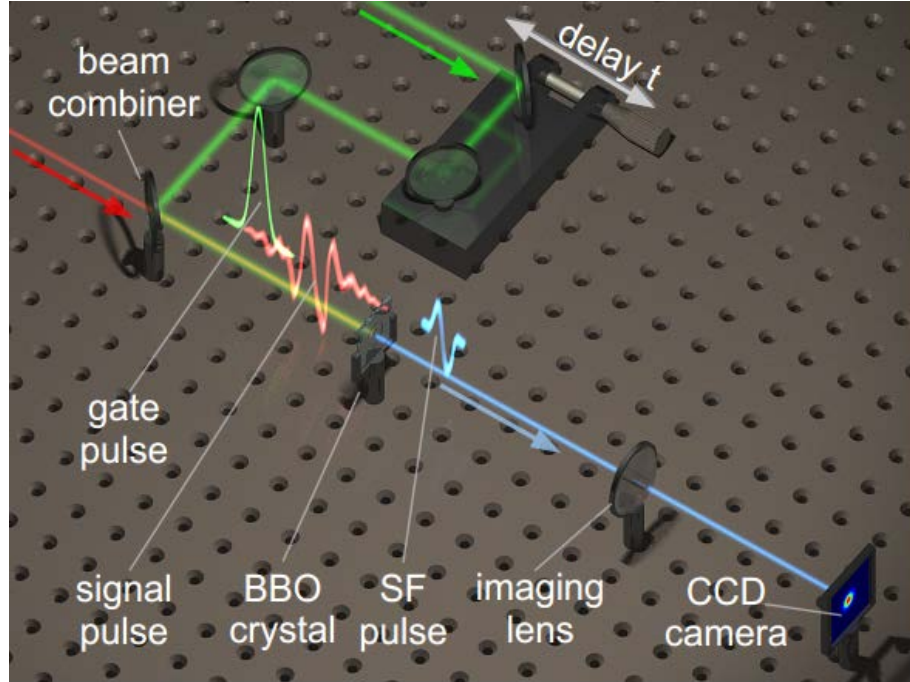


Fig. 9: Schematic representation of iXCorr setup. The reference pulse (green) with delay  $t$  gates an unknown signal pulse (red) generating sum-frequency in a  $\chi^{(2)}$ -crystal (BBO), which is imaged on a camera.

Extension of the technique to ST analysis is fairly straightforward; a scheme of the setup is depicted in Fig. 9. The signal under investigation is imaged onto the spatially extended  $\chi^{(2)}$ -crystal. The gate pulse is transmitted through the nonlinear crystal in a collimated manner. The SF field is then imaged onto a camera, the spatially resolved slow detector. The method is thus named imaging XCorr (iXCorr). The SF field is then defined as

$$I_{\text{SF}}(x, y, t) \propto \int I_{\text{Sig}}(x, y, \tau) I_{\text{Gate}}(\tau - t) d\tau, \quad (9)$$

where we have additionally assumed that the gate pulse has an arbitrarily narrow spatial

### 3. Spatiotemporal Pulse Analysis Techniques

spectrum and that the up-conversion process in the  $\chi^{(2)}$  crystal has a sufficiently broad acceptance angle range to convert all angular components of the signal with equal strength [Min03, Pot04, Min09b]. While the first two requirements can be fulfilled simultaneously with sufficiently enlarged reference pulses, the last can be fulfilled by using a very thin  $\chi^{(2)}$ -crystal.

All experiments discussed in Chapter 5, where iXCorr is employed, make use of the double-beamline facility discussed in Section 2.1. The sum frequency generation is carried out in a 25  $\mu\text{m}$  thin BBO crystal of 5 mm diameter that is cut and oriented for sum-frequency generation of the 800 nm and the 1550 nm beam line under normal incidence. The usage of distinct wavelengths for the process allows us to adjust the setup collinearly, whilst maintaining freedom from background and interference fringes. The resulting SF light's central wavelength is in the range of  $450 \text{ nm} < \lambda_{\text{SF}} < 600 \text{ nm}$ , which is helpful because CCD cameras have their sensitivity maximum in this range. It is also sufficiently well separated from the wavelength of the signal, the gate and their respective higher harmonics, such that they can be easily removed with colored glass filters and thus do not obstruct the measurement of the SF field.

The delay  $t$  is controlled by a pair of mirrors mounted on a linear motion stage, which is scanned over 300  $\mu\text{m}$  in steps of 1  $\mu\text{m}$ . A CCD camera records the SF light, while the stage is scanned at constant speed. Exposure time and scan speed are thus linked. Using this in-motion recording, measurement times are reduced to a minimum, typically in the order of 20 seconds for 300 frames, which mitigates the impact of slow laser power fluctuations. The temporal resolution is  $\delta t = 6.7 \text{ fs}$  resulting in a measurement window of  $\Delta t = 2 \text{ ps}$ . Using a spatial resolution of 1 Megapixel and an imaging depth of 16 bits this equates into a data rate of 250 Mbit/s. This is at the limit of contemporary office type computers' data processing capabilities. Therefore, we do not expect a significant further increase in the measurement speed in the near future, unless sophisticated signal processing platforms are introduced.

The role of reference and signal is interchangeable between the two beam lines. The experiments discussed in Sections 5.2, 5.3, and 5.4 have been carried out with the 1550 nm OPA pulse as the signal and 800 nm CPA as the gate, whereas the situation is vice versa in Section 5.1. We could achieve a resolution of 50 – 70 fs in the experiments discussed in Section 5.2, when no SPS was installed and a less advanced CPA system was used. In the later experiments of Sections 5.3 and 5.4 a resolution of 30 – 40 fs was achieved. Resolutions of less than 20 fs are expected in the future, with the coherent spectral broadening stage introduced in Section 2.2.4. When the 1550 nm is used as the gate a resolution of 50 fs can be achieved.

### 3.2 Imaging Cross Correlating FROG: Seeing Details

If full retrieval of the optical field including the reconstruction of the optical phase and gate deconvolution is necessary, an improvement of iXCorr must be considered. This is particularly true for experiments involving femtosecond dynamics of solitary waves or their ST counterparts, Light Bullets (LBs). In those cases deconvolution and phase retrieval is essential. However, during the last decade a whole “zoo” [Akt10] of ST phase retrieval methods has evolved.

Methods based on interference, such as SEA-TADPOLE [Bow06], STRIPED FISH [Gab04, Gab06], STARFISH [Alo10, Alo12b, Alo12a], and various subwavelength techniques [Eng07, Bal01, Bow08], are very sensitive but require full spectral overlap of the signal and reference, making them incompatible with the above described dual beamline setup.

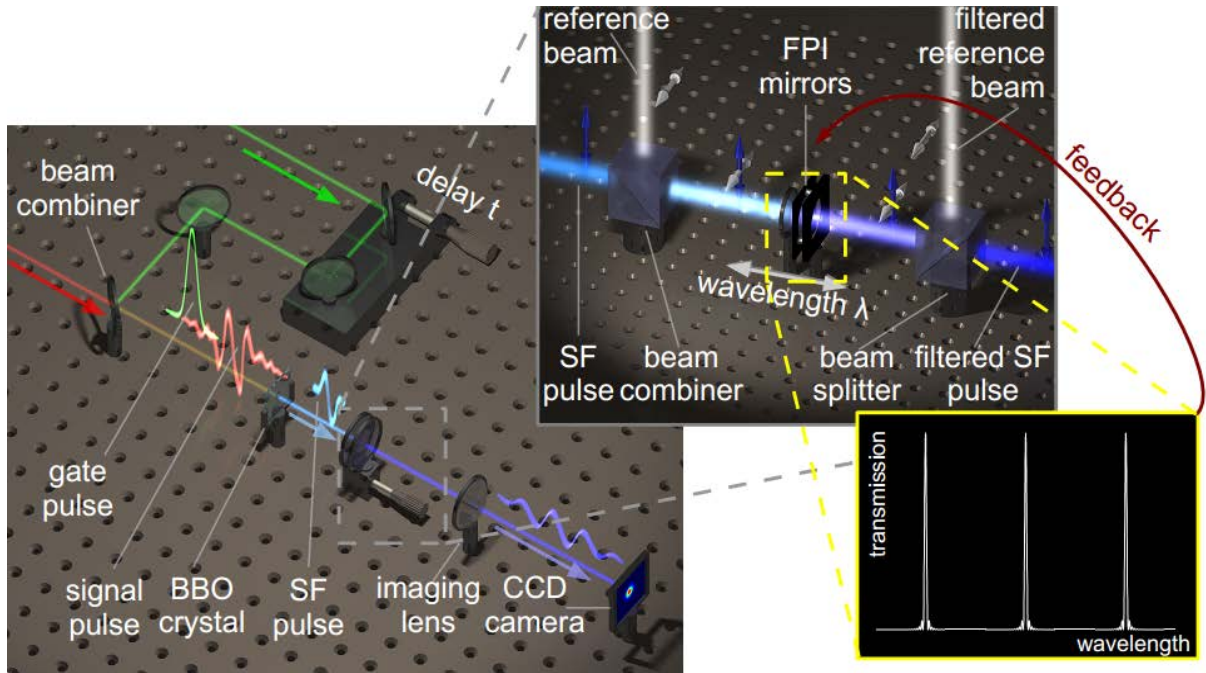


Fig. 10: Schematic representation of ImXFROG setup. The reference pulse (green) with delay  $t$  gates an unknown signal (red) generating sum-frequency in a  $\chi^{(2)}$ -crystal. Only a certain wavelength  $\lambda$  (dark blue) of the sum-frequency pulse (light blue) passes a spectral filter and is imaged on a CCD. The filter (inset) consists of two mirrors forming a tunable Fabry-Perot-Interferometer. Cross-polarized white light and a spectrometer form a feedback loop, tuning mirror parallelity and transmitted wavelength. Figure adapted from [Eil13a].

Methods based on nonlinear interaction are not limited in this way. We therefore focused on the implementations of an ST generalization of a nonlinear temporal phase retrieval technique, such as SPIDER [Iac98], SEA-SPIDER [Kos05], the FROG family [Tre02], or MIIPS [Loz04]. Either of these methods can be used to stitch spectrally resolved spatial phase measurement techniques. There the spatial phase is determined for each wavelength up to an unknown phase, which is then fixed by the above mentioned technique. This strategy was demonstrated by the SHACKLED FROG [Rub09, Bon09] and HAMSTER [Cou12] experiments. Another route towards ST retrieval, pursued in this work, is the spatial multiplexing of temporal phase retrieval

### 3. Spatiotemporal Pulse Analysis Techniques

techniques using some imaging scheme. This route was demonstrated before using spatially resolved shearing interferometry [Dor02b, Dor02a], CROAKS [Bra08], spatial SPIDER [Gal01] and spatial SEA-SPIDER [Wya06]. These techniques are, however, 1D space multiplexed and thus limited to ST pulses with cylindrical symmetry or independent variation along a single transverse dimension.

During the course of this work we developed imaging cross-correlation frequency-resolved optical gating (ImXFROG) [Eil13a]. It is a nonlinear, ultrafast, spatiotemporal pulse-retrieval technique, based on a combination of an imaging cross-correlator [Min10a, Pot04, Min03] with a Cross-Correlation FROG (XFROG) technique [Lin98]. A scheme of the setup is displayed in Fig. 10. It is designed as a plug-and-play upgrade to iXCorr, which allows us to select iXCorr or ImXFROG in a tradeoff between the desired depth of information and measurement time. The idea is as follows: a tunable spectral filter that only transmits a certain wavelength  $\lambda = 2\pi c_{\text{ph}}/\omega$  is placed between the nonlinear crystal and the CCD. Then a cross correlation is recorded for each wavelength, yielding the four dimensional dataset

$$I_{\text{SF}}^{\text{iXFROG}}(x, y, t, \omega) \propto \left| \int A_{\text{Sig}}(\tau, x, y) A_{\text{Gate}}(\tau - t) \exp(-i\omega\tau) d\tau \right|^2, \quad (10)$$

which represents an independent XFROG trace for each position  $(x, y)$ . Each of these traces can be retrieved using a generalized projections technique [Tre02], yielding the sought after complex ST field  $E(x, y, t) \exp(i\tilde{\Phi}(x, y))$  except for an unknown spatial phase  $\tilde{\Phi}(x, y)$ . This unknown phase can be determined at a certain delay  $t = t_{\text{stitch}}$ . It could, e.g. be retrieved in a single separate measurement, using, e.g., a Shack-Hartman sensor [Pla01]. Reconstruction from a second measurement in a different propagation plane in a scheme called phase-diversity [Bow12] has also been demonstrated. Phase-diversity reconstruction is an ST generalization of the classic defocus variation technique [All01] based on the Gerchberg-Saxton approach [Ger72]. Any other digital holography technique, e.g. techniques based on shadowgraphy [Eil12] or the solution of the transport of intensity equation [Tea82] could be used, too. Implementation into ImXFROG will remain subject for future work.

At the heart of ImXFROG is the tunable spectral filter. Its properties, i.e., its spectral resolution  $\delta\lambda$  and the free spectral range (FSR)  $\Delta\lambda$ , are determined by the desired length of the measurement window  $\Delta t$  and the temporal resolution  $\delta t$ :

$$\begin{aligned} \delta t &\approx \frac{\lambda_{\text{SF}}^2}{c\Delta\lambda} \\ \Delta t &= \frac{\Delta\lambda}{\delta\lambda} \delta t \end{aligned} \quad (11)$$

### 3.2 Imaging Cross Correlating FROG: Seeing Details

where  $\lambda_{\text{SF}} = 527 \text{ nm}$  is the average SF wavelength. ImXFROG was designed to analyze wavepackets that emerge from ST, nonlinear experiments in fiber arrays. The resolution  $\delta t$  must therefore be selected to be smaller than the characteristic pulse duration  $t_0$ . The meaning of  $t_0$  will be discussed in Chapter 4, however for the samples used in this thesis the minimal value is  $t_0 = 18 \text{ fs}$ , as stated in Tab. 1 on page 45. Therefore  $\delta t = 9 \text{ fs}$  was chosen. A measurement window of  $\Delta t = 900 \text{ fs}$  was selected, because simulations, such as those that will be presented in Chapter 5, suggest that ST wavepackets emerging from experiments in fiber arrays typically span over a few hundred femtoseconds.

These requirements equate into a filter resolution of  $\delta\lambda = 1 \text{ nm}$ , and an FSR of  $\Delta\lambda = 100 \text{ nm}$ , yielding a finesse of  $F^* = \Delta\lambda/\delta\lambda = 100$ , leading to a measurement window of  $1300 \text{ nm} < \lambda_{\text{Sig}} < 2400 \text{ nm}$ . The temporal resolution is as short as two optical cycles, if the  $800 \text{ nm}$  beam line is used as the gate function. The number of independently measurable points, termed temporal degrees of freedom  $\text{DoF}_t = F^* = 100$  might seem moderate at first, however one has to keep in mind that ImXFROG reconstructs one temporal trace for each spatial pixel. Therefore the total number of degrees of freedom  $\text{DoF} = \text{DoF}_x \text{ DoF}_y \text{ DoF}_t$ , where  $\text{DoF}_{x/y}$  are the number of degrees of freedom per spatial dimension, is very high. The introduction of a spatial resolution imposes further restraints on the spectral filter, namely that it must have a diameter and angular acceptance range that is compatible with the sought after spatial resolution.

The spectral filter with the desired parameters was implemented using a combination of  $10 \text{ nm}$  commercial interference filters ranging from  $500 \text{ nm}$  to  $600 \text{ nm}$  and a tunable Fabry-Perot-Interferometer (FPI), constructed from two parallel mirrors with  $85\%$  reflectivity over the same spectral range, giving a finesse of  $F_{\text{FPI}}^* = \Delta\lambda/\delta\lambda = 20$ . The FPI is operated in the  $25^{\text{th}}$  order, corresponding to a mirror separation of  $7 \mu\text{m}$ . This leads to a spectral resolution of  $\delta\lambda = 1 \text{ nm}$  and a FSR  $\Delta\lambda_{\text{FPI}} = 20 \text{ nm}$ . This combination of interference filters and an FPI reaches the total spectral resolution, FSR, and finesse as stated above. The mirrors are mounted on a one piece mount to mitigate effects from vibration and temperature variation. One end mirror is installed on a three-axis piezo-mount. Feedback is supplied by monitoring the transmission of cross-polarized white light through the FPI, with the help of a spectrometer. Piston motion is then used to set the transmitted wavelength, whereas pitch and roll are continuously adjusted to guarantee maximum mirror parallelity and thus contrast in the transmitted spectrum.

The accepted half-angle is approximated as an angle  $\theta$  under which the transmitted wavelength shifts by  $\delta\lambda/2$  and equates to  $\theta = (2F_{\text{FPI}}^*)^{-1/2} \approx 1.8 \text{ deg}$ . This angle is related to a cut-off in the angular spectrum of  $\Delta k \approx 2\pi\theta/\lambda_{\text{SF}}$ . The finite diameter  $D = 5 \text{ mm}$  imposed by mechanical

### 3. Spatiotemporal Pulse Analysis Techniques

constraints of the setup gives a lower boundary on the angular resolution  $\delta k = 2\pi/D$ , such that the spatial DoF<sub>x</sub> and the total number of independent points DoF are given by:

$$\text{DoF}_{x/y} = \frac{D}{\lambda_{\text{SF}}} \sqrt{\frac{2}{F_{\text{FPI}}^*}} \approx 300 \quad \text{DoF} = \text{DoF}_t \text{DoF}_x \text{DoF}_y = \left(\frac{D}{\lambda}\right)^2 \frac{2F^*}{F_{\text{FPI}}^*} \approx 10^7. \quad (12)$$

This should be put into perspective with other ST retrieval techniques, however few such numbers have been reported in the literature, so far. The authors of STRIPED FISH [Gab06] reported  $\text{DoF} = 10^5$ , which means that ImXFROG is a method that is suitable to resolve particularly complex ST pulses at the price of long measurement times.

Eq. (12) is also interesting from a fundamental point of view. As  $F^*/F_{\text{FPI}}^*$  is just a little larger than unity we can approximate  $\text{DoF} \approx 2(D/\lambda)^2$ . This means that the DoF is not influenced by the specific design of the spectral filter. The spectral filter just transfers spatial degrees of freedom into temporal ones. While this result has been obtained for the specific design described above, we would like to note that [Gab06] reported a similar finding, without discussing it further. We therefore would like to hypothesize that this is a fundamental limit of ST retrieval techniques.

ImXFROG's capability to retrieve and resolve ultrashort events is demonstrated in Section 5.2 in the context of LBs. Here we focus on demonstrating ImXFROG's ability to reconstruct ultra-complex ST fields. We have therefore analyzed a spatiotemporal Airy pulse. The pulse has a transform limited minimum duration of 30 fs, upon which we impose a third order chirp (TOC) of  $27 \cdot 10^3 \text{fs}^3$ , using the SPS setup discussed in Section 2.2 but without the aberration mitigation scheme discussed in Section 2.2.3. The pulse thus has a high degree of imaging aberrations introduced and also undergoes nonlinear reshaping.

Experimental results are displayed in Fig. 11. Fig. 11(a) shows an isointensity map of the ST pulse. The pulse-front with the trailing ripples that are characteristic for Airy pulses, are both immediately visible. Although the ripples are less than 25 fs short and thus shorter than the gate pulse they are fully resolved. Fig. 11(b) shows the locally resolved level of TOC. A considerable variation of the TOC over the pulse cross section is visible. In particular the TOC at the spatial boundary of the pulse is smaller than in the center. Its mean value is  $20 \pm 5 \cdot 10^3 \text{fs}^3$ . We attribute this deviation to some undetected initial TOC of  $-7 \pm 5 \cdot 10^3 \text{fs}^3$ .

Fig. 11(c)-Fig. 11(e) give a good understanding of the spatiotemporal distortions the pulse suffers in the non-optimized SPS setup. The pulse is considerably smaller in x-direction, than in y-direction, with some level of redshift in the center of the pulse, as displayed in Fig. 11(c). The center of the pulse precedes the pulse fringes, as seen in Fig. 11(d). We attribute this pulse front

bending to the greater bandwidth at the center seen in Fig. 11(e) and the interaction of the spectrum with TOC.

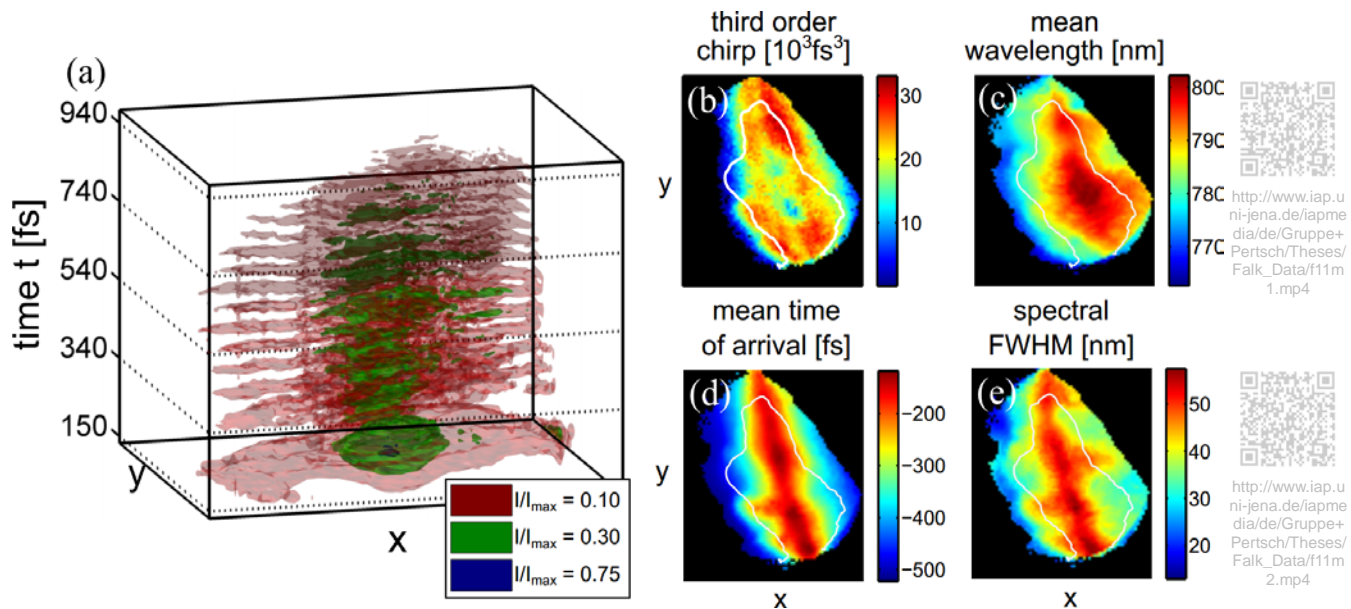


Fig. 11: ImXFROG reconstruction of an Airy pulse with spatiotemporal distortions. (a) Spatiotemporal isointensity plot. (b) Local third order chirp. (c) Local mean wavelength. (d) Local mean time of arrival. (e) Local width of the spectrum. (b-e) The white outlines mark the region containing 90% of the pulse energy; Black regions denote areas with insufficient power for pulse retrieval. Figure adapted from [Eil13a].

While this clearly demonstrates the capabilities of ImXFROG we must note at this point that this method is extremely demanding in terms of the experimental prerequisites and infrastructure. Measurement times are currently in the order of two hours; with a potential reduction to 30-60 minutes. During this time roughly 10 gigabytes of data are generated that need about 2 to 6 hours of data processing for the FROG reconstruction; reduction potential here is larger: using improved algorithms, GPU computing and parallelization we expect this number to drop below thirty minutes. Given that this potential is fully harnessed ImXFROG will become much more usable in the future but will remain an expert tool for in-depth studies of details of ST processes. For quick overviews or continuous monitoring iXCorr will remain the method of choice; however switching between the two modes of operation is as simple as removing the FPI mirrors from the setup and resetting the command and control software.

In summary in this section we have demonstrated ImXFROG, a technique that is able to fully reconstruct ST fields, except for an unknown spatial phase, which can be found in a reference experiment. ImXFROG is able to resolve few-cycle pulse features and is among all nonlinear phase retrieval methods the one which can reconstruct ST fields with the largest complexity, i.e., it has the highest published value for  $\text{DoF} = 10^7$ . It is based on a plug-and-play extension of the iXCorr technique, which is particularly handy for the experimentalist, as it makes switching between a “quick-and-dirty” and a “slow-and-in-depth” ST retrieval technique possible within

### 3. Spatiotemporal Pulse Analysis Techniques

minutes.

#### 3.3 1D Imaging Cross Correlating FROG: Fast and Accurate

With the demonstration of the ImXFROG technique in the last section there is, at least in the framework of this thesis, no need to develop ST retrieval techniques any further, as we now can retrieve the complete information from an ST pulse. In many situations, however, the system under investigation contains symmetries, which make complete analysis techniques highly redundant. Among the most prominent are systems with cylindrical symmetry, which often emerge from ST experiments in homogeneous media, and 1D systems, such as slab WGs and WAs. These systems only have a single transverse spatial dimension, e.g., the position in the 1D case and the radial coordinate for the cylindrical case, as discussed in Section 3.2. This coordinate is referred to as  $x$ .

The absence of a 2<sup>nd</sup> transverse spatial coordinate opens the possibility to use the 2<sup>nd</sup> dimension of the camera for the recording of the spectrum, eliminating the need for an external wavelength filter and time-consuming, independent scanning of the delay and wavelength axes. This facilitates a device that, by sacrificing the 2<sup>nd</sup> spatial dimension, allows FROG reconstruction of a 1D-ST signal at the speed of an iXCorr measurement. This device, called fast One dimensional imaging Cross-correlating FROG (OXFROG), was developed during this thesis and has successfully undergone characterization and first trials.

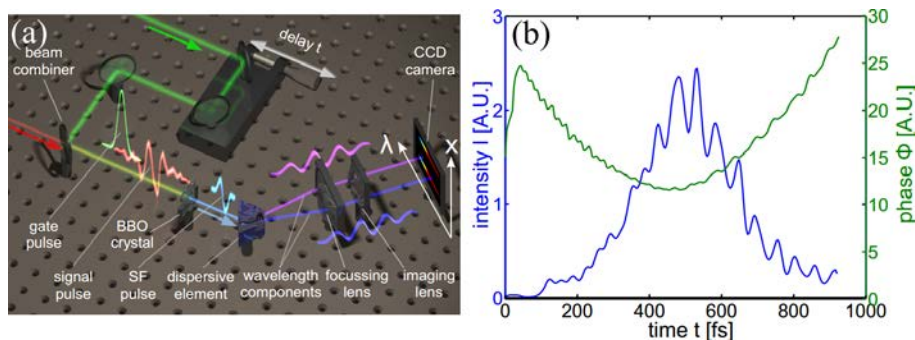


Fig. 12: (a) Schematic representation of the OXFROG setup. The reference pulse (green) with delay  $t$  gates an unknown signal (red) generating SF in a  $\chi^{(2)}$ -crystal. The SF pulse is dispersed along the horizontal axis. A horizontal, cylindrical, focusing lens images the spectrum on a CCD. A vertically curved cylindrical lens images the field on the vertical direction on the CCD, yielding spatial information. (b) Example of a pulse, which was retrieved at one given point in space, using the OXFROG technique. (blue) Instantaneous pulse power. (green) Retrieved pulse phase. The pulse FWHM duration is 284 fs with a chirp of  $13 \cdot 10^3 \text{ fs}^2$ .

After removing the FPI from the ImXFROG we had to redesign the imaging setup between the  $\chi^{(2)}$ -crystal and the CCD. Along the  $x$ -axis we are imaging onto the CCD with a cylindrical lens of  $f = 100 \text{ mm}$  with a 1:1 imaging arrangement. Along the  $y$ -axis an  $f = 150 \text{ mm}$  cylindrical collimator lens routes the light through a transmission grating with 150 lines/mm in a Littrow

setup. A focusing lens with  $f = 60$  mm in a  $2f$  setup then images the spectrum onto the CCD. The device was simulated in an optical design software prior to implementation, ensuring that the relatively simple arrangement achieves transform limited performance over the full SF spectral range of  $500 \text{ nm} < \lambda < 600 \text{ nm}$ . The optical system was built on a custom, one-piece mount, reducing adjustment degrees of freedom to a minimum. The system's dispersion was then calibrated with a collimated Xenon light source; resolution was tested with a laser source to be  $\delta\lambda = 0.35 \text{ nm}$ , which is within 10% of the transform limit and three times better than the design value for the minimum spectral resolution of the FROG scheme, discussed in Eq. (11).

A proof of principle demonstration of the OXFROG setup was done with the 1550 nm pulse as the gate and a chirped 800 nm pulse as the unknown signal. Data analysis was carried out only in one selected point in space. Results are displayed in Fig. 12(b). The measured FWHM of the signal was 284 fs, with a chirp of  $13 \cdot 10^3 \text{ fs}^2$ , which equates into an FWHM of just below 40 fs, consistent with previously determined values for the laser. The measurement took less than 20 s.

After this demonstration the OXFROG setup is scheduled to be used for the ST analysis nonlinear pulse propagation in 1D waveguide arrays (WAs) [Nol03]. Nonlinear experiments in these arrays are routinely carried out but experimental ST analysis lags behind. Analytic description on the other hand often ignores the temporal degrees of freedom altogether [Chr03, Led08, Kar11]. We therefore aim to develop OXFROG into the new “gold standard” for ST analysis of WAs.

### 3.4 Outlook: Analysis by Control

Up to now we have followed the established approach, which clearly separates the “realms” of ST pulse generation and ST analysis. In this section, however, we would like to lift this separation and show that in many situations careful mixing of the two seemingly distinct parts of the experiment can be helpful. We therefore term the concept Analysis-by-Control (AbC).

The idea is based on the assumption that the action of each stage in a (linear, time invariant) optical experiment, can be described by a filter function [Phi95] according to the definition of Eq. (7). Thus

$$E_{\text{end}}(k_x, k_y, \omega) = \prod_m A_m(k_x, k_y, \omega) \cdot B(k_x, k_y, \omega) \cdot \prod_m S_m(k_x, k_y, \omega) \cdot E^{(0)}(k_x, k_y, \omega), \quad (13)$$

where  $S_m$  describes the effect of the various pulse shaping stages,  $B$  of the experiment itself, and  $A_m$  of the pulse analysis devices. Because the product operation is commutative it does not matter in which order the operation is carried out; i.e., how the experiment is laid out [Phi95]. To give an example: it does not matter if a pulse is delayed before or after an experiment, nor does it

### 3. Spatiotemporal Pulse Analysis Techniques

matter if a delayed copy of a pulse for the purpose of autocorrelation is created before or after the experiment. One can therefore cumulate all (or at least many) optical elements of the experiment into a single filter  $F = \prod S_m \cdot \prod A_m$

$$E_{\text{end}}(k_x, k_y, \omega) = B(k_x, k_y, \omega) \cdot F(k_x, k_y, \omega) \cdot E^{(0)}(k_x, k_y, \omega). \quad (14)$$

Of course this is only possible for linear experiments; nonlinear ST experiments thwart this scheme, as Eq. (13) is not valid there.

In our case the only device which is flexible enough to cumulate arbitrary optical elements and is thus truly suitable for AbC is the SPS, which is originally a pulse control element and can now be used for analysis, too. To put matters into perspective: AbC is by no means a replacement for existing ST analysis techniques, such as those presented above. Its strength lies in the flexibility to mimic setups by simply applying the appropriate phase/amplitude function onto the SPS, without the need to physically build the setup.

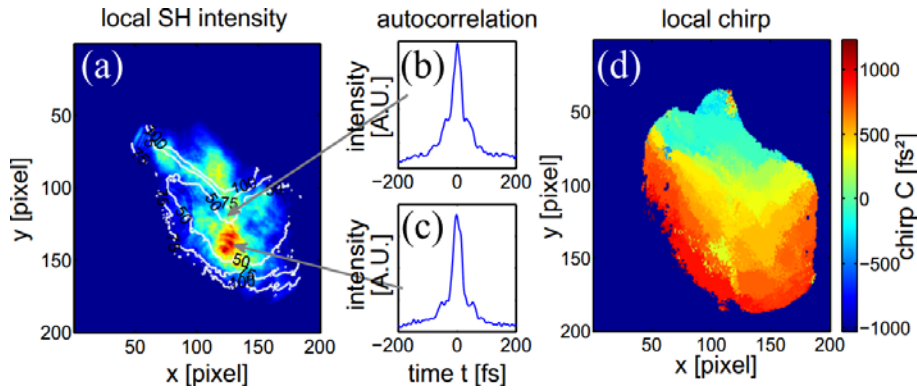


Fig. 13: Analysis of an ST pulse using the AbC scheme. (a-c) The SPS was programmed to mimic a pulse copy & delay line. A  $\chi^{(2)}$ -crystal and a CCD camera were then used to record the spatially resolved second harmonic autocorrelation. (a) Spatially resolved second harmonic intensity with (white lines) lines of equal autocorrelation FWHM duration superimposed. (b,c) Autocorrelations recorded by the AbC scheme for the points denoted with the arrow. (d) Locally resolved pulse chirp.

For example the SPS can be used to mimic a Michelson interferometer type pulse “copy & delay” stage, by applying the filter  $F(\omega) = \frac{1}{2} \cos(t\omega)$ . Building an autocorrelator is then as simple as placing an appropriate  $\chi^{(2)}$ -crystal and an SH detector in the beam path and varying the delay  $t$ . This setup was in fact used to characterize imaging aberrations of the original, non-optimized SPS setup. Some results are shown in Fig. 13(a-c).

In another example AbC was used to measure the locally resolved chirp, the results of which are displayed in Fig. 13(d). Here the same setup was used but a variable chirp  $C$  was applied according to  $F(\omega) = \exp(i/2 C \omega^2)$ . Then for each camera pixel chirp  $C_{\text{max}}$ , which generates maximum second harmonic was recorded. The initial local chirp is then simply  $-C_{\text{max}}$ . A result is displayed in Fig. 13(a-d), which shows that the pulse has a chirp that varies considerably over

its cross section.

Setting up these two experiments did not take much longer than programming the SPS and yet proved crucial in characterizing and optimizing the ST properties of the SPS setup. Given the ease, with which these results have been obtained, it seems that AbC is a technique that readily lends itself for rapid prototyping, testing, and characterization of experiments. During the course of this thesis we demonstrated that AbC has the potential to change the way in which experiments are developed; reducing development time and space requirement, while increasing accuracy and reproducibility. In the current stage of development using SPS only the temporal part of the AbC scheme, presented in Eq. (14), is implemented. Future combination with complete ST shaping techniques, as presented in Section 2.4, will harness the power of the AbC approach to the fullest.

## 4. Ultrafast Discrete Optics: Samples, Scales & Models

This chapter will introduce the class of samples used in this thesis and the physical effects to be expected when ultrafast, high-power ST pulses propagate through them. As such it complements the last two chapters in the quest for the observation of discrete Light Bullets. It focuses on the optical environments in which Light Bullets can be observed and the physical effects they are subject to. It derives typical properties of the Light Bullets, and introduces two complementary models, which can be used for the qualitative understanding of Light Bullets and their dynamic mechanisms and for quantitative prediction of the state and evolution of the optical field inside the samples used in the experiment.

A brief overview over the development of the field of nonlinear optics in discrete media in general and its role in the hunt for the Light Bullets in particular is given in Section 4.1. Then the canonical model of ST discrete optics (DO), the discrete-continuous Schrödinger equation, will be introduced in Section 4.2 and its usefulness in terms of predicting experiments will be critically examined. We will then argue that it is useful in a qualitative sense, as it is a minimal model that captures the basic principles of ST DO. Its results will be applied on experimental samples introduced Section 4.3, yielding typical temporal, spatial, and energetic scales, on which Light Bullets can be observed.

Following these predictions we will argue that the canonical model ignores a range of high order perturbations, which do not alter the characteristics of the system altogether, but drastically modify its quantitative behavior. Thus a complete model will be introduced in Section 4.4, which captures all physical effects that have a considerable impact on ST DO. This model has quantitative predicting power and will later be used extensively to verify experimental findings. The chapter is concluded by Section 4.5, which reviews all classes of physical effects, that are expected to occur during the excitation and propagation of LBs and their relative impact in various stages of the experiment.

### **4.1 *Nonlinear, Spatiotemporal, Discrete Optics: a Brief Introduction***

The experiments discussed here are carried out in DO environments, a special subclass of photonic crystals (PCs). DO environments are characterized by a periodic modulation of the refractive index  $n(x)$  in a direction transverse to the main direction of propagation. The index along the direction of propagation  $z$  is mostly homogeneous, although deviations from this part of the definition are possible. They come in 1D or (2D) versions, depending on if the periodicity stretches along both transverse directions  $x$  and  $y$ , or not. Waves in 1D DO systems are

prototypically assumed to be confined along the other transverse direction by some guiding mechanism (e.g. slab-waveguiding in the  $y$ -direction). Moreover, DO systems differ from generic PCs in that each unit cell can be considered a single- or few- [Set10, Set11c] mode WG. The impact of all other unit cells is then limited to a perturbative modification of the mode amplitude dynamics  $A_{nm}(z)$  of the WG with the 2D index  $nm$  by the nearest neighbors only. This approach is referred to as tight-binding-approximation [Kos54]. The leading term of the perturbation series is a resonant coupling term, such that DO systems can be thought of as infinite (or at least large) 1D or 2D arrays of WG couplers [Jon65]. They are hence called waveguide arrays (WA).

The linear propagation equation in frequency domain then reads:

$$\begin{aligned}
 i \frac{d}{dz} A_{nm}(z, \omega) &= \beta(\omega) A_{nm}(z, \omega) \\
 &+ c^{(1)}(\omega) [A_{n+1m}(z, \omega) + A_{n-1m}(z, \omega)] + c^{(2)}(\omega) [A_{nm+1}(z, \omega) + A_{nm-1}(z, \omega)] \\
 &+ c^{(3)}(\omega) [A_{n+1m+1}(z, \omega) + A_{n-1m-1}(z, \omega)] + c^{(4)}(\omega) [A_{n+1m-1}(z, \omega) + A_{n-1m+1}(z, \omega)],
 \end{aligned} \tag{15}$$

where  $\beta$  is the wavenumber of the isolated WG mode [Agr01],  $\omega = 2\pi c_{\text{ph}}/\lambda$  is the angular frequency of light with the vacuum wavelength  $\lambda$  and  $c_{\text{ph}}$  is the vacuum speed of light. The coupling constants  $c^{(l)}$  are calculated by an overlap integral of the modal field of a WG, with the refractive index change of the respective nearest neighbor [Sny83]. Their relations depend on the geometry of the array [Sza06a]. One dimensional arrays, displayed in Fig. 14(a), have  $c^{(2)} = c^{(3)} = c^{(4)} = 0$  and the  $m$  index is consequently ignored. Rectangular arrays, displayed in Fig. 14(b), have  $c^{(1)} = c^{(2)} \gg c^{(3)} = c^{(4)}$ , where  $c^{(1)}$  models straight connections to the nearest neighbors and  $c^{(3)}$  models diagonal connections to next-to-nearest neighbors. Hexagonal arrays, displayed in Fig. 14(c), have  $c^{(1)} = c^{(2)} = c^{(3)}$  and  $c^{(4)} = 0$ . If a single coefficient is sufficient to describe the system, as is the case for 1D and hexagonal arrays, it is just called  $c$ .

Equation (15) can be simplified if the slowly varying envelope approximation (SVEA) is adopted, chromatic variation of the coupling constants is neglected, a co-moving reference frame is introduced, and the wavenumber is expanded into a truncated Taylor series  $\beta(\omega) \approx \beta_0 + \beta_1(\omega - \omega_0) + \beta_2/2 (\omega - \omega_0)^2$ , such that:

$$\begin{aligned}
 i \frac{\partial}{\partial z} A_{nm}(z, t) &= -\frac{\beta_2}{2} \frac{\partial^2}{\partial t^2} A_{nm}(z, t) \\
 &+ c [A_{n+1m}(z, t) + A_{n-1m}(z, t) + A_{nm+1}(z, t) + A_{nm-1}(z, t) + A_{n+1m+1}(z, t) + A_{n-1m-1}(z, t)],
 \end{aligned} \tag{16}$$

where we have, without loss of generality, adopted the notation for a hexagonal array as this

#### 4. Ultrafast Discrete Optics: Samples, Scales & Models

geometry is the one that is most used in this thesis.

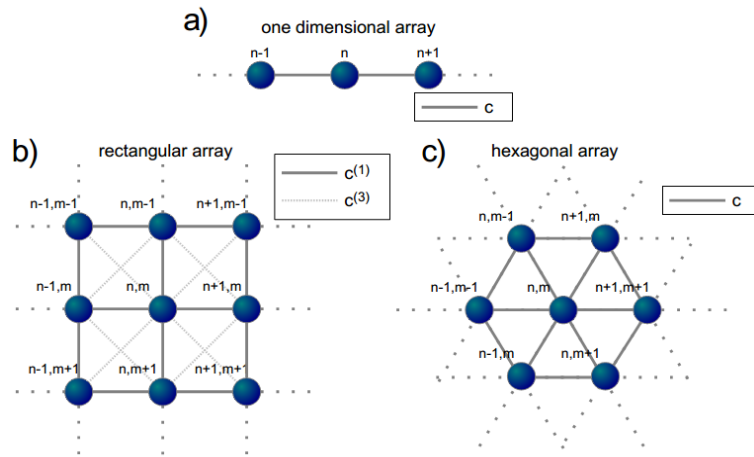


Fig. 14: Transverse layout and coupling geometries of several WA classes. (a) A 1D WA. (b) A 2D rectangular WA with nearest-neighbor and next-to-nearest-neighbor coupling. (c) A 2D hexagonal WA. Dotted lines denote continuation of the array.

Historically DO was first discussed in the context of continuous waves, i.e., in Eq. (16) with  $\beta_2 = 0$ . Then DO is a matter of spatially coupled wave propagation. The dispersion relation (DR) of the discrete coupling operator is  $\Delta\beta = 2c(\cos(\nu) + \cos(\mu) + \cos(\nu + \mu))$ , where  $\nu$  and  $\mu$  are the normalized transverse wavevector components (i.e. the Bloch-momenta) and  $\Delta\beta$  is the wavenumber shift induced by the WA. If compared with the (paraxial) free space DR one finds that in the center of the Brillouin zone the DO DR can be fitted to the free space DR. The discrete coupling process is therefore called discrete diffraction. As opposed to free space the DO DR also exhibits pronounced minima at its corners, corresponding to anomalous diffraction. Discrete diffraction can therefore mimic normal and anomalous diffraction (and everything in between), depending on the transverse wavevector, which can be tuned by varying the excitation angle [Per02]. Careful modification of transverse and/or longitudinal structures and symmetries of the system has led to the demonstration of a plethora of effects, many of which have originally been predicted and described for other discrete systems. A full account [Sza10] of these is beyond the scope of this thesis. Nevertheless, we like to mention a few results, e.g., the demonstration of Bloch Oscillations and Zener tunneling [Blo29, Zen34, Pes98, Mor99a, Per99, Tro06], Anderson localization [And58, Per04a, Sch07, Lah08, Jov11b, Jov11a, Jov12b, Jov12c, Jov12a], dynamic localization [Dun86, Lon06, Sza09],  $\mathcal{PT}$ -symmetries [Ben98, EG07, Mak08, Rüt10, Mak10, Suk10, Sza11, Jov12c], topological insulation [Kan05, Zha05, Rec13], and pseudo-magnetic optics [Rec12].

In this thesis we are interested in nonlinear optics in WAs [Chr03, Led08, Kar11]. We focus on the regime of weak nonlinearity, where the impact of the nonlinearity is assumed to be sufficiently weak that it can be considered as a perturbation of the evolution equation Eq. (16)

and then reads:

$$i \frac{\partial}{\partial z} A_{nm}(z, t) = \mathcal{L} \circ A_{nm}(z, t) + \mathcal{N}[A_{nm}(z, t)], \quad (17)$$

where the linear operator  $\mathcal{L}$  is the right hand side of Eq. (16) or any linear modification thereof.  $\mathcal{N}$  is the nonlinear perturbation. Note that “weak” means weak if compared with the waveguiding, i.e., it can still be strong, if compared with discrete diffraction. Effects based on strong nonlinearities such as wave collapse phenomena [Akh68, She76, Ber98, Sku04, Eil10], triggered by the instability of the Townes soliton [Chi64] are therefore ignored in this thesis. Depending on the host material and experimental configuration,  $\mathcal{N}$  can describe virtually any nonlinear interaction [But90, Boy03], such as, parametric interactions, nonlinear absorption, and resonant nonlinearities. Here we focus on effects that arise from the  $\chi^{(3)}$  interaction or, more specifically, the Kerr-effect, together with leading higher order perturbations, such as the stimulated Raman response and self-steepening effects [Agr01].

WAs in  $\chi^{(3)}$  media, i.e. those with Kerr nonlinearity, are particularly interesting in the context of discrete [Led08, Kar11] optical solitons [Abl91, Kiv03]. Here the existence of certain classes of solitons is linked to the combination of the type of nonlinearity (e.g. focusing or defocussing) and the shape of the dispersion relation, i.e., sign of diffraction. While the type of nonlinearity is fixed for many experimental environments, WAs offer the freedom to select a type of diffraction and thus offer ideal conditions to observe rich soliton dynamics. In fact discrete solitons [Eis02, Pes02, Led02, Led08, Kar11] in 1D WAs were first predicted by Christodoulides and Aceves [Chr88] and observed by Eisenberg et al. [Eis98]. Later experiments demonstrated discrete solitons in cascaded  $\chi^{(2)}$ -WAs [Iwa04]. The interchangeable diffraction sign also allows to observe dark discrete solitons [Kiv94a, Kob98, Mor01]. More elaborated schemes investigated, e.g., discrete vector solitons [Dar98, Mei03, Mei05a] or the discrete counterpart of gap solitons [Che87, Egg96, Mil87], by either exploiting the gap between coupled fundamental modes and coupled high order modes or by inducing a gap by inscribing a pairwise alternating lattice [Kiv93a, Suk02, Suk03b, Des03, Mor04, Man04a, Che05, Ros06].

Discrete solitons are themselves subject to modulational instability [Kiv92, Dar97, Mei04a, Bel04]. Because of their discrete nature, discrete solitons are really “just” solitary waves as they lack a sufficient number of conserved quantities. This has two interesting consequences. Their transverse motion is affected by the Peierls-Nabarro potential [Kiv93b, Ace94, Mor99b] and their coherent interaction dynamics is very rich [Ace96, Kr696, Mei04b, Mei05b]. The discrete soliton may also be used as a “blocker” to transiently reflect a probe beam via incoherent

#### 4. Ultrafast Discrete Optics: Samples, Scales & Models

interaction, which was discussed in the context of all-optical switching [Chr01, Eug01, Mei04b, Mei05c, Mei05b]. The interaction of a discrete soliton with a perturbation in the array is also of interest [Pes99].

Two-dimensional discrete solitons, which are stable against perturbation, as opposed to their continuous counterparts [Chi64], were predicted [Efr02, Efr03] and experimentally observed in photo-induced WAs [Fle03b, Fle03a, Nes03], laser written WAs [Per04b, Sza06b], and fluid filled photonic crystal fibers [Vie12].

The stability of 2D discrete solitons extends to systems with reduced symmetry [Fre06, Fis06, Fre07]. Symmetry reduction can also be of geometric origin, i.e., inscribed in the properties of the DO environment, as is the case for surface solitons [Mak05, Mak06, Sun06, Wan07, Sza07b, Sun07, Hei09a] or it can be generated by non-symmetric excitation, e.g., in the case for vortex solitons [Fir97, DT00, Mal01, Nes04, Man04b, Des05a, Des05b, Bar05, Ter08, Ter09, Ter10].

ST optics in DO systems can be viewed, to some extent, as a straightforward generalization of purely spatial DO. A driving force behind the development of this branch of photonics was the seminal work [Sil90] by Silberberg, who pointed out, that solitary waves in homogeneous Kerr media are always unstable, if they have more than a single transverse dimension. He also coined the term Light Bullet for a ST field, in which the nonlinearity simultaneously balances dispersion and diffraction in both spatial dimensions. Discrete Light Bullets (LBs) do not suffer from this instability [Ace93, Tur93, Kiv94b, Led94, Mih04]. They inherit a sufficient amount of stability from their above discussed spatial cousins to have an appreciable parameter range in which they are linearly stable. The parameter range is, however, bounded: low intensity solutions with large diameters, i.e. those which extend over many WG of the WA, tend to behave like their instable, homogeneous cousins, whereas high intensity solutions eventually leave the weak nonlinearity regime and behave like homogeneous LBs, too [Eil10]. Similar results have been predicted for Bessel lattices [Mih05, Zho10], suggesting that a complete two-dimensional patterning of the waveguide array might not be needed altogether to get stable LBs.

Stable, discrete Light Bullets have also been predicted in Bragg grating WAs [Suk06], in arrays of helical WGs [Mat10], longitudinally modulated honeycomb WAs [Lob10], and at the edge [Mih07c, Mih07b] and interface [Mih07a] of WAs.

Of course this is not only one method proposed to stabilize Light Bullets. Other strategies rely on unmodifiable intrinsic material properties, such as higher order dispersion [Fib04] and plasma effects [Ber98, Ber08], whereas the periodic modification of the refractive index is a property of the sample and can be modified to suit desired experimental parameters. Additional approaches

are currently unfeasible in an experiment, because they require the modulation of the nonlinear response [Tow02, Adh04, Tor09, Ye09], diffraction strength [Zho11], or the longitudinal modification of the WA [Bai03, Mih05, Bel08]. Other approaches weaken the concept of self-confinement, such as LBs and LB trains based on non-instantaneous [Bur09, Gur09], saturable [Ska97], resonant [Leb10], or bi-valued [Edm92] nonlinearities. Spatiotemporal spin wave packets [Bau98, Büt00] experience linear loss, such that their collapse is arrested. So-called linear LBs [VL09, Cho10, Abd10, Pik12] are infinitely extended solutions of the linear Helmholtz equations and just preserve their intensity, not their phase. Their stationarity is also not based on a nonlinear effect.

Experimental demonstration of any of these concepts lagged behind theoretical works [Wis02] in a considerable manner, prior to our work. Advances towards the observation of LBs had been made in  $\chi^{(2)}$ -media. These are of interest because  $\chi^{(2)}$ -nonlinearities can mimic the intensity-dependent phase shift, which is at the heart of the Kerr effect, via slight mismatch cascading [Ost67, DeS92, Ste96, Bur02]. In  $\chi^{(2)}$ -media LBs with two active spatial dimensions have been predicted to be stable [Skr98, Mih99, Pan05, Xu07] as opposed to those with orbital angular momentum [Mih00]. These LBs, however, require very particular properties for the fundamental and second harmonic waves and their mutual dispersive properties and have so far not been observed experimentally. However, two-color spatiotemporal solitons [Liu99, Bur02] had been observed with tilted pulses [Mar89, DT98]. Pulse tilting was required for group velocity matching of nonlinearly coupled harmonics, inducing a high level of effective anomalous dispersion, limiting this approach to a single transverse dimension. The tilted pulse technique can be generalized to another class of spatiotemporal, stationary wavepackets with two transverse dimensions, so-called X-waves. X-waves feature an angularly dispersed spatiotemporal spectrum with axial symmetry. X-waves can be spontaneously generated in  $\chi^{(2)}$ -systems [DT03, Tru04], or homogeneous [Cou03, Fac05], as well as, discrete [Con03, Kol04b, Dro05, Lah07, Jia07, Hei09b]  $\chi^{(3)}$ -media. They are, however, weakly localized and theoretically of infinite energy. Other attempts at observing LBs, even in systems with lower dimension, presumably failed due to a lack of advanced analysis techniques [Eis01, Che03] or due to an excessive amount of spurious perturbative effects [Bab07, Ben08, Ben09, Gor10].

During the course of this thesis we have been able to overcome all these difficulties. We were able to observe [Min10a] and characterize [Eil11a, Eil11b] LBs, as well as Vortex LBs [Eil13c] in fiber arrays (FAs) and also make contributions to the field of DO in WAs in general [Hei12].

## 4.2 A Qualitative Propagation Model

In the course of the thesis ST nonlinear wave propagation was investigated in WAs with instantaneous Kerr nonlinearity. Equation (17) then reads:

$$i \frac{\partial}{\partial z} A_{nm}(z, t) = -\frac{\beta_2}{2} \frac{\partial^2}{\partial t^2} A_{nm}(z, t) + \gamma |A_{nm}(z, t)|^2 A_{nm}(z, t) + c \left[ A_{n+1m}(z, t) + A_{n-1m}(z, t) + A_{nm+1}(z, t) + A_{nm-1}(z, t) + A_{n+1m+1}(z, t) + A_{n-1m-1}(z, t) \right], \quad (18)$$

where  $|A_{nm}(z, t)|^2$  is the instantaneous optical power in the WG with index  $nm$  and  $\gamma = \frac{2\pi}{\lambda} \frac{n_2}{A_{\text{eff}}}$  is the nonlinear constant, which depends on the wavelength  $\lambda$ , the material nonlinear refractive index  $n_2$  and the effective area  $A_{\text{eff}}$ , which can be calculated from the shape  $\mathcal{F}(x, y)$  of the guided, isolated mode  $A_{\text{eff}} = (\int |\mathcal{F}|^2 dx dy)^2 / \int |\mathcal{F}|^4 dx dy$  [Agr01]. Equation (18) is referred to as the discrete-continuous, generalized, nonlinear Schrödinger equation (NLSE). Again the notation for a hexagonal WA has been adopted here, different geometries are discussed in Section 4.1.

The NLSE describes (in the order of the appearance of the terms) the evolution of the instantaneous modal amplitude in the  $nm^{\text{th}}$  WG, affected by dispersion, nonlinearity, and discrete diffraction. As such it is the minimal model describing nonlinear, ST wave propagation in WAs. We will later see that, although it is quite useless for quantitative predictions, it is still extremely instructive to study, as it gives a measure of physical insight, that goes beyond the mere solution of numerical models. In particular its stationary LB solutions can be tested against experimental and numerical data to verify their very existence. Moreover, its scaling properties, discussed below, immediately allow one to study the parameter regimes of ST propagation.

For the purpose of analytically treating Eq. (18) it is useful and interesting to note that each of the free parameters is a mere parameter of scale, i.e., that it defines a characteristic granularity of the spatial and temporal axes and the typical power level of the system. More mathematically spoken Eq. (18) can be cast into an entirely dimensionless form:

$$i \frac{\partial}{\partial \zeta} a_{nm}(\zeta, \tau) = \mp \frac{1}{2} \frac{\partial^2}{\partial \tau^2} a_{nm}(\zeta, \tau) + |a_{nm}(\zeta, \tau)|^2 a_{nm}(\zeta, \tau) + \left[ a_{n+1m}(\zeta, \tau) + a_{n-1m}(\zeta, \tau) + a_{nm+1}(\zeta, \tau) + a_{nm-1}(\zeta, \tau) + a_{n+1m+1}(\zeta, \tau) + a_{n-1m-1}(\zeta, \tau) \right], \quad (19)$$

where the dimensionless quantities are linked to their physical counterparts via  $t = t_0 \tau$ ,  $z = z_0 \zeta$ , and  $A_{nm} = A_0 a_{nm}$ , where the first two scaling coefficients are the array's characteristic time  $t_0 = \sqrt{|\beta_2|/c}$  and length  $z_0 = c^{-1}$ , and the last coefficient  $A_0 = \sqrt{c/\gamma}$  can be squared to yield the characteristic power  $P_0 = c/\gamma$ .  $E_0 = P_0 t_0 = \sqrt{|\beta_2|c/\gamma}$  is the characteristic pulse energy. The

sign in front of the dispersion term has to be chosen, such that it is negative for normal dispersion and positive otherwise.

Solutions of Eq. (18) and Eq. (19) are sought after in two different manners. The evolution of any initial condition can be evaluated by direct numerical solution, e.g., with a 4<sup>th</sup> order Runge-Kutta scheme [Kut01, But87] or, more efficiently, by using a split-step Fourier method [Har73, Fis73, Agr01].

LB solutions, which are characterized by their stationarity, are solved for using the ansatz  $a_{nm}(\zeta, \tau) = \tilde{a}_{nm}(\tau) \exp(ib\zeta)$ , where  $b$  is the so-called nonlinear phase shift, i.e., the nonlinearly induced offset of the longitudinal wavenumber. The resulting set of coupled differential equations are solved by turning it into a set of coupled ordinary equations by discretization along the  $\tau$ -coordinate. Here we used a Newton-Raphson scheme, which profits from the relative ease, with which the local Jacobian of the system of equations can be determined. A set of solutions for a range of nonlinear phase shifts  $b$  can be determined, which is then termed a LB family. The stability of these solutions can be investigated by propagation, with the option of adding initial noise, by linear stability analysis, or in case of sufficiently simple solutions by application of the Vakhitov-Kolokolov theorem [Vak73].

All of the above mentioned solution methods for NLSE have been used at some point along with the experiments and respective results are discussed in Chapter 5.

### **4.3 Propagation Environments**

Over the years a number of implementations for DO system have been proposed and demonstrated, the most prominent of which shall be briefly introduced here and discussed in the context of the usability for ST experiments.

First experiments [Eis98] have been carried out in surface patterned  $\text{Al}_x\text{Ga}_{1-x}\text{As}$  arrays. They are of high quality but intrinsically limited to 1D structures. This limitation is shared by photovoltaic [Che05] and other  $\chi^{(2)}$ -WAs [Iwa04, Iwa05b]. Some of which are, however, suitable for ST experiments [Set10, Set11b]. Discrete optics in nematic liquid crystal cells [Fra04] and coupled cavities [Pes04] is unsuitable for fast ST optics due to the slow system response. Induced optical lattices [Kr698b, Kr698c, Kr698a, Den99, Pet99, Efr02, Fle03a, Pet03a, Pet03b, Kr603, Des06] in photorefractive materials and infiltrated PCF arrays [Ros07, Vie12] partially overcome this limitation but do not exhibit the required level of regularity for the unambiguous observation of LBs.

In this thesis we found femtosecond-written WAs [Nol03, Per04b] and fiber arrays [R6p07,

## 4. Ultrafast Discrete Optics: Samples, Scales & Models

Röp11] most suitable for ST experiments in DO. Both have a high degree of regularity, well defined diffraction and dispersion properties, near-instantaneous nonlinear response, high power-handling capability and low loss. The strength of fs-written WAs is their unparalleled degree of geometric flexibility. They are, however, not used for the investigation of LBs, because their linear and nonlinear response in the near infrared is largely unexplored. Fiber arrays (FAs) on the other hand are much less flexible. However, their linear and nonlinear properties over the complete transmission window of silica is extremely well understood due to the similarity of the individual WGs of the FAs to ordinary telecom fibers. Modelling of ST effects in FAs has a high level of sophistication and reliability. Both environments are briefly discussed below.

### 4.3.1 Femtosecond Written Waveguide Arrays

If a sufficiently powerful ultrashort laser pulse is focused on a transparent medium, the intensity in the focus can be so high that multi-photon absorption occurs [Boy03]. In turn this may result in plasma formation and optical material breakdown, leading to permanent modification of the material properties in the affected region in general. In particular this leads to a modification of the local refractive index. As the energy is deposited in a micron sized region only this region is modified. By moving the laser focus on an arbitrary trajectory through the material a three dimensional path of modified refractive index can be inscribed. If the refractive index modulation is positive, as is the case for silica samples, an optical WG is permanently written into the sample. Repetition of the process at different parallel paths through the sample leads to the fabrication of a WA.

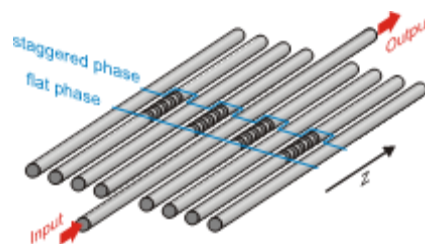


Fig. 15: Schematic representation of a segmented waveguide array. All light, which is coupled into the input WG leaves the array at the output WG, due to the staggered phase imprinted on the diffraction pattern in the middle of the array. Figure adapted from [Hei12].

The individual WGs do not necessarily have to be identical with respect to each other and may also change their properties along their length. For example, if the laser is periodically turned off during the writing process a segmented WG is produced, which, in first order approximation, has a different effective refractive index. Light propagating inside such a WG thus acquires a phase shift, with respect to light, which propagates in a non-segmented, otherwise identical, WG. If in a 1D WA every second WG is segmented in a way, that it acquires a  $\pi$ -phaseshift the effect of discrete diffraction can be completely undone [Lon08, Sza08] in a process very similar to phase

conjugation [Fis83]. For a sketch of such a structure see Fig. 15. A spatiotemporal, nonlinear experiment [Hei12] based on this concept has been evaluated in this thesis and is discussed in Section 5.1. The samples used in this experiment had a length of 100 mm, a coupling strength of  $c = 20.1 \text{ m}^{-1}$ , a nonlinearity coefficient of  $\gamma = 0.17 \cdot 10^{-3}/(\text{mW})$  and a dispersion coefficient of  $\beta_2 = 36 \cdot 10^3 \text{ fs}^2/\text{m}$  and have been operated at a carrier wavelength of  $\lambda_0 = 800 \text{ nm}$ .

### 4.3.2 Fiber Arrays

A powerful approach for the fabrication of 2D WAs which are compatible for ST experiments is derived from the fabrication technology of Photonic Crystal Fibers (PCFs) [Rus03, Kni03]. The technology is, in fact, simpler: the air holes are replaced by rods with increased refractive index and the central defect is removed. Thus a very long 2D photonic crystal with small index modulation is created, a DO environment by the definition in Section 4.1. Such WAs are called fiber arrays (FAs).

The fabrication technique itself is based on a stack and draw method. A high index rod of pure silica is placed in a depressed index tube made of fluorine doped silica glass. This choice ensured high homogeneity, without any considerable longitudinal or transversal variations of the material composition, in the WG and a high destruction threshold. The preform is then drawn and consolidated into a prefiber with a diameter of a few millimeters. Chemical vapor deposition techniques [Li85] have been used in earlier stages of the technology. The WG diameter of this prefiber is roughly one half of the outer diameter. The prefibers are then cut into pieces, sorted by size, stacked hexagonally and placed in a large jacketing tube, which is in turn drawn into the final FA with the desired diameter  $D$ .

For the complete process a very high degree of accuracy is necessary, as discrete coupling is a resonant effect and phase accuracy of much less than  $\pi$  in the up to 91 WGs of the FA has to be maintained over sample lengths of tens of centimeters, i.e.,  $\sim 10^5$  wavelengths. Therefore the complete process described above has to be designed to maintain this accuracy. Otherwise random perturbations dominate the propagation [Per04a]. Prefibers have to be selected to achieve a sample of identical diameters, prior to stacking. Further boundary rods have to be included to smoothen the transition between the hexagonal array stack and the circular jacketing tube. Details of the fabrication procedure are described in [Röp07, Röp11], a microscopic image of the FA is displayed in Fig. 16(a). Fig. 16(b) is an image of the light distribution at the end of the FA, which was excited in central WG. The FA length was several characteristic lengths and the regularity of the discrete diffraction pattern underlines the regularity of the FA.

Properties for individual WGs are typically chosen, such that they are similar to those in standard

#### 4. Ultrafast Discrete Optics: Samples, Scales & Models

telecom fibers. They are also operated in the telecom wavelength regime at a carrier wavelength of  $\lambda_0 = 1550$  nm. The refractive index difference between core and cladding is fixed and determined by the material choice, here it is  $\Delta n = 1.1 \cdot 10^{-3}$  or  $\Delta n = 3.8 \cdot 10^{-3}$ , depending on the sample. For both values  $\Delta n \ll n$  holds. The dispersion properties of the WG are then basically fixed, as the impact of the material dispersion is much stronger than that of the geometric dispersion, due to the small index difference, as can be seen in Fig. 16 (g) and (j). The material dispersion is modelled using the Sellmeier equations [Mar72, Agr01]. At the design wavelength  $\lambda = 1550$  nm the FAs dispersion is anomalous and has a typical value of  $\beta_2 = -27 \cdot 10^3 \text{fs}^2/\text{mm}$  [Mal65]. The material choice also fixes the nonlinear constant to  $n_2 = 2.7 \cdot 10^{-20} \text{m}^2/\text{W}$  [Agr01], which in turn determines the nonlinear coefficient  $\gamma$ . The variation of the values of these coefficients for different wavelengths can be found in Fig. 16 (c-e).

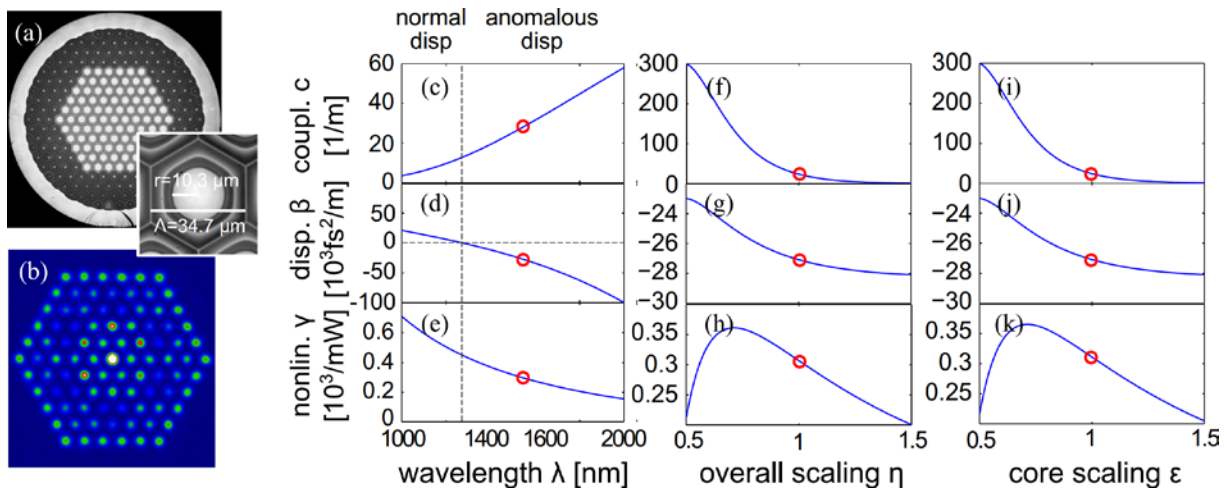


Fig. 16: (a) White light microscopy image of the front facet of a type I (see Tab. 1, below) FA, with (inset) zoom onto a single WG and geometric scales. (b) Linear diffraction pattern of centrally coupled cw-light after  $L = 100$  mm propagation length. (c-k) Variation of scale parameters (c,f,i) coupling strength  $c$ , (d,g,j) dispersion  $\beta_2$ , and (e,h,k) nonlinear constant  $\gamma$  for the FA shown in (a). (c,d,e) Variation as a function of the wavelength  $\lambda$ . (f,g,h) Variation as a function of overall scaling (i.e.  $r \rightarrow r\eta$  and  $\Lambda \rightarrow \Lambda\eta$ ) at a wavelength  $\lambda = 1550$  nm. (i,j,k) Variation as a function of the WG radius scaling (i.e.  $r \rightarrow r\epsilon$ ) at a wavelength  $\lambda = 1550$  nm. (red circles) Values for the samples used in experiments. (dotted lines) Zero dispersion line. Subfigures (a) and (b) adapted from [Eil11a].

After fixing the materials, unit cell geometry and FA geometry, the fabrication process leaves one degree of freedom: all geometric properties of the FA can be scaled by selection of appropriate drawing conditions, i.e., the selection of the outer diameter  $D$ . This simultaneously determines (i) the nonlinearity coefficient  $\gamma$  via the effective area  $A_{\text{eff}}$ , which grows more or less quadratically with  $D$ , (ii) the single-mode cutoff wavelength  $\lambda_{\text{cut}}$  also grows nearly linearly with  $D$  and determines the minimal wavelength, at which the FAs are useful, and (iii) the coupling constant  $c$ , which decreases near-exponentially with growing  $D$ , due to the decreasing overlap of the guided mode with the nearest neighbor cell. An overview over the scaling of the model parameters upon variation of the diameter  $D$ , i.e. simultaneous scaling of the core radius  $r$  and

unit cell pitch  $\Lambda$  can be found in Fig. 16 (f-h). The effects of the scaling the core radius  $r$  only is displayed in Fig. 16 (i-k). It is seen that the coupling constant  $c$  is the quantity, which depends most on the array geometry, whereas neither the dispersion coefficient  $\beta_2$  nor the nonlinear coefficient  $\gamma$  change much. The coupling constant  $c$  is therefore the most critical parameter in determining an appropriate FA geometry. A larger value of  $c$  decreases the characteristic length scale  $z_0$  and characteristic time scale  $t_0$  of the FA. Smaller FAs therefore generally demand shorter samples and shorter pulses. The lower limit of the coupling constant  $c$  is determined mostly by the length scale on which the impact of disorder becomes influential [And58, Per04a, Sch07, Lah08]. We estimate this length to be in the region of a few tens of centimeters and thus  $c > 1 \text{ m}^{-1}$ . The upper limit of the coupling constant  $c$ , on the other hand, is determined by the growing impact of short-pulse perturbations. Heuristic tests found that characteristic time scales must not drop below 15 fs, thus  $c < 100 \text{ m}^{-1}$ .

	<b>standard (type I)</b>	<b>short (type II)</b>	<b>long / irregular (type III)</b>
<b>outer diameter <math>D</math> [<math>\mu\text{m}</math>]</b>	680	580	805
<b>index step <math>\Delta n</math> [<math>10^{-3}</math>]</b>	1.1	1.1	3.8
<b>WG radius <math>r</math> [<math>\mu\text{m}</math>]</b>	9.7	8.25	6.8
<b>pitch <math>\Lambda</math> [<math>\mu\text{m}</math>]</b>	34.8	29.6	27.8
<b>effective area <math>A_{\text{eff}}</math> [<math>\mu\text{m}^2</math>]</b>	370	336	134
<b>nonlinear coeff. <math>\gamma</math> [<math>10^{-3} \text{m}^{-1} \text{W}^{-1}</math>]</b>	0.30	0.32	0.81
<b>dispersion coeff. <math>\beta_2</math> [<math>10^3 \text{fs}^2/\text{mm}</math>]</b>	-28	-26	-27
<b>coupling coeff. <math>c</math> [<math>\text{m}^{-1}</math>]</b>	27	73.4	6.7
<b>diff. length <math>L_{\text{diff}}</math> [mm]</b>	9.2	3.5	39.1
<b>char. length scale <math>z_0</math> [mm]</b>	37	13.6	149
<b>char. time scale <math>t_0</math> [fs]</b>	32	18	63
<b>char. power <math>P_0</math> [kW]</b>	90	225	7.9
<b>char. energy <math>E_0</math> [nJ]</b>	2.9	4.3	0.53

Tab. 1: Characteristic parameter values for the FA samples used in this thesis at a wavelength of  $\lambda = 1550 \text{ nm}$ .

Here we used three sets of samples. Most experiments were carried out with samples with  $D = 680 \mu\text{m}$  called type I samples, with a coupling constant that is close to neither of the limits discussed above. Type II samples with  $D = 580 \mu\text{m}$ , have been used for experiments in Section 5.3 and have a coupling constant close to the upper limit, resulting in short characteristic lengths  $z_0$  and short characteristic time scales  $t_0$ . A different class of samples, referred to as type III, has been drawn from an earlier fabrication batch. They are characterized by a smaller coupling constant close to the lower limit and hence increased characteristic lengths  $z_0$  and times  $t_0$ , mitigating the impact of higher order effects. Type II samples are, however, also much more

#### 4. Ultrafast Discrete Optics: Samples, Scales & Models

irregular, such that a distinction between disorder induced effects and pure LB propagation is conceptually difficult. Characteristic values for all three types are displayed in Tab. 1.

#### 4.4 A Quantitative Propagation Model

Although the NLSE model discussed in Section 4.2 is *the* established standard model for ST pulse propagation in WAs it is worth noting that the development of this field was mostly driven by theoretical studies, owing to the experimental difficulties discussed above. In fact, the typical scales presented in Tab. 1 are beyond the range in which the NLSE model is valid. This is in particular true for the temporal scale  $t_0$ , which is in the range of a few tens of femtoseconds. For such time scales quite a few approximations that are essential for the derivation of the NLSE break down. These are (i) the truncation of the Taylor expansion of the dispersion relation, (ii) the assumption of a constant coupling coefficient  $c$  over the pulse bandwidth, (iii) the assumption of the instantaneousness of the nonlinear response, and (iv) the validity of the SVEA itself. Issues (i), (ii), and (iii) can be fixed to a certain degree within the NLSE framework by taking into account additional terms [Agr01]. Issue (iv) however warrants introduction of an altogether new model.

Here we followed the approach of the Unidirectional Maxwell Equations (UME) [Kol04a, Kin10], adapted for the discrete-continuous nature of WAs [Bab07]. The idea is to produce a 1<sup>st</sup> order wave equation for the real field by ignoring backwards propagating waves. The result is the propagation equation [Eil11a]:

$$\begin{aligned}
 -i \operatorname{sgn}(\omega) \frac{\partial}{\partial z} E_{nm}(z, \omega) &= [\beta(\omega) - \omega \beta_1] E_{nm}(z, \omega) + c(\omega) \sum_{n'm'} C_{nm}^{n'm'} E_{n'm'}(z, \omega) \\
 &+ \frac{4}{3} \gamma(\omega) P_{nm}^{\text{NL}}(z, \omega) \\
 P_{nm}^{\text{NL}}(z, t) &= E_{nm}(z, t) \left[ (1-g) E_{nm}(z, t)^2 + g \int E_{nm}(z, t-t')^2 h(t') dt' \right] \quad (20) \\
 h(t) &= \begin{cases} 0 & t < 0 \\ \frac{\tau_1^2 + \tau_2^2}{\tau_1 \tau_2^2} \exp(-t/\tau_2) \sin(t/\tau_1) & t \geq 0 \end{cases}
 \end{aligned}$$

for the Fourier transform  $E_{nm}(z, \omega)$  of the real modal amplitude  $E_{nm}(z, t)$  in WG  $nm$ , which is related to the modal amplitude  $A_{nm}(z, t)$  of Eq. (18) via  $E_{nm}(z, t) = \frac{1}{2}(A_{nm} \exp(i\omega_0 t) + c.c.)$ , where  $\omega_0 = 2\pi v_{ph}/\lambda_0$  is the carrier frequency at the wavelength  $\lambda_0$ . Due to the reality of  $E_{nm}(z, t)$  Eq. (20) only needs to be solved for positive frequencies  $\omega > 0$ . Equation (20) models the evolution  $E_{nm}(z, \omega)$  under the influence of the full WG dispersion  $\beta(\omega)$ , in a frame of reference co-moving with a speed  $1/\beta_1$ , whose choice is arbitrary but usually taken to be  $\beta_1 = d\beta/d\omega$  at  $\omega = \omega_0$ , i.e., the group velocity at the carrier frequency. The second term

describes discrete coupling in the array, where  $c(\omega)$  models the wavelength-dependent coupling strength and the matrix  $C_{nm}^{n'm'}$  models neighborhood relationships, i.e., it is of unity value if the WGs denoted by  $nm$  and  $n'm'$  are neighbors and zero otherwise. In fact, any kind of coupling geometry can be defined with the appropriate  $C_{nm}^{n'm'}$  matrix, here we model hexagonal WAs with 91 WGs. The last term describes the influence of the nonlinear polarization. Due to its (almost) instantaneous nature it is, however, best described in time domain, as per the third line of Eq. (20). Here the first term is the instantaneous Kerr-effect and the second term is the delay stimulated Raman response of the medium. For silica glass the response function  $h(t, t')$  is given by the last line of Eq. (20), with  $\tau_1 = 12.2$  fs and  $\tau_2 = 32$  fs and a relative strength of  $g = 0.22$  [Agr01].

The functional structure of Eq. (20) is identical to that of Eq. (17), and the split step method can be used to obtain numerical solutions. A scheme for the propagation of the field by a step of length  $\delta z$  is displayed in Fig. 17. With this method the field  $E_0 = E(z = z_0)$  is first propagated by a half step  $\delta z/2$  considering only the linear part  $\mathcal{L}$  of the equation, such that  $E(z_0 + \frac{\delta z}{2}) = E_0 \exp(i\delta z/2 \mathcal{L})$ . The matrix exponential is carried out in the eigenspace of the linear propagation operator  $\mathcal{L}$ , such that  $E(z_0 + \frac{\delta z}{2}) = E_0 \cdot EVec_{\mathcal{L}} \cdot \exp(i\delta z/2 EVal_{\mathcal{L}}) \cdot EVec_{\mathcal{L}}^\dagger$ , where  $EVec_{\mathcal{L}}$  is the matrix of the eigenvectors of  $\mathcal{L}$  and  $EVal_{\mathcal{L}}$  is a diagonal matrix with the eigenvalues of  $\mathcal{L}$ . The eigenspace of the linear operator of Eq. (20) decays into a product of the temporal eigenspace and the eigenspace of the coupling matrix  $C_{nm}^{n'm'}$ , such that transformation of  $E_{nm}(z, t)$  into the eigenspace can be carried out by Fourier transform along the time axis and consecutive multiplication with the eigenvector-matrix of  $C_{nm}^{n'm'}$ . As this eigenvector-matrix neither depends on  $\omega$  nor on  $z$ , its time consuming calculation only needs to be done once. Moreover the complete transform is very fast as the temporal transform benefits from the availability of the  $\mathcal{O}(N_t \log N_t)$  scaling of the FFT algorithm and the spatial transform, which scales with  $\mathcal{O}(N_{xy}^2)$ , is not badly affected by the square scaling law because the spatial number of degrees of freedom (i.e., the number of WGs) is small. The nonlinear contribution is then added with a standard 4<sup>th</sup> order Runge-Kutta step, where the value of the linear half-step is used as a predictor value. This step is conveniently calculated in time domain, whereas the convolution of the response function  $h(t, t')$  is carried out in frequency domain, where it is a simple multiplication. The 2<sup>nd</sup> linear half-step is then done similar to the first half-step.

The solution of Eq. (20) thus scales in the same manner as the solution of an NLSE equation. The price to pay for the improved accuracy lies in the greater need for resolution. Whereas SVEA type equations must only be discretized, that the finest feature of the envelope  $A_{nm}(z, t)$

#### 4. Ultrafast Discrete Optics: Samples, Scales & Models

is resolved, UME type equations need to be discretized to resolve the carrier wave, which is a much more fine-grained discretization. The necessity to also resolve the propagation axis  $z$  in a more fine grained manner then follows automatically from the Courant criterion [Cou28].

However, this price is not as high as expected. If one takes the typical time scales from Tab. 1 as the smallest features to be resolved in a SVEA then we have to at least resolve fractions of 10 fs. The carrier wave, which we have to resolve in the UME scenario, varies on time scales close to  $\omega_0^{-1} \approx 1$  fs, which is only an order of magnitude worse.

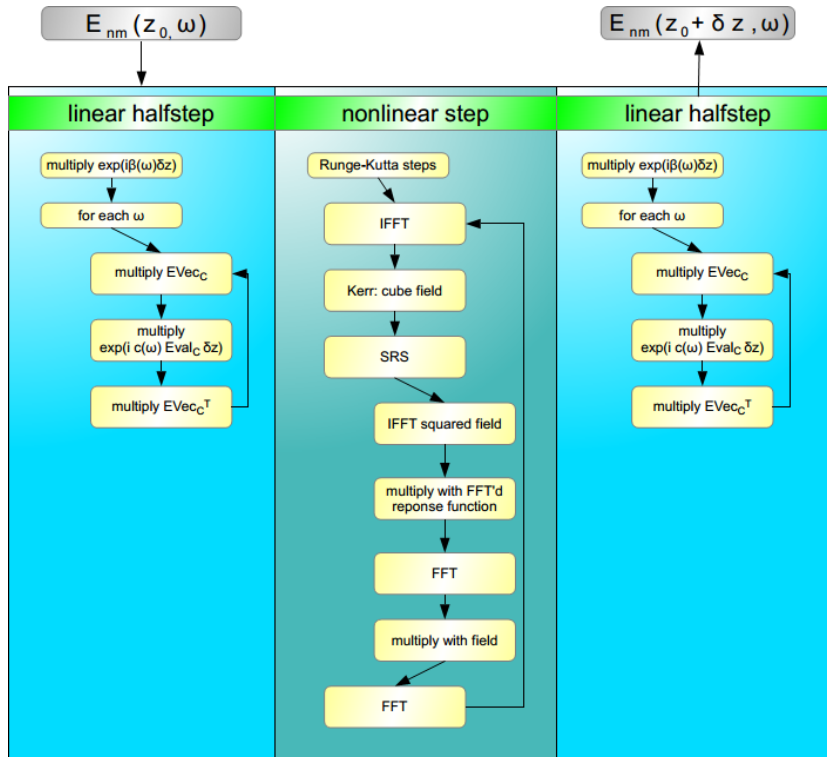


Fig. 17: Scheme of a numerical step required for the solution of the UME. FFT and IFFT are (inverse) Fourier transform steps with respect to the frequency/time axis.  $C$  denotes the coupling matrix  $C_{nm}^{n'm'}$  and  $EVec_C$  and  $EVal_C$  are its eigenvector and eigenvalue matrices. Indentation denotes subordinate steps.

We therefore argue that UME type equations are the tool of choice to realistically and quantitatively model ST pulse propagation in WAs. They are only a little more computationally demanding to implement than SVEA type solvers, which give wrong (or at least imprecise) predictions of experiments, anyway. Here we used a parallel implementation of the UME to model pulse propagation; many results of these simulations are discussed in Chapter 5. However, one should note, that split-step solvers have limits on parallelizability: the calculation of each propagation phase is computationally cheap and the expensive transform steps need to operate on the full dataset, such that the solver speed quickly becomes limited by the available memory bandwidth. For future systems with a high number of transverse degrees of freedom a different approach might therefore be necessary for efficient solution of the UME.

## 4.5 Scales and Dominating Effects

With the introduction of the UME many new effects have to be considered. This section gives an overview over their relative strength and will re-justify the introduction of the characteristic scales in Section 4.2. To compare the relative strength of each effect we have to judge their impact on Eq. (20) in a common framework, i.e., the length scale upon which the effect leads to a considerable change of the shape of a pulse with energy  $E$  and FWHM duration  $t_0$ , in the absence of all other effects. For the dispersion we have the dispersion length of order  $N$  termed  $L_{\text{Disp}}^{(N)}$ , which is the length after which a pulse of duration  $t^{(0)}$  has broadened considerably.

$$L_{\text{Disp}}^{(N)} = \frac{\left(t^{(0)} / 1.66\right)^N}{|\beta_N|}, \quad (21)$$

where  $\beta_N = d^N \beta / d\omega^N$  is taken at the carrier wavelength [Agr01]. For the coupling it is the diffraction length  $L_{\text{Diff}}$ , which is the length after which an initial excitation in a single WG has lost roughly 1/3 of the initial energy by coupling to its neighbours.

$$L_{\text{Diff}} = \frac{1}{\text{NN}} \frac{\pi}{2c} = \frac{1}{\text{NN}} L_C = \frac{1}{\text{NN}} \frac{\pi}{2} z_0, \quad (22)$$

where  $\text{NN} = 6$  is the number of nearest neighbors,  $c$  is taken at the carrier wavelength,  $z_0 = c^{-1}$  is defined in Section 4.2, and  $L_C$  is the half-beat length of a discrete coupler [Jon65]. The typical length scale for the Kerr effect is the nonlinear length  $L_{\text{NL}}$ , which is the length after SPM has reshaped the pulse spectrum considerably.

$$L_{\text{NL}} = (\gamma P_0)^{-1} = \frac{t^{(0)}}{\gamma E}, \quad (23)$$

where the nonlinear coefficient is taken at the carrier wavelength [Agr01]. The impact of the higher order parts of the nonlinearity, i.e., the self-steepening and the stimulated Raman effect, can be judged with the Raman-length  $L_{\text{Raman}}$ ; the length after which the pulse has shifted in frequency by its bandwidth. A good approximation is [Agr01]:

$$L_{\text{Raman}} = 0.3 \text{fs}^{-1} \frac{t^{(0)^2}}{\gamma E}. \quad (24)$$

The effects can now be compared for a given fiber geometry and excitation wavelength as a function of pulse duration  $t^{(0)}$  and pulse energy  $E$ . The dominating effect is the effect, which for a given combination of  $t^{(0)}$  and  $E$  yields the minimal length. Results for a type I FA at  $\lambda = 1550$  nm are plotted in Fig. 18. Linear effects dominate at low powers, whereas nonlinear

#### 4. Ultrafast Discrete Optics: Samples, Scales & Models

effects dominate at high powers. Temporal effects dominate for short pulses and spatial effects for long pulses. LBs should occur close to the equilibrium point between dispersion, diffraction, and the Kerr-effect, which is marked by the green circle. We therefore expect LBs to have a typical pulse duration of  $t^{(0)} \sim 10$  fs and a typical energy of  $E \sim 10$  nJ, a prediction which coincides with the characteristic energy  $E_0$  and duration  $t_0$  in Tab. 1. This prediction is beyond the validity of the NLSE, such that the introduction of the UME model is a-posteriori justified.

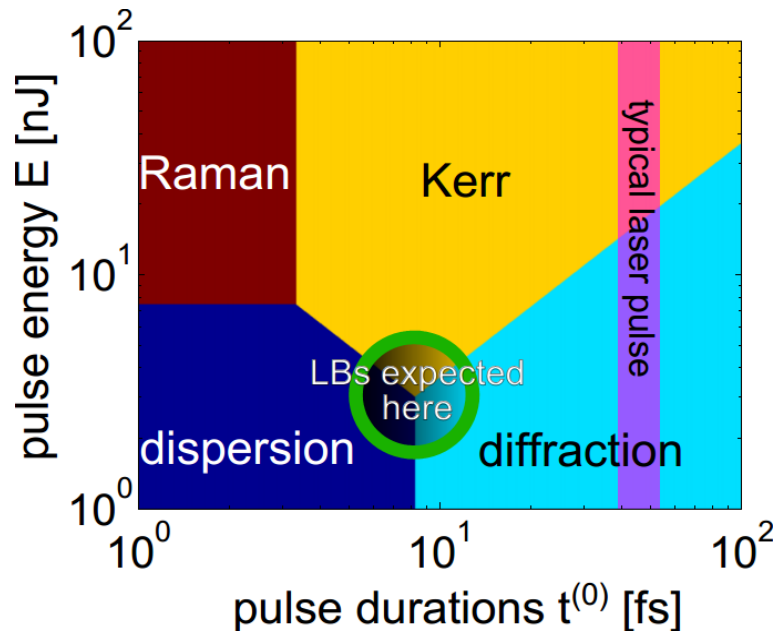


Fig. 18: Dominating effect vs. pulse duration  $t_0$  and pulse energy  $E$  for a type I FA at a wavelength of  $\lambda = 1550$  nm. A typical laser pulse has a duration of approximately 30 – 50 fs with variable energy. LBs are expected at the intersection of dispersion-, diffraction-, and Kerr-dominated areas, where all effects are balanced. LBs should thus have a duration of  $\sim 10$  fs and  $\sim 10$  nJ energy.

Two more important conclusions can be drawn from Fig. 18 regarding the temporal dynamics of ST optics in FAs: (i) the pulse parameter region of Raman/self-steepening dominance is “uncomfortably” close to the parameter region, where LBs are expected and (ii) there is a considerable mismatch between the duration of the laser pulse used for the excitation in the experiment and the expected duration of the LB. The former will, in the best case, facilitate self-induced red-shift [Dia85, Mit86, Gor86] on solitary waves. It is, however, also known to induce instability of high order temporal solitons [Gol85, Ohk87, Tai88, Hus01, Her02]. The latter means that in an experiment one has to rely on self-contraction [Nak81, Sha82] to excite a LB. This typically means that an excessive amount of energy has to be injected in the FA. Solitary wave formation, at least in a simple fiber, then occurs as part of the generation of supercontinua [Dud06, Alf06] via the stages of modulation instability [Kar67, Kar69, Has70], leading to the formation of Akhmediev breathers [Akh86, Akh09] and soliton fission. The close spectral vicinity of the excitation to the zero-dispersion wavelength at  $\lambda(\beta_2 = 0) = 1270$  nm then lead to the generation of blue-shifted waves by resonant radiation [Akh95]. These are shifted further

due to radiation trapping [Gor07b] by the group-velocity event horizon [Unr81, Unr05, Phi08, Eil13b] formed by the red-shifting and thus decelerating solitary waves. Because this process is noise induced and self-amplifying, as strong solitary waves draw energy [Erk10] from weaker ones in the presence of the Raman-effect, we also cannot rule out the generation of Rouge-waves [Sol07, Sol08, Dud08, Bir13] at this point.

While the impact of this cascade is well understood in purely temporal experiments, e.g., in single core fibers, this was not the case for ST DO systems, prior to this thesis. Moreover, given the multitude of effects, which can and will occur if ultrashort pulses propagate through FAs, it was prior to this thesis unclear, if LBs would propagate in FAs in a stable manner at all. The reason was that their prediction was based on the overly simple NLSE model, which was discussed in Section 4.1. The expected generation of LBs in conjunction with a supercontinuum of radiation was also one of the driving forces for the development of the ST analysis techniques, discussed in Chapter 3.

In summary, we now have a better understanding of the role of DO in the realm of ST photonics, and of the importance of DO systems in the physics of Light Bullets, which are nonlinearity self-confined in all transverse dimensions. The NLSE was introduced as the standard model for the description of nonlinear ST pulse propagation. The two systems, in which ST experiments have been carried out in the course of the thesis, have been introduced and the relations of their geometric parameters and the model coefficients have been discussed. Using typical values of these coefficients we have derived characteristic spatial, temporal, and energetic scales, in which true ST dynamics can be expected. This prediction led us to the introduction of the UME model, which we argue is the new “gold-standard” for the modelling of ultrashort pulse propagation in ST DO systems. A careful reconsideration of typical scales, has reconfirmed the predicted parameter range for LB propagation but also pointed out that higher order effects will have considerable effect on the ST dynamics of ultrashort pulses in DO systems. The impact of these higher order effects on ST pulses and LBs in particular had not been at the focus of ST photonics prior to this thesis. The base of knowledge was in fact so small, that the question if LBs could be observed at all in an experiment, in the face of the many perturbations they would experience, remained inconclusive prior to this thesis. The answer to this question is discussed in detail in the next chapter, which will not only make use of the conceptual basis developed here but also exploit the experimental methods introduced in Chapters 2 and 3.

### 5. Results of Experiments and Simulations

This chapter focuses on the main results of this thesis. It will make heavy use of the methods discussed in the previous chapters. Successful implementation of the experiments described here, was the main driving force for the development of the pulse generation, analysis methods and simulation tools introduced in the previous chapters. These techniques did, in fact, evolve in parallel to the experiments presented here. Thus advanced methods, such as ImXFROG and the SPS, were not available for early experiments. Furthermore, input pulse durations and attainable resolution of iXCorr experiments were oftentimes much worse than the best values stated in the chapters above. Specific values will be given where appropriate. Experimental results and data from simulations are presented in a tightly knit manner, as they are continuously used for cross-validation and to expand the available toolbox that allows us to understand the nonlinear propagation of ST waves. The repeated jumping between experiment and simulations, which might seem unmotivated at times, should thus be viewed as the natural process that organically fosters understanding of the complex ST dynamics and evolution behavior, which will be encountered in the following sections.

The main topic of this chapter and of the thesis as a whole has been the experimental analysis of the propagation of ST pulses through WAs, with special emphasis on the observation and characterization of various classes of Light Bullets in fiber arrays. The chapter thus starts with the investigation of fundamental ST propagation effects and then continuously progresses towards more complex ST excitations, with reduced symmetry.

The chapter starts with the analysis of the nonlinear propagation of ultrashort pulses in fs-written segmented WAs in Section 5.1 and investigates their suitability for the implementation of an all-optical limiting device. These experiments are chosen as an entry point to this chapter, because due to the absence of LBs at the operation wavelength their nonlinear dynamics is much less involved than the dynamics introduced in later chapters.

In Section 5.2 we report on the existence, observation, and evolution of fundamental LBs, who are mainly located in a single, high-symmetry WG at the center of the array. Note that the term “Light Bullet” is used somewhat redundantly for the class of solitary ST excitations in general and also for fundamental LBs, the prototypical, albeit specific member of this class. The meaning is explicitly stated where it might not be clear from the context.

After the fundamental proof of the experimental observation of stable discrete LBs, we will argue that reduction of symmetry induces novel LB dynamics, which had not been previously discussed and can only be observed in high dimensional solitary waves. We will first focus on

internal asymmetries, which are an intrinsic part of the propagation environment. They couple spatial, temporal, and nonlinear contributions to propagation dynamics and have a strong impact on LB dynamics. Effects related to these couplings are discussed in Sections 5.2 and 5.3. Section 5.2 focuses on LB evolution and the self-induced decay, related to the non-instantaneous, nonlinear response of the host material and the high-dimensional nature of the LBs. Section 5.3 deals with effects related to the wavelength-dependence of the discrete coupling strength and shows that it has profound impact on the static and dynamic properties of LBs.

Then we will focus on extrinsic asymmetries, which can be imposed on the system externally. In Section 5.4 we observe and characterize Vortex LBs, ST solitary waves with optical angular momentum, where the asymmetry is imprinted on the excitation field by a pulse shaping technique discussed in Chapter 2. We argue that these are the most complex spatiotemporal solitary waves observed, so far. Their successful observation marks the end of this chapter.

### **5.1 Nonlinear Self-Limiting in Segmented Waveguide Arrays**

In this section we explore the nonlinear propagation of ultrashort pulses in fs-written waveguide arrays. WAs are operated in the normal dispersion regime, such that they are not suitable for the observation of LBs. In conjunction with them having just a single transverse dimension they are characterized by a much less involved level of internal, nonlinear dynamics and thus serve as an entry point for the observation of ST effects in DO systems. The somewhat lower level of complexity on the one hand and the greater flexibility of the fabrication technique on the other hand allow us to observe and understand effects related to more complex geometries and aim for actual applications. Here we investigate the feasibility of segmented waveguide arrays (SWA) for the implementation of an all-optical limiting scheme.

WG segmentation was initially designed as a measure to induce perfect imaging, i.e., to perfectly reproduce the input field pattern of a SWA with length  $L$  at its end. Image formation is, of course, driven by diffraction. Thus for perfect imaging one has to devise a way to undo diffraction. Diffraction adds a phase onto the spatial spectrum, which dephases the pulse's spectral components in the 1<sup>st</sup> half of the WA. To achieve perfect imaging propagation in the 2<sup>nd</sup> half of the WA must add a negative spectral phase until at the end of the WA both phases add up to zero and the spectral components are again in constructive interference.

Undoing diffraction is therefore a question of being able to invert the DR  $\beta = \beta(\mu)$ , where  $\beta$  is the difference of the longitudinal wavenumber of the WAs Bloch mode with respect to the wavenumber of the individual WG and  $\mu$  is the dimensionless transverse wavenumber. In homogeneous WAs this relation can be obtained from Eq. (15), assuming that cw-light is

## 5. Results of Experiments and Simulations

propagating through the array. The DR is then  $\beta(\mu) = 2c \cdot \cos(\mu)$ .

According to this equation inversion can be achieved by inverting the sign of the coupling constant  $c$  or by shifting  $\mu$  by  $\pi$ . Inversion of the coupling constant is, in principle, possible for WAs, however, only for higher order [Man03, Set11a] modes and/or guided modes in arrays of photonic crystals waveguides of appropriate symmetry [Bro10, Bro12]. Array segmentation exploits the latter approach; the inversion is achieved by inducing a  $\pi$ -shift in the transverse wavenumber  $\mu$ , inverting the cosine term. A  $\pi$ -shift in the transverse wavenumber equates into adding an alternating sign, i.e., a  $\pi$ -phaseshift onto the mode of every second WG. This inverts the curvature of the dispersion relation and undoes the action of discrete diffraction. Any excitation at the beginning of the WA will be reproduced at its end [Lon08, Sza08] in intensity and phase, as opposed to nonlinear schemes which only reproduce the intensity pattern [Yan11].

The  $\pi$ -phaseshift is achieved for a particular operating wavelength  $\lambda_0$  by modifying the effective index of every second WG in the section close to the length-wise middle of the WA. The refractive index is modified by periodically blocking the inscription laser, while it writes the WA into the host material. If the length of the section is chosen appropriately a  $\pi$ -phaseshift can be achieved, due to the reduced effective index of the WG section. The periodic blocking also results in the inscription of a grating, its Bragg wavelength is, however, far from the operating wavelength and thus ignored.

Here the SWA was 100 mm, with a length of the segmentation section of 5.2 mm, written with a laser duty cycle of 50%. A schematic of the sample was presented in Fig. 15 in Section 4.3.1, where more parameters of the WA have been discussed.

In this thesis we aimed for a better understanding of the ST, nonlinear behavior of these SWAs. The above discussion only applies to low power, linear waves. The propagation of pulsed, nonlinear waves in SWAs was unexplored prior to this thesis. The SWA induces a  $\pi$ -phaseshift only for a certain wavelength and linear propagation. The segmentation further results in a loss of  $\sim 3$  dB for light travelling in the segmented WGs. Higher order ST effects, such as those discussed in Sections 4.4 and 4.5 and the effect of asymmetric excitation pulses had been ignored prior to this thesis.

The ultimate aim was to test the feasibility SWA for optical limiting (OL) of powerful pulses. The application is driven by the aim for developing integrated, all-optical data processing devices [Ji10, Vo10, Egg11, Vo12], which are deemed a key element in future all-optical terabit data networks. Of particular interest for long-haul opto-optical networks are all-optical 3R stages, which re-amplify, re-time, and re-shape pulsed data streams, without expensive, bulky,

and power-hungry electronic systems. In this scheme OLs are typically used to shape the peak section of on-off or phase-keyed pulse trains, mitigating high-power noise and nonlinear propagation effects and reducing radio-frequency sideband generation. An OL is a device, which has a saturable transmission curve, i.e., its transmission drops for increasing input energy. Previous suggestions are mainly based on the nonlinear, optical absorption of complex molecules [Tut93, Per96]. They lead to on-chip absorption and generation of heat and are hard to integrate, as opposed to SWAs, which reroute “unwanted” power. The opposite of OL, i.e., saturable absorption-like behavior, was demonstrated in ordinary WAs [Pro05] for laser mode-locking.

Various other linear mechanisms may also give rise to the revival of an initial input distribution and are therefore in principle suited for OL. The discrete Talbot effect [Tal36, Iwa05a] reproduces only spatially periodic input patterns. Photonic Bloch oscillations [Blo29, Mor99a] and dynamic localization [Dun86, Lon06, Dre08b] rely on specific transverse potential gradients to reconstruct arbitrary wave packets and are susceptible to disorder [Sch08, Dre08a]. Continuous longitudinal modulations of the lattice allows for the suppression of transverse broadening [Zha10], whereas transverse modulation of the WA can induce defect states, suppressing discrete diffraction. In [Hei12] we, however, showed that SWA based OL is superior to any of those schemes.

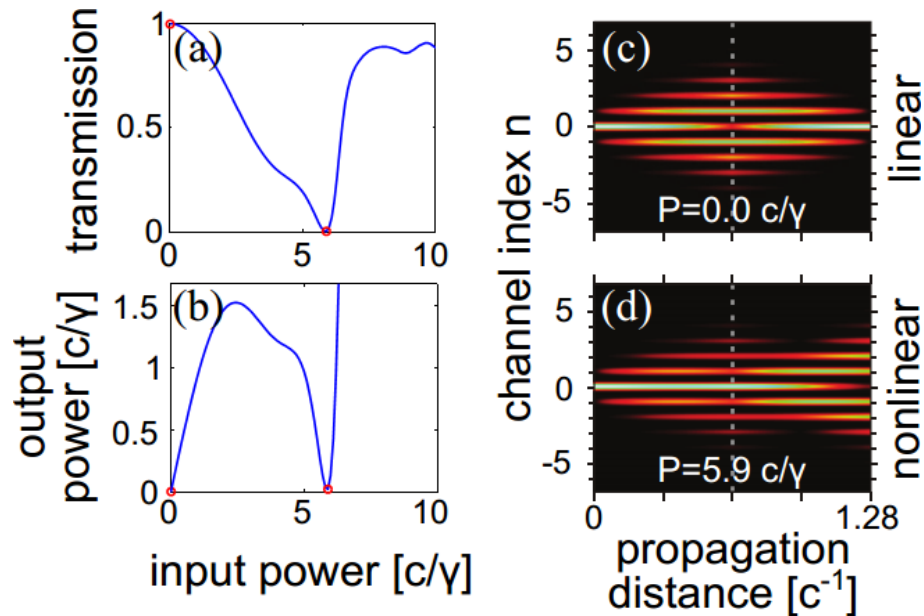


Fig. 19: NLSE simulation of the power dependent continuous wave transmission behavior for the SWA based OL scheme. (a) Transmission in central WG vs. input power. (b) Output power vs. input power. (c) Field pattern inside the SWA at  $P = 0$ . (d) Field pattern inside the WA at the minimum transmission. Power levels in (c) and (d) are marked in (a) and (b) by the red circles. Figure adapted from [Hei12].

Preliminary analysis of SWA based OL was carried out in the simplified NLSE scheme, i.e., by the solution of the appropriate version of Eq. (17) with Kerr-nonlinearity, under cw-excitation and the absence of dispersion. The results are displayed in Fig. 19, where the transmission, i.e.,

## 5. Results of Experiments and Simulations

the fraction of the input power leaving the central WG of the SWA, is plotted as a function of the input power. The SWA based OL scheme has a minimum transmission is 0.4%, i.e., its switching contrast is 22 dB. Moreover the output power has the desired dependence on the input power, i.e., a near linear growth for  $P < 1.7c/\gamma$  and a nearly constant output power for  $1.7c/\gamma < P < 4.7c/\gamma$ . SWAs are therefore a good candidate for OL and a realistic investigation based on the UME model introduced in Section 4.4 was thus carried out.

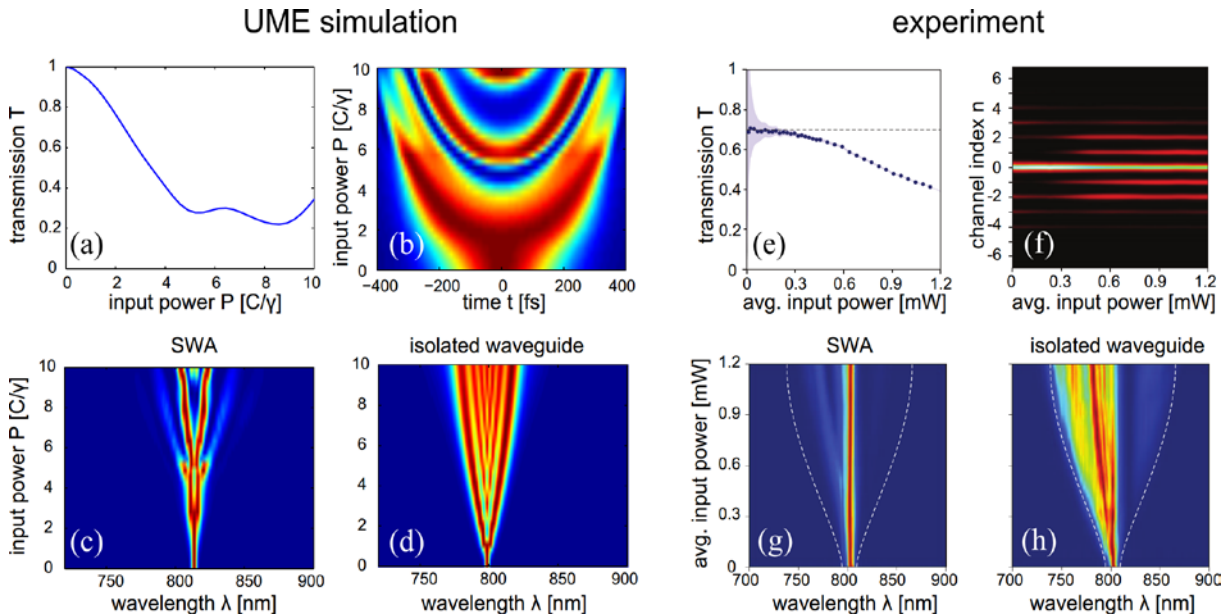


Fig. 20: (a-d) UME simulation of nonlinear ST pulse propagation in an SWA. (a) Transmission curve. (b) Temporal output pulse shape as for varying input powers. (c) Output spectrum of the SWA. (d) Output of an isolated WG. (e-h) Experimental data for a ST pulse propagating through an SWA. An average input power of 1.2 mW corresponds to roughly  $7.0 C/\gamma$ . (e) Transmission curve. (f) Field distribution at the SWA output as a function of the input power. (g) Output spectrum of the SWA. (h) Output spectrum of an isolated WG. Direct comparison of simulation and experimental power scales is impossible due to uncertainties of the input pulse shape. Figure adapted from [Hei12].

Results of UME simulations, where the excitation was a Gaussian pulse with a duration of 300 fs at a carrier wavelength of  $\lambda_0 = 800$  nm, are displayed in Fig. 20. Subfigure (a) displays the transmission as a function of the input peak power. While the shape of the curve is initially similar to the above discussed model it settles out at roughly 25% transmission and does then remain at roughly this value, reducing the switching contrast to 6 dB. The reason for this behavior can be seen in Fig. 20 (b), where the instantaneous optical power in the central WG at the end of the SWA is plotted as a function of the peak input power. Especially for high input powers the pulse no longer leaves the SWA as a cohesive entity but in parts. This is not unexpected for pulses propagating in the normal dispersion regime, where no LBs exist, which would force the pulse to act in a cohesive manner. The splitting into sub-pulses is attributed to the fact, that for each time slice the pulse has a certain instantaneous power, for which the SWA imaging either works, fails, or a spatial soliton is generated. Nevertheless SWA are still an

## 5.1 Nonlinear Self-Limiting in Segmented Waveguide Arrays

attractive candidate for OL, as long as the input power is kept below  $4c/\gamma$ , where nonlinear effects are weak and the pulse still emerges intact.

It is interesting to note, that in this regime the spectrum of the light transiting the SWA is broadened very little, as displayed in Fig. 20(c). The lack of spectral broadening is particularly evident if compared to the broadening occurring in an isolated WG for the same input pulses, as depicted in Fig. 20(d). SWAs are thus not only interesting candidates for OL but also for spectral stabilization, where a high power signal can be transmitted without the level of spectral deterioration usually encountered. One can think of SWA based spectral stabilization as a means to increase the effective area of a mode, by transiently distributing its power onto many WGs.

Results of the experimental verification of OL and spectral stabilization in SWAs are presented in Fig. 20 (f). Note that direct comparison of simulation and experimental power scales is impossible due to uncertainties of the input pulse shape. It shows the power dependent output pattern of the SWA, which was excited at the central WG only. At low input powers nearly all energy is leaving from the same WG, thus segmentation imaging works. Increase of power leads to a continuous increase of the amount of energy, which is leaving the other WGs, as expected for OL operation. The experimentally transmission curve is presented in Fig. 20(e). OL is clearly visible, proving the scheme works as expected. Fig. 20(g) and Fig. 20(h) show power dependent output spectra for (h) an isolated WG and (g) the SWA. The spectral stabilization effect is obvious, as for the SWA the spectrum does not visibly expand, whereas for the isolated WG it expands from less than 10 nm to more than 50 nm. The spectral asymmetry is due to residual third order chirp in the input pulse and can be reproduced by appropriate UME simulations. Experiments with input pulses modified by SPS (see Section 2.2) and OXFROG retrieval (see Section 3.3) are currently under way.

In summary we have exemplarily shown that WAs can be used to construct complex, nonlinear, all-optical elements. As such they are an interesting candidate for on-chip integration of ultrafast, all-optical devices in future terabit networks. More specifically we have demonstrated that SWAs can take the role of optical limiters. Rigorous ST modelling of pulse propagation in WAs is absolutely necessary to understand and to reliably predict their operation, even in the normally dispersive regime. Advanced ST analysis techniques will help us to further understand ST pulse propagation in WAs, in particular if operated in the near infrared, where anomalous dispersion causes the formation of LBs and the spatial and temporal aspects of pulse propagation will interact in a complex manner.

## 5. Results of Experiments and Simulations

### 5.2 Fundamental Light Bullets

A discussion of LBs in the context of nonlinear optics in WAs is given in Section 4.1. Here we shall concentrate on their observation and characterization in FAs.

At first, however, it is extremely useful to find steady state solutions of the NLSE Eq. (19). As discussed above this equation is “just” a qualitative model for ST pulse propagation. Similarly to Section 4.5 it is, however, helpful to determine the temporal scale, spatial size, and energy requirements of LBs with a certain level of accuracy. In fact, Eq. (19) is the only available model that features strictly stationary solutions. Moreover, Eq. (19) supplies a convenient framework to evaluate LB stability, something which cannot be done with simple analysis of scale arguments. Although these solutions are idealized (they are hence termed idealized LBs), they are pivotal in the verification of LB observation, as they represent a set of parameters against which experimental and numerical data can be tested. These solutions are therefore a conceptual device, the role of which is somewhat similar to the role of Kerr-solitons in supercontinuum generation [Dud06, Alf06]. There solitons do not exist in the sense of strict stationarity, however, certain features in the pulse dynamics have properties that locally approach that of solitons. Their specific properties might change slowly during propagation or abruptly during scattering events, however, they retain a robustness against dispersion, which is characteristic for solitary waves.

Properties of fundamental stationary solutions of Eq. (19) are depicted in Fig. 21, i.e., those solutions which are spatially located in a single WG and temporally in a single pulse. In the following sections we will discuss more complex solutions. The fundamental solutions constitute a one-parameter family of solitary waves, i.e. LBs, where the family parameter is the nonlinear phase shift  $b$ . There is a minimum value  $b_{\min}$  below which no LB solution exists, because the LB solution branches from the top of the dispersion relation at  $\Delta\beta = 6c$ . As opposed to spatial discrete solitons here  $b_{\min} > 6$ , which we attribute to dispersion, that has to be overcome, too. If the minimal phase shift is approached  $E(b \rightarrow b_{\min}) = \infty$ , i.e., they have infinite energy, as seen in Fig. 21(a). This is different from 1D solutions, where the energy goes to zero and from 2D solutions, where it approaches a finite value. These differences can be understood by arguments of scale [Sil90], as spatially broad solutions can be approximated by solutions of the continuous NLSE [Eil10].

The impact of discreteness, however, is evident for larger nonlinear phase shifts  $b$ . At a certain threshold nonlinear phase shift  $b_{\text{thresh}} \approx 8.43$  a minimum energy of  $E_{\text{thresh}} \approx 9.05E_0 \approx 27$  nJ is reached. All solutions with larger  $b$  have higher energy. This behavior was already described for 2D discrete spatial solitons [Eil10], its consequences for LB stability and dynamics are essential.

As seen in the inset of Fig. 21(a) at  $b_{\text{thresh}}$  the largest perturbation eigenvalue, attained from linear stability analysis [Hil00], becomes negative and all LB solutions with  $b > b_{\text{thresh}}$  are thus linearly stable. This finding is in agreement with the predictions of the Vakhitov-Kolokolov theorem [Vak73]. As all LBs, which we can hope to observe, in an experiment must be stable, they will have a minimum energy and, as can be seen from Fig. 21(b-d), a minimum power and a minimum of temporal and spatial localization. In particular, we cannot observe LBs with a duration of more than 15 fs for type I samples. These numbers reconfirm the predictions from Sections 4.3.2 and 4.5. Properties of particular solutions are outlined in Fig. 21(f-k), giving an impression of field distributions of LB solutions and of the general trend of increasing localization and power as a function of increasing nonlinear phase shift  $b$ .

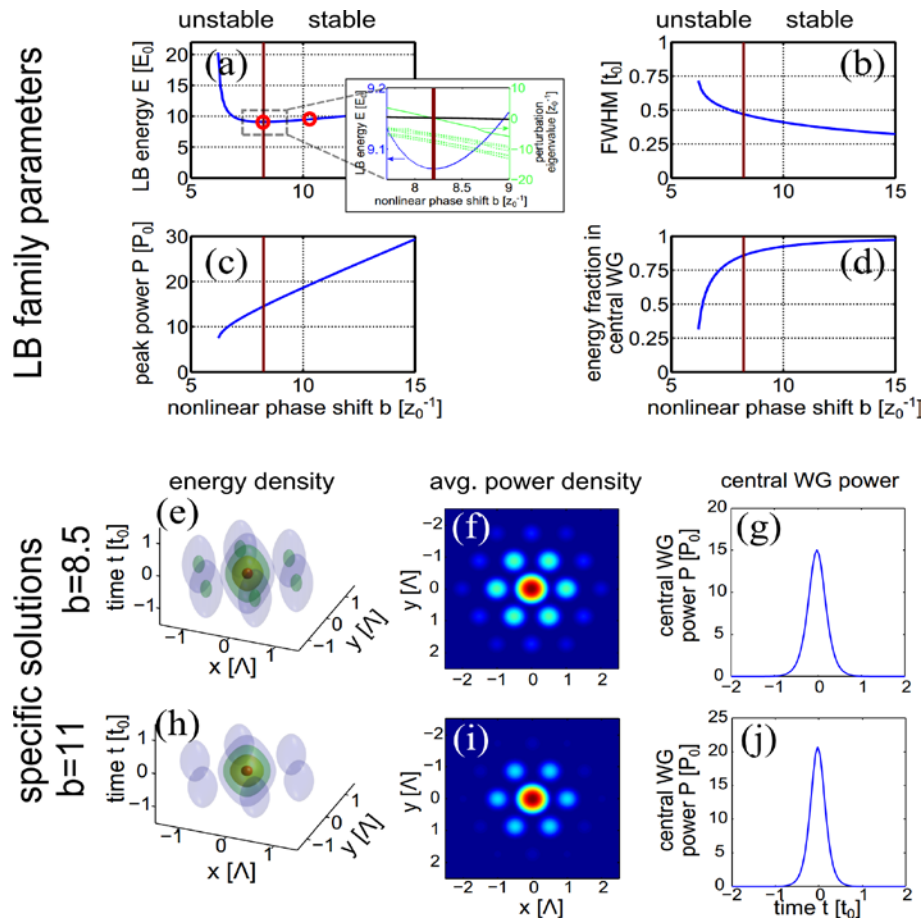


Fig. 21: (a-d) Parameters of the fundamental LB family as a function of the nonlinear phase shift  $b$ . (a) LB energy. (b) LB FWHM duration. (c) LB peak power. (d) Fraction of energy in the central WG. (a, inset) Zoom into (a) close the point of minimal energy ( $b_{\text{thresh}}$ ,  $E_{\text{thresh}}$ ). The green line displays the largest perturbation eigenvalues. The transition from linear instability (at least one positive eigenvalue) to stability (all eigenvalues negative) occurs at  $b_{\text{thresh}}$ , and is marked by the red line, as (a-d), too. (e-j) Exemplary features for LB solutions marked with red circles in (a). (e,h) 3D ST isointensity plots. (f,i) Energy density as would be recorded by a camera, i.e., a slow spatial detector. (g,j) Pulse power in the central WG. Subfigures (a)-(d) adapted from [Eil11a].

It is now instructive to investigate the result of simulations of the UME model. Due to the limitation of pulse duration and pulse shaping capabilities direct excitation of LBs is impossible.

## 5. Results of Experiments and Simulations

Moreover, it must be noted that our first experiments in this direction had been made with an older laser system, which only delivered 170 fs pulses at 1550 nm, instead of the 50 fs stated in Section 2.1 and the reference pulse duration was close to 60 fs. Thus the iXCorr resolution was not nearly good enough to measure the LB duration, nor the absence of linear broadening. Rigorous numerical modelling then proved to be a key element in the observation of LBs.

Results of the solutions of the UME model (Eq. (20)) with an input pulse duration of  $t^{(0)} = 170$  fs and an energy of  $E = 153$  nJ are shown in Fig. 22. This is roughly five times the expected minimum energy  $E_{\text{thresh}} = 27$  nJ, such that sufficient power overhead is available for the nonlinear pulse contraction. In fact, we have later shown that only 80 nJ are necessary to excite a LB. Fig. 22(a) shows the pulse power evolution in the central WG of the FA. The evolution is split into three phases. In phase I at  $z < 15$  mm the pulse contracts to a duration of roughly 25 fs. In phase II at  $15 \text{ mm} < z < 40$  mm two distinct, short pulses separate from the main peak and decelerate, i.e. they propagate at a lower group velocity than the dispersive waves. The trailing waves quickly disperse. In phase III the two short pulses decay themselves. The properties of the most retarded pulse are displayed in Fig. 22(b) and Fig. 22(c). Here we have plotted the pulse duration, wavelength, and fraction of the total energy contained in this pulse. The pulse's duration is nearly stationary. The temporal broadening of a hypothetical pulse of the same duration, affected by linear dispersion only, is shown by the dashed line in Fig. 22(b). This pulse would disperse quickly, whereas the pulse we actually observe is subdispersive. The same argument applies to the energy content of the LB. It is slowly decreasing but much slower than would be expected for a field that is affected by discrete diffraction only.

The behavior observed in phase II is driven by the evolution of the central wavelength, which grows steadily during propagation, reducing propagation speed and increasing pulse delay. Such behavior is typical for solitary waves affected by SRS. Its influence on ST pulse propagation is, however, much more complex. As seen in Section 4.3.2 all linear effects become more influential for longer wavelengths, whereas the nonlinear coefficient decreases. Therefore the characteristic energy  $E_0$  grows rapidly for increasing wavelength. A once excited LB, which has a fixed energy, must thus react to the growing  $E_0$  by evolving towards a smaller normalized energy. It then shifts from its initial excitation point on the  $E(b)$  curve in Fig. 21(a), towards lower normalized energy and lower values of  $b$ . This is necessarily accompanied by a reduction of the spatial and temporal localization. The ST field distribution is displayed Fig. 22(d), which shows an isointensity plot of the field at the end of phase II, together with a projection onto the  $x - t$ . The most retarded pulse is already decaying, whereas the second pulse is still constitutes a well-confined LB. Both pulses are preceded by delocalized dispersive radiation.

## type I sample

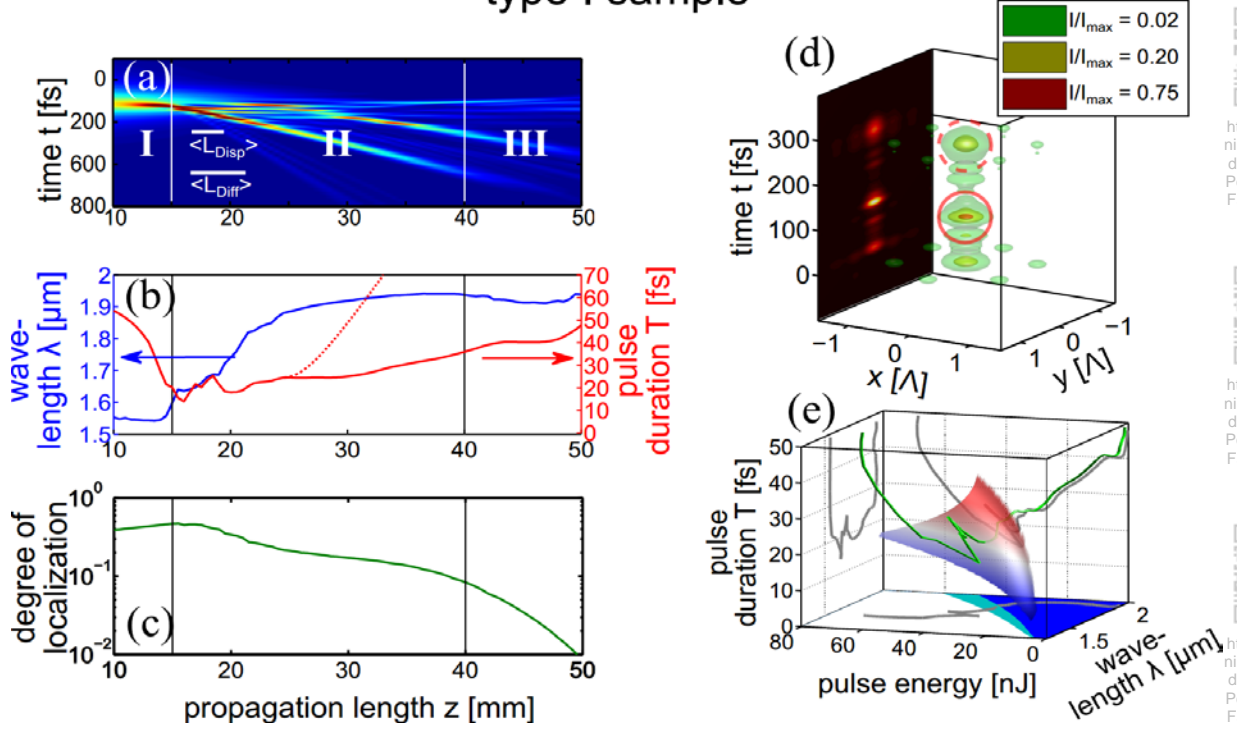


Fig. 22: UME simulations of LB formation, evolution, and decay in a type I FA with  $E = 150$  nJ excitation energy. (a) Instantaneous power vs. propagation length in central WG. (I), (II), (III) Evolution phases. Lines mark their limits. Scale bars mark averaged dispersion and diffraction lengths. (b) Wavelength and pulse duration of the most retarded peak vs. propagation length. (c) Fraction of the total energy in the central WG of the most retarded peak. (d) Isointensity plots at  $z = 35$  mm. Red, solid circles indicate LB locations. Red, dashed circles indicate LB leftovers after decay. The color plot is a projection onto  $y - t$ -plane. (e) Trajectory of properties of the most retarded pulse in the energy-duration-wavelength space. The colored surface indicates the locations of stationary NLSE solutions. The gray lines are projections of the green line. No LB solutions on the dark blue surface, LB solutions unstable on the bright blue surface, and LB solutions stable on the white surface. Subfigures (a), (b), (c) adapted from [Eil11a].

Due to the increasing wavelength both the dispersion length  $L_{\text{Disp}}$  and diffraction length  $L_{\text{Diff}}$  are modified. To measure the length of phase II in terms of these quantities we therefore modify Eqs. (21) and (22), introducing an average dispersion length  $\langle L_{\text{Disp}} \rangle$  and diffraction length  $\langle L_{\text{Diff}} \rangle$

$$\begin{aligned} \langle L_{\text{Diff}} \rangle &= (z_2 - z_1)^{-1} \int_{z_1}^{z_2} \frac{\pi}{12c [\lambda_c(\tilde{z})]} d\tilde{z} \\ \langle L_{\text{Disp}} \rangle &= (z_2 - z_1)^{-1} \int_{z_1}^{z_2} \frac{(T(\tilde{z})/1.66)^2}{|\beta_2[\lambda_c(\tilde{z})]|} d\tilde{z}, \end{aligned} \quad (25)$$

where  $\lambda_c$  is the local carrier wavelength of the pulse and  $z_1$  and  $z_2$  mark the limits of phase II. The pulse propagates over a LB length  $L_{\text{LB}} = z_2 - z_1$  of roughly  $5.3\langle L_{\text{Diff}} \rangle$  and  $9.0\langle L_{\text{Disp}} \rangle$  in a stationary manner, such that one can speak of the existence of LBs with good justification.

The transition into phase III is marked by a sudden loss of LB energy and the onset of dispersive broadening. It is the natural consequence of the above described evolution. As the LB increases in wavelength and evolves due to the increase of the characteristic energy  $E_0$ , its energy content

## 5. Results of Experiments and Simulations

is eventually equal to the threshold energy for LB formation  $E_{\text{thresh}}$ . This is the point, which marks the transition into phase III, where LBs become unstable and consequentially decay.

This line of argumentation is augmented by the data displayed in Fig. 22(e). The curved surface shows the duration of idealized LBs as a function of the wavelength and the energy content in the central WG. It was synthesized from the curves in Fig. 21 and the wavelength dependent parameters in Fig. 16. The line is compiled from the pulse parameter trajectory in Fig. 22(b). The bounding surfaces display projections onto corresponding subspaces. The trajectory approaches the surface of idealized LB solutions in phase I, it then remains close to this surface in phase II, during which it moves into the region with unstable solutions and eventually into the region without solutions altogether. This transition marks the beginning of phase III, in which the pulse trajectory leaves the surface. Evolution of the trajectory towards the surface proves that LB solutions serve as a nonlinear attractor of the systems dynamics, again underlining the nature of LBs being solitary waves.

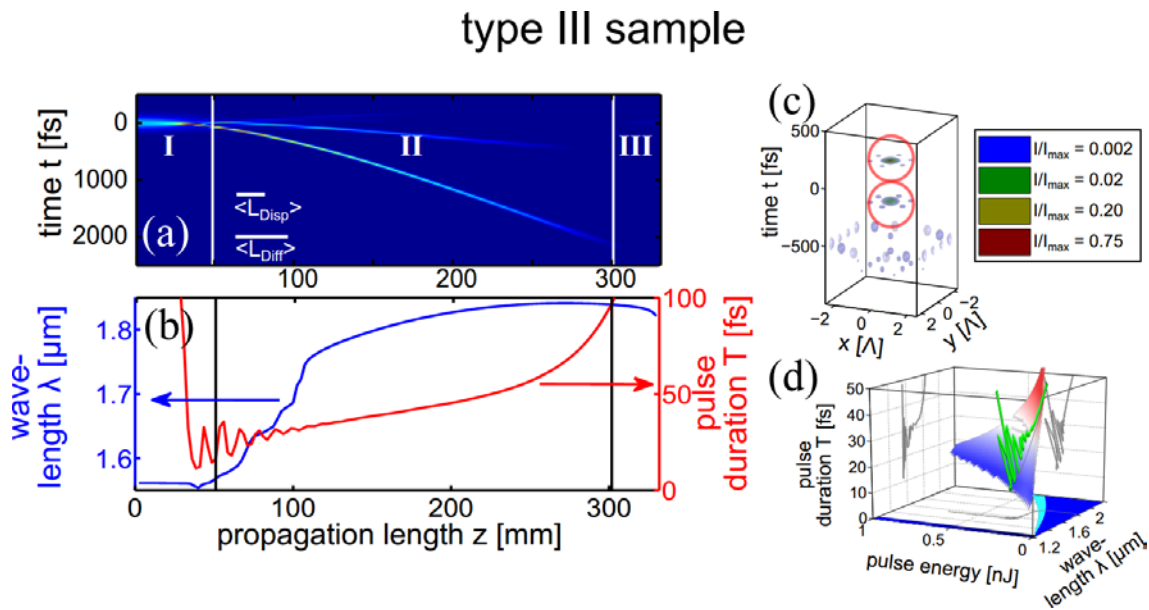


Fig. 23: UME simulations of LB formation, evolution, and decay in a type III FA with  $E = 9$  nJ excitation energy. (a) Instantaneous power vs. propagation length in central WG. (I), (II), (III) Evolution phases. Lines mark their limits. Scale bars mark averaged dispersion and diffraction lengths. (b) Wavelength and pulse duration of the most retarded peak vs. propagation length. (c) Isointensity plots at  $z = 200$  mm. Red, solid circles indicate LB locations. (e) Trajectory of properties of the most retarded pulse in the energy-duration-wavelength space. The colored surface indicates the locations of stationary NLSE solutions. The gray lines are projections of the green line. No LB solutions on the dark blue surface, LB solutions unstable on the bright blue surface, and LB solutions stable on the white surface. Figure adapted from [Eil11a].

It must be noted however, that the pulse duration settles out at no less than 25 fs, whereas the idealized solutions in this wavelength range predict a maximum LB duration of 15 – 19 fs. This discrepancy is due to the comparatively strong impact of higher order effects, e.g., high order dispersion. This is proven by another simulation in a type III fiber, where the characteristic time

$t_0$  is roughly twice as long, mitigating higher order effects. Data of this simulation is displayed in Fig. 23. Here an input energy of 9 nJ was used and we observe the same three evolution phases, as can be seen from the power evolution in the central WG in Fig. 23(a). The pulse parameter evolution curve is displayed in Fig. 23(b). A snapshot of the ST intensity distribution towards the end of phase II is displayed Fig. 23(c). Here a separation of two well-localized LBs trailing a set of diffracted waves is clearly visible. In type III samples the trajectory of the LB parameters approaches the ideal LB surface very closely, as can be seen in Fig. 23(d). The measured pulse duration is 35 fs and the duration of the idealized solution is 31 – 40 fs, supporting the notion of the idealized LBs acting as a nonlinear attractor for the ST pulse dynamics in DO systems.

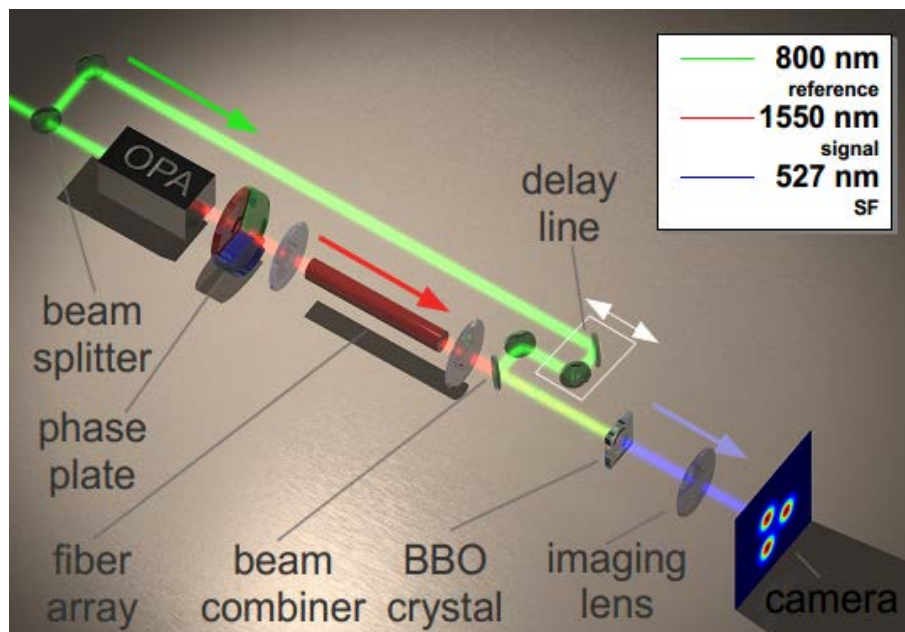


Fig. 24: Scheme of the LB and VLB experiments with iXCorr analysis stage. Beam propagation left to right. An  $\lambda = 800$  nm pulse (green) is split. The 1<sup>st</sup> part bypasses the experiment through a delay line and impinges on a BBO crystal. The 2<sup>nd</sup> part is converted to  $\lambda = 1550$  nm in an OPA (red). It is focused onto the front of the FA, exciting a Vortex LB or an ordinary LB if the phase plate is removed. A 2<sup>nd</sup> lens images the output onto the BBO crystal. This crystal generates sum-frequency light (blue), which is imaged onto a CCD, recording iXCorr data at the FA end. The phase plate is only present for VLB experiments (see Section 5.4). Figure adapted from [Eil13c].

The  $L_{LB}$  for type III FAs is of course longer. In terms of diffraction and dispersion lengths one gets  $L_{LB} = 6.4\langle L_{Diff} \rangle = 11.2\langle L_{Disp} \rangle$ , which is slightly more than for type I FAs. An estimate of the dependence of  $L_{LB}$  on the array properties was carried out in [Eil11a], where we found that  $L_{LB}/\langle L_{Diff} \rangle \sim c^{-q}$ , where  $1/2 < q < 1$ . Here the value is  $q = 0.19$ , somewhat smaller than predicted. Nevertheless, either value underlines, that a reduction of the coupling strength will extend the normalized LB lifetime, but only at a very moderate rate.

## 5. Results of Experiments and Simulations

Now that we have established important parameters for the propagation of LBs, such as required pulse energies and sample lengths, we can tackle the experimental observation of LBs. A schematic representation of the experimental setup is displayed in Fig. 24. An 800 nm pulse is split. The first part is used to pump an OPA, emitting a pulse at 1550 nm, which is focused onto the central WG of the FA (the phase plate is only present for Vortex Light Bullets experiments, discussed later in Section 5.4). The back surface of the FA is imaged onto a  $\chi^{(2)}$ -crystal. The second part of the 800 nm pulse is used as a reference, which co-propagates through the crystal. The part of the experiment after the crystal forms an iXCorr setup, the details of which are discussed in Section 3.1.

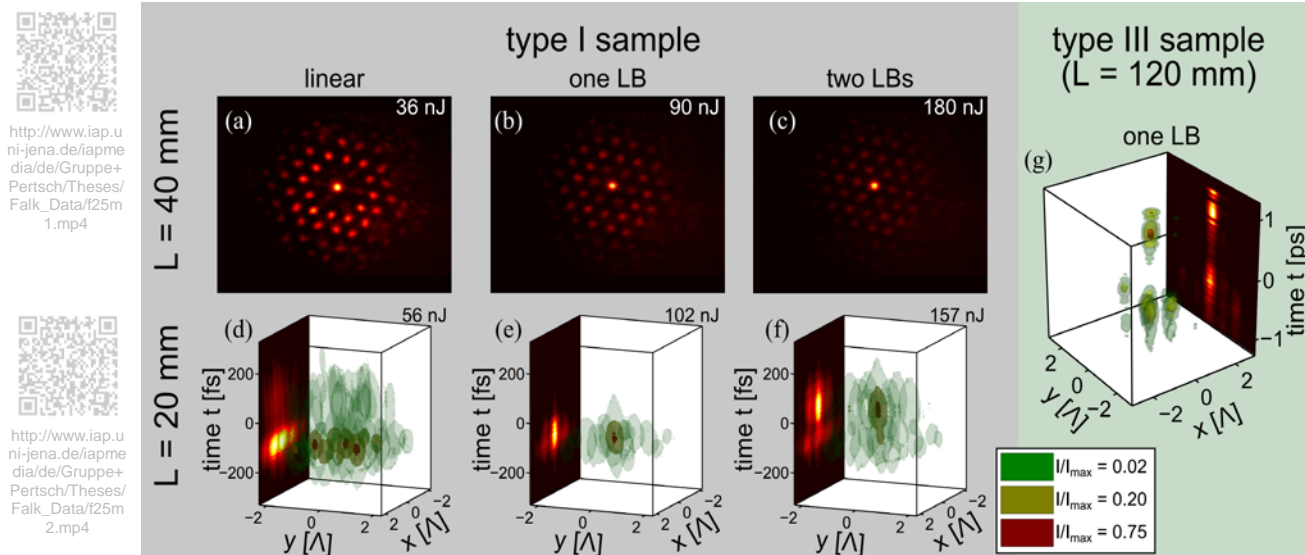


Fig. 25: Experimental data of iXCorr analysis of LB propagation in (a-f) a type I FA of (a-c)  $L = 40$  mm and (d-f)  $L = 20$  mm and (g) a type III FA of  $L = 120$  mm. (a-c) Time averaged camera images at different input energy levels in (a) the linear regime, (b) the single LB regime, and (c) the double LB regime. (d-g) iXCorr isointensity plots in the same input energy regimes. Subfigures (a)-(c) adapted from [Eil11a].

Results for the experiment are displayed in Fig. 25. In Fig. 25(a-c) camera images of the output facet of a type I fiber with a length of  $L = 40$  mm for varying input energies are displayed. The first image is below the LB threshold energy and linear broadening is observed. Increase of power leads to some degree of spatial localization. More instructive is the data obtained from iXCorr traces, displayed in Fig. 25(d-f). ST broadening is visible in the low power case. In the  $E = 102$  nJ experiment full ST reshaping of the light field is observed, where a ST localized wavepacket, with a length that is equal to the iXCorr resolution, contains almost all energy of the LB. Increase of the energy to  $E = 157$  nJ generates a similar pattern with more dispersive waves preceding the localized wavepacket. The temporal separation of the localized wave from the dispersive wave is roughly 150 fs. These results are in agreement with the above discussed simulations. An iXCorr trace from a similar experiment in a type III fiber with a length of  $L = 120$  mm is displayed in Fig. 25(g). Here the temporal separation of the LB from the

dispersive background is even more obvious, due to the longer sample, which maps a similar increase in wavelength into a larger delay.

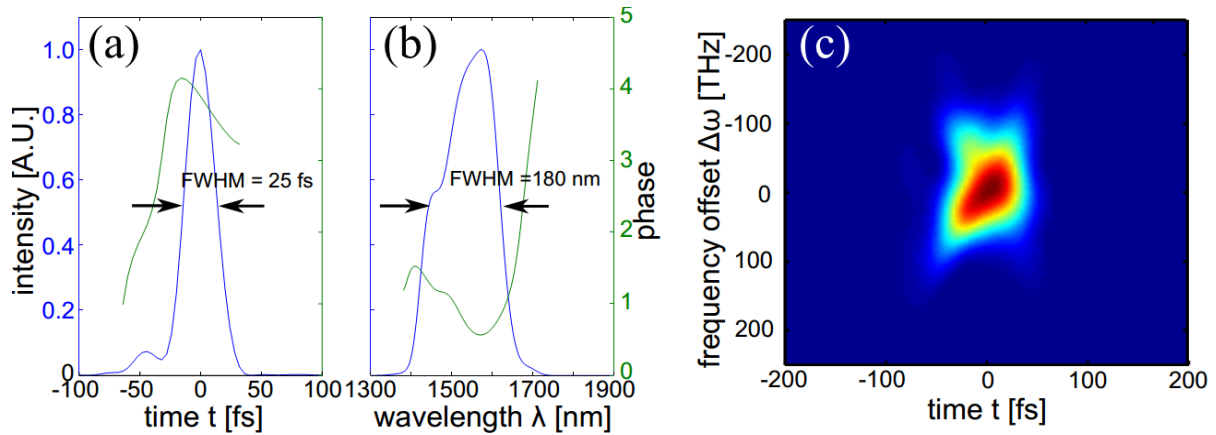


Fig. 26: ImXFROG reconstruction of a LB in a 30 mm type I FA. The excitation pulse is a 50 fs Gaussian at 1550 nm. (a) Temporal, (b) spectral, and (c) spectrographic representation. The pulse is composed of a leading, blue-shifted, dispersive part, trailed by a red-shifted LB. The pulse is essentially transform-limited. Figure adapted from [Eil13a].

The validation of the compression to the value predicted from the solution of the UME equations was carried out in a later experiment [Eil13a] with an  $L = 30$  mm type I sample and the laser system introduced in Section 2.1, using the ImXFROG technique (see Section 3.2). Results are displayed in Fig. 26. We observe a transform limited  $T = 25$  fs pulse with a bandwidth of 180 nm and a time-bandwidth product of  $< 1.2$ . The pulse is redshifted from the excitation wavelength and is preceded by a blue-shifted pedestal of dispersive waves. Linear broadening over the sample length would lead to a duration of roughly 90 fs and strong pulse chirp. Freedom of chirp and the correct prediction of the pulse duration are the definite proof of the dispersion-freeness of the pulse and of the solitary nature of LBs.

More systematic experiments reproduce all other essential features of the evolution dynamics. A set of low-resolution ImXFROG measurements of the central WG pulse in type I samples of various lengths and an input energy of  $E = 150$  nJ are shown in Fig. 27, together with their numeric counterparts. Both sets of data agree very well. Low-resolution ImXFROG traces have been recorded with the ImXFROG setup (see Section 3.2), but only with coarse IF filters and no FPI. Retrieval of the signal from the FROG traces was thus impossible. However, extraction of overview data and comparison of the FROG traces with numerical results was still found to be helpful. The FROG trace of the shortest sample shows the onset of the development of two redshifted LBs, together with a blueshifted dispersive wave. The redshift is much more pronounced for the  $L = 40$  mm samples; the most retarded LB has already left the measurement window. Only residual radiation can be observed for the  $L = 60$  mm sample.

## 5. Results of Experiments and Simulations

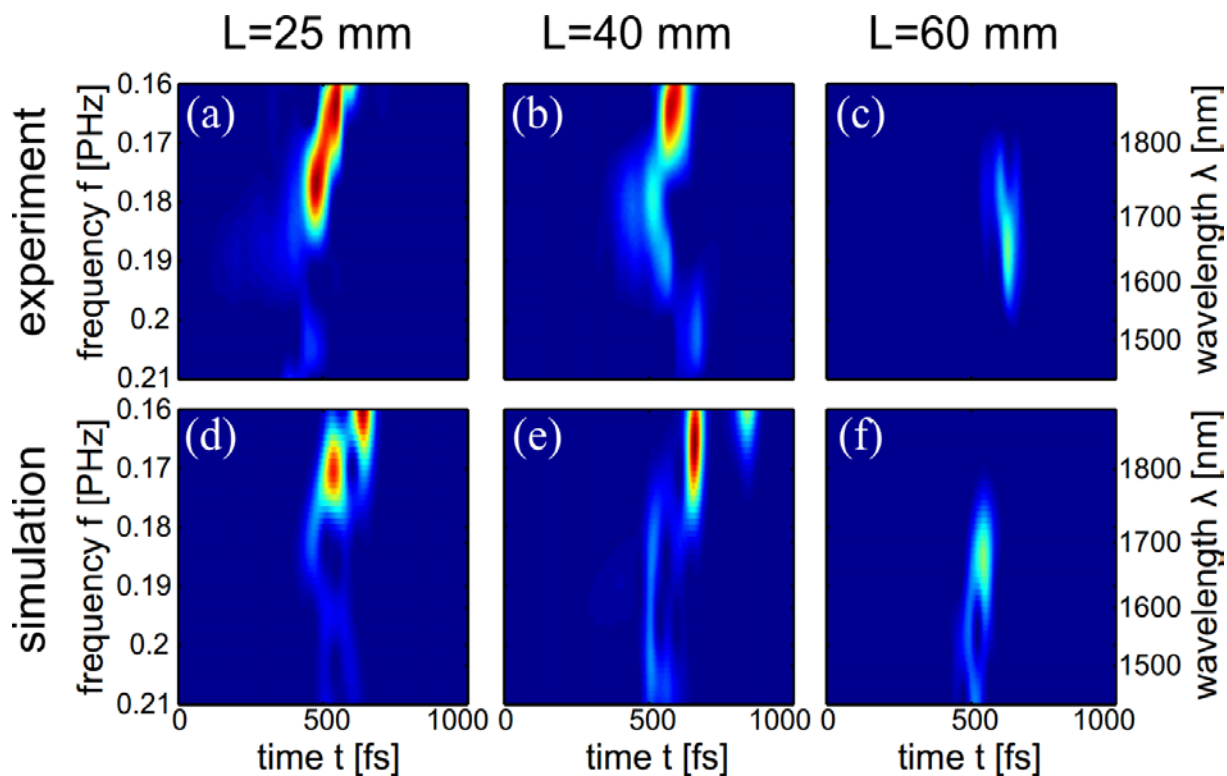


Fig. 27:(a-c) Experimental and (d-f) simulated low-resolution ImXFROG traces of the field in the central WG of a type I FA with a  $T = 170$  fs excitation pulse of  $E = 150$  nJ energy. Shown are sample lengths (a,d) 25 mm, (b,e) 40 mm, and (c,f) 60 mm. Two red-shifted and delayed LBs are visible at 25 mm. At 40 mm the more red-shifted LB has left the wavelength window of the detector, only a small part is still visible in the simulation. Short wavelength residual radiation is preceding the LBs. Only dispersive radiation is detectable at 60 mm. Figure adapted from [Eil11a].

Fig. 28 displays measured cross correlation traces of the central WG of a type I FA with a length of  $L = 20$  mm and therefore at the initial stages of the LB formation process and with a length of  $L = 60$  mm after all LBs have decayed. All traces are plotted for a range of excitation energies, which span from the linear regime, well into the LB regime and have been made with an input pulse duration of  $T = 50$  fs. For the short sample red-shifting induced delay, whose magnitude grows with increasing input power is observed, together with a weak peak of leading dispersive radiation. Pulse contraction cannot be observed due to the limited resolution of the iXCorr system. Pulse splitting related to the excitation of multiple LBs cannot be observed due to the short sample length. No LBs can be observed for the long samples. Nevertheless we observe weak peaks of delayed radiation. The number of the peaks grows by one for roughly every 80 nJ of input energy. These are the leftover of LBs, which have decayed after they reached the end of their life cycle in phase III. Although they broaden and loose energy they still propagate at a considerably slower speed than the dispersive radiation and can thus be distinguished.

Moreover from this data we conclude that for the excitation of a single LB an energy of roughly

$E = 80$  nJ] is required for an input pulse duration of 50 fs. As the LB has a minimal energy of  $E_{\text{thesh}} = 9.05E_0 = 31$  nJ], this means that LBs can be excited with a efficiency of roughly 40% for type I samples. This finding is backed up by simulations.

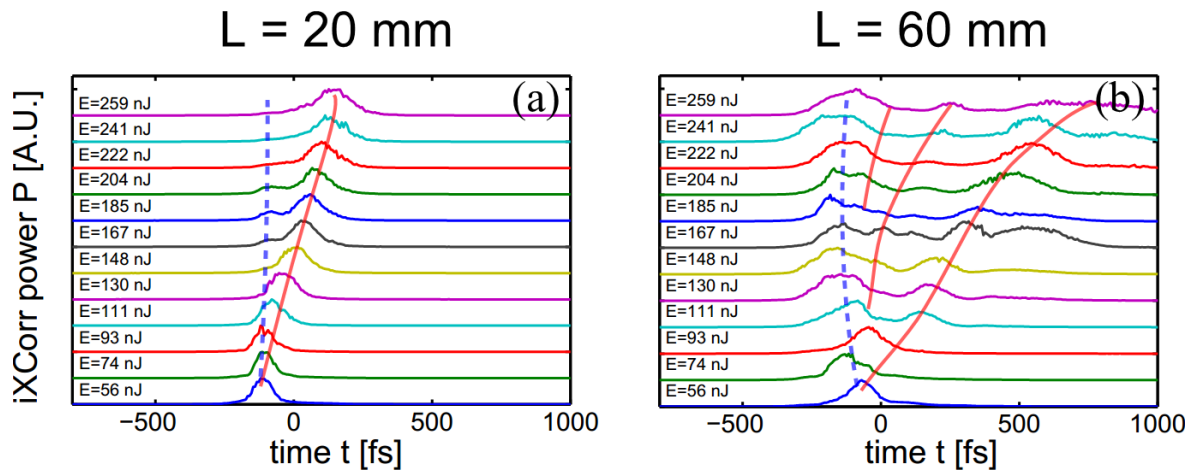


Fig. 28: Cross-correlation measurements of light leaving the central WG of a type I FA. (a) after the point of creation of the first LB at  $L = 20$  mm and (b) after the point of LB decay at  $L = 60$  mm for various input intensities. Marked are (blue, dashed) the dispersive wave peak, (red, solid) the LBs (20 mm sample), and the residual leftovers of decayed LBs (60 mm sample) and how they move as a function of the input energy  $E$ . Figure adapted from [Eil11a].

In summary we have shown that stable LBs exist in FAs and that they can be excited and observed in an experiment. As opposed to their low dimensional cousins they have a maximum duration and minimum energy threshold. They are locally robust against perturbations such as higher order dispersion, the Raman effect and self-steepening, and the wavelength dependence of the coupling. They exhibit a novel kind of evolution behavior that is driven by the Raman redshift. This behavior can be broadly characterized by three phases: generation by self-contraction, stationary propagation with adiabatic redshift, and decay through the growth of the energy threshold. This phenomenon is linked to the thresholds mentioned above, thus a consequence of the dimensionality, and therefore a genuinely ST effect. It limits the possible propagation length of LBs in FAs of the basic design considered here to a few tens of dispersion lengths. More advanced sample designs might surpass this limitation but are beyond the scope of this work.

### 5.3 Direct Spacetime Coupling

We have seen in the last chapter that the intriguing LB evolution behavior is triggered by the intrinsic, temporal asymmetry of the Raman response. We will now closely investigate the consequence of another type of intrinsic asymmetry: the wavelength dependence of the coupling strength  $c(\omega)$ . On the one hand it constitutes a temporal asymmetry, similar to the delayed Raman response, because any frequency dependent factor in the propagation model acts like a convolution with a non-instantaneous response function in time domain. On the other hand it is

## 5. Results of Experiments and Simulations

qualitatively different in that it does not mix dispersion and nonlinearity, as the delayed Raman response does, but it mixes diffraction and dispersion. Such a mixing on the level of the propagation equation (i.e., without mediation by the field) is referred to as direct space-time-coupling (DSC).

DSC is closely related to the concept of group velocity in multi-modal systems. The group velocity in systems with DSC is by no means bounded to the speed of light in a medium. In fact, superluminal, as well as, subluminal propagation of light pulses have been reported in various media [Dog01b, Dog01a, Ste93, Kuz01, Ste03], raising the discussion if signals could propagate faster than light [Nim99]. However group- and signal velocity are two different measurables. The limits of relativity do apply to the latter [Ste03]. Superluminal as well as subluminal pulse propagation in systems with DSC can be explained on the basis of the Gouy phase [Por02, Por03]. The characterization of superluminal pulse propagation in the context of LBs in FAs is at the focus of Section 5.3.2.

The coupling of spatial and temporal frequency components also leads to a non-factorizable ST structure of pulses. While these pulses can be generated using linear optical elements, another established route to achieve such coupling is to exploit non-linear pulse reshaping to generate fields with DSC. Some examples are tilted pulses [Mar89], and their axially symmetric generalization (X-like waves [Saa97]), as well as helical beams in Raman media [Gor07a]. They can be generated in quadratic [DT03] and Kerr nonlinear media with normal dispersion, sustaining the spontaneous generation of X-like waves [Fac06, Min09a, Blo09] propagating sub- or superluminally. In 1D nanowire WAs the coupling of spatial and temporal dispersion makes the zero-dispersion wavelength dependent on the supermode and thus on the excitation condition. This has a strong impact on quasisoliton-induced Supercontinuum-generation [Ben09, Ben08, Gor10]. In Section 5.3.1 we will show how the nonlinear effects associated with LB propagation imprint a dependence of spatial and temporal coordinates in the spectrum onto a previously factorizable ST pulse.

At this point, we first explore the origin of the DSC in FAs and compare it to DSC in homogeneous materials. DSC occurs if the curvature (i.e., the Hessian matrix) of the dispersion relation cannot be factored into a spatial and temporal part, that is, if  $D_{21} = D_{12} \neq 0$  or  $D_{13} = D_{31} \neq 0$ , where

$$D_{nm} = \frac{\partial^2 \beta}{\partial \xi_n \partial \xi_m}, \quad \xi_1 = \omega, \xi_2 = \mu, \xi_3 = \nu, \quad (26)$$

where  $\mu$  and  $\nu$  are the transverse wave vector components,  $\omega$  is the frequency and  $\beta =$

$\beta(\omega, \mu, \nu)$  is the longitudinal wavevector component of the medium (or of a certain Bloch band in case of a periodic medium). In this sense DSC acts like a form of spatiotemporal anisotropy: it forces the eigenvectors of  $D_{nm}$  to have both spatial and temporal, non-zero components. Thus wave propagation is not a superposition of purely spatial diffraction and purely temporal dispersion, both effects are intermixed instead. Eq. (26) can be derived from the propagation equation. In case of a FA the propagation equation takes a generalized form of Eq. (19), which reads as

$$i \frac{\partial}{\partial \zeta} a_{nm}(\zeta, \tau) = \mp \frac{1}{2} \frac{\partial^2}{\partial \tau^2} a_{nm}(\zeta, \tau) + |a_{nm}(\zeta, \tau)|^2 a_{nm}(\zeta, \tau) + \left(1 + i\alpha_1 \frac{\partial}{\partial \tau}\right) [a_{n\pm 1m}(\zeta, \tau) + a_{nm\pm 1}(\zeta, \tau) + a_{n\pm 1m\pm 1}(\zeta, \tau)], \quad (27)$$

where  $\alpha_1 = c_1(c_0|\beta_2|)^{-1/2}$  is the dimensionless STC coefficient. It is related to the wavelength dependence of the coupling coefficient  $c(\omega)$ , which was expanded into a Taylor series around the carrier wavelength  $\lambda_0 = 2\pi c/\omega_0$  and cut off after the linear term  $c(\omega) \approx c_0 + c_1(\omega - \omega_0)$ . A plot of the magnitude of  $\alpha_1$  is given in Fig. 29 for type I and type II FAs. It is evident that both arrays exhibit negative STC, as  $\alpha_1 < 0$ , which is due to the increase of  $c$  with increasing wavelength, i.e., the increase of  $c$  with decreasing frequency  $\omega$ . The quantity of  $\alpha_1$  can be influenced by selection of the FA type. Here we consider only type I and type II arrays. Both have a considerable magnitude of STC, i.e., we can expect a measurable impact of STC on LB propagation. Moreover, we note that  $\alpha_1$  is nearly constant over the wavelength range  $1500 \text{ nm} < \lambda < 2000 \text{ nm}$ , which is relevant for LB propagation. Thus the linear cutoff of the series expansion of  $c(\omega)$  is justified. Experiments in this section are carried out in type II FAs, due the larger magnitude of their STC coefficient  $\alpha_1$ .

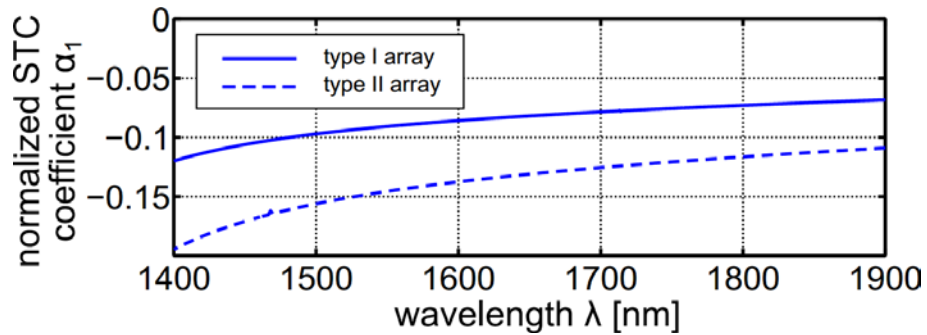


Fig. 29: Dimensionless STC coefficient  $\alpha_1$  vs carrier wavelength for (solid) type I FAs and (dashed) type II FAs. Figure adapted from [Eil11b].

The dispersion relation in physical units including STC is

$$\beta(\omega) = \beta_0(\omega) + 2[c_0 + c_1(\omega - \omega_0)](\cos(\nu) + \cos(\mu) + \cos(\nu + \mu)). \quad (28)$$

The dispersion relation for homogeneous space can be obtained from the Helmholtz-Equation

## 5. Results of Experiments and Simulations

with the approximation of forward-moving waves

$$\beta^{(\text{hom})} = k(\omega) - \frac{k_x^2 + k_y^2}{2k_0} \left[ 1 - \frac{\omega - \omega_0}{k_0 v_g} \right], \quad (29)$$

with  $k_0$  representing the wavevector at the central frequency  $\omega_0$ , the corresponding group velocity  $v_g$ , and the transverse wavevector components  $k_x$  and  $k_y$  in place for  $\mu$  and  $\nu$ . The cross diagonal entries  $D_{13} = D_{31}$  for the Hessian matrices are then

$$\begin{aligned} D_{13} &= D_{31} = -2c_1 (\sin(\nu) + \sin(\nu + \mu)) \\ D_{13}^{(\text{hom})} &= D_{31}^{(\text{hom})} = \frac{k_y}{k_0^2 V_g^0}. \end{aligned} \quad (30)$$

Thus, both wave propagation in homogeneous media and in DO systems are influenced by STC. The influence is, however, quantitatively different and can be approximated by comparing the magnitude of the diagonal and cross-diagonal elements of the respective Hessian matrices. If we assume for both that the excitation is a more or less transform limited pulse with duration  $t^{(0)}$ , such that  $\omega - \omega_0 \approx 1/t^{(0)}$ , we can derive a minimal pulse duration  $t_{\min}$ , which is needed for the cross diagonal terms to become influential:

$$\begin{aligned} t_{\min} &\approx \frac{c_1}{c_0} = 100 \text{ fs} \\ t_{\min}^{(\text{hom})} &\approx \omega_0^{-1} = 1.2 \text{ fs}, \end{aligned} \quad (31)$$

where the values have been obtained for light with a wavelength of  $\lambda = 1500$  nm and a type II FA. The value  $t_{\min}$  is to be understood in the sense that for longer pulses the effect of STC is of increasingly less influence. Thus STC based effects in homogeneous media can only be observed for almost single-cycle pulses, for which Eq. (29) fails anyway. In DO systems we can observe effects based on STC for reasonably short pulses. DO systems are therefore an ideal system to study STC effects. Moreover, one can tune the degree of STC by changing the wavelength dependence of the WG coupling, e.g., by varying the array geometry.

Now that we have established that STC is an important effect in the propagation of ultrashort pulses in FAs we will turn to the details and see how it affects the static properties of LBs in Section 5.3.1, as well as, their dynamic evolution in Section 5.3.2.

### 5.3.1 Spectral Symmetry Breaking of Light Bullets

The stationary properties of idealized LBs have been discussed in Section 5.2, with an overview of their properties given in Fig. 21. Among other approximations we had assumed that the

coupling coefficient  $c$  does not depend on the wavelength. We now lift this assumption and solve for stationary solutions of Eq. (27), instead of Eq. (19).

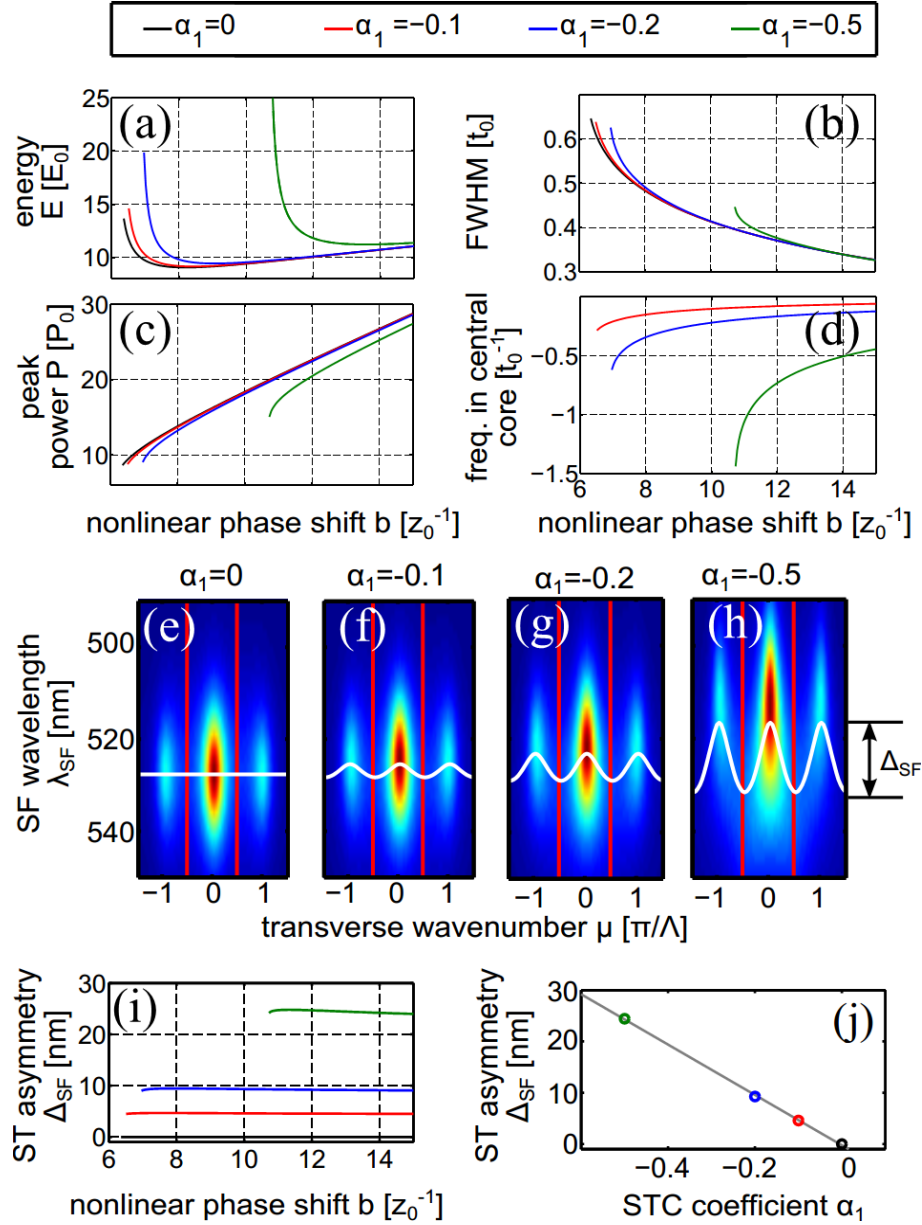


Fig. 30: (a-d) Parameters of the LB family as a function of the nonlinear phase shift  $b$  for four levels of STC. For  $\alpha_1 = 0$  the results of Fig. 21 are reproduced. (a) LB energy. (b) LB FWHM duration. (c) LB peak power. (d) Frequency shift in the central WG of the FA compared to the carrier frequency. (e-h) ST spectra for LBs with  $b = 15$ .  $\mu$  is the transverse wavenumber along one dimension whereas  $\nu = 0$ .  $\lambda_{SF}$  is the wavelength of the sum-frequency light for a carrier wavelength of  $\lambda = 1550$  nm a reference wavelength of  $\lambda_{Ref} = 800$  nm and a type II FAs. (White lines) denote the mean wavelength vs the transverse wavenumber. The ST asymmetry value  $\Delta_{SF}$  is the peak-to-valley-value of this mean wavelength. (i) ST asymmetry value  $\Delta_{SF}$  for the four LB families as a function of the nonlinear phase shift  $b$ . (j) Mean ST asymmetry value vs. STC coefficient for (points) the data taken from (i) and (gray line) linear fit. Figure adapted from [Eil11b].

Properties of these LB solutions are displayed in Fig. 30. Subfigures (a-c) display energy, duration and peak power as a function of the nonlinear phase shift for various values of the STC coefficient  $\alpha_1$ . Note that typical values for type II FAs, used for the experiments discussed here, are in the range between  $-0.2 < \alpha_1 < -0.1$  as can be seen from Fig. 29. The curves for  $\alpha_1 = 0$

## 5. Results of Experiments and Simulations

are the same as those presented in Fig. 21(a-c) and serve as a reference. It can be seen that an increase in the STC coefficient leads to an increase in the minimal nonlinear phase shift  $b_{\min}$ , which we attribute to the larger effective coupling coefficient experienced by the long-wavelength components of the LBs. LBs with higher values of  $\alpha_1$  also need more peak power and have a shorter duration. Fig. 30(d) shows the shift of the mean frequency in the central WG of the FA with respect to the carrier frequency. The light in the central WG of the FA is thus shifted to considerably lower frequencies and thus longer wavelengths.

A better overview over the spectral properties of the LB spectra is given in Fig. 30(e-h). Here we have plotted the ST spectra of LBs with  $b = 15z_0^{-1}$  for the four discussed values of the STC coefficient  $\alpha_1$ . These graphs have been generated by looking the Fourier transform of the steady state solution with respect to  $n$ ,  $m$  and  $t$  and then taking a cross section at the center of the first transverse wavenumber, thus  $\nu = 0$ . The spectra are then multiplied with the Fourier transform of the modal field and plotted over three Brillouin-zones. The wavelength axis has been rescaled using the parameters for a type II FA and assuming up-conversion of the spectrum with an 800 nm reference pulse. These transformations will later be helpful to ease visual comparison with experimental data. It can be clearly seen that an increase of  $\alpha_1$  leads to ST distortion of the spectra. At  $\alpha_1 = 0$  the plot can be factorized into a spatial and temporal part, whereas there is a growing interdependence visible for larger STC coefficients. The effect can mainly be attributed to a widening of the spatial spectra for increasing wavelengths, which means that long wavelength components are more localized than short wavelength components.

The level of interdependence is quantified by calculating the spectral centers of gravity as a function the transverse wavenumber. They are then plotted as white curves over the ST spectra. Their peak-to-valley-value  $\Delta_{\text{SF}}$  is termed ST asymmetry value and plotted for all solutions as a function of the nonlinear phase shift  $b$  in Fig. 30(i). Interestingly we find that  $\Delta_{\text{SF}}$  is almost independent of  $b$  and thus on the LB energy. It is therefore a measure of the STC value  $\alpha_1$ . The relation between  $\Delta_{\text{SF}}$  and  $\alpha_1$  is clarified in Fig. 30(j). The circles mark the data taken from Fig. 30(i) and the gray line is a linear fit. It can be seen that the linear fit is a good approximation and that the ST asymmetry value is therefore proportional to the STC coefficient of the system with

$$\Delta_{\text{SF}}[\text{nm}] \approx -45 \alpha_1 \left( \frac{3.5 \text{ mm}}{L_{\text{Dif}}} \right)^{1/2}. \quad (32)$$

For type II FAs, where we simplify the data from Fig. 29 to  $\alpha_1 \approx -0.12$  in the wavelength range of  $1550 \text{ nm} < \lambda < 2000 \text{ nm}$ , which is relevant for LB propagation, we therefore expect to measure a ST asymmetry value of  $\Delta_{\text{SF}} \approx 5.4 \text{ nm}$ , which is easily measurable in an experiment

and  $\Delta_{\text{SF}} \approx 2.5$  nm for type I FAs, which we will investigate numerically.

Experimental verification of the STC is then carried out as follows: the iXCorr setup discussed in Section 3.1 is modified after the BBO crystal. Instead of imaging the SF field onto a CCD we Fourier transform it in space, using a lens and a  $2f$ -setup. A slit then selects only the cross section of the data with  $\nu = 0$ . A second lens images this data slice onto the input slit of an imaging spectrograph, which generates the temporal Fourier transform of the input field along the direction perpendicular to the slit. The resulting ST spectra are recorded by a CCD. In these experiments the delay stage is not scanned, instead it is fixed at the position, which generates a maximum of SF light. This delay is assumed to coincide with the (temporal) location of the LB. Hence, the correlator is used to cut a temporal section of the duration of the reference pulse, here 60 fs, resulting in a discrimination of dispersive radiation from the measurement, which is temporally separated from the LB, as discussed in Section 5.2.

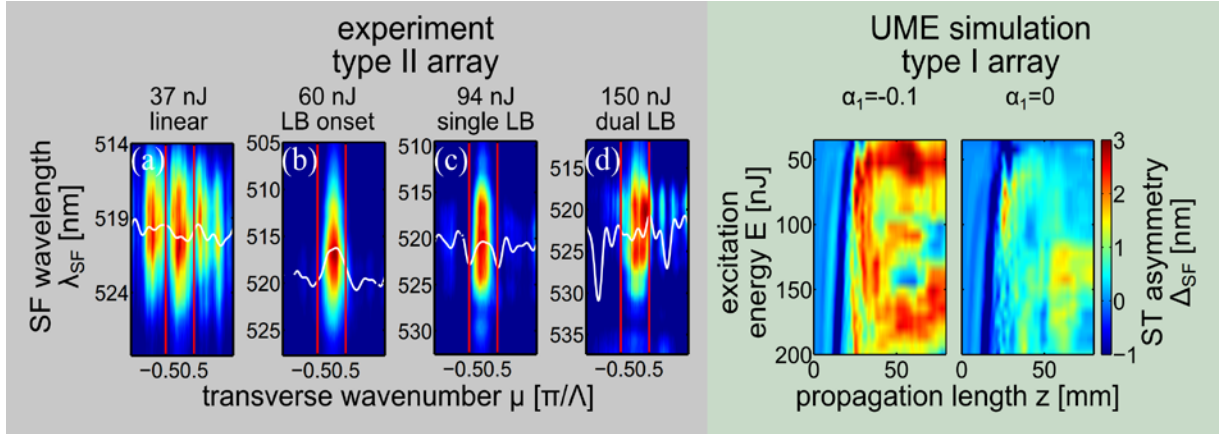


Fig. 31: (a-d) Experimental ST spectra of an  $L = 25$  mm type II FA for various input pulse energies. The iXCorr delay was adjusted to the peak delay of the cross-correlation trace. (white lines) Spectral centre of mass. (red lines) Borders of the 1<sup>st</sup> Brillouin zone. (a) Insufficient energy for LB excitation at low input energy levels, no asymmetry observed. (b,c) Excitation of a single LB. Measured spectral asymmetry  $\Delta_{\text{SF}} \approx 4.0$  nm at 60 nJ and 2.8 nm at 94 nJ. (d) Multiple LBs excited, no asymmetry observed. (e,f) ST asymmetry as predicted by UME simulations for type I FAs (e) with  $\alpha_1 = -0.1$  and (f) without STC for range of input powers and propagation lengths. Figure adapted from [Eil11b].

Results for a type II FA with a length of  $L = 25$  mm for various input energies are displayed in Fig. 31. For low input energies, depicted in Fig. 31(a), there is no measurable spectral symmetry breaking, which is clear because the exciting pulse is spatiotemporally symmetric, and there is not enough input power for the spectrally asymmetric LB to act as a nonlinear attractor. If, however, the input power is increased sufficiently to generate a LB, as can be seen in Fig. 31(b) and (c), spatiotemporal asymmetry is observed, as expected. The observed value of  $\Delta_{\text{SF}}(60 \text{ nJ}) = 4.0$  nm coincides well with the expected value of 5.4 nm. The weaker asymmetry at  $\Delta_{\text{SF}}(94 \text{ nJ}) = 2.8$  nm might be either due to the stronger redshift at higher input powers, with, e.g.,  $\Delta_{\text{SF}}(1800 \text{ nm}) = 3.1$  nm or the existence of more temporally non-separated dispersive

## 5. Results of Experiments and Simulations

waves, which are spectrally symmetric. If the input energy is increased to be sufficient for the excitation of a second LB, as has been done in Fig. 31(d), no spectral asymmetry is again observed, which might be explained by the fact that the second LB is not yet fully developed and not temporally separated. However, given the uncertainties of the experiment and the very indirect method of measuring the ST asymmetry in the temporal vicinity of the LB we claim, that the semi-numeric prediction of above is in good agreement with experimental data.

This notion is supported by results from UME simulations displayed in Fig. 31(e) and (f). The two panes display the ST asymmetry in a time slice of 60 fs around the position of the LB center for various excitation energies and propagation lengths in a type I FA with (e) and without STC (f). Here the predicted value for the asymmetry was  $\Delta_{\text{SF}} \approx 2.5$  nm. Almost no symmetry breaking of the ST spectra is measured in the absence of STC, a clear symmetry breaking is observed if STC is present. Then the asymmetry takes values between  $1.5 \text{ nm} < \Delta_{\text{SF}} < 3 \text{ nm}$ , in agreement with the expected value. It also becomes clear that the ST asymmetry develops together with the LBs, because it is initially zero and starts to form at  $z \approx 15$  mm, which we have identified in Section 5.2 as the approximate length of phase I, after which the initial wavepacket has shaped itself into a LB.

Thus, STC is responsible for the breaking of the ST symmetry of ultrashort wavepackets propagating through FAs. STC imprints asymmetry onto the spectra of LBs, to which all excitations of sufficient energy are attracted. While spectral asymmetry is a property of the stationary solution, in the next section we will show how it also influences the dynamics of LB evolution.

### 5.3.2 Superluminally Decaying Light Bullets

In Section 5.2 we have discussed the LB decay mechanism, which is driven by the growth of the coupling constant experienced by the LB, that is undergoing Raman-induced red-shift. In this chapter we have found that the increase of the coupling strength with increasing wavelength is the very essence of STC. It is thus obvious that STC and LB decay are linked and the LB decay must be influenced by STC. We have also discussed that STC is linked to the concept of group velocity, and we will thus evaluate the group velocity of the LB, especially its behavior during decay.

By now it should have become clear that it is good practice to first investigate Eq. (27), the STC extended NLSE model. Here specifically we investigate the deviation of the pulse's center of gravity from that predicted by assuming propagation with the group velocity of the isolated WG  $v_g^{(0)}$ , which we term *luminality*. It is defined as

$$\begin{aligned}
 \frac{d}{d\zeta}\langle T \rangle &= (v_g)^{-1} - (v_g^{(0)})^{-1} \\
 &= \frac{d}{d\zeta} \sum_{nm} \int d\tau \tau |a_{nm}|^2 \\
 &= \mathfrak{A} + 2\alpha_1 \mathfrak{B} \quad \left\{ \begin{array}{l} \mathfrak{A} = \sum_{nm} \int d\tau \Im m(a_{nm,\tau}^* a_{nm}) \\ \mathfrak{B} = \sum_{nm} \int d\tau \Re e([a_{n+1m} + \dots] a_{nm}^*), \end{array} \right. \quad (33)
 \end{aligned}$$

where  $a_{nm,\tau}$  is the time derivative of the modal amplitude. As per the construction of the LB solutions they are stationary. This means that they move with  $v_g^{(0)}$ , i.e., the group velocity of the isolated WG, without acceleration. The two terms in the third line of Eq. (33) are therefore in equilibrium. After straightforward, albeit lengthy calculation, one can show that the first term is always constant, i.e.,  $d\mathfrak{A}/d\zeta = 0$ , such that any acceleration of the pulse, if there is any, is proportional to the STC coefficient  $\alpha_1$ . One can further show that  $d\mathfrak{B}/d\zeta$  and thus the acceleration of the pulse location  $d^2\langle T \rangle/d\zeta^2$  has only nonlinear contributions of the order  $\mathcal{O}(a^4)$ . Thus, there is no pulse acceleration after the LB has decayed into low-power dispersive waves with low peak energy. Acceleration can thus only take place during LB decay when the non-accelerating stationary solutions no longer apply but powers are still sufficiently high to have a considerable value of  $\mathfrak{B}$ . A closer analysis of  $\mathfrak{B}$  reveals, that it is essentially a discrete, spatial autocorrelation function. For a hexagonal lattice its values are limited to  $-3 \leq \mathfrak{B} \leq 6$ , where the high value applies to in-phase Bloch-waves in the center of the Brillouin zone and the low value applies to Bloch-waves at its edge. For a completely localized solution, which is a decent approximation for high power LBs  $\mathfrak{B} = 0$ . As the LB bifurcates from the top of the band-structure, and thus from the mode in the centre of the first Brillouin zone, the LB preferably decays into this mode and we expect  $\mathfrak{B}$  to grow from  $\mathfrak{B} = 0$  to  $\mathfrak{B} = 6$  during LB decay.

These simple considerations already give a pretty good idea on the limits of group-velocity evolution of a LB. The LB initially propagates with  $v_g^{(0)}$  and retains this velocity as long as it is stationary, i.e., until it decays. During decay this equilibrium slowly breaks and acceleration, proportional to  $\alpha_1$  occurs until power levels have dropped and bring the acceleration to a halt. The final result is a wavepacket with a luminality of  $d\langle T \rangle/dz$  of less than but close to  $12\alpha_1$ .

The validity of the hypothesis was tested using a dynamic simulation of the NLSE. As an initial condition we took a LB with an energy of  $E_0 = 11.06$  and propagated it numerically using Eq. (27) and a value of  $\alpha_1 = -0.1$ . No decay and therefore no speedup can be observed, because the LB is, per definition, a stationary solution of this equation and does not change upon

## 5. Results of Experiments and Simulations

propagation, in particular if there is no Raman term, which leads to redshift and LB decay. However, we introduced additional, artificial loss, such that the energy dropped according to  $E(\zeta) = E_0 \exp(-0.06\zeta)$  and the LB decays at  $\zeta = 2.65$ , because there its energy has dropped to the threshold value of  $E_{\min} = 9.44$ .

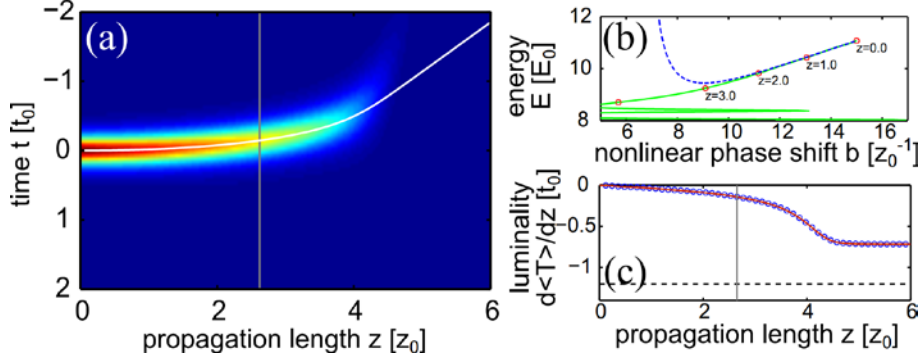


Fig. 32: (a) Power evolution in the central WG of a FA for a LB with  $\alpha = -0.1$  under the action of Eq. (27) with artificial loss, such that LB decay sets in at  $\zeta = 2.65$  (gray line). The (white) line marks the the center of gravity  $\langle T \rangle$ . (b, green line) Pulse energy and nonlinear phase shift of the pulse in (a), where the (red dots) mark certain propagation lengths on the trajectory. The (blue, dotted) line represents possible LB solutions with  $\alpha = -0.1$ . A separation of both lines marks LB decay. (c) Luminality  $d\langle T \rangle/d\zeta$  (red line) as measured from (a) and (blue circles) as calculated from Eq. (33). The decay point is marked by the (grey) line. The (black, dotted) line is the limit of the luminality of  $12\alpha_1$ . Figure adapted from [Eil11b]).

Results of this simulation are displayed in Fig. 32. Subfigure (a) shows the evolution of the power in the central WG of the FA. The pulse, which is initially stationary, accelerates close to the region of decay and then again settles out at a constant speed. The validity of the location of the point of decay is confirmed by Fig. 32(b). The trajectory of the pulse’s energy and phase shift follows that of the LB solutions, until its energy drops below the threshold energy  $E_{\min}$ , close to the predicted decay position at  $\zeta = 2.65$ . Fig. 32(c) displays the luminality, derived from the center of gravity curve in Fig. 32(a) and the calculated value as per Eq. (33), which coincide perfectly. The above established maximal value for the luminality of  $12\alpha_1$  is marked by the dashed line and approached, as predicted. A similar simulation without STC did not show any sign of pulse acceleration.

Thus, the dynamics outlined above have been confirmed: STC indeed leads to superluminal pulse propagation after the decay of LBs. For a more physical understanding of the STC induced acceleration process we resort to a “nutshell” explanation. The central point is that LBs bifurcate from (and decay into) the mode at the center of the Brillouin zone, which has  $\mu = \nu = 0$ . Its inverse group velocity is given by  $v_g^{-1} = \beta_1 + 12c_1$ . The LB, however, is well-localized and can, for the sake of simplicity, be described as propagating through a (nonlinearly) isolated WG. Its inverse group velocity is  $(v_g^{(0)})^{-1} = \beta_1$ , where  $\beta_1$  is the derivative of the longitudinal wavenumber of the WG at the carrier frequency, as introduced in Chapter 4. The difference

between the two values is nothing but the luminality  $d\langle T \rangle/d\zeta$ . The STC induced superluminal pulse propagation during LB decay is therefore a consequence of the modal dependence of the group velocity of the FA. In fact, very large values for the modal dependence of the group velocity dispersion in 1D silicon nanowire arrays [Gor10] have been reported before – STC based effects could therefore be even more dominant in such systems.

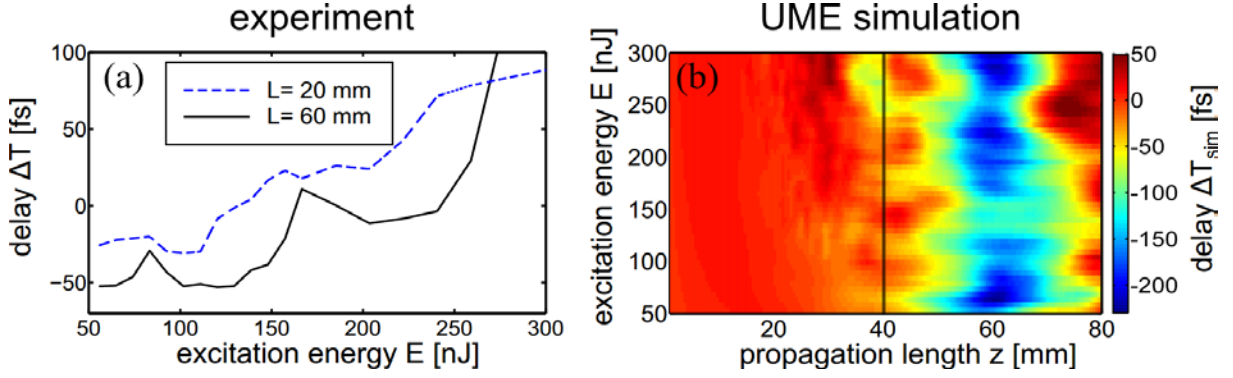


Fig. 33: (a) Experimental delay measurement for a type I sample with (blue, dotted line)  $L = 20$  mm and (black, solid line)  $L = 60$  mm as a function of the excitation pulse energy. Roughly 80 nJ are needed to excite a LB. (b) Pulse arrival difference between a  $\alpha_1 = 0$  and  $\alpha_1 = -0.1$  simulation. Very little difference is observed for  $z < 40$  mm, where LB are stable. Pulses with STC (i.e.,  $\alpha_1 = -0.1$ ) arrive considerably earlier if  $z > 40$  mm, i.e., after LB decay. Figure adapted from [Eil11b]).

The relative pulse speedup for type I FAs can be estimated to be  $\delta v_g/v_g^{(0)} \approx 10^{-4} \dots 10^{-3}$ . Experimental verification of the superluminal decay, however, needs an indirect approach. The group velocity cannot be directly observed outside of a sample. Direct observation of speedup in this scale is unpractical as it would require a very precise sample-cutback technique with an extremely repeatable coupling scheme. Time-of-flight measurements are, however, feasible. Under the conservative assumption of a relative speedup of  $2 \cdot 10^{-4}$  during decay and a length of 20 mm after the point of decay the time of arrival will change in the order of 20 fs. This is well above the 1 fs level of accuracy and repeatability of the iXCorr scheme.

Time-of-flight measurements need a well-defined reference time. Due to a lack of other references we resort to use the dispersive waves generated early in the LB evolution process as a reference. They do not experience speedup. As the LB is concentrated mostly in the central WG, whereas the dispersive waves are spread throughout the FA, we measure the delay  $\Delta T = \langle T_C \rangle - \langle T_O \rangle$ , where  $\langle T_C \rangle$  is the temporal center of gravity of the pulse in the central WG of the FA and  $\langle T_O \rangle$  is the temporal center of gravity of the pulses of all other WGs.

Results for such measurements in type I samples are displayed in Fig. 33(a). The dashed line represents a short sample with  $L = 20$  mm where the LBs have not yet decayed and no speedup is expected and the solid lines represents a long sample with  $L = 60$  mm, where the LBs have decayed 10 to 20 mm before the end of the sample. Both curves exhibit a general trend towards

## 5. Results of Experiments and Simulations

later arrival for pulses with more input energy. This is due to the stronger redshift and thus lower average group velocity experienced by pulses with higher input energy. For the short sample the increase of the delay is more or less monotonic. However, for the long sample this monotonic increase is interrupted by periodic decreases. The ditches have a periodicity of roughly 80 nJ. Similar energy levels have been identified with the excitation of the first and second LB in Section 5.2. The depths of the ditches have a value in the range of 20 to 30 fs and coincide well with the expected reduction of the delay of 20 fs.

We therefore argue that the observed ditches are an experimental proof for superluminal pulse propagation induced by the decay of the LBs. They are a direct consequence of STC. They occur only for energies which are sufficient for the creation of LBs, only for lengths where LBs have already decayed, and with a magnitude very close to the expected value.

These results are augmented by numerical simulations of the UME model. As opposed to the experimental scenario here we can turn STC off at will and also measure the relative delay at any propagation distance. Fig. 33(b) therefore displays the difference in the delay for otherwise identical simulations with  $\alpha_1 = 0$  and with the level of STC expected for a type I FA. This difference is termed simulated model delay  $\Delta T_{\text{sim}}$ . It can be seen that the two models exhibit no considerable timing difference for samples up to a length of 40 mm, consistent with the assumption that superluminality is linked to LB decay. After the point of decay at  $z > 40$  mm the pulses of the model with STC, however, appear much earlier than those of the model without STC, which further proves the validity of our model. The reduction of  $\Delta T_{\text{sim}}$  for very long samples can be explained by the fact that the leftovers of the LB have then spread over the complete FA and the applied definition of the delay  $\Delta T$  is no longer meaningful.

We have therefore shown that STC is responsible for superluminal propagation and profoundly affects the dynamics of ultrashort pulse propagation in FAs. Moreover, we have given a simple and physical explanation of the underlying physics and have been able to demonstrate the effect experimentally. In summary, we have shown that ST wave propagation in DO is an interesting system to study the effects of STC. More specifically, we have investigated the impact of STC on LBs and have shown that it influences the static, as well as, the dynamic properties of LBs in a way which is both measurable and can be understood from fundamental physical concepts.

### **5.4 Vortex Light Bullets**

Up to now we have mainly investigated fundamental LBs and the impact that intrinsic asymmetries have on their static and dynamic properties. Section 5.2 dealt to a large extent with the impact of the temporal asymmetry of the nonlinear response, whereas Section 5.3, was

dealing with the temporal asymmetry of the spatial response of the system. All of these asymmetries are, however, fixed for a certain experimental system. They can be tuned by changing the system's geometry but to some extent only. The logical next step on the road towards a comprehensive understanding of LBs is to investigate the impact of a tunable asymmetry that can be superimposed externally onto the system.

Here we focus on the effects of a particular, spatial asymmetry that can be imposed by the variation of the spatial shape of the excitation. More specifically, we investigate the propagation of DO ST wavepackets with orbital angular momentum (OAM).

Optical wavepackets are said to have OAM [Poy09, Jac06, MT07], if they have an azimuthal variation of the optical phase around a certain center of symmetry, such that the optical phase varies by an integer multiple  $M$  of  $2\pi$  during one revolution [Nye74].  $M$  is called the topological charge of the field and is quantum optically [Enk92] related to the angular momentum of the photons propagating in this mode. It is related to the polarization state of the light in the same way that angular momentum is related to spin [Bet36, He95, Sim97]. The most prominent examples of fields with OAM in free space are Gauss-Laguerre modes [All92], which can be generated from Gauss-Hermite laser modes [Bei93]. Other techniques for the generation of OAM fields are based on imprinting a spiral phase with an appropriately shaped phase plate [Bei93] or using static [Baz90] or dynamic [Cur02] gratings with an  $M$ -fold fork dislocation. A generalization of the grating concept is to nonlinearly generate [Blo12] or modify [She13] OAM fields in twisted photonic crystals.

Fields with OAM [All99, FA08] have recently gained a lot of attention, due to their mutual orthogonality, which allows them to be used in mode division multiplexing schemes for high-throughput parallel data transmission [Gib04, Wan12].

The interaction of OAM with nonlinear waves in DO systems has so far resulted in the observation of discrete Vortex Solitons of various flavors [Fir97, DT00, Mal01, Nes04, Des05a, Ter09, Ter10] and the deviation of a simple stability rule [Kar05]. See also Section 4.1 for an overview. Here we just mention that 2D FAs, which support discrete solitons, in general also support discrete vortex solitons. In the course of this section we will show that the same is true for VLBs. More precisely we investigate compact triangular VLBs in type I fiber FAs. These have been subject of a previous numerical study LeBlond et al. [Leb11], where they have been found to be numerically stable in an NLSE model. This report showed similar results for VLBs with a larger spatial extent and follows a similar numerical investigation of VLBs [Leb08] in square arrays with comparable results. We therefore claim that the fundamental compact triangular VLB, although the simplest discrete VLB possible, is generic for a large class of

## 5. Results of Experiments and Simulations

VLBs.

Compact triangular VLBs are compound LBs, where the main part of the energy is equally distributed in a triangle of three neighboring WGs. The pulse shape in each of these WGs is synchronized and identical with that in the other two WGs but has a mutual phase shift of  $\pm 2\pi/3$  with respect to the other two WGs. As such compact triangular VLBs only exist with OAMs of  $M = \pm 1$ , where the sign is of basically no influence because the FA exhibits helical symmetry, i.e. it is not twisted long the axis of propagation.

Following the established route we start by investigating the stationary VLB solutions of Eq. (19) to establish their parameters and check for stability. The solution method for this intrinsically complex field is the same as the one introduced in Section 5.3, however, we neglect STC. We solved for fundamental LBs, triplet LBs (LB compounds similar to VLBs but without OAM), and VLBs by applying appropriate initial conditions and symmetry restraints on the solutions.

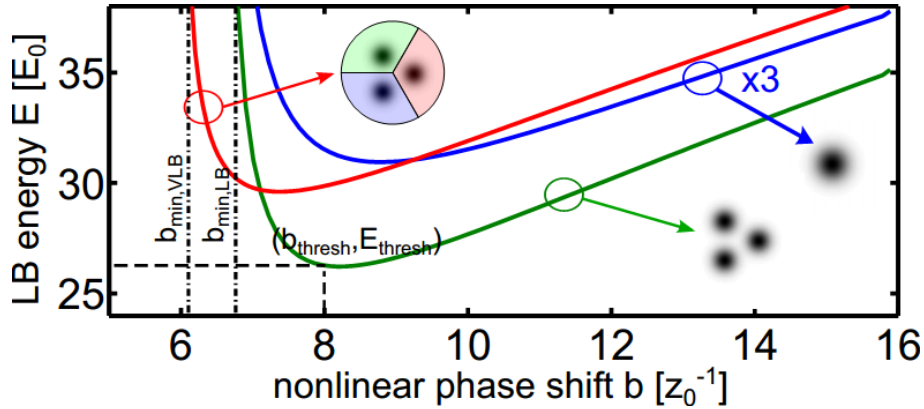


Fig. 34: Families of various LB solutions of the NLSE. Displayed is the energy  $E$  vs. the nonlinear phase shift  $b$  of (red) VLBs, (Green) triplet LBs, and (blue) fundamental LBs (energy multiplied by three). (black, dashed) The minimal energy  $E_{\text{thresh}}$  and the corresponding nonlinear phase shift  $b_{\text{thresh}}$ . (black, dash-dotted) The solution with the minimal nonlinear phase shift  $b_{\text{min}}$ . Figure adapted from [Eil13c].

Results are displayed in Fig. 34, which displays the VLB energy as a function of the nonlinear phase shift  $b$ . As the average energy of the compound LBs is, of course, higher than the energy of a fundamental LB, the curve for the fundamental LB is magnified by a factor of three. The reduced minimum wavenumber  $b_{\text{min}}$  for VLBs, if compared to triplet LB and fundamental LBs, shows that VLBs do not bifurcate from the top of the Bloch-band. This is not surprising because the flat-phase mode in the center of the Brillouin-zone and any field with OAM  $M \neq 0$  are orthogonal. In comparison VLBs have the largest energy at any fixed value of  $b > 9$ , such that, from an energetic point of view, a decay into a triplet LB or three fundamental LBs seems possible.

Next we investigated the stability of the three classes of LBs. In Section 5.2 we had found that

for fundamental LBs all solutions with  $b > b_{\text{thresh}}$  are stable, which was consistent with the Vakhitov-Kolokolov theorem [Vak73]. This theorem, however, only applies to the first nonlinear state, i.e., the one with lowest energy and thus not to compound LBs. The stability analysis for triplet LBs and VLBs was thus carried out by numerically propagating the fields with numerical noise. Noise sources were uncertainties of the initial field and integration errors. Their impact has been tested by varying the temporal resolution, the integrator step size, and by adding noise onto the initial solutions. No qualitative impact on the evolution of the solutions was evident.

We found that, as expected, triplet LBs are always unstable. The situation is more difficult for VLBs. The evolution of the deviation  $\varepsilon$  from the initial field shape as a function of the nonlinear phase shift  $b$  for a fixed propagation length is plotted in Fig. 35(a). Two regimes can be clearly distinguished. VLBs with a small nonlinear phase shift  $b < b_{\text{crit}} = 19.2 z_0^{-1}$  are unstable, exhibiting exponential noise growth, as can be seen in Fig. 35(b). They decay into a fundamental LB and into dispersive radiation, as is shown in Fig. 35(c). Solutions with large nonlinear phase shift  $b > b_{\text{crit}}$  have a different evolution behavior. They initially seem to be stable until the three main constituents desynchronize into three fundamental LBs, as shown in Fig. 35(d). This transition is accompanied by sudden, non-exponential noise growth, as can be seen in Fig. 35(b). Exponential growth would, however, be expected for modulational instability. We therefore term these VLBs to be semistable. Because the transition occurs on length scales, which are much larger than typical sample lengths (e.g.,  $L \approx 140$  mm, for type I arrays), they can be considered stable in the context of our experiments.

This desynchronization decay of semistable VLBs is another nonlinearity-triggered, spatiotemporal transition of LBs. It coincides with the findings of [Leb08], predicting similar results for square arrays. Our findings complement those in [Leb11], who, in the same hexagonal geometry, predict a slightly lower value for  $b_{\text{crit}} \approx 16.4 z_0^{-1}$  and stability for all  $b > b_{\text{crit}}$ . The difference might be due to the “temporal filtering” method employed in [Leb11].

The experimental setup is the same as that for experiments with fundamental LBs, discussed in Section 5.2, employing the iXCorr scheme introduced and discussed in Section 3.1. A schematic representation was already shown in Fig. 24 in Section 5.2. OAM is imprinted onto the excitation field with a threefold-symmetric, discrete phase plate, the details of which have been described in Section 2.3. The discrete phase plate is an adaptation of the spiral phase plate technique for discrete optical systems and generates a focal field distribution that is sufficiently similar to the field distribution of VLBs to guarantee a high coupling efficiency to the discrete vortex field.

## 5. Results of Experiments and Simulations

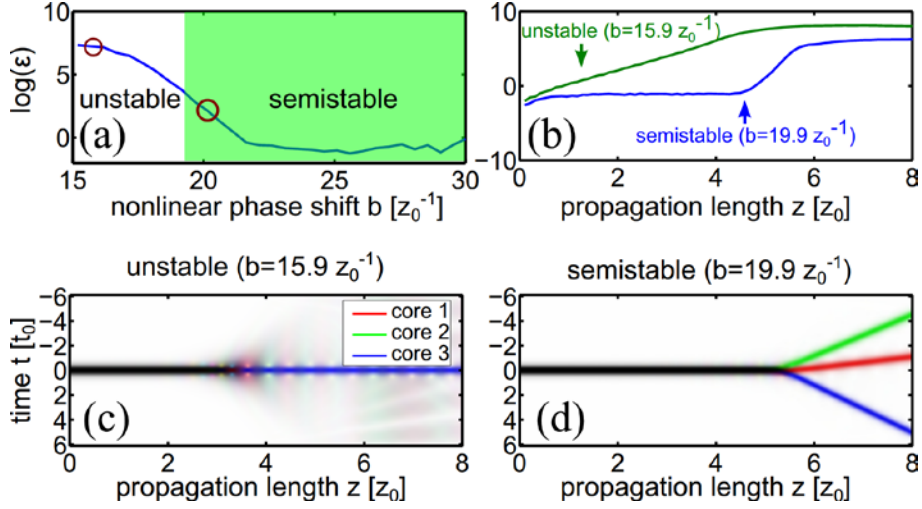


Fig. 35: Stability of VLBs. (a) Perturbation  $\log(\epsilon)$  at  $z = 3.4 z_0$ . Stability transition at  $b \approx 19.2 z_0^{-1}$ . More details given in (b-d) for the circled values. (b) Growth of perturbation  $\log(\epsilon)$  as function of propagation length, where  $\epsilon = \sum \int (|a_{nm}^{(0)}(t)| - |a_{nm}(z, t)|)$  is the deviation of the modulus of the solution  $a_{nm}(z, t)$  from the initial state  $a_{nm}^{(0)}(t)$ . Exponential growth for the unstable (green) and sudden onset growth for the semistable (blue) solution. (c,d) Evolution of the temporal pulse intensity for the three main WGs for (c) an unstable solution and (d) a semistable solution. The WGs are color coded into the red-green-blue (RGB) channel respectively. Figure adapted from [Eil13c].

Already in the linear regime a considerable difference in the propagation of discrete and continuous vortices is evident at the end of the FA. In homogeneous media the vortex character of the field in general has to be visualized using interference with a reference field of different OAM, producing a characteristic spiral mode-beating pattern [All03, FA08]. This is not the case for discrete vortices. In Fig. 36(a) and (b) experimental and simulated images of the light distribution after linear propagation of the vortex field through 17 mm of a type I FA are displayed. The triangular symmetry of the field is obvious. The OAM of the field is directly manifested in the observed intensity. One can observe a diffraction pattern with interdependent radial and azimuthal field distributions in a distinct corkscrew pattern in Fig. 36(a) and (b). The peculiar properties of discrete diffraction in WA can therefore be used to directly image vorticity in optical fields. We therefore propose to use FAs for the interference-free measurement of OAM modes [Min10b].

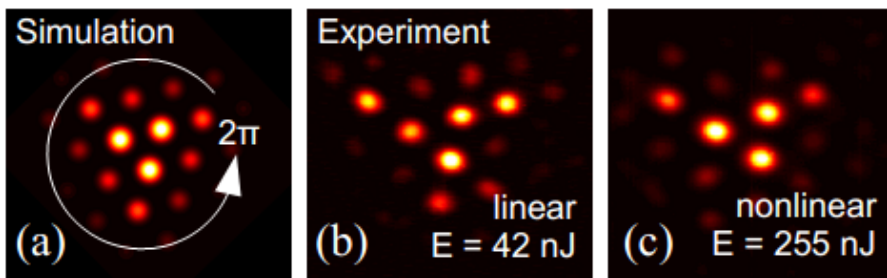


Fig. 36: (a) Simulated and (b) experimental diffraction patterns in the linear power regime of a type I FA of  $L = 17$  mm. (c) Experimental diffraction pattern in the same FA in the VLB power range. Increased contrast of the center compared to the outer WGs is observed. Figure adapted from [Eil13c].

Fig. 36(c) shows an image of the light distribution at the end of the same FA but at a much higher input energy. The energy was chosen such as to be roughly three times the input energy that was determined to be required for the excitation of a fundamental LB. An increase in localization is observed. This increase of spatial contrast can be observed for  $250 \text{ nJ} < E < 300 \text{ nJ}$  and we will confirm below that VLBs are actually observed in this energy range.

We will now again turn to UME simulations to identify energy ranges and sample lengths for which stable VLBs can be observed in type I FAs. A thorough analysis of the UME data is again necessary because at this point it is still unclear if and how VLBs are robust against the intrinsic asymmetries of the realistic model and against the residual extrinsic asymmetries that are related to a possibly asymmetric and imbalanced excitation of the three main WGs of the FA. To differentiate between these two perturbation mechanisms we ran two sets of simulations. In the first set of simulations we injected three  $2\pi/3$  phase shifted, otherwise identical 50 fs Gaussian pulses into the three central WGs of the FA to determine the energy range and sample length range in which VLBs can be observed. Both of these values cannot be taken directly from the NLSE data discussed above, because the laser pulse duration is much longer than the VLB duration and thus their excitation is accompanied by dispersive wave generation as discussed before.

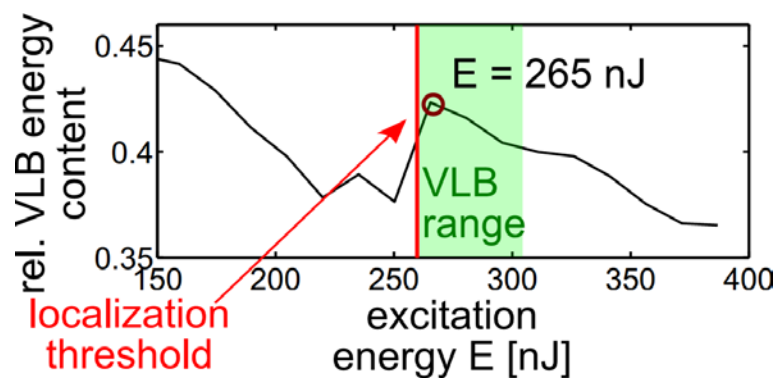


Fig. 37: UME simulation of the relative energy content of the brightest pulse in the three main WGs as a function of the input energy. A sudden increase at  $E \approx 260 \text{ nJ}$  denotes the localization threshold. The VLB energy range is marked in (green). Figure adapted from [Eil13c].

For the UME simulation we find an increase of roughly 20% in the localization of the output field distribution in the energy range of  $260 \text{ nJ} < E < 300 \text{ nJ}$ , as can be seen in Fig. 37. Typical propagation dynamics in this energy range are displayed in Fig. 38. The pulse duration in the central WG is consistently below 30 fs if the sample length is shorter than  $z_{\text{max}} < 17 \text{ mm}$ , as displayed Fig. 38(b). Moreover, in this sample length range the evolution of the pulse duration is subdispersive as can be seen by comparing with the pulse broadening behavior of hypothetical, dispersively broadened pulses, marked by the purple lines. The three pulses are also temporally synchronized in this range, as can be seen from Fig. 38(c). Subfigure (d) proves that the pulses in

## 5. Results of Experiments and Simulations

all three WGs are phase-locked to a nonlinear attractor. It is located at a relative phase shift of  $\Delta\varphi_{12} = 2\pi/3$  and  $\Delta\varphi_{13} = 4\pi/3$ , where  $\Delta\varphi_{12}$  is the phase shift between the 1<sup>st</sup> and 2<sup>nd</sup> and  $\Delta\varphi_{13}$  is the phase shift between the 1<sup>st</sup> and 3<sup>rd</sup> WG of the FA. Both phase shifts are measured at the respective pulse peaks. The figure shows the trajectory of  $\Delta\varphi_{12}$  and  $\Delta\varphi_{13}$ . The state of the system orbits around the phase lock point in the center on a damped trajectory. This behavior is expected for a stable VLB solution, which is a nonlinear attractor. The initial pulse contraction takes roughly  $Z_{\min} = 5$  mm, such that we observe VLB propagation for  $L_{\text{VLB}} = 12$  mm, equating into  $L_{\text{VLB}} = 2.5 \langle L_{\text{Disp}} \rangle \approx 1.5 \langle L_{\text{Diff}} \rangle$ . VLBs are therefore stable for identical excitations with a stability range of roughly half that of fundamental LBs as seen by comparing to the values stated in Section 5.2.

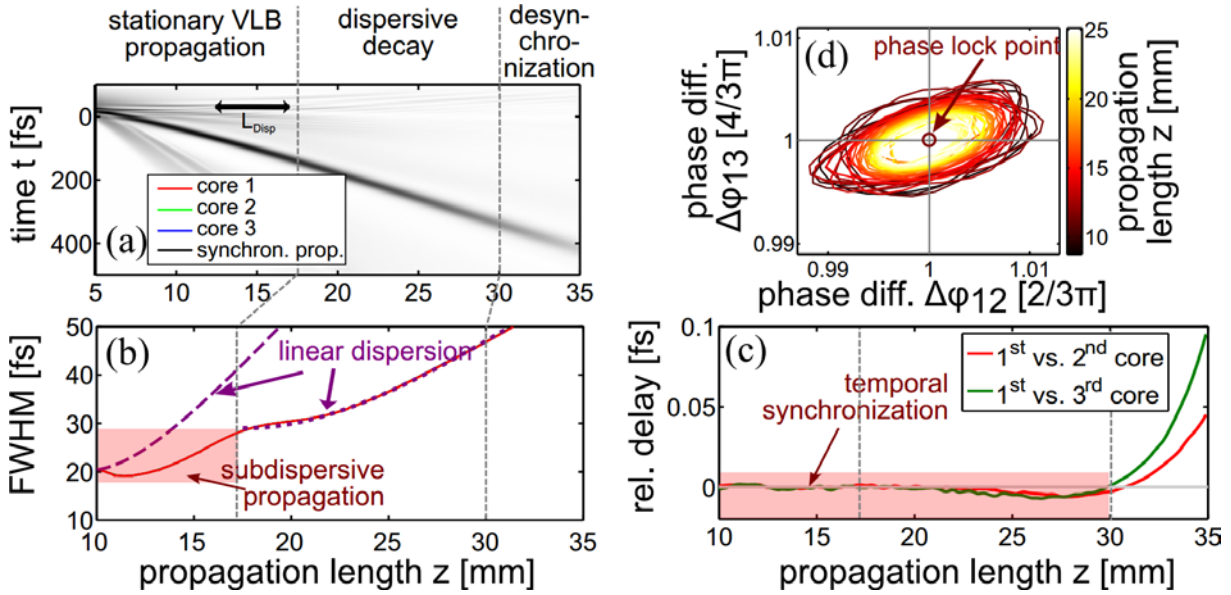


Fig. 38: UME Simulation of VLB propagation for excitation with three identical 50 fs pulses with  $2\pi/3$  relative phase shift and total energy  $E = 265$  nJ in a type I sample. (a) Power evolution in the three central WGs of the FA. Each WG's contribution is coded into the image's RGB channel - gray denotes synchronous propagation. (b) FWHM in the central WGs. The (purple, dashed) line shows hypothetic linear dispersive broadening. The (purple, dotted) line shows that linear dispersive broadening describes pulse's behavior well after  $z > 17$  mm. (c) Peak delay of the pulse in the 2<sup>nd</sup> and 3<sup>rd</sup> WG with respect to the 1<sup>st</sup> as a function of the propagation length. Onset of desynchronization for distances  $z > 30$  mm. (d) Phase difference of the pulse in the 2<sup>nd</sup> and 3<sup>rd</sup> WG with respect to the 1<sup>st</sup>. Propagation length  $z$  color coded. Figure adapted from [Eil13c].

The purpose of the second set of simulations is to establish the stability of VLBs against inevitable, residual coupling asymmetries. We therefore repeated the first set of simulations, however with the energy of the input pulse in the second WG reduced by 5% and in the third by 10% with respect to that in the first, while maintaining a constant total energy. Linear excitation with  $E \ll 100$  nJ does not produce VLBs but no temporal desynchronization and other symmetry breaking is observed due to the absence of nonlinearity. In the slightly nonlinear regime, with  $100 \text{ nJ} < E < 260 \text{ nJ}$  we observe rapid energetic desynchronization, i.e.,

fundamental LBs develop in one or two of the WGs but no VLB. This is consistent with the decay scenario of unstable VLBs discussed in the initial paragraphs of this section. If the energy is in the range of  $260 \text{ nJ} < E < 300 \text{ nJ}$ , we observe spatial localization and temporal, as well as, energetic synchronization and phase locking, hence VLB propagation. If the input energy is too large  $E > 300 \text{ nJ}$  we observe rapid temporal and energetic desynchronization and the generation of individual, desynchronized fundamental LBs in all of the central WGs.

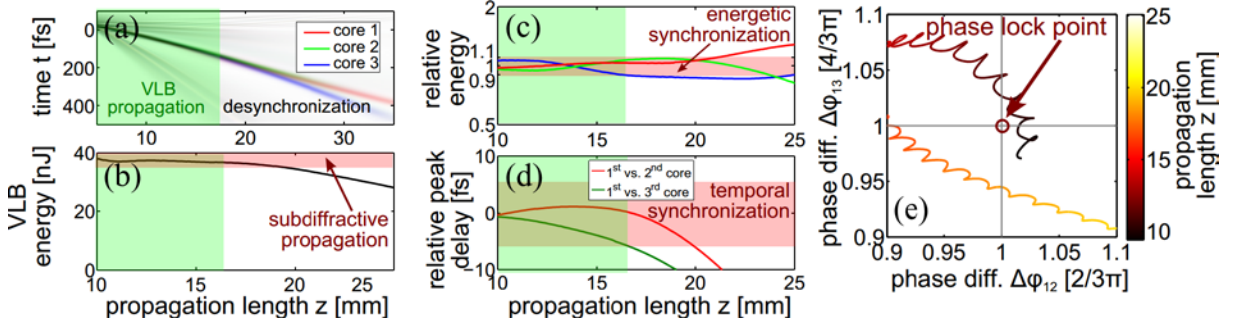


Fig. 39: UME Simulation of VLB propagation for excitation with three 50 fs pulses with  $2\pi/3$  relative phase shift and initial energy reduction of 5% in the 2<sup>nd</sup> and 10% in the 3<sup>rd</sup> WG at a total energy of  $E = 265 \text{ nJ}$ . (a) Instantaneous power in the three central WGs. Each WG's power is coded into one of the image's RGB channel. Gray denotes synchronous propagation. Regions of stationary VLB propagation are shaded in green. Regions with desynchronization are white. (b) VLB energy content during propagation. The subdiffractive region ( $z < 20 \text{ mm}$ ) is red. (c) Relative energy content of each WG compared to average energy. Regions with energy synchronization ( $z < 17 \text{ mm}$ ) are red. (d) Peak delay of the pulse in the 2<sup>nd</sup> and 3<sup>rd</sup> WG with respect to the 1<sup>st</sup>. Regions with temporal synchronization ( $z < 17 \text{ mm}$ ) are red. (f) Evolution of phase shift of the 1<sup>st</sup> WG with respect to the 2<sup>nd</sup> and 3<sup>rd</sup>. Propagation length color coded. Figure adapted from [Eil13c].

A typical simulation result in the VLB regime for  $E = 265 \text{ nJ}$  is displayed in Fig. 39. We observe temporal synchronization to less than 5 fs for  $z < 17 \text{ mm}$  as displayed in Fig. 39(a) and (d), with phase synchronization to less than 10% of the respective phase difference of  $2\pi/3$  as shown in Fig. 39(e). The data in Fig. 39(b) underlines the sub-diffractiveness of the wavepacket. As opposed to higher powers the peaks exchange energy periodically, as seen in Fig. 39(c), and approach equilibrium for  $z < 17 \text{ mm}$ . At longer propagation lengths desynchronization into multiple fundamental LBs in all three WGs is observed. This is again consistent with the decay by desynchronization for semistable VLBs discussed in the initial part of this section.

Thus for a specific range of energies VLB propagate for lengths up to 17 mm, even with slightly asymmetric excitation. Longer samples and larger energies do not support VLBs, but desynchronized fundamental LBs.

Experimental observation of VLBs relies on indirect observation methods. We have investigated type I samples of three different lengths, where the shortest has a length of  $L = 13.6 \text{ mm}$ , such that VLBs can be observed. The second sample has a length of 16.9 mm, slightly too long for VLB observation, yet short enough to observe the immediate products of VLB decay, i.e., three

## 5. Results of Experiments and Simulations

temporally desynchronized fundamental LBs. Note that from simulation data for samples with a length of 16.9 mm we should still observe VLBs, whereas in experiments we found that the maximal length for VLBs is roughly 15 mm. We attribute the difference to having a larger coupling asymmetry than assumed in the simulations. The longest sample with  $L = 29.9$  mm is much too long for VLB observation and is used to study the decay products of VLBs and their consistency with the energy ranges predicted in the simulations.

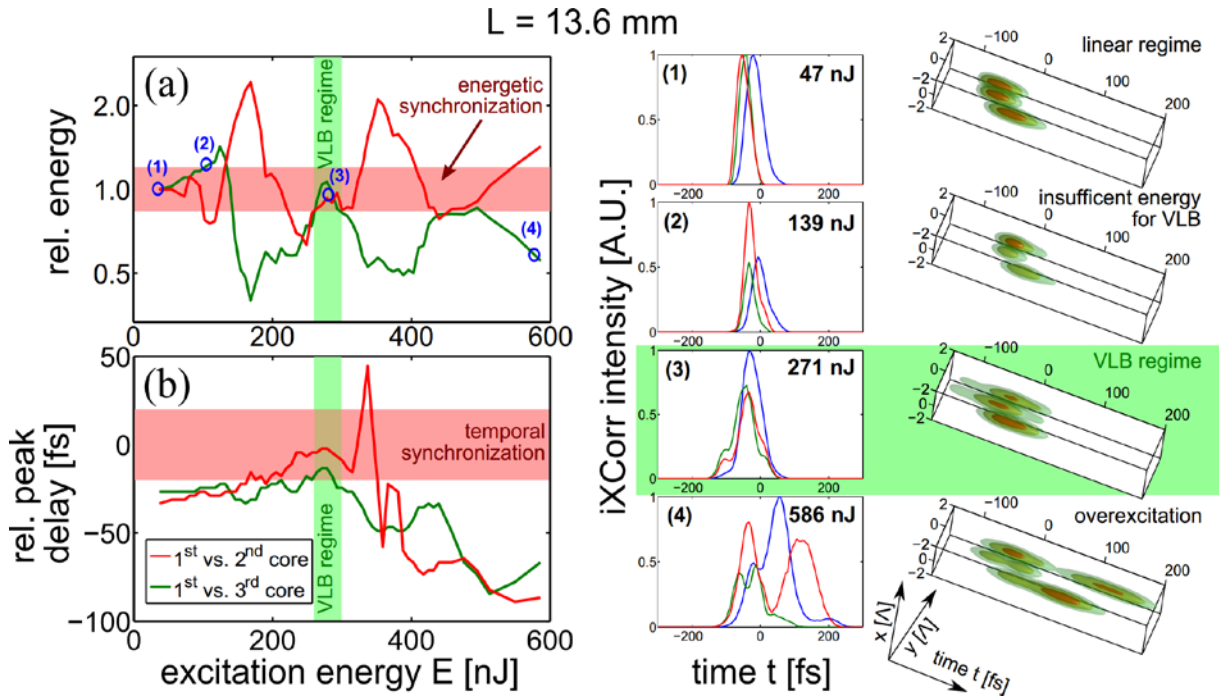


Fig. 40: iXCorr data for a short type I sample. (a) Relative energy content of the 2<sup>nd</sup> and 3<sup>rd</sup> WG with respect to the 1<sup>st</sup>. (b) Relative peak delay of the 2<sup>nd</sup> and 3<sup>rd</sup> WG with respect to the 1<sup>st</sup>. (red bands) Regions of energetic and temporal synchronization are defined by the respective uncertainties. (green bands) Regions of VLB existence are judged by predicted energy ranges, temporal, and energetic synchronization. (1-4, left column) Spatiotemporal iXCorr data of the three central WG modes at energies denoted in (a). (1-4, right column) 3D cross-correlation, iso-intensity plots of the same data. Figure adapted from [Eil13c].

For all samples we have carried out power scans to observe the four characteristic regimes discussed above: linear propagation at  $E \ll 100$  nJ, decay into individual LBs for  $100$  nJ  $< E < 250$  nJ, VLBs for  $250$  nJ  $< E < 300$  nJ, and generation of multiple, unsynchronized, fundamental LBs for  $E > 300$  nJ. We consider VLBs to be present, if simultaneous energetic and temporal synchronization in the three central WGs of the FA is observed. Energetic synchronization means that the quotient of the energy in the 2<sup>nd</sup> or 3<sup>rd</sup> WG with respect to the 1<sup>st</sup> is between 0.9 and 1.1, i.e. not larger than the energetic asymmetry of the excitation. Temporal synchronization is achieved if the center of gravity of the main pulse of the 2<sup>nd</sup> and 3<sup>rd</sup> WG are delayed with respect to the 1<sup>st</sup> WG by no more than 10 fs, i.e. no pulse is shifted with respect to the other ones by more than a single optical cycle.

Results for the short sample are displayed in Fig. 40. Subfigure (a) displays the relative energy in

the 2<sup>nd</sup> and 3<sup>rd</sup> WG with respect to the 1<sup>st</sup> WG. Fig. 40(b) displays the relative delay between the main peak in the 2<sup>nd</sup> and 3<sup>rd</sup> WG with respect to the 1<sup>st</sup> WG. In the linear regime, where no nonlinear reshaping takes place the pulses are initially energetically synchronized and almost temporally synchronized. As soon and the energy is increased into the nonlinear regime to energies that are not yet sufficient for the generation of VLBs the energy becomes unevenly distributed with a pulse in single WG having the highest energy. In the predicted VLB energy range  $250 \text{ nJ} < E < 300 \text{ nJ}$  this asymmetry is lifted and the pulses appear at the end of the FA temporally and energetically synchronized to within the accuracies of the measurement method. Higher energies again lead to the excitation of asynchronous waves. A more detailed insight into the pulse shape for an exemplary pulse energy in each of the regimes is given in the right half of Fig. 40. Here the cross correlation traces of the three central WGs and their representative 3D plots are displayed. This underlines the qualitative difference in the four regimes: no reshaping for linear excitation, excitation of a fundamental LB for intermediate energies, consistent with the decay of an unstable VLB, excitation of fully synchronized VLBs for higher energies, and excitation for multiple, fundamental LBs for excessively high energies. All these findings are constituent with the simulations discussed above.

Results for the longer samples are displayed in Fig. 41. No synchronization and thus no VLBs are observed, as expected. Note, however, that the  $L = 16.9 \text{ mm}$  sample, which is just a little bit longer than the maximum VLB range, exhibits an onset of synchronization, with almost identical energies in all three WGs and very little delay between the pulses in the 1<sup>st</sup> and 2<sup>nd</sup> WG visible in Fig. 41(a) and Fig. 41(c). This is in accordance with simulations, predicting decay into temporally desynchronized, fundamental LBs at maximum VLB propagation length. Data for a much longer sample is displayed in Fig. 41(b) und Fig. 41(d). Here even more asymmetry can be observed, an onset of synchronization is no longer visible. Subfigures (1) and (2) depict exemplary cross-correlation data for an energy where VLBs would be observed in shorter samples.

In summary in this section we have shown that VLBs, i.e., LBs with OAM, can be excited and observed in FAs. These VLBs are so far the, arguably, most complex solitary waves ever observed in an experiment. Using rigorous simulations we have established that the OAM is a key element in stabilizing these compound LBs against decay. They exhibit a new mode of stability, which we termed semi-stability, that is characterized by a considerable length of stationary propagation and then decay into temporally desynchronized, fundamental LBs. This stability is retained under the influence of intrinsic asymmetries, such as higher order dispersion, the Raman effect and discrete space-time coupling. VLBs are also robust against a certain level

## 5. Results of Experiments and Simulations

of asymmetries caused by inevitable, experimental issues.

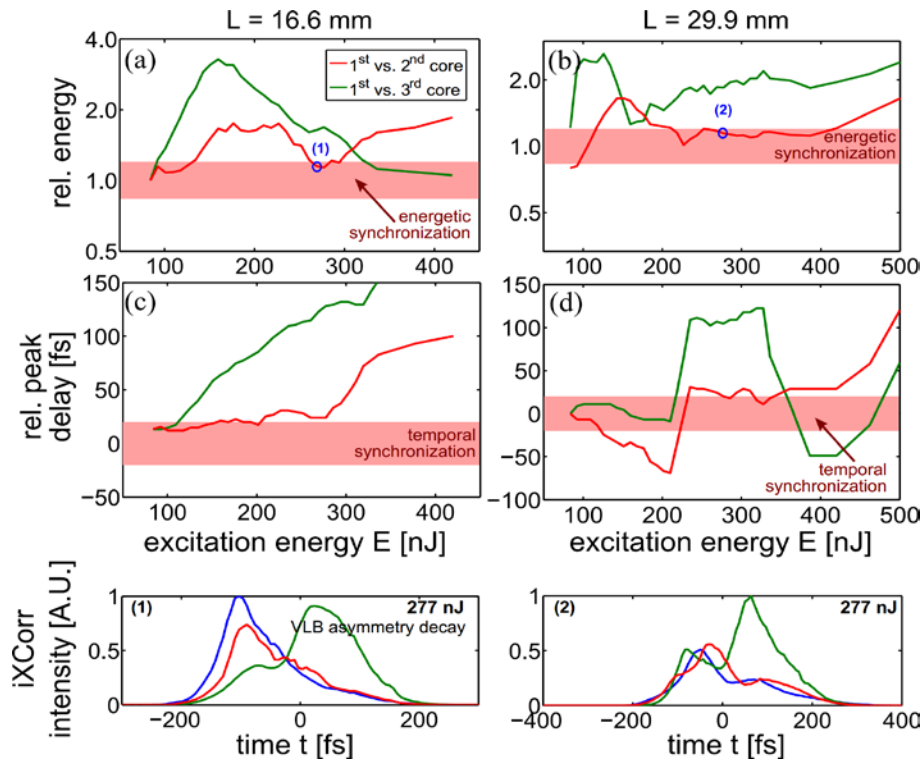


Fig. 41: iXCorr data for longer type I samples. (left) A sample with length  $L = 16.9$  mm, just longer than maximal experimental VLB propagation range. (right) A sample with  $L = 29.9$  mm. (a,b) Relative energy content of the 2<sup>nd</sup> and 3<sup>rd</sup> WG with respect to the 1<sup>st</sup>. (c,d) Relative peak delay of the 2<sup>nd</sup> and 3<sup>rd</sup> WG with respect to the 1<sup>st</sup>. (red bands) Regions of energetic and temporal synchronization. (1,2) Spatiotemporal iXCorr data of the three central WG modes at energies and samples denoted in (a) and (b). Figure adapted from [Eil13c].

If considered together with the results of Sections 5.2 and 5.3, VLBs are not just an even more complex version of fundamental LBs. They are rather a first experimental demonstration of the richness of the physics of spatiotemporal solitary waves, that can be achieved by explicitly arranging for external asymmetries, here the introduction of OAM. As opposed to internal asymmetries discussed in the prior sections, external asymmetries are not a fixed part of the system but can be chosen arbitrarily. VLBs therefore open the route towards a versatile LB “chemistry”, where fundamental spatiotemporal constituents can be fused into compound objects with entirely novel properties.

The observation and characterization of LBs and VLBs, although they put an end to the long scientific debate as to whether LBs can really be observed in an experiment, are therefore not a singular, solitary scientific event but, as we firmly believe, open an entirely new perspective for nonlinear wave research adding a very interesting field of possible future exploration.

## 6. Conclusions & Outlook

In this thesis, we have made a contribution towards the development of spatiotemporal, nonlinear optics. Contributions in the field of spatiotemporal pulse generation and analysis have been driven by the quest for the observation, characterization, and understanding of various families of discrete Light Bullets (LBs) and developed in parallel to that. In this chapter we shall first give a brief summary of the results that have been obtained in this thesis and then discuss potential ramifications thereof as well as possible future directions of research, which are indicated as potentially fruitful by the results obtained here.

Starting from commercial facilities for the generation of high-power, femtosecond, pulsed light sources at variable wavelengths in the near infrared we have implemented a spectral pulse shaper to generate pulses with arbitrary temporal profiles, at high peak powers, with a high throughput and without imaging aberrations. Spatial pulse shaping into a pulse with discrete orbital angular momentum was demonstrated with a discrete spiral phase plate technique. We gave an outlook onto a concept that might eventually lead to a truly spatiotemporal pulse shaping device. The concept is based on recent advances in the field of multicolor metamaterial holograms and would extend the concept of metasurface beam shaping into the spatiotemporal domain.

Equally essential for the observation of LBs was the development of spatiotemporal pulse analysis techniques with femtosecond resolution. Initial experiments have been carried out with a spatiotemporal cross-correlation technique (iXCorr), which reconstructs the spatiotemporal intensity of a pulse with a resolution of 30 ... 70 fs. The technique is, however, unable to reconstruct the optical phase, and it is unsuitable for reference pulse deconvolution. On the other side it is a relatively simple and robust technique and does not require long measurement times.

Aiming to mitigate all disadvantages of iXCorr, we developed an imaging cross correlation FROG scheme (ImXFROG). It is implemented by augmenting the iXCorr setup with a tunable, interferometric wavelength filter. We demonstrated the transform-limitedness of LBs and analyzed a spatiotemporally distorted Airy pulse. ImXFROG achieves a resolution of less than 10 fs and can measure the spatiotemporal intensity and phase of a pulse on more than  $10^7$  independent voxels. It is, to the best of our knowledge, the nonlinear, non-interferometric measurement technique with the highest number of independent data points presented, so far.

Further developments include the construction of a scaled-down version of ImXFROG, called OXFROG. This device reconstructs spatiotemporal pulses with a single spatial dimension. It is therefore ideally suited to investigate the spatiotemporal dynamics of one-dimensional waveguide arrays or of highly symmetric two-dimensional systems, where full three-dimensional

## 6. Conclusions & Outlook

mapping would be overkill. The former is an interesting perspective as nonlinear, spatiotemporal dynamics in waveguide arrays is underdeveloped, considering the amount of research that has been dedicated to their physics. OXFROG dispenses with the interferometric filter, yielding a simpler and more robust setup. It also reduces measurement times and thus allows for rapid data acquisition.

In perspective we aim for the development of an inline spatiotemporal pulse analysis device, that can reconstruct spatiotemporal fields in a single-shot manner. The idea would be to arrange an array of downsized GRENOUILLE [O'S01] FROG devices in a plane just before a large size image sensor. Such an arrayed GRENOUILLE would then reconstruct one FROG trace per array element, much like a Shack-Hartman sensor [Pla01] reconstructs one intensity and phase information from each element of the microlens array in front of the camera sensor. Already with commercially available contemporary image sensors [gol06], e.g., with  $\sim 100$  megapixels and  $9\ \mu\text{m}$  pixel pitch, one could reconstruct  $40 \times 40$  spatial FROG traces with  $256 \times 256$  pixels per FROG trace. The GRENOUILLE elements would have to be scaled down to  $\sim 2 \times 2\ \text{mm}^2$ , which is not too far from its current size of roughly  $20 \times 20\ \text{mm}^2$ . Ongoing developments in the field of large area, high resolution image sensors will further relax these requirements.

We also presented Analysis-by-Control, a new concept for the rapid prototyping of experimental setups. It relies on the flexibility of contemporary pulse shaping devices and on the commutativity of linear optical elements. It aims for the unification of pulse generation and analysis. We demonstrated the locally resolved measurement of chirp and of the autocorrelation function of a spatiotemporally distorted pulse. However, just temporal and spatial adaptive pulse shaping is currently available, the full power of the concept will only be harnessed by emerging concepts for spatiotemporal pulse shaping.

The concepts and devices for the spatiotemporal pulse generation and analysis have been developed in the service of the quest for the observation of discrete LBs. For this end we have also investigated the properties of various two-dimensional discrete optical environments for their spatiotemporal properties. We have identified femtosecond laser-written waveguide arrays and drawn fiber arrays as being suitable in this regard. We concentrated on drawn fiber arrays (FAs) for their regularity, high damage threshold, and ability to operate in the anomalous dispersion regime.

The arrays' properties, i.e. the strength of discrete diffraction, the dispersive properties, and nonlinear response, and their dependence on geometric variations, wavelength, and on each other have been investigated. We have argued that most of these properties modify a certain scale and

have no impact on the fundamental physics. They determine a typical sample length, pulse duration, and pulse energy. The most critical parameter is the temporal scale, which is just a few tens of femtoseconds for all feasible FAs. Such time scales are beyond the validity range of nonlinear Schrödinger models, we resorted to an advanced model for quantitative numerical simulations. This model includes dispersion to all orders, wavelength dependent discrete diffraction, and the instantaneous and non-instantaneous contributions to the Kerr effect. A systematic estimate of the relative impact of all important effects on pulses lead to the conclusion, that experimentally LBs would be generated together with a background of dispersive, supercontinuum radiation and that they would redshift.

At the heart of this thesis was the experimental observation and characterization of various classes of LBs and the understanding of static and dynamics effects related to their evolution. We first focused on the observation of fundamental LBs. Fundamental LBs are those which are mainly concentrated in the central waveguide of the FA. They are, nevertheless, truly spatiotemporal entities, with static and dynamic properties that cannot be explained in the context of a temporal soliton in an isolated waveguide.

Using a mixture of iXCorr measurements and rigorous simulations, later augmented by high-resolution ImXFROG traces, we have shown that LBs indeed propagate in a stable manner through FAs for roughly ten dispersion lengths. They are shifted towards longer carrier wavelengths due to the non-instantaneous Kerr effect. This redshift induces the limited propagation length of LBs, because the LB energy threshold grows with increasing wavelength. Being a truly spatiotemporal effect that had neither been observed nor anticipated before, this evolution and decay mechanism was carefully investigated.

The LB decay mechanism is driven by the asymmetric, non-instantaneous nonlinear response of the material, or to put it more abstract, by a mixture of the nonlinear and temporal response of the system. Another intrinsic source of such an asymmetric mixture of effects was thus also investigated, namely the wavelength dependence of the waveguide coupling strength, constituting a coupling of the spatial and temporal response of the system. Such a direct spacetime coupling (DSC) is currently a hot topic, as on superficial consideration it seemingly allows one to violate causality. DSC can be observed in FAs for pulses that are two orders of magnitude longer than in homogeneous environments. This makes FAs a potential playground for experimental verification of DSC effects. Here we found DSC did affect static and dynamic properties of the LBs. The former manifests in asymmetric spatiotemporal LB spectra, whereas the latter manifests in pulse speedup during LB decay. Both effects could be observed experimentally with results matching predictions from numerical and semi-analytic methods.

## 6. Conclusions & Outlook

In a next step we investigated the impact of external asymmetry, imposed by exciting the sample with a pulse with discrete orbital angular momentum (OAM). We excited Vortex Light Bullets (VLB), which are located in a triangle of three neighboring waveguides and possess OAM. We found that VLBs have an intricate stability behavior: unstable, low-power solutions decay into a single, fundamental LB and dispersive waves. Their higher-power counterparts are semistable. They propagate over a considerable length without change until they desynchronize into three fundamental LBs without dispersive waves. VLBs have been observed experimentally. They can be found for samples up to a particular length and manifest in the simultaneous energetic and temporal synchronization of the light pulses in the three central waveguides of the FA at a particular range of excitation energies. These and other experimental findings agree perfectly with numerical simulations. We claim to have observed the most complex stationary, spatiotemporal, so far. Moreover, we have opened the perspective for the observation and understanding of ever more complex compounds of LB, whose diversity might be orders of magnitude richer than that for lower dimensional systems. As an example we like to emphasize that OAM for spatial waves is a scalar quantity, i.e. the symmetry axis of the vortex is fixed to the propagation axis, whereas for spatiotemporal waves the vortex may rotate around any axis in the  $(x, y, t)$ -space. As such we have just observed a very special kind of a whole class of VLBs.

The thesis originally set out as a project to exploit the properties of drawn fiber arrays to push for the first observation of the discrete LB and “just” confirm their theoretical prediction. From a theoretical point of view LBs had been predicted to be highly symmetric entities of limited complexity and little internal dynamics. In reality we have found quite the opposite to be true. Light Bullets are highly active, dynamically evolving entities with unexpectedly complicated behavior. Thus we claim that we have opened the path to a new and exciting experimental research field in optics: the understanding of the dynamic effects of high-dimensional, spatiotemporal solitary waves and their interaction with the geometric properties of highly structured environments. Moreover, the unexpected and unpredicted richness of the dynamic features of Light Bullets has forced us to push the technological limits of pulse generation, pulse analysis and modelling, to a point where the progress made in these peripheral fields stand out as research results in their own right. Many results have potential application beyond the problems they have originally been conceived for.

In the course of this thesis we could show that new and unexpected physics arises mainly from the perturbation of symmetries. While entities with broken symmetries are often less appealing from a fundamental point of view, we argue that they lead to a much deeper physical understanding of the system and themselves contain potential for possible future applications. As

such we propose that further investigation should follow the path established here of investigating LBs in reduced symmetry environments. So far we have analyzed the impact of intrinsic asymmetries and those that can be imprinted by asymmetric excitations. All experiments did, however, deal with periodic, longitudinally homogeneous lattices. It would therefore be of paramount interest to investigate the behavior of Light Bullets in non-periodic and/or inhomogeneous lattices. The former symmetry could, e.g., be broken by looking at LBs, which are located at edges or corners [Mih89, Pon91, Mak05, Sza07a, Hei09a] or by looking at LBs in geometries with defects [Mor03, MM06, Fre06]. Inhomogeneous lattices would require FAs with longitudinal variation. With the existing samples one might look, e.g., into the interaction of LBs with longitudinally twisted FAs [Ale09, Won12]. This would be interesting in the context of the generation and conversion of OAM [Blo12, She13] and has recently been investigated in the context of topological isolators [Rec13].

Another option for future investigations regarding the propagation of spatiotemporal solitary waves would be to study the collision of LBs, for which extremely rich dynamics has been predicted [Ait91b, Edm93, Xi06, Mih09b, Mih09a]. The interaction of any kind of solitary waves is of fundamental physical interest. This is particularly true for LBs because they are simultaneously affected by intrinsic asymmetries and have a high and anisotropic mobility due to their high-dimensional and discrete-continuous nature. Appropriate initial conditions could be achieved by installing a spectral pulse shaper in the excitation beam line of the experiment and/or by appropriate spatial pulse shaping setups.

Even more geometric flexibility would be achieved by being able to excite LBs in laser written waveguide arrays, with arbitrary transversal and longitudinal geometries. The analysis of spatiotemporal effects in segmented waveguide arrays, which we have carried out, has demonstrated the potential of such an approach to design all-optical devices. In conjunction with the above proposed LB scattering experiments this could, e.g., again put LB routing and all-optical switching of ultrashort pulses on the list of possible applications. Current spatiotemporal experiments in laser-written waveguide arrays are, however, not meaningful in the context of LBs. The reason is that laser-written waveguide arrays are currently not well-characterized in the anomalous dispersion regime. However, only in this regime can bright LBs be excited with the focusing Kerr nonlinearity. Fundamental work would thus have to be carried out until results may be expected.

Another development in contemporary photonics with potential interest with regard to this thesis, is the development of fiber lasers with structured, active cores [Akh05]. Adoption of this technique into the fabrication of FAs would allow one to investigate dissipative effects that are

## 6. Conclusions & Outlook

related to spatiotemporal gain, i.e. non-Hamiltonian spatiotemporal optics. Particularly interesting in this respect is the development of arrays of coupled-phase locked laser sources [Che01], with the vision of either surpassing the Townes limit or with the aim of building active optical, phased-array laser sources [Tan94, McM96, Han09, Sun13]. Another field, which would be opened with the introduction of gain, would be the investigation of spatiotemporal effects in two-dimensional  $\mathcal{PT}$ -symmetric [Ben98] structures. Continuous wave experiments in one-dimensional  $\mathcal{PT}$ -symmetric [EG07, Mak08, Rüt10, Mak10, Suk10] structures are currently a hot topic as unexpected behavior, such as directional transmission [Ram10] or directional invisibility [Lin11] has been reported.

While this outlook did, so far, largely focus on possible future developments that would be related to the spatiotemporal physics of LBs in waveguide arrays, we would also like to discuss the applicability of our results. The first observation of LBs and VLBs is of course interesting from a fundamental point of view. It is even more so as it catches up on almost twenty years of theoretical research. Nevertheless, judging from the perspective of an experimentalist, the range of immediate technical application for LBs is limited. Many applications, which have been proposed in the past, be they for the transport of quantized pieces of information and energy [Mol88, Nak91, Mec91] or for the self-routing [Ace96, Mor99b, Suk03a, Wil11] of data packets in large fiber interconnects might be realized in a simpler manner by other systems.

Nevertheless, this thesis has, in our opinion three important effects on research and technology that deals with nonlinear waves and spatiotemporal optics. The impact for spatiotemporal optics is immediately evident: the methods and devices developed in this thesis, which we needed to generate and analyze LBs, are by no means bounded to this area of nonlinear optics. The technical improvements, that we made for the spectral pulse shaper allowed us to generate arbitrary pulse shapes, with a high throughput and very high beam quality. ImXFROG has demonstrated the reconstruction of spatiotemporal pulses of unprecedented complexity and pushed the limit for measurable pulse complexity in its class of techniques by two orders of magnitude. OXFROG promises to achieve the same for spatiotemporal pulses with one spatial dimension or radial symmetry. Moreover, it has the potential to turn the ImXFROG concept into a robust turn-key device without interferometers and without semiautomatic feedback loops.

The impact on nonlinear wave research is more subtle. First it is interesting to note that although more than 15 years passed between the first prediction of the stability of discrete LBs and their observation, surprisingly little of the theoretical research of this period on the subject of LBs could be used directly for the observation of LBs or for the understanding of their evolution. This is particularly noteworthy as all the physical models and parameters, which we used in this

thesis, are well established and have been so for many years. We like to read this notion as a testimony to the essential purpose of experiments in physics and its role as a “pacemaker” of physical research. This is particularly noteworthy as photonics is a research area, where mathematical models are highly developed and can be solved, at least numerically, with comparatively little effort. Experiments in this respect act as an anchor for theoretical efforts, giving feedback as into which direction realistic models should be investigated and expanded.

A third important impact is rooted in the role that nonlinear optics has often played in the understanding of nonlinear waves in general. As discussed in the introduction, nonlinear optics might be the experimentally most accessible environment to study nonlinear waves, which are ubiquitous in nature and technical systems. A recent example in this respect is the contribution of nonlinear optics to the understanding of Rogue waves [Sol07, Sol08, Akh09, Erk10]. Many systems, which support nonlinear waves are, however, intrinsically of higher dimension. In fact, ocean Rogue waves [Dra66, Hav04, Cha11] have two transverse degrees of freedom [Bir13]; transfer of results from fiber optical experiments into the realm of Rogue waves is therefore conceptually difficult. This thesis adds to the understanding of high-dimensional systems, not only by contributing to the observation and understanding of truly spatiotemporal solitary waves and nonlinear wave phenomena in general but also by developing and implementing methods, which will make future research in the same direction considerably easier and more fruitful.

## 7. Zusammenfassung

Ziel der vorliegenden Arbeit war die Beobachtung und Charakterisierung raumzeitlich selbstlokalisierter, solitärer Wellenpakete in zweidimensionalen, diskreten Wellenleiterstrukturen, sogenannter diskreter Light Bullets.

Um dieses zu erreichen wurden Untersuchungen zu nichtlinearen, raumzeitlichen Propagationseffekten ultrakurzer Lichtpulse angestellt. Dabei wurde Augenmerk auf die Umsetzung, Weiter- und Neuentwicklung von Methoden zur Erzeugung und Charakterisierung raumzeitlicher Pulse und auf die numerische Modellierung raumzeitlicher Propagationseffekte von ultrakurzen, oktavenspannenden Pulsen gelegt. Da die Untersuchung raumzeitlicher, ultrakurzer Pulse eine aktive und junge Teildisziplin der Photonik ist, kann im Allgemeinen nicht auf etablierte Methoden zurückgegriffen werden. Entsprechende Techniken müssen aktiv und begleitend zum eigentlichen Experiment entwickelt und maßgeschneidert werden. Diese Herausforderung unterstreicht die Rolle der raumzeitlichen Optik als treibende Teildisziplin der Photonik. Es gilt Methoden aus verschiedenen Teilgebieten der Optik, wie der räumlichen Optik, der Optik ultrakurzer Pulse und der nichtlinearen Optik zu vereinen.

In Bezug auf die Erzeugung und Formung raumzeitlicher Lichtpulse konnten in dieser Arbeit die zeitliche und räumliche Manipulation von Lichtfeldern demonstriert werden, ausgehend von Kurzpulslasern und Verstärkern, sowie optisch-parametrischen Verstärkern. Es wurde ein spektraler Pulsformungsaufbau für Laserpulse mit mehreren zehn Gigawatt Spitzenleistung implementiert und im Hinblick auf geringe optische Aberrationen hin optimiert. Dabei konnten die Parameter kommerziell erhältlicher Systeme in Bezug auf Transmissionseffizienz, Leistungsverträglichkeit und Abbildungsqualität deutlich verbessert werden.

Die räumliche Formung ultrakurzer Pulse wurde benutzt, um einen Puls mit optischem Drehimpuls (orbital angular momentum) und diskret azimuthaler Struktur zu erzeugen. Zu diesem Zweck wurde die etablierte Spiralphasenplattentechnik modifiziert, d.h. der Puls propagiert durch ein transparentes Medium mit stufenweise, spiralförmig anwachsender Dicke. Die Intensität der Fernfeldverteilung hat die gleiche Anzahl diskreter Peaks, wie die Phasenplatte Stufen hat. Diese Technik ist geeignet optische Wirbelfelder in diskreten Strukturen anzuregen.

Ausblickend wurde das Potential von Metamaterialoberflächen zur raumzeitlichen Pulsformung eruiert, da es zurzeit noch keine tragfähigen Konzepte zur statischen oder rekonfigurierbaren Formung beliebiger, raumzeitlicher Pulse gibt. Das Konzept basiert auf einem holographischen Element, welches für jede Frequenzkomponente des Pulses ein anderes, beliebig einstellbares Hologramm produziert. Die notwendige Dispersion und Designfreiheit der spektralen Antwort

jedes einzelnen Pixels soll erreicht werden, in dem jedes Pixel aus einem oder mehreren resonanten Nanostrukturen besteht, deren kumulative Antwort auf ein Anregungsfeld frei designt werden kann. Das Vorhaben fußt auf einer Untersuchung zu mehrfarbigen Metamaterialhologrammen. Die Erweiterung auf ein durchgehendes Spektrum ist konzeptionell klar, in der technischen Umsetzung jedoch an fundamentale Limits verfügbarer Materialien und Strukturierungstechniken gebunden.

Die hier implementierten und entwickelten, raumzeitlichen Analysetechniken basieren auf der räumlichen Parallelisierung von Pulscharakterisierungsverfahren. Es wurden drei raumzeitliche Analysetechniken eingesetzt. Zuerst wurde ein abbildender Kreuzkorrelator als „Arbeitspferd“ aufgebaut. Dabei propagiert der zu charakterisierende Signalpuls mit einem bekannten Referenzpuls durch einen nichtlinearen Kristall. Signal- und Referenzpuls sind über eine Verzögerungsstrecke in der Ankunftszeit variabel. Im entsprechend angepassten nichtlinearen Kristall entsteht Summenfrequenzlicht. Wird dieses Summenfrequenzlicht auf eine Kamera abgebildet und die Verzögerungsstrecke „durchgefahren“ kann eine raumzeitliche Intensitätsverteilung des Signals rekonstruiert werden. Die zeitliche Auflösung wird dabei von der Dauer des Referenzpulses bestimmt und konnte im Laufe der Arbeit von mehr als 70 fs auf 30 fs reduziert werden.

Zur Analyse kürzerer Ereignisse wurde der Kreuzkorrelator zum abbildenden Kreuzkorrelations-FROG (ImXFROG) ausgebaut. Dazu wurde ein einstellbares Fabry-Perot-Interferometer entwickelt, das lediglich eine bestimmte Frequenzkomponente des Summenfrequenzlichtes transmittiert. Der Aufbau erreicht eine zeitliche Auflösung von 9 fs bei einem Messfeld von 900 fs und  $300 \times 300$  Pixeln räumlicher Auflösung. Er ist in der Lage Intensität und Phase des Pulses auf  $10^7$  Voxeln unabhängig voneinander zu rekonstruieren. Damit wurde die Anzahl unabhängiger Voxel für diese Klasse von Analysetechnik um zwei Größenordnungen gesteigert.

Als Alternative zu ImXFROG wurde ein eindimensionaler Kreuzkorrelations-FROG (OXFROG) entwickelt, der die Abbildung entlang einer Achse „opfert“, um entlang dieser die Wellenlänge zu bestimmen. Der Aufbau benötigt kein aktiv stabilisiertes Interferometer, sondern wird mit einem Gitter betrieben. OXFROG erreicht die zeitliche Auflösung von ImXFROG bei einer Messdauer von wenigen Sekunden. OXFROG soll bei der raumzeitlichen Charakterisierung der Pulspropagation in eindimensionalen Wellenleiterarrays eingesetzt werden.

In einem weiteren Teilprojekt dieser Arbeit wurde das Potential flexibler Pulsformungstechniken erforscht, um die Unterteilung zwischen Pulsformung und Pulsanalyse aufzubrechen. Damit werden experimentelle Aufbaue in der linearen Optik vereinfacht. Das Konzept basiert auf der

## 7. Zusammenfassung

Austauschbarkeit der linear-optischen Bauteile und stellt deren kumulative Wirkung mittels eines raumzeitlichen Pulsshapers dar. Der spektrale Pulsformer wurde benutzt, um zeitliche Bauelemente darzustellen, so z.B. ein Michelson-Interferometer und einen Pulskompressor. Damit konnten Pulse raumzeitlich analysiert werden, ohne einen entsprechenden physischen Aufbau zu realisieren.

Kern der Arbeit und Anlass für die Methodenentwicklung war die Beobachtung und Charakterisierung diskreter Light Bullets (LBs). Die Vorhersage ihrer Beobachtbarkeit erfolgte bereits Mitte der Neunziger Jahre des vergangenen Jahrhunderts. Die spezifischen Eigenschaften hexagonaler Faserarrays sind hervorragend geeignet, um LBs zu beobachten. Die Dispersion bei relevanten Wellenlängen ist jedoch gering. Deshalb haben LBs typische Dauern von wenigen zehn Femtosekunden und eine kritische Überprüfung der etablierten, numerischen Modelle war nötig. Modelle, die auf der nichtlinearen Schrödingergleichung basieren, beschreiben die Propagation solcher Pulse ungenau, dienen aber der Vorhersage der Existenz und Stabilität diskreter LBs. Die bekannten Lösungen wurden deshalb mit einem erweiterten Modell evaluiert, das die Vorwärts-Maxwell-Gleichungen löst und die Evolution des reellen Feldes quantitativ beschreibt.

Damit wurden entscheidende Grundlagen für die Beobachtung diskreter LBs gelegt. Diese gelang durch Korrelations- und ImXRFOG-Experimente sowie durch rigorose Simulationen. Anregungen hinreichender Leistung kontrahieren zu LBs und dispersiven Wellen. Die direkte Messung ihrer Zeitdauer und Dispersionsfreiheit gelang mit dem ImXFROG.

LBs werden durch den Raman-Effekt zu längeren Wellenlängen verschoben und propagieren langsamer als die dispersiven Wellen. LBs sind deshalb von dispersiven Wellen raumzeitlich getrennt. Die Rotverschiebung begrenzt die Lebensdauer der LBs. Dies ist ein inhärent hochdimensionaler Effekt, da solitäre Wellen hoher Dimension eine Minimalenergie haben, die proportional zur Stärke der diskreten Beugung ist, die mit der Wellenlänge anwächst. Sobald die LBs über eine gewisse Grenzwellenlänge rotverschoben wird zerfällt sie deshalb. Wir konnten nachweisen, dass diskrete LBs über mehr als 10 Dispersionslängen stationär sind.

Dieser selbstinduzierte Zerfall ist das Ergebnis der zeitlichen Asymmetrie der nichtlinearen Antwort des Materials. Eine weitere intrinsische Asymmetrie, ist die Wellenlängenabhängigkeit der diskreten Beugung, also der direkten Kopplung von räumlichen und zeitlichen Effekten. Dies manifestiert sich in raumzeitlicher Asymmetrie des Spektrums der LBs. Experimentell wurde nachgewiesen, dass LBs einer raumzeitlich symmetrischen Anregung das vorhergesagte Maß an Asymmetrie aufprägen. Dies führt zum experimentell messbaren, superluminalen Zerfall der LBs. Ähnliche Effekte in homogenen Medien sind experimentell unzugänglicher.

Im letzten Teil der Arbeit wurde der Einfluss asymmetrischer Anregungen untersucht. Es wurden Vortex Light Bullets (VLBs), also LBs mit einer azimuthalen Phasenschraube mittels der Phasenplattentechnik angeregt. Es konnte gezeigt werden, dass VLBs gegen experimentell auftretende Störungen für ca. die Hälfte der stationären Länge der einfachen LBs stationär sein können. Instabile, niederenergetische VLBs zerfallen in ein einfaches LB und dispersive Wellen. Hochenergetische, teilstabile VLBs propagieren stationär und desynchronisieren. Der experimentelle Nachweis erfolgt, in dem man die zeitliche und energetische Synchronizität der Pulse in den drei zentralen Wellenleitern untersucht. Im relevanten Energiebereich lässt sich diese beobachten, VLBs propagieren hier.

Im Rahmen dieser Arbeit ist es gelungen diskrete LBs in einem experimentellen System nachzuweisen und damit deren theoretische Vorhersage nachprüfen. Darüber hinaus kann man hier schlaglichtartig den Wert experimenteller Physik ablesen. Im Gegensatz zu den stark vereinfachten und idealisierten Lösungen, mittels derer die Stabilität diskreter LBs vorhergesagt wurde, konnte gezeigt werden das tatsächliche LBs eine deutlich komplexere Dynamik aufweisen. Es konnten neuartige Effekte der nichtlinearen, raumzeitlichen Wellenausbreitung dargestellt werden. Dieses Feld ist beliebig erweiterbar; komplexe, raumzeitliche Interaktionsszenarien von LBs können untersucht werden, genauso wie die Interaktion von LBs mit geometrischen Störungen.

Die Verbesserung und Neuentwicklung von Methoden zur Erzeugung, Messung und Modellierung von raumzeitlichen Pulsen sind in keiner Weise nur auf diskrete LBs beschränkt, sondern werden in der raumzeitlichen Photonik ihren Platz finden.

Abschließend sei ein weiterer wichtiger Aspekt der Untersuchung nichtlinearer, raumzeitlicher Prozesse genannt. Wie einleitend beschrieben ist die experimentelle, nichtlineare Optik unverzichtbarer Impulsgeber für das Verständnis nichtlinearer Wellenphänomene. Viele dieser Prozesse sind intrinsisch hochdimensional. Deshalb ist davon auszugehen, dass die hier gezeigten Ergebnisse das Verständnis hochdimensionaler Wellenphänomene im Allgemeinen fördern werden.



## Appendix A: References

- [Abd10] D. Abdollahpour, S. Suntsov, D. G. Papazoglou, and S. Tzortzakis. *Spatiotemporal Airy Light Bullets in the Linear and Nonlinear Regimes*. Phys. Rev. Lett., **105** 253901 (2010).
- [Ab191] M. A. Ablowitz and P. A. Clarkson. *Solitons, Nonlinear Evolution Equations and Inverse Scattering*. Cambridge University Press (1991).
- [Ace93] A. B. Aceves and C. D. Angelis. *Spatiotemporal pulse dynamics in a periodic nonlinear waveguide*. Opt. Lett., **18** 110 (1993).
- [Ace94] A. B. Aceves, S. Trillo, S. Wabnitz, and C. D. Angelis. *Storage and steering of self-trapped discrete solitons in nonlinear waveguide arrays*. Opt. Lett., **19** 332 (1994).
- [Ace96] A. Aceves, C. De Angelis, T. Peschel, R. Muschall, F. Lederer, S. Trillo, and S. Wabnitz. *Discrete self-trapping, soliton interactions, and beam steering in nonlinear waveguide arrays*. Phys. Rev. E, **53** 1172 (1996).
- [Adh04] S. Adhikari. *Stabilization of a light bullet in a layered Kerr medium with sign-changing nonlinearity*. Phys. Rev. E, **70** 36608 (2004).
- [Agr01] G. Agrawal. *Nonlinear Fiber Optics*. Academic Press (2001).
- [Aie12a] F. Aieta, P. Genevet, M. A. Kats, N. Yu, R. Blanchard, Z. Gaburro, and F. Capasso. *Aberration-Free Ultrathin Flat Lenses and Axicons at Telecom Wavelengths Based on Plasmonic Metasurfaces*. Nano Lett., **12** 4932 (2012).
- [Aie12b] F. Aieta, P. Genevet, N. Yu, M. A. Kats, Z. Gaburro, and F. Capasso. *Out-of-Plane Reflection and Refraction of Light by Anisotropic Optical Antenna Metasurfaces with Phase Discontinuities*. Nano Lett., **12** 1702 (2012).
- [Ait90] J. S. Aitchison, A. M. Weiner, Y. Silberberg, M. K. Oliver, J. L. Jackel, D. E. Leaird, E. M. Vogel, and P. W. E. Smith. *Observation of spatial optical solitons in a nonlinear glass waveguide*. Opt. Lett., **15** 471 (1990).
- [Ait91a] J. S. Aitchison, Y. Silberberg, A. M. Weiner, D. E. Leaird, M. K. Oliver, J. L. Jackel, E. M. Vogel, and P. W. E. Smith. *Spatial optical solitons in planar glass waveguides*. J. Opt. Soc. Am. B, **8** 1290 (1991).
- [Ait91b] J. S. Aitchison, A. M. Weiner, Y. Silberberg, D. E. Leaird, M. K. Oliver, J. L. Jackel, and P. W. E. Smith. *Experimental observation of spatial soliton interactions*. Opt. Lett., **16** 15 (1991).
- [Akh68] S. A. Akhmanov, A. P. Sukhorukov, and R. V. Khokhlov. *Self-focusing and Diffraction of Light in a Nonlinear Medium*. Soviet Physics Uspekhi, **10** 609 (1968).
- [Akh86] N. Akhmediev and V. Korneev. *Modulation instability and periodic solutions of the nonlinear Schrödinger equation*. Theor. Mat. Phys., **69** 1089 (1986).
- [Akh95] N. Akhmediev and M. Karlsson. *Cherenkov radiation emitted by Solitons in optical fibers*. Phys. Rev. A, **51** 2602 (1995).
- [Akh05] N. Akhmediev and A. Ankiewicz, editors. *Dissipative Solitons*. Springer (2005).
- [Akh09] N. Akhmediev, A. Ankiewicz, and M. Taki. *Waves that appear from nowhere and disappear without a trace*. Phys. Lett. A, **373** 675 (2009).
- [Akt10] S. Akturk, X. Gu, P. Bowlan, and R. Trebino. *Spatio-temporal couplings in ultrashort laser pulses*. J. Opt., **12** 093001 (2010).
- [Ale09] C. N. Alexeyev, E. V. Borshak, A. V. Volyar, and M. A. Yavorsky. *Angular momentum conservation and coupled vortex modes in twisted optical fibres with torsional stress*. J. Opt. A, **11** 094011 (2009).
- [Alf06] R. Alfano. *The Supercontinuum Laser Source*. Springer (2006).
- [All92] L. Allen, M. W. Beijersbergen, R. J. C. Spreeuw, and J. P. Woerdman. *Orbital angular momentum of light and the transformation of Laguerre-Gaussian laser modes*. Phys. Rev. A, **45** 8185 (1992).
- [All99] L. Allen, M. Padgett, and M. Babiker. *The Orbital Angular Momentum of Light*. volume 39 of *Progress in Optics*, 291 – 372. Elsevier (1999).
- [All01] L. J. Allen and M. P. Oxley. *Phase retrieval from series of images obtained by defocus variation*. Opt. Commun., **199** 65 (2001).
- [All03] L. Allen, S. M. Barnett, and M. J. Padgett. *Optical angular momentum*. CRC Press (2003).
- [Alo10] B. Alonso, I. J. Sola, O. Varela, J. Hernández-Toro, C. Méndez, J. S. Román, A. Zair, and L. Ro. *Spatiotemporal amplitude-and-phase reconstruction by Fourier-transform of interference spectra of high-complex-beams*. J. Opt. Soc. Am. B, **27** 933 (2010).

- [Alo12a] B. Alonso, R. Borrego-Varillas, O. Mendoza-Yero, I. J. Sola, J. S. Román, G. Mínguez-Vega, and L. Roso. *Frequency resolved wavefront retrieval and dynamics of diffractive focused ultrashort pulses*. J. Opt. Soc. Am. B, **29** 1993 (2012).
- [Alo12b] B. Alonso, M. Miranda, I. J. Sola, and H. Crespo. *Spatiotemporal characterization of few-cycle laser pulses*. Opt. Express, **20** 17880 (2012).
- [And58] P. W. Anderson. *Absence of Diffusion in Certain Random Lattices*. Phys. Rev., **109** 1492 (1958).
- [Arm62] J. A. Armstrong, N. Bloembergen, J. Ducuing, and P. S. Pershan. *Interactions between Light Waves in a Nonlinear Dielectric*. Phys. Rev., **127** 1918 (1962).
- [Bab07] I. Babushkin, A. Husakou, J. Herrmann, and Y. S. Kivshar. *Frequency-selective self-trapping and supercontinuum generation in arrays of coupled nonlinear waveguides*. Opt. Express, **15** 11978 (2007).
- [Bai03] B. B. Baizakov, B. A. Malomed, and M. Salerno. *Multidimensional solitons in periodic potentials*. EPL, **63** 642 (2003).
- [Bal01] M. L. M. Balistreri, H. Gersen, J. P. Korterik, L. Kuipers, and N. F. van Hulst. *Tracking Femtosecond Laser Pulses in Space and Time*. Science, **294** 1080 (2001).
- [Bar85] A. Barthelemy, S. Maneuf, and C. Froehly. *Propagation soliton et auto-confinement de faisceaux laser par non linearité optique de kerr*. Opt. Commun., **55** 201 (1985).
- [Bar05] G. Bartal, O. Manela, O. Cohen, J. W. Fleischer, and M. Segev. *Observation of Second-Band Vortex Solitons in 2D Photonic Lattices*. Phys. Rev. Lett., **95** 053904 (2005).
- [Bau98] M. Bauer, O. Büttner, S. O. Demokritov, B. Hillebrands, V. Grimalsky, Y. Rapoport, and A. N. Slavin. *Observation of Spatiotemporal Self-Focusing of Spin Waves in Magnetic Films*. Phys. Rev. Lett., **81** 3769 (1998).
- [Baz90] V. Y. Bazhenov, M. Vasnetsov, and M. Soskin. *Laser beams with screw dislocations in their wavefronts*. JETP Lett., **52** 429 (1990).
- [Bäc73] A. V. Bäcklund. *Einiges über Curven- und Flächentransformationen*. Lunds Universitets Arsskrift, Afdelningen for Mathematik och Naturetenskap, **X** 1 (1873).
- [Bäc75] A. Bäcklund. *Über Flächentransformationen*. Math. Ann., **9** 297 (1875).
- [Bäc80] A. Bäcklund. *Zur Theorie der partiellen Differentialgleichung erster Ordnung*. Math. Ann., **17** 285 (1880).
- [Bäc81] A. Bäcklund. *Zur Theorie der Flächentransformationen*. Math. Ann., **19** 387 (1881).
- [Bei93] M. Beijersbergen, L. Allen, H. van der Veen, and J. Woerdman. *Astigmatic laser mode converters and transfer of orbital angular momentum*. Opt. Commun., **96** 123 (1993).
- [Bel04] M. Belic, M. Petrovic, D. Jovic, A. Strinic, D. Arsenovic, K. Motzek, F. Kaiser, P. Jander, C. Denz, M. Tlidi, and P. Mandel. *Transverse modulational instabilities of counterpropagating solitons in photorefractive crystals*. Opt. Express, **12** 708 (2004).
- [Bel08] M. Belic, N. Petrovic, W.-P. Zhong, R.-H. Xie, and G. Chen. *Analytical Light Bullet Solutions to the Generalized (3+1)-Dimensional Nonlinear Schrödinger Equation*. Phys. Rev. Lett., **101** 123904 (2008).
- [Ben98] C. M. Bender and S. Boettcher. *Real Spectra in Non-Hermitian Hamiltonians Having PT Symmetry*. Phys. Rev. Lett., **80** 5243 (1998).
- [Ben08] C. J. Benton, A. V. Gorbach, and D. V. Skryabin. *Spatiotemporal quasisolitons and resonant radiation in arrays of silicon-on-insulator photonic wires*. Phys. Rev. A, **78** 033818 (2008).
- [Ben09] C. J. Benton and D. V. Skryabin. *Coupling induced anomalous group velocity dispersion in nonlinear arrays of silicon photonic wires*. Opt. Express, **17** 5879 (2009).
- [Ber98] L. Bergé. *Wave collapse in physics: principles and applications to light and plasma waves-weak turbulence, condensates and collapsing filaments in the nonlinear Schrodinger equation*. Phys. Rep., **303** 259 (1998).
- [Ber07] L. Bergé, S. Skupin, R. Nuter, J. Kasparian, and J.-P. Wolf. *Ultrashort filaments of light in weakly ionized, optically transparent media*. Rep. Prog. Phys., **70** 1633 (2007).
- [Ber08] L. Bergé and S. Skupin. *Few-Cycle Light Bullets Created by Femtosecond Filaments*. Phys. Rev. Lett., **100** 113902 (2008).
- [Bet36] R. A. Beth. *Mechanical Detection and Measurement of the Angular Momentum of Light*. Phys. Rev., **50** 115 (1936).
- [Bin00] P. Binder, D. Abraimov, A. V. Ustinov, S. Flach, and Y. Zolotaryuk. *Observation of Breathers in Josephson Ladders*. Phys. Rev. Lett., **84** 745 (2000).

- [Bir13] S. Birkholz, E. T. J. Nibbering, C. Brée, S. Skupin, A. Demircan, G. Genty, and G. Steinmeyer. *Spatiotemporal Rogue Events in Optical Multiple Filamentation*. Phys. Rev. Lett., **111** 243903 (2013).
- [Blo29] F. Bloch. *Über die Quantenmechanik der Elektronen in Kristallgittern*. Zeitschrift für Physik, **52** 555 (1929).
- [Blo09] I. Blonskyi, V. Kadan, O. Shpotyuk, and I. Dmitruk. *Manifestations of sub- and superluminality in filamented femtosecond laser pulse in fused silica*. Opt. Commun., **282** 1913 (2009).
- [Blo12] N. V. Bloch, K. Shemer, A. Shapira, R. Shiloh, I. Juwiler, and A. Arie. *Twisting Light by Nonlinear Photonic Crystals*. Phys. Rev. Lett., **108** 233902 (2012).
- [Boc03] E. J. Bochove, P. K. Cheo, and G. G. King. *Self-organization in a multicore fiber laser array*. Opt. Lett., **28** 1200 (2003).
- [Bon09] F. Bonaretti, D. Faccio, M. Clerici, J. Biegert, and P. D. Trapani. *Spatiotemporal Amplitude and Phase Retrieval of Bessel-X pulses using a Hartmann-Shack Sensor*. Opt. Express, **17** 9804 (2009).
- [Bor99] M. Born and E. Wolf. *Principles of optics: electromagnetic theory of propagation, interference and diffraction of light*. Cambridge University Press (1999).
- [Bou71] J. Boussinesq. *Théorie de l'intumescence liquide appelée onde solitaire ou de translation se propageant dans un canal rectangulaire*. Comptes Rendus Acad. Sci (Paris), **72** 755 (1871).
- [Bow06] P. Bowlan, P. Gabolde, A. Shreenath, K. McGresham, R. Trebino, and S. Akturk. *Crossed-beam spectral interferometry: a simple, high-spectral-resolution method for completely characterizing complex ultrashort pulses in real time*. Opt. Express, **14** 11892 (2006).
- [Bow08] P. Bowlan, U. Fuchs, R. Trebino, and U. D. Zeitner. *Measuring the spatiotemporal electric field of tightly focused ultrashort pulses with sub-micron spatial resolution*. Opt. Express, **16** 13663 (2008).
- [Bow12] P. Bowlan and R. Trebino. *Using phase diversity for the measurement of the complete spatiotemporal electric field of ultrashort laser pulses*. J. Opt. Soc. Am. B, **29** 244 (2012).
- [Boy03] R. W. Boyd. *Nonlinear optics*. Academic press (2003).
- [Bra95] A. Braun, G. Korn, X. Liu, D. Du, J. Squier, and G. Mourou. *Self-channeling of high-peak-power femtosecond laser pulses in air*. Opt. Lett., **20** 73 (1995).
- [Bra96] P. Brandt, W. Alpers, and J. O. Backhaus. *Study of the generation and propagation of internal waves in the Strait of Gibraltar using a numerical model and synthetic aperture radar images of the European ERS 1 satellite*. Journal of Geophysical Research: Oceans, **101** 14237 (1996).
- [Bra08] F. Bragheri, D. Faccio, F. Bonaretti, A. Lotti, M. Clerici, O. Jedrkiewicz, C. Liberale, S. Henin, L. Tartara, V. Degiorgio, and P. D. Trapani. *Complete retrieval of the field of ultrashort optical pulses using the angle-frequency spectrum*. Opt. Lett., **33** 2952 (2008).
- [Bré12] C. Brée. *Nonlinear optics in the filamentation regime*. Springer (2012).
- [Bro10] J. S. Brownless, S. Mahmoodian, K. B. Dossou, F. J. Lawrence, L. C. Botten, and C. M. de Sterke. *Coupled waveguide modes in hexagonal photonic crystals*. Opt. Express, **18** 25346 (2010).
- [Bro12] J. S. Brownless, F. J. Lawrence, S. Mahmoodian, K. B. Dossou, L. C. Botten, and C. M. de Sterke. *Supermodes of hexagonal lattice waveguide arrays*. J. Opt. Soc. Am. B, **29** 1338 (2012).
- [Büt00] O. Büttner, M. Bauer, A. Rueff, S. Demokritov, B. Hillebrands, A. Slavin, M. Kostylev, and B. Kalinikos. *Space- and time-resolved Brillouin light scattering from nonlinear spin-wave packets*. Ultrasonics, **38** 443 (2000).
- [Bur99] S. Burger, K. Bongs, S. Dettmer, W. Ertmer, K. Sengstock, A. Sanpera, G. V. Shlyapnikov, and M. Lewenstein. *Dark Solitons in Bose-Einstein Condensates*. Phys. Rev. Lett., **83** 5198 (1999).
- [Bur02] A. V. Buryak, P. D. Trapani, D. V. Skryabin, and S. Trillo. *Optical solitons due to quadratic nonlinearities: from basic physics to futuristic applications*. Phys. Rep., **370** 63 (2002).
- [Bur09] I. B. Burgess, M. Peccianti, G. Assanto, and R. Morandotti. *Accessible Light Bullets via Synergetic Nonlinearities*. Phys. Rev. Lett., **102** 203903 (2009).
- [But87] J. C. Butcher. *The numerical analysis of ordinary differential equations: Runge-Kutta and general linear methods*. Wiley-Interscience (1987).
- [But90] P. Butcher and D. Cotter. *The Elements of Nonlinear Optics*. Cambridge University Press (1990).
- [Cai10] W. Cai and V. M. Shalae. *Optical metamaterials*, volume 10. Springer (2010).
- [Cha11] A. Chabchoub, N. P. Hoffmann, and N. Akhmediev. *Rogue Wave Observation in a Water Wave Tank*. Phys. Rev. Lett., **106** 204502 (2011).
- [Che87] W. Chen and D. L. Mills. *Gap solitons and the nonlinear optical-response of superlattices*. Phys. Rev. Lett., **58** 160 (1987).

- [Che01] P. Cheo, A. Liu, and G. King. *A high-brightness laser beam from a phase-locked multicore Yb-doped fiber laser array*. IEEE Photon. Tech. L., **13** 439 (2001).
- [Che03] D. Cheskis, S. Bar-Ad, R. Morandotti, J. Aitchison, H. Eisenberg, Y. Silberberg, and D. Ross. *Strong Spatiotemporal Localization in a Silica Nonlinear Waveguide Array*. Phys. Rev. Lett., **91** 223901 (2003).
- [Che05] F. Chen, M. Stepi, C. Rüter, D. Runde, D. Kip, V. Shandarov, O. Manela, and M. Segev. *Discrete diffraction and spatial gap solitons in photovoltaic LiNbO<sub>3</sub> waveguide arrays*. Opt. Express, **13** 4314 (2005).
- [Chi64] R. Y. Chiao, E. Garmire, and C. H. Townes. *Self-Trapping of Optical Beams*. Phys. Rev. Lett., **13** 479 (1964).
- [Chi10] S. L. Chin. *Femtosecond laser filamentation*, volume 55. Springer (2010).
- [Cho10] A. Chong, W. Renninger, D. Christodoulides, and F. Wise. *Airy–Bessel wave packets as versatile linear light bullets*. Nature Photon., **4** 103 (2010).
- [Chr88] D. Christodoulides and R. Joseph. *Discrete self-focusing in nonlinear arrays of coupled waveguides*. Opt. Lett., **13** 794 (1988).
- [Chr01] D. N. Christodoulides and E. D. Eugenieva. *Blocking and Routing Discrete Solitons in Two-Dimensional Networks of Nonlinear Waveguide Arrays*. Phys. Rev. Lett., **87** 233901 (2001).
- [Chr03] D. Christodoulides, F. Lederer, and Y. Silberberg. *Discretizing light behaviour in linear and nonlinear waveguide lattices*. Nature, **424** 817 (2003).
- [Cla81] R. Clarke, R. Smith, and D. Reid. *The morning glory of the Gulf of Carpentaria: an atmospheric undular bore*. Mon. Wea. Rev., **109** 1726 (1981).
- [Cla03] T. Clausnitzer, J. Limpert, K. Zöllner, H. Zellmer, H.-J. Fuchs, E.-B. Kley, A. Tünnermann, M. Jupé, and D. Ristau. *Highly Efficient Transmission Gratings in Fused Silica for Chirped-Pulse Amplification Systems*. Appl. Opt., **42** 6934 (2003).
- [Con03] C. Conti, S. Trillo, P. Di Trapani, G. Valiulis, A. Piskarskas, O. Jedrkiewicz, and J. Trull. *Nonlinear Electromagnetic X Waves*. Phys. Rev. Lett., **90** 170406 (2003).
- [Cou28] R. Courant, K. Friedrichs, and H. Lewy. *Über die partiellen Differenzgleichungen der mathematischen Physik*. Math. Ann., **100** 32 (1928).
- [Cou03] A. Couairon. *Light bullets from femtosecond filamentation*. EPJ D, **27** 159 (2003).
- [Cou06] F. Couny, F. Benabid, and P. S. Light. *Large-pitch kagome-structured hollow-core photonic crystal fiber*. Opt. Lett., **31** 3574 (2006).
- [Cou07] A. Couairon and A. Mysyrowicz. *Femtosecond filamentation in transparent media*. Phys. Rep., **441** 47 (2007).
- [Cou12] S. L. Cousin, J. M. Bueno, N. Forget, D. R. Austin, and J. Biegert. *Three-dimensional spatiotemporal pulse characterization with an acousto-optic pulse shaper and a Hartmann-Shack wavefront sensor*. Opt. Lett., **37** 3291 (2012).
- [Cun10] S. Cundiff and A. Weiner. *Optical arbitrary waveform generation*. Nature Photon., **4** 760 (2010).
- [Cur02] J. E. Curtis, B. A. Koss, and D. G. Grier. *Dynamic holographic optical tweezers*. Opt. Commun., **207** 169 (2002).
- [Dar97] S. Darmanyan, I. Relke, and F. Lederer. *Instability of continuous waves and rotating solitons in waveguide arrays*. Phys. Rev. E, **55** 7662 (1997).
- [Dar98] S. Darmanyan, A. Kobayakov, E. Schmidt, and F. Lederer. *Strongly localized vectorial modes in nonlinear waveguide arrays*. Phys. Rev. E, **57** 3520 (1998).
- [Dau06] T. Dauxois and M. Peyard. *Physics of Solitons*. Cambridge University Press (2006).
- [Dav73] A. Davydov and N. Kislukha. *Solitary excitons in one-dimensional molecular chains*. Phys. Status Solidi B, **59** 465 (1973).
- [Dav77] A. Davydov. *Solitons and energy transfer along protein molecules*. J. Theor. Biol., **66** 379 (1977).
- [Dav91] A. S. Davydov. *Solitons in molecular systems*, volume 61. Springer (1991).
- [Den92] B. Denardo, B. Galvin, A. Greenfield, A. Larraza, S. Putterman, and W. Wright. *Observations of localized structures in nonlinear lattices: Domain walls and kinks*. Phys. Rev. Lett., **68** 1730 (1992).
- [Den99] C. Denz, W. Królikowski, J. Petter, C. Weillnau, T. Tschudi, M. R. Belic, F. Kaiser, and A. Stepken. *Dynamics of formation and interaction of photorefractive screening solitons*. Phys. Rev. E, **60** 6222 (1999).

- [Den00] J. Denschlag, J. E. Simsarian, D. L. Feder, C. W. Clark, L. A. Collins, J. Cubizolles, L. Deng, E. W. Hagley, K. Helmerson, W. P. Reinhardt, S. L. Rolston, B. I. Schneider, and W. D. Phillips. *Generating Solitons by Phase Engineering of a Bose-Einstein Condensate*. Science, **287** 97 (2000).
- [DeS92] R. DeSalvo, D. J. Hagan, M. Sheik-Bahae, G. Stegeman, E. W. V. Stryland, and H. Vanherzeele. *Self-focusing and self-defocusing by cascaded second-order effects in KTP*. Opt. Lett., **17** 28 (1992).
- [Des03] A. S. Desyatnikov, E. A. Ostrovskaya, Y. S. Kivshar, and C. Denz. *Composite Band-Gap Solitons in Nonlinear Optically Induced Lattices*. Phys. Rev. Lett., **91** 153902 (2003).
- [Des05a] A. S. Desyatnikov, Y. S. Kivshar, and L. Torner. *Optical vortices and vortex solitons*. volume 47 of *Progress in Optics*, 291 – 391. Elsevier (2005).
- [Des05b] A. S. Desyatnikov, D. Mihalache, D. Mazilu, B. A. Malomed, C. Denz, and F. Lederer. *Two-dimensional solitons with hidden and explicit vorticity in bimodal cubic-quintic media*. Phys. Rev. E, **71** 026615 (2005).
- [Des06] A. S. Desyatnikov, N. Sagemerten, R. Fischer, B. Terhalle, D. Träger, D. N. Neshev, A. Dreischuh, C. Denz, W. Krolikowski, and Y. S. Kivshar. *Two-dimensional self-trapped nonlinear photonic lattices*. Opt. Express, **14** 2851 (2006).
- [Dia85] E. Dianov and V. Mamyshev. *Stimulated-Raman conversion of multisoliton pulses in*. JETP Lett., **41** (1985).
- [Dir13] C. A. Dirdal and J. Skaar. *Superpositions of Lorentzians as the class of causal functions*. Phys. Rev. A, **88** 033834 (2013).
- [Dog01a] A. Dogariu, A. Kuzmich, H. Cao, and L. Wang. *Superluminal light pulse propagation via rephasing in a transparent anomalously dispersive medium*. Opt. Express, **8** 344 (2001).
- [Dog01b] A. Dogariu, A. Kuzmich, and L. J. Wang. *Transparent anomalous dispersion and superluminal light-pulse propagation at a negative group velocity*. Phys. Rev. A, **63** 053806 (2001).
- [Dor02a] C. Dorrer, E. Kosik, and I. Walmsley. *Spatio-temporal characterization of the electric field of ultrashort optical pulses using two-dimensional shearing interferometry*. Appl. Phys. B, **74** s209 (2002).
- [Dor02b] C. Dorrer, E. M. Kosik, and I. A. Walmsley. *Direct space time-characterization of the electric fields of ultrashort optical pulses*. Opt. Lett., **27** 548 (2002).
- [Dra66] L. Draper. *'Freak' ocean waves*. Weather, **21** 2 (1966).
- [Dre08a] F. Dreisow, M. Heinrich, A. Szameit, S. Doering, S. Nolte, A. Tünnermann, S. Fahr, and F. Lederer. *Spectral resolved dynamic localization in curved fs laser written waveguide arrays*. Opt. Express, **16** 3474 (2008).
- [Dre08b] F. Dreisow, A. Szameit, M. Heinrich, T. Pertsch, S. Nolte, and A. Tünnermann. *Second-order coupling in femtosecond-laser-written waveguide arrays*. Opt. Lett., **33** 2689 (2008).
- [Dro05] S. Droulias, K. Hizanidis, J. Meier, and D. Christodoulides. *X - waves in nonlinear normally dispersive waveguide arrays*. Opt. Express, **13** 1827 (2005).
- [DT98] P. Di Trapani, D. Caironi, G. Valiulis, A. Dubietis, R. Danielius, and A. Piskarskas. *Observation of Temporal Solitons in Second-Harmonic Generation with Tilted Pulses*. Phys. Rev. Lett., **81** 570 (1998).
- [DT00] P. Di Trapani, W. Chinaglia, S. Minardi, A. Piskarskas, and G. Valiulis. *Observation of Quadratic Optical Vortex Solitons*. Phys. Rev. Lett., **84** 3843 (2000).
- [DT03] P. Di Trapani, G. Valiulis, A. Piskarskas, O. Jedrkiewicz, J. Trull, C. Conti, and S. Trillo. *Spontaneously Generated X-Shaped Light Bullets*. Phys. Rev. Lett., **91** 093904 (2003).
- [Dud06] J. M. Dudley, G. Genty, and S. Coen. *Supercontinuum generation in photonic crystal fiber*. Rev. Mod. Phys., **78** 1135 (2006).
- [Dud08] J. M. Dudley, G. Genty, and B. J. Eggleton. *Harnessing and control of optical rogue waves in supercontinuum generation*. Opt. Express, **16** 3644 (2008).
- [Dun86] D. H. Dunlap and V. M. Kenkre. *Dynamic localization of a charged particle moving under the influence of an electric field*. Phys. Rev. B, **34** 3625 (1986).
- [Edm92] D. E. Edmundson and R. H. Enns. *Robust bistable light bullets*. Opt. Lett., **17** 586 (1992).
- [Edm93] D. E. Edmundson and R. H. Enns. *Fully three-dimensional collisions of bistable light bullets*. Opt. Lett., **18** 1609 (1993).
- [Efr02] N. Efremidis, S. Sears, D. Christodoulides, J. Fleischer, and M. Segev. *Discrete solitons in photorefractive optically induced photonic lattices*. Phys. Rev. E, **66** 46602 (2002).
- [Efr03] N. K. Efremidis, J. Hudock, D. N. Christodoulides, J. W. Fleischer, O. Cohen, and M. Segev. *Two-Dimensional Optical Lattice Solitons*. Phys. Rev. Lett., **91** 213906 (2003).

- [EG07] R. El-Ganainy, K. G. Makris, D. N. Christodoulides, and Z. H. Musslimani. *Theory of coupled optical PT-symmetric structures*. Opt. Lett., **32** 2632 (2007).
- [Egg96] B. J. Eggleton, R. E. Slusher, C. M. de Sterke, P. A. Krug, and J. E. Sipe. *Bragg grating solitons*. Phys. Rev. Lett., **76** 1627 (1996).
- [Egg11] B. Eggleton, B. Luther-Davies, and K. Richardson. *Chalcogenide photonics*. Nature Photon., **5** 141 (2011).
- [Eil10] F. Eilenberger, A. Szameit, and T. Pertsch. *Transition from discrete to continuous Townes solitons in periodic media*. Phys. Rev. A, **82** 043802 (2010).
- [Eil11a] F. Eilenberger, S. Minardi, A. Szameit, U. Röpke, J. Kobelke, K. Schuster, H. Bartelt, S. Nolte, L. Torner, F. Lederer, A. Tünnermann, and T. Pertsch. *Evolution dynamics of discrete-continuous light bullets*. Phys. Rev. A, **84** 013836 (2011).
- [Eil11b] F. Eilenberger, S. Minardi, A. Szameit, U. Röpke, J. Kobelke, K. Schuster, H. Bartelt, S. Nolte, A. Tünnermann, and T. Pertsch. *Light bullets in waveguide arrays: spacetime-coupling, spectral symmetry breaking and superluminal decay*. Opt. Express, **19** 23171 (2011).
- [Eil12] F. Eilenberger, S. Minardi, D. Pliakis, and T. Pertsch. *Digital holography from shadowgraphic phase estimates*. Opt. Lett., **37** 509 (2012).
- [Eil13a] F. Eilenberger, A. Brown, S. Minardi, and T. Pertsch. *Imaging cross-correlation FROG: measuring ultrashort, complex, spatiotemporal fields*. Opt. Express, **21** 25968 (2013).
- [Eil13b] F. Eilenberger, I. Kabakova, M. de Sterke, B. Eggleton, and T. Pertsch. *Cavity Optical Pulse Extraction: ultra-short pulse generation as seeded Hawking radiation [accepted]*. Sci. Rep., 260 (2013).
- [Eil13c] F. Eilenberger, K. Prater, S. Minardi, R. Geiss, U. Röpke, J. Kobelke, K. Schuster, H. Bartelt, S. Nolte, A. Tünnermann, and T. Pertsch. *Observation of Discrete, Vortex Light Bullets*. Phys. Rev. X, **3** 041031 (2013).
- [Eis98] H. Eisenberg, Y. Silberberg, R. Morandotti, A. Boyd, and J. Aitchison. *Discrete Spatial Optical Solitons in Waveguide Arrays*. Phys. Rev. Lett., **81** 3383 (1998).
- [Eis01] H. Eisenberg, R. Morandotti, Y. Silberberg, S. Bar-Ad, D. Ross, and J. Aitchison. *Kerr Spatiotemporal Self-Focusing in a Planar Glass Waveguide*. Phys. Rev. Lett., **87** 43902 (2001).
- [Eis02] H. S. Eisenberg, R. Morandotti, Y. Silberberg, J. M. Arnold, G. Pennelli, and J. S. Aitchison. *Optical discrete solitons in waveguide arrays. I. Soliton formation*. J. Opt. Soc. Am. B, **19** 2938 (2002).
- [Eng80] S. W. Englander, N. R. Kallenbach, A. J. Heeger, J. A. Krumhansl, and S. Litwin. *Nature of the open state in long polynucleotide double helices: possibility of soliton excitations*. Proc. Natl. Acad. Sci. U.S.A., **77** 7222 (1980).
- [Eng07] R. J. Engelen, Y. Sugimoto, H. Gersen, N. Ikeda, K. Asakawa, and L. K. Kuipers. *Ultrafast evolution of photonic eigenstates in k-space*. Nature Physics, **3** 401 (2007).
- [Enk92] S. van Enk and G. Nienhuis. *Eigenfunction description of laser beams and orbital angular momentum of light*. Opt. Commun., **94** 147 (1992).
- [Erk10] M. Erkintalo, G. Genty, and J. M. Dudley. *Giant dispersive wave generation through soliton collision*. Opt. Lett., **35** 658 (2010).
- [Eug01] E. D. Eugenieva, N. K. Efremidis, and D. N. Christodoulides. *Design of switching junctions for two-dimensional discrete soliton networks*. Opt. Lett., **26** 1978 (2001).
- [FA08] S. Franke-Arnold, L. Allen, and M. Padgett. *Advances in optical angular momentum*. Laser Photon. Rev., **2** 299 (2008).
- [Fac05] D. Faccio, P. D. Trapani, S. Minardi, A. Bramati, F. Bragheri, C. Liberale, V. Degiorgio, A. Dubietis, and A. Matijosius. *Far-field spectral characterization of conical emission and filamentation in Kerr media*. J. Opt. Soc. Am. B, **22** 862 (2005).
- [Fac06] D. Faccio, M. A. Porras, A. Dubietis, F. Bragheri, A. Couairon, and P. Di Trapani. *Conical Emission, Pulse Splitting, and X-Wave Parametric Amplification in Nonlinear Dynamics of Ultrashort Light Pulses*. Phys. Rev. Lett., **96** 193901 (2006).
- [Fer55] E. Fermi, J. Pasta, and S. T. M. Ulam. *Studies of Nonlinear Problems I*. Los Alamos National Laboratory (LANL) Technical Report, **LA-1940** (1955).
- [Fer05] A. Ferrando, M. Zacarés, M.-A. Garc-March, J. A. Monsoriu, and P. F. de Córdoba. *Vortex Transmutation*. Phys. Rev. Lett., **95** 123901 (2005).
- [Fer11] F. Ferdous, H. Miao, D. Leaird, K. Srinivasan, J. Wang, L. Chen, L. Varghese, and A. Weiner. *Spectral line-by-line pulse shaping of on-chip microresonator frequency combs*. Nature Photon. (2011).
- [Fib04] G. Fibich and B. Ilan. *Optical light bullets in a pure Kerr medium*. Opt. Lett., **29** 887 (2004).

- [Fil89] F. Fillaux and C. Carlile. *Collective rotation of methyl groups in isotopic mixtures of 4-methylpyridine at low temperature. Inelastic neutron scattering spectra.* Chem. Phys. Lett., **162** 188 (1989).
- [Fir97] W. J. Firth and D. V. Skryabin. *Optical Solitons Carrying Orbital Angular Momentum.* Phys. Rev. Lett., **79** 2450 (1997).
- [Fis73] R. A. Fisher and W. Bischel. *The role of linear dispersion in plane-wave self-phase modulation.* Appl. Phys. Lett., **23** 661 (1973).
- [Fis83] R. A. Fisher, editor. *Optical phase conjugation.* Academic Press (1983).
- [Fis06] R. Fischer, D. Trager, D. Neshev, A. Sukhorukov, W. Krolikowski, C. Denz, and Y. Kivshar. *Reduced-Symmetry Two-Dimensional Solitons in Photonic Lattices.* Phys. Rev. Lett., **96** 023905 (2006).
- [Fle03a] J. Fleischer, T. Carmon, M. Segev, N. Efremidis, and D. Christodoulides. *Observation of Discrete Solitons in Optically Induced Real Time Waveguide Arrays.* Phys. Rev. Lett., **90** 23902 (2003).
- [Fle03b] J. Fleischer, M. Segev, N. Efremidis, and D. Christodoulides. *Observation of two-dimensional discrete solitons in optically induced nonlinear photonic lattices.* Nature, **422** 147 (2003).
- [Fra61] P. A. Franken, A. E. Hill, C. W. Peters, and G. Weinreich. *Generation of Optical Harmonics.* Phys. Rev. Lett., **7** 118 (1961).
- [Fra04] A. Fratallocchi, G. Assanto, K. A. Brzdakiewicz, and M. A. Karpierz. *Discrete propagation and spatial solitons in nematicliquid crystals.* Opt. Lett., **29** 1530 (2004).
- [Fre06] B. Freedman, G. Bartal, M. Segev, R. Lifshitz, D. N. Christodoulides, and J. W. Fleischer. *Wave and defect dynamics in nonlinear photonic quasicrystals.* Nature, **440** 1166 (2006).
- [Fre07] B. Freedman, R. Lifshitz, J. W. Fleischer, and M. Segev. *Phason dynamics in nonlinear photonic quasicrystals.* Nat. Mater., **6** 776 (2007).
- [Gab04] P. Gabolde and R. Trebino. *Self-referenced measurement of the complete electric field of ultrashort pulses.* Opt. Express, **12** 4423 (2004).
- [Gab06] P. Gabolde and R. Trebino. *Single-shot measurement of the full spatio-temporal field of ultrashort pulses with multi-spectral digital holography.* Opt. Express, **14** 11460 (2006).
- [Gal01] L. Gallmann, G. Steinmeyer, D. H. Sutter, T. Rupp, C. Iaconis, I. A. Walmsley, and U. Keller. *Spatially resolved amplitude and phase characterization of femtosecond optical pulses.* Opt. Lett., **26** 96 (2001).
- [Gar67] C. S. Gardner, J. M. Greene, M. D. Kruskal, and R. M. Miura. *Method for Solving the Korteweg-de Vries Equation.* Phys. Rev. Lett., **19** 1095 (1967).
- [Gar74] C. S. Gardner, J. M. Greene, M. D. Kruskal, and R. M. Miura. *Korteweg-devries equation and generalizations. VI. methods for exact solution.* Commun. Pur. Appl. Math., **27** 97 (1974).
- [Gar12] E. Garmire. *Nonlinear Optics*, chapter Overview of Nonlinear Optics. Intech Open Science (2012).
- [Gar13] E. Garmire. *Nonlinear optics in daily life.* Opt. Express, **21** 30532 (2013).
- [Gel51] I. M. Gel'fand and B. M. Levitan. *On the determination of a differential equation from its spectral function.* Izvestiya Rossiiskoi Akademii Nauk. Seriya Matematicheskaya, **15** 309 (1951).
- [Ger72] R. W. Gerchberg and W. O. Saxton. *A practical algorithm for the determination of phase from image and diffraction plane pictures.* Optik (Stuttgart), **35** 227– (1972).
- [Gib04] G. Gibson, J. Courtial, M. Padgett, M. Vasnetsov, V. Pas'ko, S. Barnett, and S. Franke-Arnold. *Free-space information transfer using light beams carrying orbital angular momentum.* Opt. Express, **12** 5448 (2004).
- [Gla98] P. Glas, M. Naumann, A. Schirmacher, and T. Pertsch. *The multicore fiber – a novel design for a diode pumped fiber laser.* Opt. Commun., **151** 187 (1998).
- [Gol85] E. Golovchenko, E. Dianov, A. Prokhorov, and V. Serkin. *Decay of optical solitons.* JETP Lett., **42** 87 (1985).
- [gol06] golem.de. *CCD-Sensor mit 111 Megapixeln entwickelt* (2006).
- [Goo11] M. Goodwin. *Photonics - Our Vision for a Key Enabling Technology of Europe* (2011).
- [Gor86] J. P. Gordon. *Theory of the soliton self-frequency shift.* Opt. Lett., **11** 662 (1986).
- [Gor07a] A. V. Gorbach and D. V. Skryabin. *Cascaded Generation of Multiply Charged Optical Vortices and Spatiotemporal Helical Beams in a Raman Medium.* Phys. Rev. Lett., **98** 243601 (2007).
- [Gor07b] A. V. Gorbach and D. V. Skryabin. *Light trapping in gravity-like potentials and expansion of supercontinuum spectra in photonic-crystal fibres.* Nature Photon., **1** 653 (2007).
- [Gor10] A. V. Gorbach, W. Ding, O. K. Staines, C. E. de Nobrega, G. D. Hobbs, W. J. Wadsworth, J. C. Knight, D. V. Skryabin, A. Samarelli, M. Sorel, and R. M. De La Rue. *Spatiotemporal nonlinear optics in arrays of subwavelength waveguides.* Phys. Rev. A, **82** 041802 (2010).

- [Gur09] H. C. Gurgov and O. Cohen. *Spatiotemporal pulse-train solitons*. Opt. Express, **17** 7052 (2009).
- [Hac03] M. Hacker, G. Stobrawa, R. Sauerbrey, T. Buckup, M. Motzkus, M. Wildenhain, and A. Gehner. *Micromirror SLM for femtosecond pulse shaping in the ultraviolet*. Appl. Phys. B, **76** 711 (2003).
- [Han09] R. C. Hansen. *Phased array antennas*, volume 213. John Wiley & Sons (2009).
- [Har73] R. H. Hardin and F. D. Tappert. *Application of the split-step Fourier method to the numerical solution of nonlinear and variable coefficient wave equations*. SIAM Rev., **15** 423 (1973).
- [Has70] A. Hasegawa. *Observation of Self-Trapping Instability of a Plasma Cyclotron Wave in a Computer Experiment*. Phys. Rev. Lett., **24** 1165 (1970).
- [Has73] A. Hasegawa and F. Tappert. *Transmission of stationary nonlinear optical pulses in dispersive dielectric fibers. I. Anomalous dispersion*. Appl. Phys. Lett., **23** 142 (1973).
- [Hav04] S. Haver. *A possible freak wave event measured at the Draupner Jacket January 1 1995*. In *Rogue Waves* (2004).
- [He95] H. He, M. E. J. Friese, N. R. Heckenberg, and H. Rubinsztein-Dunlop. *Direct Observation of Transfer of Angular Momentum to Absorptive Particles from a Laser Beam with a Phase Singularity*. Phys. Rev. Lett., **75** 826 (1995).
- [Hec11] O. H. Heckl, C. J. Saraceno, C. R. E. Baer, T. Südmeyer, Y. Y. Wang, Y. Cheng, F. Benabid, and U. Keller. *Temporal pulse compression in a xenon-filled Kagome-type hollow-core photonic crystal fiber at high average power*. Opt. Express, **19** 19142 (2011).
- [Hei05] T. Heimburg and A. D. Jackson. *On soliton propagation in biomembranes and nerves*. Proc. Natl. Acad. Sci. U. S. A., **102** 9790 (2005).
- [Hei09a] M. Heinrich, Y. V. Kartashov, A. Szameit, F. Dreisow, R. Keil, S. Nolte, A. Tünnermann, V. A. Vysloukh, and L. Torner. *Observation of two-dimensional coherent surface vector lattice solitons*. Opt. Lett., **34** 1624 (2009).
- [Hei09b] M. Heinrich, A. Szameit, F. Dreisow, R. Keil, S. Minardi, T. Pertsch, S. Nolte, A. Tünnermann, and F. Lederer. *Observation of Three-Dimensional Discrete-Continuous X Waves in Photonic Lattices*. Phys. Rev. Lett., **103** 113903 (2009).
- [Hei12] M. Heinrich, F. Eilenberger, R. Keil, F. Dreisow, E. Suran, F. Louradour, A. Tünnermann, T. Pertsch, S. Nolte, and A. Szameit. *Optical limiting and spectral stabilization in segmented photonic lattices*. Opt. Express, **20** 27299 (2012).
- [Her64] M. Hercher. *Laser-induced damage in transparent media author:hercher*. In *Program of the 1964 Spring Meeting of the Optical Society of America, Incorporated*, volume 54, 563. Optical Society of America (1964).
- [Her02] J. Herrmann, U. Griebner, N. Zhavoronkov, A. Husakou, D. Nickel, J. Knight, W. Wadsworth, P. Russell, and G. Korn. *Experimental Evidence for Supercontinuum Generation by Fission of Higher-Order Solitons in Photonic Fibers*. Phys. Rev. Lett., **88** 173901 (2002).
- [Hil00] R. C. Hilborn. *Chaos and nonlinear dynamics: an introduction for scientists and engineers*. Oxford University Press (2000).
- [Hod52] A. Hodgkin and A. Huxley. *A quantitative description of membrane current and its application to conduction and excitation in nerve*. J. Physiol., **117** 500 (1952).
- [Hol59a] T. Holstein. *Studies of polaron motion: Part I. The molecular-crystal model*. Ann. Phys, **8** 325 (1959).
- [Hol59b] T. Holstein. *Studies of polaron motion: Part II. The "small" polaron*. Ann. Phys, **8** 343 (1959).
- [Hus01] A. V. Husakou and J. Herrmann. *Supercontinuum Generation of Higher-Order Solitons by Fission in Photonic Crystal Fibers*. Phys. Rev. Lett., **87** 203901 (2001).
- [Iac98] C. Iaconis and I. Walmsley. *Spectral phase interferometry for direct electric-field reconstruction of ultrashort optical pulses*. Opt. Lett., **23** 792 (1998).
- [Iwa04] R. Iwanow, R. Schiek, G. Stegeman, T. Pertsch, F. Lederer, Y. Min, and W. Sohler. *Observation of Discrete Quadratic Solitons*. Phys. Rev. Lett., **93** 113902 (2004).
- [Iwa05a] R. Iwanow, D. May-Arrijoja, D. Christodoulides, G. Stegeman, Y. Min, and W. Sohler. *Discrete Talbot Effect in Waveguide Arrays*. Phys. Rev. Lett., **95** 53902 (2005).
- [Iwa05b] R. Iwanow, G. Stegeman, R. Schiek, Y. Min, and W. Sohler. *Discrete modulational instability in periodically poled lithium niobate waveguide arrays*. Opt. Express, **13** 7794 (2005).
- [Jac06] J. D. Jackson. *Klassische Elektrodynamik*. Walter de Gruyter (2006).
- [Ji10] H. Ji, M. Galili, H. Hu, M. Pu, L. Oxenlowe, K. Yvind, J. Hvam, and P. Jeppesen. *1.28-Tb/s Demultiplexing of an OTDM DPSK Data Signal Using a Silicon Waveguide*. Photonics Technology Letters, IEEE, **22** 1762 (2010).

- [Jia07] S. Jia, W. Wan, and J. Fleischer. *Dispersive Shock Waves in Nonlinear Arrays*. Phys. Rev. Lett., **99** 223901 (2007).
- [Joh72] P. B. Johnson and R. W. Christy. *Optical Constants of the Noble Metals*. Phys. Rev. B, **6** 4370 (1972).
- [Jol11] N. Y. Joly, J. Nold, W. Chang, P. Hölzer, A. Nazarkin, G. K. L. Wong, F. Biancalana, and J. Russell, P. St. *Bright Spatially Coherent Wavelength-Tunable Deep-UV Laser Source Using an Ar-Filled Photonic Crystal Fiber*. Phys. Rev. Lett., **106** 203901 (2011).
- [Jon65] A. Jones. *Coupling of optical fibers and scattering in fibers*. J. Opt. Soc. Am, **55** 261 (1965).
- [Jov11a] D. M. Jovic, M. R. Belic, and C. Denz. *Transverse localization of light in nonlinear photonic lattices with dimensionality crossover*. Phys. Rev. A, **84** 043811 (2011).
- [Jov11b] D. M. Jovic, Y. S. Kivshar, C. Denz, and M. R. Belic. *Anderson localization of light near boundaries of disordered photonic lattices*. Phys. Rev. A, **83** 033813 (2011).
- [Jov12a] D. Jovic and C. Denz. *Disorder-induced localization of light in one- and two-dimensional photonic lattices*. Phys. Scr., **2012** 014042 (2012).
- [Jov12b] D. M. Jovic, M. R. Belic, and C. Denz. *Anderson localization of light at the interface between linear and nonlinear dielectric media with an optically induced photonic lattice*. Phys. Rev. A, **85** 031801 (2012).
- [Jov12c] D. M. Jovic, C. Denz, and M. R. Belic. *Anderson localization of light in PT-symmetric optical lattices*. Opt. Lett., **37** 4455 (2012).
- [Kan93] D. Kane and R. Trebino. *Characterization of arbitrary femtosecond pulses using frequency-resolved optical gating*. IEEE J. Quant. Electron., **29** 571 (1993).
- [Kan05] C. L. Kane and E. J. Mele. *Quantum Spin Hall Effect in Graphene*. Phys. Rev. Lett., **95** 226801 (2005).
- [Kar67] V. Karpman. *Self-modulation of nonlinear plane waves in dispersive media*. J. Exp. Theor. Phys., **6** 277 (1967).
- [Kar69] V. Karpman and E. Krushkal'. *Modulated Waves in Nonlinear Dispersive Media*. JETP, **55** 277 (1969).
- [Kar05] Y. V. Kartashov, A. Ferrando, A. A. Egorov, and L. Torner. *Soliton Topology versus Discrete Symmetry in Optical Lattices*. Phys. Rev. Lett., **95** 123902 (2005).
- [Kar11] Y. V. Kartashov, B. A. Malomed, and L. Torner. *Solitons in nonlinear lattices*. Rev. Mod. Phys., **83** 247 (2011).
- [Kin10] P. Kinsler. *Unidirectional optical pulse propagation equation for materials with both electric and magnetic responses*. Phys. Rev. A, **81** 023808 (2010).
- [Kiv92] Y. S. Kivshar and M. Peyrard. *Modulational instabilities in discrete lattices*. Phys. Rev. A, **46** 3198 (1992).
- [Kiv93a] Y. Kivshar. *Self-localization in arrays of defocusing waveguides*. Opt. Lett, **18** 1147 (1993).
- [Kiv93b] Y. S. Kivshar and D. K. Campbell. *Peierls-Nabarro potential barrier for highly localized nonlinear modes*. Phys. Rev. E, **48** 3077 (1993).
- [Kiv94a] Y. Kivshar, W. Królikowski, and O. Chubykalo. *Dark solitons in discrete lattices*. Phys. Rev. E, **50** 5020 (1994).
- [Kiv94b] Y. Kivshar and S. Turitsyn. *Spatiotemporal pulse collapse on periodic potentials*. Phys. Rev. E, **49** 2536 (1994).
- [Kiv00] Y. S. Kivshar and D. E. Pelinovsky. *Self-focusing and transverse instabilities of solitary waves*. Phys. Rep., **331** 117 (2000).
- [Kiv03] Y. Kivshar and G. Agrawal. *Optical Solitons*. Academic Press, San Diego (2003).
- [Kni03] J. Knight. *Photonic crystal fibres*. Nature, **424** 847 (2003).
- [Kob98] A. Kobayakov, S. Darmanyan, F. Lederer, and E. Schmidt. *Dark spatial solitons in discrete cubic media with self-and cross-phase modulation*. Opt. Quantum. Electron., **30** 795 (1998).
- [Kol04a] M. Kolesik and J. V. Moloney. *Nonlinear optical pulse propagation simulation: From Maxwell's to unidirectional equations*. Phys. Rev. E, **70** 036604 (2004).
- [Kol04b] M. Kolesik, E. M. Wright, and J. V. Moloney. *Dynamic Nonlinear X Waves for Femtosecond Pulse Propagation in Water*. Phys. Rev. Lett., **92** 253901 (2004).
- [Kom95] T. S. Komatsu and S.-i. Sasa. *Kink soliton characterizing traffic congestion*. Phys. Rev. E, **52** 5574 (1995).
- [Kor95] D. Korteweg and G. De Vries. *XLI. On the change of form of long waves advancing in a rectangular canal, and on a new type of long stationary waves*. Philosophical Magazine Series 5, **39** 422 (1895).

- [Kos54] G. F. Koster and J. C. Slater. *Wave Functions for Impurity Levels*. Phys. Rev., **95** 1167 (1954).
- [Kos05] E. M. Kosik, A. S. Radunsky, I. A. Walmsley, and C. Dorrer. *Interferometric technique for measuring broadband ultrashort pulses at the sampling limit*. Opt. Lett., **30** 326 (2005).
- [Kr696] W. Królikowski and Y. Kivshar. *Soliton-based optical switching in waveguide arrays*. J. Opt. Soc. Am. B, **13** 876 (1996).
- [Kr698a] W. Królikowski, C. Denz, A. Stepken, M. Saffman, and B. Luther-Davies. *Interaction of spatial photorefractive solitons*. Quant. Semiclass. Opt. Euro. Opt. Soc. B, **10** 823 (1998).
- [Kr698b] W. Królikowski, M. Saffman, B. Luther-Davies, and C. Denz. *Anomalous Interaction of Spatial Solitons in Photorefractive Media*. Phys. Rev. Lett., **80** 3240 (1998).
- [Kr698c] W. Królikowski, B. Luther-Davies, C. Denz, and T. Tschudi. *Annihilation of photorefractive solitons*. Opt. Lett., **23** 97 (1998).
- [Kr603] W. Królikowski, B. Luther-Davies, and C. Denz. *Photorefractive solitons*. IEEE J. Quant. Electron., **39** 3 (2003).
- [Kra27] H. Kramers. *La diffusion de la lumière par les atomes* (1927).
- [Kro26] R. D. L. Kronig. *On the theory of dispersion of X-rays*. J. Opt. Soc. Am., **12** 547 (1926).
- [Kur95] D. A. Kurtze and D. C. Hong. *Traffic jams, granular flow, and soliton selection*. Phys. Rev. E, **52** 218 (1995).
- [Kut01] M. W. Kutta. *Beitrag zur näherungsweise Integration totaler Differentialgleichungen*. Z. Mat. Phys., **46** 435 (1901).
- [Kuz01] A. Kuzmich, A. Dogariu, L. J. Wang, P. W. Milonni, and R. Y. Chiao. *Signal Velocity, Causality, and Quantum Noise in Superluminal Light Pulse Propagation*. Phys. Rev. Lett., **86** 3925 (2001).
- [Lah07] Y. Lahini, E. Frumker, Y. Silberberg, S. Droulias, K. Hizanidis, R. Morandotti, and D. N. Christodoulides. *Discrete X-Wave Formation in Nonlinear Waveguide Arrays*. Phys. Rev. Lett., **98** 023901 (2007).
- [Lah08] Y. Lahini, A. Avidan, F. Pozzi, M. Sorel, R. Morandotti, D. N. Christodoulides, and Y. Silberberg. *Anderson Localization and Nonlinearity in One-Dimensional Disordered Photonic Lattices*. Phys. Rev. Lett., **100** 013906 (2008).
- [Lan60] L. D. Landau, E. M. Lifšic, J. B. Sykes, J. S. Bell, M. Kearsley, and L. P. Pitaevskii. *Electrodynamics of continuous media*, volume 364. Pergamon press Oxford (1960).
- [Lan75] L. D. Landau and E. M. Lifšic. *The classical theory of fields*, volume 2. Butterworth-Heinemann (1975).
- [Leb08] H. Leblond, B. A. Malomed, and D. Mihalache. *Spatiotemporal vortices in optical fiber bundles*. Phys. Rev. A, **77** 063804 (2008).
- [Leb10] H. Leblond and D. Mihalache. *Ultrashort light bullets described by the two-dimensional sine-Gordon equation*. Phys. Rev. A, **81** 063815 (2010).
- [Leb11] H. Leblond, B. A. Malomed, and D. Mihalache. *Spatiotemporal vortex solitons in hexagonal arrays of waveguides*. Phys. Rev. A, **83** 063825 (2011).
- [Led94] F. Lederer and W. Biehlig. *Bright solitons and light bullets in semiconductor waveguides*. Electron. Lett., **30** 1871 (1994).
- [Led02] F. Lederer and Y. Silberberg. *Discrete Solitons*. Opt. Photon. News, **13** 48 (2002).
- [Led08] F. Lederer, G. I. Stegeman, D. N. Christodoulides, G. Assanto, M. Segev, and Y. Silberberg. *Discrete solitons in optics*. Phys. Rep., **463** 1 (2008).
- [Lev05] H. J. Levinson. *Principles of lithography*, volume 146. SPIE press (2005).
- [LF99] B. La Fontaine, F. Vidal, Z. Jiang, C. Y. Chien, D. Comtois, A. Desparois, T. W. Johnston, J.-C. Kieffer, H. Pépin, and H. P. Mercure. *Filamentation of ultrashort pulse laser beams resulting from their propagation over long distances in air*. Phys. Plasmas, **6** 1615 (1999).
- [Li85] T. Li. *Optical Fiber Communications: Fiber Fabrication*. Academic Press (1985).
- [Lie74] S. Lie. *Begründung einer Invarianten-Theorie der Berührungs-Transformationen*. Math. Ann., **8** 215 (1874).
- [Lie80a] S. Lie. *Zur Theorie der Flächen konstanter Krümmung III*. Archiv for matematik og naturvidenskab, **5** 282 (1880).
- [Lie80b] S. Lie. *Zur Theorie der Flächen konstanter Krümmung III*. Archiv for matematik og naturvidenskab, **5** 328 (1880).
- [Lin98] S. Linden, H. Giessen, and J. Kuhl. *XFROG — A New Method for Amplitude and Phase Characterization of Weak Ultrashort Pulses*. Phys. Status Solidi (B), **206** 119 (1998).

- [Lin11] Z. Lin, H. Ramezani, T. Eichelkraut, T. Kottos, H. Cao, and D. N. Christodoulides. *Unidirectional Invisibility Induced by PT-Symmetric Periodic Structures*. Phys. Rev. Lett., **106** 213901 (2011).
- [Liu99] X. Liu, L. J. Qian, and F. W. Wise. *Generation of Optical Spatiotemporal Solitons*. Phys. Rev. Lett., **82** 4631 (1999).
- [Lob10] V. E. Lobanov, Y. V. Kartashov, and L. Torner. *Light Bullets by Synthetic Diffraction-Dispersion Matching*. Phys. Rev. Lett., **105** 033901 (2010).
- [Lon06] S. Longhi, M. Marangoni, M. Lobino, R. Ramponi, P. Laporta, E. Cianci, and V. Foglietti. *Observation of Dynamic Localization in Periodically Curved Waveguide Arrays*. Phys. Rev. Lett., **96** 243901 (2006).
- [Lon08] S. Longhi. *Image reconstruction in segmented waveguide arrays*. Opt. Lett., **33** 473 (2008).
- [Loz04] V. V. Lozovoy, I. Pastirk, and M. Dantus. *Multiphoton intrapulse interference IV: Ultrashort laserpulse spectral phase characterization and compensation*. Opt. Lett., **29** 775 (2004).
- [Mai60] T. H. Maiman. *Stimulated optical radiation in ruby*. Nature, **187** 493 (1960).
- [Mak05] K. Makris, S. Suntsov, D. Christodoulides, G. Stegeman, and A. Hache. *Discrete surface solitons*. Opt. Lett., **30** 2466 (2005).
- [Mak06] K. G. Makris, J. Hudock, D. N. Christodoulides, G. I. Stegeman, O. Manela, and M. Segev. *Surface lattice solitons*. Opt. Lett., **31** 2774 (2006).
- [Mak08] K. G. Makris, R. El-Ganainy, D. N. Christodoulides, and Z. H. Musslimani. *Beam Dynamics in PT Symmetric Optical Lattices*. Phys. Rev. Lett., **100** 103904 (2008).
- [Mak10] K. G. Makris, R. El-Ganainy, D. N. Christodoulides, and Z. H. Musslimani. *PT-symmetric optical lattices*. Phys. Rev. A, **81** 063807 (2010).
- [Mal65] I. H. Malitson. *Interspecimen Comparison of the Refractive Index of Fused Silica*. J. Opt. Soc. Am., **55** 1205 (1965).
- [Mal01] B. Malomed and P. Kevrekidis. *Discrete vortex solitons*. Phys. Rev. E, **64** 26601 (2001).
- [Mal05] B. A. Malomed, D. Mihalache, F. Wise, and L. Torner. *Spatiotemporal optical solitons*. J. Opt. B, **7** R53 (2005).
- [Man03] D. Mandelik, H. S. Eisenberg, Y. Silberberg, R. Morandotti, and J. S. Aitchison. *Band-Gap Structure of Waveguide Arrays and Excitation of Floquet-Bloch Solitons*. Phys. Rev. Lett., **90** 053902 (2003).
- [Man04a] D. Mandelik, R. Morandotti, J. S. Aitchison, and Y. Silberberg. *Gap Solitons in Waveguide Arrays*. Phys. Rev. Lett., **92** 093904 (2004).
- [Man04b] O. Manela, O. Cohen, G. Bartal, J. W. Fleischer, and M. Segev. *Two-dimensional higher-band vortex lattice solitons*. Opt. Lett., **29** 2049 (2004).
- [Mar64] E. Marcatili and R. Schmeltzer. *Hollow metallic and dielectric waveguides for long distance optical transmission and lasers (Long distance optical transmission in hollow dielectric and metal circular waveguides, examining normal mode propagation)*. Bell System Technical Journal, **43** 1783 (1964).
- [Mar72] D. Marcuse. *Light transmission optics* (1972).
- [Mar86] V. A. Marchenko. *Sturm-Liouville operators and applications*. American Mathematical Soc. (1986).
- [Mar89] O. Martinez. *Achromatic phase matching for second harmonic generation of femtosecond pulses*. IEEE J. Quantum. Electron., **25** 2464 (1989).
- [Mar95] P. Marquié, J. M. Bilbault, and M. Remoissenet. *Observation of nonlinear localized modes in an electrical lattice*. Phys. Rev. E, **51** 6127 (1995).
- [Mat10] M. Matuszewski, I. L. Garanovich, and A. A. Sukhorukov. *Light bullets in nonlinear periodically curved waveguide arrays*. Phys. Rev. A, **81** 043833 (2010).
- [McM96] P. McManamon, T. Dorschner, D. Corkum, L. Friedman, D. Hobbs, M. Holz, S. Liberman, H. Nguyen, D. Resler, R. Sharp, and E. Watson. *Optical phased array technology*. IEEE J. Proc., **84** 268 (1996).
- [Mec91] A. Mecozzi, J. D. Moores, H. A. Haus, and Y. Lai. *Soliton transmission control*. Opt. Lett., **16** 1841 (1991).
- [Mei03] J. Meier, J. Hudock, D. Christodoulides, G. Stegeman, Y. Silberberg, R. Morandotti, and J. S. Aitchison. *Discrete Vector Solitons in Kerr Nonlinear Waveguide Arrays*. Phys. Rev. Lett., **91** 143907 (2003).
- [Mei04a] J. Meier, G. I. Stegeman, D. N. Christodoulides, Y. Silberberg, R. Morandotti, H. Yang, G. Salamo, M. Sorel, and J. S. Aitchison. *Experimental Observation of Discrete Modulational Instability*. Phys. Rev. Lett., **92** 163902 (2004).

- [Mei04b] J. Meier, G. I. Stegeman, Y. Silberberg, R. Morandotti, and J. S. Aitchison. *Nonlinear Optical Beam Interactions in Waveguide Arrays*. Phys. Rev. Lett., **93** 093903 (2004).
- [Mei05a] J. Meier, J. Hudock, D. N. Christodoulides, G. I. Stegeman, H. Yang, G. Salamo, R. Morandotti, J. S. Aitchison, and Y. Silberberg. *Excitation of strongly confined scalar and vector self-trapped beams in one-dimensional arrays of Kerr-nonlinear channel waveguides*. J. Opt. Soc. Am. B, **22** 1432 (2005).
- [Mei05b] J. Meier, G. Stegeman, D. Christodoulides, R. Morandotti, M. Sorel, H. Yang, G. Salamo, J. Aitchison, and Y. Silberberg. *Nonlinear beam interactions in 1D discrete Kerr systems*. Opt. Express, **13** 1797 (2005).
- [Mei05c] J. Meier, G. I. Stegeman, D. N. Christodoulides, Y. Silberberg, R. Morandotti, H. Yang, G. Salamo, M. Sorel, and J. S. Aitchison. *Beam interactions with a blocker soliton in one-dimensional arrays*. Opt. Lett., **30** 1027 (2005).
- [Mes97] D. Meshulach, D. Yelin, and Y. Silberberg. *Adaptive ultrashort pulse compression and shaping*. Opt. Commun., **138** 345 (1997).
- [Mih89] D. Mihalache, M. Bertolotti, and C. Sibilia. *{IV} Nonlinear Wave Propagation in Planar Structures*. volume 27 of *Progress in Optics*, 227 – 313. Elsevier (1989).
- [Mih99] D. Mihalache, D. Mazilu, J. Dörring, and L. Torner. *Elliptical light bullets*. Opt. Commun., **159** 129 (1999).
- [Mih00] D. Mihalache, D. Mazilu, L.-C. Crasovan, B. A. Malomed, and F. Lederer. *Azimuthal instability of spinning spatiotemporal solitons*. Phys. Rev. E, **62** R1505 (2000).
- [Mih04] D. Mihalache, D. Mazilu, F. Lederer, Y. V. Kartashov, L.-C. Crasovan, and L. Torner. *Stable three-dimensional spatiotemporal solitons in a two-dimensional photonic lattice*. Phys. Rev. E, **70** 055603 (2004).
- [Mih05] D. Mihalache, D. Mazilu, F. Lederer, B. Malomed, Y. Kartashov, L. Crasovan, and L. Torner. *Stable Spatiotemporal Solitons in Bessel Optical Lattices*. Phys. Rev. Lett., **95** 23902 (2005).
- [Mih07a] D. Mihalache, D. Mazilu, F. Lederer, and Y. S. Kivshar. *Interface discrete light bullets in waveguide arrays*. Opt. Lett., **32** 2091 (2007).
- [Mih07b] D. Mihalache, D. Mazilu, F. Lederer, and Y. S. Kivshar. *Spatiotemporal surface solitons in two-dimensional photonic lattices*. Opt. Lett., **32** 3173 (2007).
- [Mih07c] D. Mihalache, D. Mazilu, F. Lederer, and Y. S. Kivshar. *Stable discrete surface light bullets*. Opt. Express, **15** 589 (2007).
- [Mih09a] D. Mihalache, D. Mazilu, F. Lederer, and Y. S. Kivshar. *Collisions between discrete surface spatiotemporal solitons in nonlinear waveguide arrays*. Phys. Rev. A, **79** 013811 (2009).
- [Mih09b] D. Mihalache, D. Mazilu, F. Lederer, and Y. S. Kivshar. *Discrete light bullets in two-dimensional photonic lattices: Collision scenarios*. Opt. Commun., **282** 3000 (2009).
- [Mil87] D. L. Mills and S. E. Trullinger. *Gap solitons in nonlinear periodic structures*. Phys. Rev. B, **36** 947 (1987).
- [Min03] S. Minardi, J. Yu, G. Blasi, A. Varanavicius, G. Valiulis, A. Berzanskis, A. Piskarskas, and P. Di Trapani. *Red Solitons: Evidence of Spatiotemporal Instability in  $\chi^{(2)}$  Spatial Soliton Dynamics*. Phys. Rev. Lett., **91** 123901 (2003).
- [Min09a] S. Minardi, A. Gopal, A. Couairon, G. Tamošauskas, R. Piskarskas, A. Dubietis, and P. D. Trapani. *Accurate retrieval of pulse-splitting dynamics of a femtosecond filament in water by time-resolved shadowgraphy*. Opt. Lett., **34** 3020 (2009).
- [Min09b] S. Minardi, J. Trull, and M. A. C. Potenza. *Holographic Properties of Parametric Image Conversion for Spatiotemporal Imaging of Ultrashort Laser Pulses*. J. Holography Speckle, **5** 85 (2009).
- [Min10a] S. Minardi, F. Eilenberger, Y. V. Kartashov, A. Szameit, U. Röpke, J. Kobelke, K. Schuster, H. Bartelt, S. Nolte, L. Torner, F. Lederer, A. Tünnermann, and T. Pertsch. *Three-Dimensional Light Bullets in Arrays of Waveguides*. Phys. Rev. Lett., **105** 263901 (2010).
- [Min10b] S. Minardi and T. Pertsch. *Interferometric beam combination with discrete optics*. Opt. Lett., **35** 3009 (2010).
- [Mit86] F. M. Mitschke and L. F. Mollenauer. *Discovery of the soliton self-frequency shift*. Opt. Lett., **11** 659 (1986).
- [MM06] L. Morales-Molina and R. A. Vicencio. *Trapping of discrete solitons by defects in nonlinear waveguide arrays*. Opt. Lett., **31** 966 (2006).
- [Mol80] L. F. Mollenauer, R. H. Stolen, and J. P. Gordon. *Experimental Observation of Picosecond Pulse Narrowing and Solitons in Optical Fibers*. Phys. Rev. Lett., **45** 1095 (1980).

- [Mol88] L. F. Mollenauer and K. Smith. *Demonstration of soliton transmission over more than 4000 km in fiber with loss periodically compensated by Raman gain*. Opt. Lett., **13** 675 (1988).
- [Mon10] A. Monmayrant, S. Weber, and B. Chatel. *A newcomer's guide to ultrashort pulse shaping and characterization*. J. Phys. B: At., Mol. Opt. Phys., **43** 103001 (2010).
- [Mor99a] R. Morandotti, U. Peschel, J. Aitchison, H. Eisenberg, and Y. Silberberg. *Experimental Observation of Linear and Nonlinear Optical Bloch Oscillations*. Phys. Rev. Lett., **83** 4756 (1999).
- [Mor99b] R. Morandotti, U. Peschel, J. S. Aitchison, H. S. Eisenberg, and Y. Silberberg. *Dynamics of Discrete Solitons in Optical Waveguide Arrays*. Phys. Rev. Lett., **83** 2726 (1999).
- [Mor01] R. Morandotti, H. S. Eisenberg, Y. Silberberg, M. Sorel, and J. S. Aitchison. *Self-Focusing and Defocusing in Waveguide Arrays*. Phys. Rev. Lett., **86** 3296 (2001).
- [Mor03] R. Morandotti, H. S. Eisenberg, D. Mandelik, Y. Silberberg, D. Modotto, M. Sorel, C. R. Stanley, and J. S. Aitchison. *Interactions of discrete solitons with structural defects*. Opt. Lett., **28** 834 (2003).
- [Mor04] R. Morandotti, D. Mandelik, Y. Silberberg, J. S. Aitchison, M. Sorel, D. N. Christodoulides, A. A. Sukhorukov, and Y. S. Kivshar. *Observation of discrete gap solitons in binary waveguide arrays*. Opt. Lett., **29** 2890 (2004).
- [MT07] G. Molina-Terriza, J. P. Torres, and L. Torner. *Twisted photons*. Nature Physics, **3** 305 (2007).
- [Nak81] H. Nakatsuka, D. Grischkowsky, and A. C. Balant. *Nonlinear Picosecond-Pulse Propagation through Optical Fibers with Positive Group Velocity Dispersion*. Phys. Rev. Lett., **47** 910 (1981).
- [Nak91] M. Nakazawa, E. Yamada, H. Kubota, and K. Suzuki. *10 Gbit/s soliton data transmission over one million kilometres*. Electron. Lett., **27** 1270 (1991).
- [Nes03] D. Neshev, E. Ostrovskaya, Y. Kivshar, and W. Krolikowski. *Spatial solitons in optically induced gratings*. Opt. Lett., **28** 710 (2003).
- [Nes04] D. Neshev, T. Alexander, E. Ostrovskaya, Y. Kivshar, H. Martin, I. Makasyuk, and Z. Chen. *Observation of Discrete Vortex Solitons in Optically Induced Photonic Lattices*. Phys. Rev. Lett., **92** 123903 (2004).
- [Nim99] G. Nimtz. *Evanescence modes are not necessarily Einstein causal*. EPJ B, **7** 523 (1999).
- [Nis96] M. Nisoli, S. De Silvestri, and O. Svelto. *Generation of high energy 10 fs pulses by a new pulse compression technique*. Appl. Phys. Lett., **68** 2793 (1996).
- [Nis97] M. Nisoli, S. Stagira, S. De Silvestri, O. Svelto, S. Sartania, Z. Cheng, M. Lenzner, C. Spielmann, and F. Krausz. *A novel-high energy pulse compression system: generation of multigigawatt sub-5-fs pulses*. Appl. Phys. B, **65** 189 (1997).
- [Nol03] S. Nolte, M. Will, J. Burghoff, and A. Tünnermann. *Femtosecond waveguide writing: a new avenue to three-dimensional integrated optics*. Appl. Phys. A, **77** 109 (2003).
- [Nol10] J. Nold, P. Hölzer, N. Y. Joly, G. K. L. Wong, A. Nazarkin, A. Podlipensky, M. Scharrer, and P. S. Russell. *Pressure-controlled phase matching to third harmonic in Ar-filled hollow-core photonic crystal fiber*. Opt. Lett., **35** 2922 (2010).
- [Nye74] J. F. Nye and M. V. Berry. *Dislocations in Wave Trains*. Proc. R. Soc. A, **336** 165 (1974).
- [Ohk87] K. Ohkuma, Y. H. Ichikawa, and Y. Abe. *Soliton propagation along optical fibers*. Opt. Lett., **12** 516 (1987).
- [O'S01] P. O'Shea, M. Kimmel, X. Gu, and R. Trebino. *Highly simplified device for ultrashort-pulse measurement*. Opt. Lett., **26** 932 (2001).
- [Ost67] L. Ostrovskii. *Self-action of light in crystals*. JETP, **5** 272 (1967).
- [Ouz05] D. Ouzounov, C. Hensley, A. Gaeta, N. Venkateraman, M. Gallagher, and K. Koch. *Soliton pulse compression in photonic band-gap fibers*. Opt. Express, **13** 6153 (2005).
- [Pan05] N.-C. Panoiu, R. M. Osgood, B. A. Malomed, F. Lederer, D. Mazilu, and D. Mihalache. *Parametric light bullets supported by quasi-phase-matched quadratically nonlinear crystals*. Phys. Rev. E, **71** 036615 (2005).
- [Pen99] J. Pendry, A. J. Holden, D. J. Robbins, and W. J. Stewart. *Magnetism from conductors and enhanced nonlinear phenomena*. IEEE Trans. Microw. Theory Tech., **47** 2075 (1999).
- [Per96] J. W. Perry, K. Mansour, I.-Y. S. Lee, X.-L. Wu, P. V. Bedworth, C.-T. Chen, D. Ng, S. R. Marder, P. Miles, T. Wada, M. Tian, and H. Sasabe. *Organic Optical Limiter with a Strong Nonlinear Absorptive Response*. Science, **273** 1533 (1996).
- [Per99] T. Pertsch, P. Dannberg, W. Elflein, A. Bräuer, and F. Lederer. *Optical Bloch Oscillations in Temperature Tuned Waveguide Arrays*. Phys. Rev. Lett., **83** 4752 (1999).
- [Per02] T. Pertsch, T. Zentgraf, U. Peschel, A. Bräuer, and F. Lederer. *Anomalous Refraction and Diffraction in Discrete Optical Systems*. Phys. Rev. Lett., **88** 93901 (2002).

- [Per04a] T. Pertsch, U. Peschel, J. Kobelke, K. Schuster, H. Bartelt, S. Nolte, A. Tünnermann, and F. Lederer. *Nonlinearity and Disorder in Fiber Arrays*. Phys. Rev. Lett., **93** 53901 (2004).
- [Per04b] T. Pertsch, U. Peschel, F. Lederer, J. Burghoff, M. Will, S. Nolte, and A. Tünnermann. *Discrete diffraction in two-dimensional arrays of coupled waveguides in silica*. Opt. Lett., **29** 468 (2004).
- [Pes98] U. Peschel, T. Pertsch, and F. Lederer. *Optical Bloch oscillations in waveguide arrays*. Opt. Lett., **23** 1701 (1998).
- [Pes99] U. Peschel, R. Morandotti, J. S. Aitchison, H. S. Eisenberg, and Y. Silberberg. *Nonlinearly induced escape from a defect state in waveguide arrays*. Appl. Phys. Lett., **75** 1348 (1999).
- [Pes02] U. Peschel, R. Morandotti, J. M. Arnold, J. S. Aitchison, H. S. Eisenberg, Y. Silberberg, T. Pertsch, and F. Lederer. *Optical discrete solitons in waveguide arrays. 2. Dynamic properties*. J. Opt. Soc. Am. B, **19** 2637 (2002).
- [Pes04] U. Peschel, O. Egorov, and F. Lederer. *Discrete cavity solitons*. Opt. Lett., **29** 1909 (2004).
- [Pet99] J. Petter, C. Weillna, C. Denz, A. Stepken, and F. Kaiser. *Self-bending of photorefractive solitons*. Opt. Commun., **170** 291 (1999).
- [Pet03a] M. Petrovic, D. Träger, A. Strinic, M. Belic, J. Schröder, and C. Denz. *Solitonic lattices in photorefractive crystals*. Phys. Rev. E, **68** 055601 (2003).
- [Pet03b] J. Petter, J. Schröder, D. Träger, and C. Denz. *Optical control of arrays of photorefractive screening solitons*. Opt. Lett., **28** 438 (2003).
- [Phi95] C. L. Philips, J. M. Parr, and E. Riskin. *Signals, systems, and transforms*. Prentice Hall (1995).
- [Phi08] T. G. Philbin, C. Kuklewicz, S. Robertson, S. Hill, F. König, and U. Leonhardt. *Fiber-Optical Analog of the Event Horizon*. Science, **319** 1367 (2008).
- [Pik12] P. Piskarv, H. Valtna-Lukner, A. Valdmann, M. L. ohmus, R. Matt, and P. Saari. *Temporal focusing of ultrashort pulsed Bessel beams into Airy-Bessel light bullets*. Opt. Express, **20** 17220 (2012).
- [Pla01] B. Platt and R. Shack. *History and principles of Shack-Hartmann wavefront sensing*. JRS, **17** 573 (2001).
- [Pon91] H.-E. Ponath and G. I. Stegeman. *Nonlinear surface electromagnetic phenomena*. Elsevier (1991).
- [Por02] M. A. Porras, R. Borghi, and M. Santarsiero. *Superluminality in Gaussian beams*. Opt. Commun., **203** 183 (2002).
- [Por03] M. A. Porras, I. Gonzalo, and A. Mondello. *Pulsed light beams in vacuum with superluminal and negative group velocities*. Phys. Rev. E, **67** 066604 (2003).
- [Pot04] M. A. C. Potenza, S. Minardi, J. Trull, G. Blasi, D. Salerno, A. Varanavicius, A. Piskarskas, and P. D. Trapani. *Three dimensional imaging of short pulses*. Opt. Commun., **229** 381 (2004).
- [Poy09] J. H. Poynting. *The Wave Motion of a Revolving Shaft, and a Suggestion as to the Angular Momentum in a Beam of Circularly Polarised Light*. Proc. R. Soc. A, **82** 560 (1909).
- [Pro05] J. L. Proctor and J. N. Kutz. *Passive mode-locking by use of waveguide arrays*. Opt. Lett., **30** 2013 (2005).
- [Raj87] R. Rajaraman. *Solitons and Instantons: An Introduction to Solitons and Instantons in Quantum Field Theory*. North-Holland Personal Library (1987).
- [Ram10] H. Ramezani, T. Kottos, R. El-Ganainy, and D. N. Christodoulides. *Unidirectional nonlinear PT-symmetric optical structures*. Phys. Rev. A, **82** 043803 (2010).
- [Ray76] L. Rayleigh. *On waves*. Philos. Mag., **ser. 5, vol. 1** 257 (1876).
- [Rec12] M. C. Rechtsman, J. M. Zeuner, A. Tünnermann, S. Nolte, M. Segev, and A. Szameit. *Strain-induced pseudomagnetic field and photonic Landau levels in dielectric structures*. Nature Photonics, **7** 153 (2012).
- [Rec13] M. C. Rechtsman, J. M. Zeuner, Y. Plotnik, Y. Lumer, S. Nolte, M. Segev, and A. Szameit. *Photonic Floquet Topological Insulators*. Nature, **496** 196 (2013).
- [Ros06] C. R. Rosberg, D. N. Neshev, W. Krolikowski, A. Mitchell, R. A. Vicencio, M. I. Molina, and Y. S. Kivshar. *Observation of Surface Gap Solitons in Semi-Infinite Waveguide Arrays*. Phys. Rev. Lett., **97** 083901 (2006).
- [Ros07] C. R. Rosberg, F. H. Bennet, D. N. Neshev, P. D. Rasmussen, O. Bang, W. Krolikowski, A. Bjarklev, and Y. S. Kivshar. *Tunable diffraction and self-defocusing in liquid-filled photonic crystal fibers*. Opt. Express, **15** 12145 (2007).
- [Rot11] J. Rothhardt, S. Hädrich, H. Carstens, N. Herrick, S. Demmler, J. Limpert, and A. Tünnermann. *1 MHz repetition rate hollow fiber pulse compression to sub-100-fs duration at 100 W average power*. Opt. Lett., **36** 4605 (2011).

- [Röp07] U. Röpke, H. Bartelt, S. Unger, K. Schuster, and J. Kobelke. *Two-dimensional high-precision fiber waveguide arrays for coherent light propagation*. *Opt. Express*, **15** 6894 (2007).
- [Röp11] U. Röpke, H. Bartelt, S. Unger, K. Schuster, and J. Kobelke. *Fiber waveguide arrays as model system for discrete optics*. *Appl. Phys. B*, **104** 481 (2011).
- [Rub09] E. Rubino, D. Faccio, L. Tartara, P. K. Bates, O. Chalus, M. Clerici, F. Bonaretti, J. Biegert, and P. D. Trapani. *Spatiotemporal amplitude and phase retrieval of space-time coupled ultrashort pulses using the Shackled-FROG technique*. *Opt. Lett.*, **34** 3854 (2009).
- [Rus44] J. Russell. *Report on waves*. In *14th meeting of the British Association for the Advancement of Science*, 311–390. York, UK (1844).
- [Rus03] P. Russell. *Photonic Crystal Fibers*. *Science*, **299** 358 (2003).
- [Rüt10] C. E. Rüter, K. G. Makris, R. El-Ganainy, D. N. Christodoulides, M. Segev, and D. Kip. *Observation of parity–time symmetry in optics*. *Nature Physics*, **6** 192 (2010).
- [Saa97] P. Saari and K. Reivelt. *Evidence of X-Shaped Propagation-Invariant Localized Light Waves*. *Phys. Rev. Lett.*, **79** 4135 (1997).
- [Sal91] B. E. Saleh and M. C. Teich. *Fundamentals of photonics*, volume 22. Wiley New York (1991).
- [Sat03] M. Sato, B. E. Hubbard, A. J. Sievers, B. Ilic, D. A. Czaplewski, and H. G. Craighead. *Observation of Locked Intrinsic Localized Vibrational Modes in a Micromechanical Oscillator Array*. *Phys. Rev. Lett.*, **90** 044102 (2003).
- [Sat04] M. Sato and A. Sievers. *Direct observation of the discrete character of intrinsic localized modes in an antiferromagnet*. *Nature*, **432** 486 (2004).
- [Sch99] U. T. Schwarz, L. Q. English, and A. J. Sievers. *Experimental Generation and Observation of Intrinsic Localized Spin Wave Modes in an Antiferromagnet*. *Phys. Rev. Lett.*, **83** 223 (1999).
- [Sch05] U. Schnars and W. Jueptner. *Digital Holography*. In *Digital Holography*, 41–69. Springer Berlin Heidelberg (2005).
- [Sch07] T. Schwartz, G. Bartal, S. Fishman, and M. Segev. *Transport and Anderson localization in disordered two-dimensional photonic lattices*. *Nature*, **446** 52 (2007).
- [Sch08] T. Schulte, S. Drenkelforth, G. K. Büning, W. Ertmer, J. Arlt, M. Lewenstein, and L. Santos. *Dynamics of Bloch oscillations in disordered lattice potentials*. *Phys. Rev. A*, **77** 023610 (2008).
- [Set10] F. Setzpfandt, A. A. Sukhorukov, D. N. Neshev, R. Schiek, Y. S. Kivshar, and T. Pertsch. *Phase Transitions of Nonlinear Waves in Quadratic Waveguide Arrays*. *Phys. Rev. Lett.*, **105** 233905 (2010).
- [Set11a] F. Setzpfandt, D. Neshev, A. Sukhorukov, R. Schiek, R. Ricken, Y. Min, Y. Kivshar, W. Sohler, F. Lederer, A. Tünnermann, and T. Pertsch. *Nonlinear dynamics with higher-order modes in lithium niobate waveguide arrays*. *Appl. Phys. B*, **104** 487 (2011).
- [Set11b] F. Setzpfandt, A. A. Sukhorukov, D. N. Neshev, R. Schiek, A. S. Solntsev, R. Ricken, Y. Min, W. Sohler, Y. S. Kivshar, and T. Pertsch. *Spectral pulse transformations and phase transitions in quadratic nonlinear waveguide arrays*. *Opt. Express*, **19** 23188 (2011).
- [Set11c] F. Setzpfandt, A. A. Sukhorukov, and T. Pertsch. *Discrete quadratic solitons with competing second-harmonic components*. *Phys. Rev. A*, **84** 053843 (2011).
- [Sha72] A. Shabat and V. Zakharov. *Exact theory of two-dimensional self-focusing and one-dimensional self-modulation of waves in nonlinear media*. *J. Exp. Theor. Phys*, **34** 62 (1972).
- [Sha82] C. Shank, R. Fork, R. Yen, R. Stolen, and W. J. Tomlinson. *Compression of femtosecond optical pulses*. *Appl. Phys. Lett.*, **40** 761 (1982).
- [She76] Y. R. Shen. *Recent advances in nonlinear optics*. *Rev. Mod. Phys.*, **48** 1 (1976).
- [She13] K. Shemer, N. Voloch-Bloch, A. Shapira, A. Libster, I. Juwiler, and A. Arie. *Azimuthal and radial shaping of vortex beams generated in twisted nonlinear photonic crystals*. *Opt. Lett.*, **38** 5470 (2013).
- [Sie88] A. J. Sievers and S. Takeno. *Intrinsic Localized Modes in Anharmonic Crystals*. *Phys. Rev. Lett.*, **61** 970 (1988).
- [Sil90] Y. Silberberg. *Collapse of optical pulses*. *Opt. Lett.*, **15** 1282 (1990).
- [Sim97] N. B. Simpson, K. Dholakia, L. Allen, and M. J. Padgett. *Mechanical equivalence of spin and orbital angular momentum of light: an optical spanner*. *Opt. Lett.*, **22** 52 (1997).
- [Ska97] V. Skarka, V. I. Berezhiani, and R. Miklaszewski. *Spatiotemporal soliton propagation in saturating nonlinear optical media*. *Phys. Rev. E*, **56** 1080 (1997).
- [Skr98] D. V. Skryabin and W. J. Firth. *Generation and stability of optical bullets in quadratic nonlinear media*. *Opt. Commun.*, **148** 79 (1998).

- [Sku04] S. Skupin, U. Peschel, L. Bergé, and F. Lederer. *Stability of weakly nonlinear localized states in attractive potentials*. Phys. Rev. E, **70** 16614 (2004).
- [Sku06] S. Skupin, G. Stibenz, L. Bergé, F. Lederer, T. Sokollik, M. Schnürer, N. Zhavoronkov, and G. Steinmeyer. *Self-compression by femtosecond pulse filamentation: Experiments versus numerical simulations*. Phys. Rev. E, **74** 056604 (2006).
- [Sny83] A. Snyder and J. Love. *Optical Waveguide Theory*. Chapman & Hall (1983).
- [Sol07] D. Solli, C. Ropers, P. Koonath, and B. Jalali. *Optical rogue waves*. Nature, **450** 1054 (2007).
- [Sol08] D. R. Solli, C. Ropers, and B. Jalali. *Active Control of Rogue Waves for Stimulated Supercontinuum Generation*. Phys. Rev. Lett., **101** 233902 (2008).
- [Ste93] A. M. Steinberg, P. G. Kwiat, and R. Y. Chiao. *Measurement of the single-photon tunneling time*. Phys. Rev. Lett., **71** 708 (1993).
- [Ste96] G. I. Stegeman, D. J. Hagan, and L. Torner.  $\chi^{(2)}$  *cascading phenomena and their applications to all-optical signal processing, mode-locking, pulse compression and solitons*. Opt. Quantum. Electron., **28** 1691 (1996).
- [Ste03] M. Stenner, D. Gauthier, and M. Neifeld. *The speed of information in a 'fast-light' optical medium*. Nature, **425** 695 (2003).
- [Su80] W. P. Su, J. R. Schrieffer, and A. J. Heeger. *Soliton excitations in polyacetylene*. Phys. Rev. B, **22** 2099 (1980).
- [Su83] W. P. Su, J. R. Schrieffer, and A. J. Heeger. *Erratum: Soliton excitations in polyacetylene*. Phys. Rev. B, **28** 1138 (1983).
- [Sue04] K. Sueda, G. Miyaji, N. Miyanaga, and M. Nakatsuka. *Laguerre-Gaussian beam generated with a multilevel spiral phase plate for high intensity laser pulses*. Opt. Express, **12** 3548 (2004).
- [Suk02] A. A. Sukhorukov and Y. Kivshar. *Discrete gap solitons in modulated waveguide arrays*. Opt. Lett., **27** 2112 (2002).
- [Suk03a] A. Sukhorukov, Y. Kivshar, H. Eisenberg, and Y. Silberberg. *Spatial optical solitons in waveguide arrays*. IEEE J. Quantum. Electron., **39** 31 (2003).
- [Suk03b] A. A. Sukhorukov and Y. Kivshar. *Generation and stability of discrete gap solitons*. Opt. Lett., **28** 2345 (2003).
- [Suk06] A. A. Sukhorukov and Y. S. Kivshar. *Slow-Light Optical Bullets in Arrays of Nonlinear Bragg-Grating Waveguides*. Phys. Rev. Lett., **97** 233901 (2006).
- [Suk10] A. A. Sukhorukov, Z. Xu, and Y. S. Kivshar. *Nonlinear suppression of time reversals in PT-symmetric optical couplers*. Phys. Rev. A, **82** 043818 (2010).
- [Sun06] S. Suntsov, K. G. Makris, D. N. Christodoulides, G. I. Stegeman, A. Haché, R. Morandotti, H. Yang, G. Salamo, and M. Sorel. *Observation of Discrete Surface Solitons*. Phys. Rev. Lett., **96** 063901 (2006).
- [Sun07] S. Suntsov, K. G. Makris, D. N. Christodoulides, G. I. Stegeman, R. Morandotti, M. Volatier, V. Aimez, R. Arès, C. E. Rüter, and D. Kip. *Optical modes at the interface between two dissimilar discrete meta-materials*. Opt. Express, **15** 4663 (2007).
- [Sun13] J. Sun, E. Timurdogan, A. Yaacobi, E. S. Hosseini, and M. R. Watts. *Large-scale nanophotonic phased array*. Nature, **493** 195 (2013).
- [Swa99] B. I. Swanson, J. A. Brozik, S. P. Love, G. F. Strouse, A. P. Shreve, A. R. Bishop, W.-Z. Wang, and M. I. Salkola. *Observation of Intrinsically Localized Modes in a Discrete Low-Dimensional Material*. Phys. Rev. Lett., **82** 3288 (1999).
- [Sza06a] A. Szameit, D. Blömer, J. Burghoff, T. Pertsch, S. Nolte, and A. Tünnermann. *Hexagonal waveguide arrays written with fs-laser pulses*. Appl. Phys. B, **82** 507 (2006).
- [Sza06b] A. Szameit, J. Burghoff, T. Pertsch, S. Nolte, A. Tünnermann, and F. Lederer. *Two-dimensional soliton in cubic fs laser written waveguide arrays in fused silica*. Opt. Express, **14** 6055 (2006).
- [Sza07a] A. Szameit, Y. Kartashov, F. Dreisow, T. Pertsch, S. Nolte, A. Tünnermann, and L. Torner. *Observation of Two-Dimensional Surface Solitons in Asymmetric Waveguide Arrays*. Phys. Rev. Lett., **98** 173903 (2007).
- [Sza07b] A. Szameit, T. Pertsch, F. Dreisow, S. Nolte, A. Tünnermann, U. Peschel, and F. Lederer. *Light evolution in arbitrary two-dimensional waveguide arrays*. Phys. Rev. A, **75** 53814 (2007).
- [Sza08] A. Szameit, F. Dreisow, M. Heinrich, T. Pertsch, S. Nolte, A. Tünnermann, E. Suran, F. Louradour, A. Barthelemy, and S. Longhi. *Image reconstruction in segmented femtosecond laser-written waveguide arrays*. Appl. Phys. Lett., **93** 181109 (2008).

- [Sza09] A. Szameit, I. L. Garanovich, M. Heinrich, A. A. Sukhorukov, F. Dreisow, T. Pertsch, S. Nolte, A. Tünnermann, and Y. S. Kivshar. *Polychromatic dynamic localization in curved photonic lattices*. Nature Physics, **5** 271 (2009).
- [Sza10] A. Szameit and S. Nolte. *Discrete optics in femtosecond-laser-written photonic structures*. J. Phys. B: At., Mol. Opt. Phys., **43** 163001 (2010).
- [Sza11] A. Szameit, M. C. Rechtsman, O. Bahat-Treidel, and M. Segev. *PT-symmetry in honeycomb photonic lattices*. Phys. Rev. A, **84** 021806 (2011).
- [Tai88] K. Tai, A. Hasegawa, and N. Bekki. *Fission of optical solitons induced by stimulated Raman effect*. Opt. Lett., **13** 392 (1988).
- [Tal36] H. Talbot. *LXXVI. Facts relating to optical science. No. IV*. Philosophical Magazine Series 3, **9** 401 (1836).
- [Tan94] A. Tanone, Z. Zhang, C.-M. Uang, F. T. S. Yu, and D. A. Gregory. *Optical beam steering using a liquid-crystal television panel*. Microwave and Optical Technology Letters, **7** 285 (1994).
- [Tan12] J. Tang, R. N. Germain, and M. Cui. *Superpenetration optical microscopy by iterative multiphoton adaptive compensation technique*. Proc. Natl. Acad. Sci. U.S.A. (2012).
- [Tea82] M. R. Teague. *Irradiance moments: their propagation and use for unique retrieval of phase*. J. Opt. Soc. Am., **72** 1199 (1982).
- [Ter08] B. Terhalle, T. Richter, A. S. Desyatnikov, D. N. Neshev, W. Krolikowski, F. Kaiser, C. Denz, and Y. S. Kivshar. *Observation of Multivortex Solitons in Photonic Lattices*. Phys. Rev. Lett., **101** 013903 (2008).
- [Ter09] B. Terhalle, T. Richter, K. J. H. Law, D. Gories, P. Rose, T. J. Alexander, P. G. Kevrekidis, A. S. Desyatnikov, W. Krolikowski, F. Kaiser, C. Denz, and Y. S. Kivshar. *Observation of double-charge discrete vortex solitons in hexagonal photonic lattices*. Phys. Rev. A, **79** 043821 (2009).
- [Ter10] B. Terhalle, D. Gories, T. Richter, P. Rose, A. S. Desyatnikov, F. Kaiser, and C. Denz. *Anisotropy-controlled topological stability of discrete vortex solitons in optically induced photonic lattices*. Opt. Lett., **35** 604 (2010).
- [Tor09] L. Torner and Y. V. Kartashov. *Light bullets in optical tandems*. Opt. Lett., **34** 1129 (2009).
- [Tow02] I. Towers and B. Malomed. *Stable  $(2+1)$ -dimensional solitons in a layered medium with sign-alternating Kerr nonlinearity*. J. Opt. Soc. Am. B, **19** 537 (2002).
- [Tre02] R. Trebino. *Frequency-Resolved Optical Gating: The Measurement of Ultrashort Laser Pulses*. Kluwer Academic Publishers (2002).
- [Tri00] E. Trias, J. J. Mazo, and T. P. Orlando. *Discrete Breathers in Nonlinear Lattices: Experimental Detection in a Josephson Array*. Phys. Rev. Lett., **84** 741 (2000).
- [Tro01] A. Trombettoni and A. Smerzi. *Discrete Solitons and Breathers with Dilute Bose-Einstein Condensates*. Phys. Rev. Lett., **86** 2353 (2001).
- [Tro06] H. Trompeter, W. Krolikowski, D. Neshev, A. Desyatnikov, A. Sukhorukov, Y. Kivshar, T. Pertsch, U. Peschel, and F. Lederer. *Bloch Oscillations and Zener Tunneling in Two-Dimensional Photonic Lattices*. Phys. Rev. Lett., **96** 53903 (2006).
- [Tru04] J. Trull, O. Jedrkiewicz, P. Di Trapani, A. Matijosius, A. Varanavicius, G. Valiulis, R. Danielius, E. Kucinskis, A. Piskarskas, and S. Trillo. *Spatiotemporal three-dimensional mapping of nonlinear X waves*. Phys. Rev. E, **69** 026607 (2004).
- [Tur93] S. K. Turitsyn. *Collapse criterion for pulse dynamics in a periodic nonlinear waveguide*. Opt. Lett., **18** 1493 (1993).
- [Tut93] L. W. Tutt and T. F. Boggess. *A review of optical limiting mechanisms and devices using organics, fullerenes, semiconductors and other materials*. Prog. Quant. Electron., **17** 299 (1993).
- [Unr81] W. G. Unruh. *Experimental Black-Hole Evaporation?* Phys. Rev. Lett., **46** 1351 (1981).
- [Unr05] W. G. Unruh and R. Schützhold. *Universality of the Hawking effect*. Phys. Rev. D, **71** 024028 (2005).
- [Vak73] N. Vakhitov and A. Kolokolov. *Stationary solutions of the wave equation in a medium with nonlinearity saturation*. Radiophys. Quantum Electron., **16** 783 (1973).
- [Vie12] M. Vieweg, T. Gissibl, Y. V. Kartashov, L. Torner, and H. Giessen. *Spatial solitons in optofluidic waveguide arrays with focusing ultrafast Kerr nonlinearity*. Opt. Lett., **37** 2454 (2012).
- [VL09] H. Valtna-Lukner, P. Bowlan, M. L. ohmus, P. Piksarv, R. Trebino, and P. Saari. *Direct spatiotemporal measurements of accelerating ultrashort Bessel-type light bullets*. Opt. Express, **17** 14948 (2009).

- [Vo10] T. D. Vo, H. Hu, M. Galili, E. Palushani, J. Xu, L. K. Oxenløwe, S. J. Madden, D.-Y. Choi, D. A. P. Bulla, M. D. Pelusi, J. Schröder, B. Luther-Davies, and B. J. Eggleton. *Photonic chip based transmitter optimization and receiver demultiplexing of a 1.28 Tbit/s OTDM signal*. Opt. Express, **18** 17252 (2010).
- [Vo12] T. Vo, J. Schröder, B. Corcoran, J. Van Erps, S. Madden, D.-Y. Choi, D. A. P. Bulla, B. Luther-Davies, M. Pelusi, and B. Eggleton. *Photonic-Chip-Based Ultrafast Waveform Analysis and Optical Performance Monitoring*. IEEE J. Sel. Top. Quant. Electron., **18** 834 (2012).
- [Voz05] C. Vozzi, M. Nisoli, G. Sansone, S. Stagira, and S. De Silvestri. *Optimal spectral broadening in hollow-fiber compressor systems*. Appl. Phys. B, **80** 285 (2005).
- [Wal12] B. Walther, C. Helgert, C. Rockstuhl, F. Setzpfandt, F. Eilenberger, E.-B. Kley, F. Lederer, A. Tünnermann, and T. Pertsch. *Spatial and Spectral Light Shaping with Metamaterials*. Adv. Mater., **24** 6300 (2012).
- [Wan07] X. Wang, A. Bezryadina, Z. Chen, K. Makris, D. Christodoulides, and G. Stegeman. *Observation of Two-Dimensional Surface Solitons*. Phys. Rev. Lett., **98** 123903 (2007).
- [Wan11] Y. Y. Wang, N. V. Wheeler, F. Couny, P. J. Roberts, and F. Benabid. *Low loss broadband transmission in hypocycloid-core Kagome hollow-core photonic crystal fiber*. Opt. Lett., **36** 669 (2011).
- [Wan12] J. Wang, J. Yang, I. Fazal, N. Ahmed, Y. Yan, H. Huang, Y. Ren, Y. Yue, S. Dolinar, M. Tur, *et al.* *Terabit free-space data transmission employing orbital angular momentum multiplexing*. Nature Photon., **6** 488 (2012).
- [Wei95] A. M. Weiner. *Femtosecond optical pulse shaping and processing*. Prog. Quant. Electron., **19** 161 (1995).
- [Wei00] A. M. Weiner. *Femtosecond pulse shaping using spatial light modulators*. Rev. Sci. Instrum., **71** 1929 (2000).
- [Wei11] A. Weiner. *Ultrafast optics*, volume 72. Wiley. com (2011).
- [Whi11] G. B. Whitham. *Linear and nonlinear waves*, volume 42. John Wiley & Sons (2011).
- [Wil11] M. Williams and J. Kutz. *Generating and routing light-bullets using slab waveguide arrays*. Opt. Quantum. Electron., 1–7 (2011).
- [Wis02] F. Wise and P. D. Trapani. *Spatiotemporal Solitons*. Opt. Photon. News, **13** 28 (2002).
- [Won12] G. K. L. Wong, M. S. Kang, H. W. Lee, F. Biancalana, C. Conti, T. Weiss, and P. S. J. Russell. *Excitation of Orbital Angular Momentum Resonances in Helically Twisted Photonic Crystal Fiber*. Science, **337** 446 (2012).
- [Wya06] A. S. Wyatt, I. A. Walmsley, G. Stibenz, and G. Steinmeyer. *Sub-10 fs pulse characterization using spatially encoded arrangement for spectral phase interferometry for direct electric field reconstruction*. Opt. Lett., **31** 1914 (2006).
- [Xi06] T.-T. Xi, X. Lu, and J. Zhang. *Interaction of Light Filaments Generated by Femtosecond Laser Pulses in Air*. Phys. Rev. Lett., **96** 025003 (2006).
- [Xu07] H. Xu and H. Zeng. *Spontaneously generated walking X-shaped light bullets*. Opt. Lett., **32** 1944 (2007).
- [Yan11] J. Yang, P. Zhang, M. Yoshihara, Y. Hu, and Z. Chen. *Image transmission using stable solitons of arbitrary shapes in photonic lattices*. Opt. Lett., **36** 772 (2011).
- [Ye09] F. Ye, Y. V. Kartashov, B. Hu, and L. Torner. *Light bullets in Bessel optical lattices with spatially modulated nonlinearity*. Opt. Express, **17** 11328 (2009).
- [Yel97] D. Yelin, D. Meshulach, and Y. Silberberg. *Adaptive femtosecond pulse compression*. Opt. Lett., **22** 1793 (1997).
- [Zab65] N. J. Zabusky and M. D. Kruskal. *Interaction of "Solitons" in a Collisionless Plasma and the Recurrence of Initial States*. Phys. Rev. Lett., **15** 240 (1965).
- [Zak68] V. E. Zakharov. *Stability of periodic waves of finite amplitude on the surface of a deep fluid*. Journal of Applied Mechanics and Technical Physics, **9** 190 (1968).
- [Zen34] C. Zener. *A Theory of the Electrical Breakdown of Solid Dielectrics*. Proc. R. Soc. A, **145** 523 (1934).
- [Zha05] Y. Zhang, Y.-W. Tan, H. L. Stormer, and P. Kim. *Experimental observation of the quantum Hall effect and Berry's phase in graphene*. Nature, **438** 201 (2005).
- [Zha10] P. Zhang, N. K. Efremidis, A. Miller, Y. Hu, and Z. Chen. *Observation of coherent destruction of tunneling and unusual beam dynamics due to negative coupling in three-dimensional photonic lattices*. Opt. Lett., **35** 3252 (2010).
- [Zho10] W.-P. Zhong, M. Belic, and T. Huang. *Three-dimensional Bessel light bullets in self-focusing Kerr media*. Phys. Rev. A, **82** 033834 (2010).

- [Zho11] W.-P. Zhong, M. Belic, G. Assanto, B. A. Malomed, and T. Huang. *Light bullets in the spatiotemporal nonlinear Schrödinger equation with a variable negative diffraction coefficient*. Phys. Rev. A, **84** 043801 (2011).

## Appendix B: Bibliography

### Peer Reviewed Journal Papers

- [1] N. C. Becker, F. Eilenberger, N. K. Efremidis, and T. Pertsch. Generation and Characterization of ultrashort Airy Pulses. *Opt. Lett.*, submitted (2014).
- [2] F. Eilenberger, K. Prater, S. Minardi, R. Geiss, U. Röpke, J. Kobelke, K. Schuster, H. Bartelt, S. Nolte, A. Tünnermann, and T. Pertsch. *Observation of Discrete, Vortex Light Bullets*. *Phys. Rev. X*, **3** 041031 (2013).
- [3] F. Eilenberger, I. V. Kabakova, C. M. de Sterke, B. J. Eggleton, and T. Pertsch. *Cavity Optical Pulse Extraction: ultra-short pulse generation as seeded Hawking radiation*. *Scientific reports*, **3** 2607 (2013).
- [4] F. Eilenberger, A. Brown, S. Minardi, and T. Pertsch. *Imaging cross-correlation FROG: measuring ultrashort, complex, spatiotemporal fields*. *Opt. Express*, **21** 25968 (2013).
- [5] M. Bache, F. Eilenberger, and S. Minardi. *Higher-order Kerr effect and harmonic cascading in gases*. *Opt. Lett.*, **37** 4612 (2012).
- [6] F. Eilenberger, S. Minardi, D. Pliakis, and T. Pertsch. *Digital holography from shadowgraphic phase estimates*. *Opt. Lett.*, **37** 509 (2012).
- [7] N. Gutman, A. A. Sukhorukov, F. Eilenberger, and C. M. de Sterke. *Bistability suppression and low threshold switching using frozen light at a degenerate band edge waveguide*. *Opt. Express*, **20** 27363 (2012).
- [8] M. Heinrich, F. Eilenberger, R. Keil, F. Dreisow, E. Suran, F. Louradour, A. Tünnermann, T. Pertsch, S. Nolte, and A. Szameit. *Optical limiting and spectral stabilization in segmented photonic lattices*. *Opt. Express*, **20** 27299 (2012).
- [9] B. Walther, C. Helgert, C. Rockstuhl, F. Setzpfandt, F. Eilenberger, E.-B. Kley, F. Lederer, A. Tünnermann, and T. Pertsch. *Spatial and Spectral Light Shaping with Metamaterials*. *Advanced Materials*, **24** 6300 (2012).
- [10] F. Eilenberger, S. Minardi, A. Szameit, U. Röpke, J. Kobelke, K. Schuster, H. Bartelt, S. Nolte, L. Torner, F. Lederer, A. Tünnermann, and T. Pertsch. *Evolution dynamics of discrete-continuous light bullets*. *Phys. Rev. A*, **84** 013836 (2011).
- [11] F. Eilenberger, S. Minardi, A. Szameit, U. Röpke, J. Kobelke, K. Schuster, H. Bartelt, S. Nolte, A. Tünnermann, and T. Pertsch. *Light bullets in waveguide arrays: spacetime-coupling, spectral symmetry breaking and superluminal decay*. *Opt. Express*, **19** 23171 (2011).
- [12] S. Minardi, F. Eilenberger, Y. V. Kartashov, A. Szameit, U. Röpke, J. Kobelke, K. Schuster, H. Bartelt, S. Nolte, L. Torner, F. Lederer, A. Tünnermann, and T. Pertsch. *Three-Dimensional Light Bullets in Arrays of Waveguides*. *Phys. Rev. Lett.*, **105** 263901 (2010).
- [13] F. Eilenberger, C. M. de Sterke, and B. J. Eggleton. *Soliton mediated optical quantization in the transmission of one-dimensional photonic crystals*. *Opt. Express*, **18** 12708 (2010).
- [14] F. Eilenberger, A. Szameit, and T. Pertsch. *Transition from discrete to continuous Townes solitons in periodic media*. *Phys. Rev. A*, **82** 043802 (2010).

### Invited Talks

- [1] F. Eilenberger, S. Skirlo, I. Kabakova, C. M. de Sterke, B. J. Eggleton, and T. Pertsch. *Cavity Optical Pulse Extraction: ultra-short pulse generation as seeded Hawking radiation*. In *Quantum Gravity Laboratory Seminar*. University of Nottingham, Nottingham, UK (2014).
- [2] F. Eilenberger. *Nonlinear Light Bullets in Discrete Media*. In *CeNoS Seminar*. Center for Nonlinear Science, Westfälische Wilhelms-Universität Münster, Münster, Germany (2014).
- [3] F. Eilenberger, S. Minardi, F. Lederer, J. Kobelke, K. Schuster, Y. Kartashov, L. Torner, U. Peschel, and T. Pertsch. *Nonlinear spatio-temporal dynamics in microstructured fibers*. In *Nonlinear Schrödinger Equation: Theory and Applications*. Heraklion, Greece (2013).
- [4] F. Eilenberger, K. Prater, S. Minardi, and T. Pertsch. *Discrete Light Bullet Vortices*. In *Workshop on Nonlinear Photonics*. Sudak, Ukraine (2013).
- [5] S. Minardi, F. Eilenberger, Y. Kartashov, A. Szameit, U. Röpke, J. Kobelke, K. Schuster, H. Bartelt, S. Nolte, L. Torner, F. Lederer, A. Tünnermann, and T. Pertsch. *Three-dimensional light bullets*. In *Photonics West*. San Francisco (2012).
- [6] T. Pertsch, F. Eilenberger, K. P. amd Alex Brown, S. Minardi, and F. Setzpfandt. *Nonlinear Spatiotemporal Photonics*. In *FANS & ANPh XVI*. Minsk, Belarus (2012).

- [7] N. Gutman, A. A. Sukhorukov, F. Eilenberger, and M. de C. Sterke. Low-Power All-Optical Switching through Frozen Light at Degenerate Band Edges. In *Nonlinear Photonics, JW4D.2*. Optical Society of America, Colorado Spring, Colorado, USA (2012).
- [8] F. Eilenberger, M. de Sterke, and B. Eggleton. *Self-induced Transmission Limits in Bandedge Structures*. In *10th CUDOS Workshop*. Port Stephens, Australia (2011).
- [9] F. Eilenberger, S. Minardi, E. Pshenay-Severin, Y. Kartashov, A. Szameit, U. Röpke, J. Kobelke, K. Schuster, L. Torner, H. Bartelt, S. Nolte, F. Lederer, A. Tünnermann, and T. Pertsch. *Observation of nonlinear Light Bullets in waveguide arrays*. In *CLEO, QMD5*. Baltimore, MD, USA (2011).
- [10] T. Pertsch, F. Eilenberger, S. Minardi, Y. Kartashov, A. Szameit, U. Röpke, J. Kobelke, K. Schuster, L. Torner, H. Bartelt, S. Nolte, F. Lederer, and A. Tünnermann. Light Bullets. In *CLEO Pacific Rim*. Sydney, Australia (2011).
- [11] F. Eilenberger, M. de Sterke, and B. Eggleton. *Soliton Mediated Optical Quantization in Bragg Gratings*. In *PECS 8*. Sydney, Australia (2009).

## Conference Talks

- [1] N. Becker, F. Eilenberger, and T. Pertsch. *Airy pulses and pulses with arbitrary temporal trajectories*. In *DoKDoK*. Suhl, Germany (2013).
- [2] F. Eilenberger, I. Kabakova, C. M. de Sterke, B. J. Eggleton, and T. Pertsch. *Black Holes and Revelations: on the Extraction of Optical Pulses from Cavities*. In *DoKDoK*. Suhl, Germany (2013).
- [3] F. Eilenberger, I. Kabakova, C. M. de Sterke, B. J. Eggleton, and T. Pertsch. *Cavity Optical Pulse Extraction: A Novel, Ultrashort Light Source Based on Nonlinearly Seeded Hawking Radiation*. In *NLO, NW3A.4*. Kohala Coast, Hawaii, USA (2013).
- [4] F. Eilenberger, K. Prater, S. Minardi, U. Röpke, J. Kobelke, K. Schuster, H. Bartelt, and S. Nolte. *Vortex Light Bullets in Fibre Arrays - Properties, Decay and Experimental Schemes*. In *CLEO Europe, IF-2.1 SUN*. Munich, Germany (2013).
- [5] F. Eilenberger, A. Brown, S. Minardi, and T. Pertsch. *Spatio-Temporal Complex Electric Fields: Analysis & Generation*. In *DoKDoK2012*. Abbe School of Photonics, Oppurg, Germany (2012).
- [6] F. Eilenberger, S. Minardi, A. Szameit, U. Röpke, J. Kobelke, K. Schuster, H. Bartelt, S. Nolte, A. Tünnermann, and T. Pertsch. *Nonlinear Spectral Symmetry Breaking of Light Bullets in Waveguide Arrays*. In *CLEO*. San Jose (2012).
- [7] A. Solntsev, A. Clark, F. Setzpfandt, M. Collins, C. Xiong, A. Wu, F. Eilenberger, A. Schreiber, F. Katzschmann, R. Schiek, et al. *Simultaneous Photon-Pair Generation and Quantum Walks in a Waveguide Array*. In *Frontiers in Optics, FTu4D.2*. Optical Society of America, Rochester, NY, USA (2012).
- [8] A. S. Solntsev, F. Setzpfandt, F. Eilenberger, C. W. Wu, D. Neshev, A. A. Sukhorukov, T. Pertsch, and Y. S. Kivshar. *Observation of spontaneous parametric down-conversion in quadratic nonlinear waveguide arrays*. In *Nonlinear Photonics, NTu4D.2*. Optical Society of America, Colorado Springs, Colorado, United States (2012).
- [9] A. S. Solntsev, A. A. Sukhorukov, M. J. Collins, A. S. Clark, C. Xiong, F. Setzpfandt, A. Wu, F. Eilenberger, R. Schiek, A. Mitchell, B. J. Eggleton, T. Pertsch, D. N. Neshev, and Y. S. Kivshar. *Active quantum circuits: integrated photon pair generation and quantum walks*. In *15th International Conference on Laser Optics, TuR8-15*. SPIE, St. Petersburg, Russia (2012). Talk, 3rd place Best Student Paper Award.
- [10] F. Eilenberger, M. Bache, S. Minardi, and T. Pertsch. *Nonlocal quintic nonlinearity by cascaded THG in dispersive media*. In *CLEO Europe*. Munich, Germany (2011).
- [11] F. Eilenberger, S. Minardi, and T. Pertsch. *Nonlinear pulse propagation in waveguide arrays and evolution of Light Bullets*. In *DoKDoK*. Naumburg, Germany (2011).
- [12] F. Eilenberger, S. Minardi, and T. Pertsch. *Superluminally Decaying Light Bullets in Arrays of Waveguides*. In *Nonlinear Optics (NLO)*. Kauai, HI, USA (2011).
- [13] S. Minardi, F. Eilenberger, Y. Kartashov, A. Szameit, U. Röpke, J. Kobelke, K. Schuster, L. Torner, H. Bartelt, S. Nolte, F. Lederer, A. Tünnermann, and T. Pertsch. *Dynamics of Light Bullets in Two-Dimensional Arrays of Waveguides*. In *CLEO Europe, QMD5*. Munich, Germany (2011).
- [14] E. Pshenay-Severin, A. Chipouline, J. Petschulat, U. Hübner, F. Eilenberger, F. Setzpfandt, A. Tünnermann, and T. Pertsch. *Magnetic properties of asymmetric double-wire structures*. In *CLEO, QTuD7*. Baltimore, MD, USA (2011).
- [15] F. Setzpfandt, M. Falkner, R. Schiek, F. Eilenberger, E. Pshenay-Severin, and T. Pertsch. *Bandstructure measurements of lithium niobate waveguide arrays*. In *CLEO, QMD3*. Baltimore, MD, USA (2011).

- [16] F. Setzpfandt, A. Sukhorukov, D. Neshev, R. Schiek, A. Solntsev, F. Eilenberger, S. Minardi, R. Ricken, Y. Min, W. Sohler, Y. Kivshar, and T. Pertsch. *Nonlinear evolution of laser pulses in lithium niobate waveguide arrays*. In *Nonlinear Optics (NLO)*, NThB7. Kauaii, HI, USA (2011).
- [17] F. Eilenberger, D. Pliakis, S. Minardi, and T. Pertsch. *Digital holography from shadowgraphic phase estimates*. In C. Gorecki, A. K. Asundi, and W. Osten, eds., *SPIE Photonics Europe 2010*, vol. 7718, 771804. SPIE, Brussels, Belgium (2010).
- [18] C. Menzel, C. Rockstuhl, T. Paul, C. Helgert, J. Petschulat, E.-B. Kley, F. Eilenberger, T. Pertsch, and F. Lederer. *Asymmetric Transmission of Linearly Polarized Light through Low Symmetry Metamaterials*. In *CLEO/QELS*, CFI6. San Jose, USA (2010).
- [19] F. Eilenberger, S. Minardi, T. Pertsch, S. Nolte, F. Lederer, A. Tünnerman, U. Röpke, J. Kobelke, K. Schuster, H. Bartelt, Y. Khartashov, and L. Torner. *Observation of Discrete-Continuous Optical Bullets*. In *CLEO Europe*. Munich, Germany (2009).
- [20] F. Eilenberger, M. de Sterke, and B. Eggleton. *Soliton Mediated Optical Quantization of Fibre-Bragg-Gratings*. In *ACOFT/ACOLS*. Adelaide, Australia (2009).
- [21] F. Eilenberger, M. de Sterke, and B. Eggleton. *Soliton Mediated Optical Quantization in Bragg Gratings*. In *Complex Phenomena in Nonlinear Physics*. Erice, Italy (2009).
- [22] T. Pertsch, F. Eilenberger, S. Minardi, S. Nolte, F. Lederer, A. Tünnermann, U. Röpke, J. Kobelke, K. Schuster, H. Bartelt, Y. Kartashov, and L. Torner. *Light propagation in complex two-dimensional waveguide lattices*. In *LEOS Winter Topicals 2009*. Innsbruck, Austria (2009).
- [23] F. Eilenberger, S. Minardi, T. Pertsch, Y. Kartashov, S. Nolte, F. Lederer, U. Röpke, J. Kobelke, K. Schuster, H. Bartelt, and A. Tünnermann. *Nonlinear propagation of ultrashort pulses in 2-D fibre arrays – towards the observation of 3-D solitons*. In *KOALA (Conference on Optics And Laser Applications)*. Brisbane, Australia (2008).
- [24] F. Eilenberger, T. Pertsch, S. Nolte, F. Lederer, U. Röpke, J. Kobelke, K. Schuster, H. Bartelt, and A. Tünnermann. *Nonlinear, discrete-continuous propagation of ultrashort pulses in 2-dimensional, periodic fibre arrays*. In *OECC/ACOFT*. Sydney, Australia (2008).
- [25] T. Pertsch, F. Eilenberger, S. Nolte, F. Lederer, U. Röpke, J. Kobelke, K. Schuster, H. Bartelt, A. Tünnermann, K. Y., and L. Torner. *Spatio-temporal Effects in Nonlinear Fiber Arrays*. In *SIAM Conference on Nonlinear Waves and Coherent Structures*. Rome, Italy (2008).
- [26] F. Eilenberger, A. Szameit, T. Pertsch, S. Nolte, F. Lederer, R. U., J. Kobelke, K. Schuster, H. Bartelt, and A. Tünnermann. *Discrete-continuous spatio-temporal light localization in nonlinear fiber arrays*. In *CLEO Europe*. Munich, Germany (2007).

## Conference Poster

- [1] M. Bache, F. Eilenberger, and S. Minardi. *Higher-order Kerr effect and harmonic cascading in gases*. In *CLEO Europe*, IF/IE-P.41 WED. Munich, Germany (2013).
- [2] F. Eilenberger, M. Bache, S. Minardi, and T. Pertsch. *Pressure tunable cascaded third order nonlinearity and temporal pulse switching*. In *CLEO Europe*, IF-P.2 SUN. Munich, Germany (2013).
- [3] K. Prater, F. Eilenberger, S. Minardi, and T. Pertsch. *Vortex Light Bullets: a Discrete Revolution*. In *DoKDoK2012. Abbe School of Photonics*, Oppurg, Germany (2012).
- [4] F. Eilenberger, S. Minardi, and T. Pertsch. *Characterization of ultrashort, nonlinearly self-confined wavepackets in waveguide arrays*. In *10th CUDOS Workshop*. Port Stephens, Australia (2011).
- [5] F. Eilenberger, C. M. de Sterke, and B. J. Eggleton. *Soliton mediated quantization transmission in Bragg-gratings*. In *PhoNa Kick-Off Meeting*. Jena, Germany (2010).
- [6] F. Eilenberger, S. Minardi, and T. Pertsch. *Spatiotemporal characterization of ultrashort, nonlinear excitations in waveguide arrays*. In *UNO-2*. Bad Dürkheim, Germany (2010).
- [7] F. Eilenberger, D. Pliakis, S. Minardi, and T. Pertsch. *Digital In-Line Holography with the Iterative Shadowgraphic Method*. In *CLEO/QELS*, JWA32. San Jose, USA (2010).
- [8] F. Eilenberger, M. de Sterke, and B. Eggleton. *Soliton Mediated Optical Quantization*. In *8th CUDOS Workshop*. Lake Crackenback, Australia (2009).
- [9] F. Eilenberger, T. Pertsch, S. Nolte, F. Lederer, U. Röpke, J. Kobelke, K. Schuster, H. Bartelt, and A. Tünnermann. *Nonlinear, discrete-continuous propagation of ultrashort pulses in 2-dimensional, periodic fibre arrays*. In *407th Heraeus-Seminar “Discrete Optics and Beyond”*. Bad Honnef, Germany (2008).
- [10] E. Pshenay-Severin, F. Eilenberger, F. Setzpfandt, and T. Pertsch. *Tailoring light propagation in microstructured materials*. In *386th Heraeus-Seminar “Computational Nano-Photonics”*. Bad Honnef, Germany (2007).

## Appendix C: Acknowledgements

The somewhat outdated colloquial name for the Friedrich Schiller University is “Alma Mater Jenensis”, which roughly translates into “the nurturing mother of Jena”. And that she indeed is: a giver of scientific bread, in the form of money and equipment, and a scientific home, which is, of course, much more than a desk and a lab. It is a place to feel comfortable, a place to grow, and mature into an independent scientist.

Not quite as outdated is the term “Doktorvater”, i.e., “doctoral father” for the name of the supervisor of a doctoral thesis; a complement for the scientific “mother” in a sense. The Doktorvater in my case was Prof. Thomas Pertsch and the term could not be more suitable: being bright and modest, guiding and supportive, friendly, patient and open-minded I am deeply indebted to him and proud to have been able to work with him.

The scientific family is, however, much larger.

I would like to particularly thank my colleagues Jörg Petschulat, Frank Setzpfandt, Christian Helgert, Katja Pshenay-Severin, Matthias Zilk, Angela Klein, Reinhard Geiss, Michael Steinert, Jörg Reinhold, Daniel Füßel, Carsten Schmidt, Benny Walther, Thomas Kaiser, Stefan Fasold, Anton Sergejev, Rachel Grange, Sina Saravi and Norik Janunts for the help and support in many physical and non-physical problems and for just putting up with me. The latter is also true for the Wednesday lunch group, which consists of Florian Just, Kevin Füchsel, Tino Eidam and Alexander Hartung, and which is so much more than just a group of old friends that have a meal together now and then.

Stefano Minardi brought the Imaging Cross Correlator and lots of spatiotemporal insight in the labs. Without him the Light Bullets might still linger somewhere in the eternal darkness of noise.

Benny Walter devised and designed the amazing two color-metamaterial holograms and gave testimony to the fact, that scientific progress is 99% transpiration and 1% inspiration. Although I am sure that in the end Benny’s figures add up to more than just 100%.

Jan Sperrhake, Marcel Wille, Katja Puschkarsky, Kevin LeCalvez, Pierre Lheritier, Scott Skirlo and Brenda Doherty were so daring as to spend an internship in the dark dungeon of the Bullet lab. Not all of the projects were successful but you all did a great job. Even more noteworthy are the contributions of Alexander Brown, who co-developed the ImXFROG and Karin Prater, who co-observed the Vortex Light Bullets. The thesis of Nils Becker did not even make it into this document, nevertheless it was a great job with an even greater potential. No supervised students have been harmed in the process of writing this thesis.

Ulrich Röpke, Kay Schuster, Jens Kobelke, and Prof. Hartmut Bartelt of the IPHT, in a superhuman effort, managed to build the fiber arrays, which have been the very basis of this thesis.

Some of the results presented here, in particular those related to the spectral pulse shaper and the Vortex Light Bullets, could not have been achieved without the superb skill and awesome reliability of the Microfabrication team of Ernst-Bernhard Kley. In particular I am indebted to Christiane Otto, Reinhard Geiss, Stefan Steiner, Thomas Käsebier, and Stefanie Krockner. Prof. Herbert Gross of the IAP's optical systems design group helped simulate the imaging properties of the spectral pulse shaper and turned this device into a truly useful one, with reproducible, superior performance. Julia Vetter, Christin Weber, Annelie Zapfe, Bodo Martin, Holger Hartung, Sabine Rockstroh, and Carola Steinberg did not contribute scientifically to this thesis, but without their continuous toil the bustling, busy Institute would immediately come to a grinding halt.

I am indebted to all fellow organizers of the DoKDoK conference, in particular Thomas Kaiser, Dorit Schmidt, and all the generous sponsors. It was a great experience to see DoKDoK come to life, just as I had envisioned on a long trip over the endless, sandy dunes of Fraser Island. It was an even greater experience to see how DoKDoK matured into DoKDoK 2012 and DoKDoK 2013. I am sorry for the burning bus.

Many external collaborators did contribute to the success of this thesis. Yaroslav Kartashov and Prof. Lluís Torner from the ICFO in Barcelona suggested and helped us to upgrade our modelling efforts to the UME scheme. Irina Kabakova, Martijn de Sterke, and Benjamin Eggleton from the University of Sydney contributed to the success of the COPE project, which is not mentioned in this thesis. Morten Bache from DTU Fotonik in Copenhagen helped us better understand the mysterious ways of the cascaded third harmonic and wrote one paper with us on the topic and crafted the other one by relentlessly pushing for the improvement of the manuscript and model. Matthias Heinrich devised and carried out the segmented waveguide array experiment and proved that science and efficiency are not mutually exclusive. The paper on nonlinear frozen light was written by Nadav Gutman, I still owe him a Whiskey.

No scientific results of my time in Australia made it into this thesis. It, nevertheless, is an integral part of my doctoral time. I would particularly thank Prof. Benjamin Eggleton, Prof. Martijn de Sterke, and Chris Walsh for the scientific and organizational support. Cameron Smith, Bill Corcoran, and Sahand Mahmoodian have become trusted friends during that time.

This is a thesis in experimental physics. I am painfully aware that without a whole s\*\*\*load of

money, equipment, and trust it could neither have been conceived, nor carried out. There are many people that I have to thank in this respect: apart from those mentioned before these are in particular Prof. Stefan Nolte, Prof. Andreas Tünnermann, and Prof. Falk Lederer and the numerous funding agencies, of course.

Some fine day, I promise, I will sit down, learn to speak slowly and get an intelligible handwriting. Until this fine day comes I am obliged to thank all students for being patient with me. It was great fun teaching you. If you only learned half as much, as I did, then I am happy. Keep on thinking, keep on asking!

At the end of this long list of people that have scientifically contributed to this thesis, I would like to thank all non-superficial reviewers that took their time and tried to really understand the, sometimes convolved, ways of our papers and my sentences. There are not many of you, especially among those that work for high-rank journals. Please, keep up the effort!

Last but not least, I would like to thank my family for the continuous support. I am sure that most of you did not understand much of the gibberish I told you from my work. Thanks for nodding, anyway. And thanks for always being there.

*This was tale of a journey of the mind. The much greater tale  
of the journey of the heart remains untold.*

*Thank you Bine, thank you Sarah. You are the Greatest.*

## **Appendix D: Curriculum Vitae**

### ***Schulausbildung***

08/1988 – 07/2001            Schulbesuch  
Abschluss                    Abitur, Note 1,2

### ***Studium***

10/2002 – 03/2008            Physik an der Friedrich-Schiller-Universität, Jena  
Abschluss                    Diplom, Note 1,0 (mit Auszeichnung)  
Thema der Diplomarbeit      Untersuchung der nichtlinearen Raum-Zeit-Dynamik von  
Lichtpulsen in Faserarrays

### ***wissenschaftliche Laufbahn***

06/2008 – 06/2009            Visiting Scholar am Centre for Ultrahigh bandwidth Devices for  
Optical Systems (CUDOS), University of Sydney  
seit 04/2008                  Doktorand am Institut für angewandte Physik der Friedrich-  
Schiller-Universität, Jena

### ***Lehre***

09/2004 – 10/2004            Seminarleiter Mathematik-Vorkurs für Studienanfänger der  
09/2005 – 10/2005            Physik  
04/2005 – 02/2006            Praktikumsassistent Elektronikpraktikum  
10/2007 – 02/2008            Praktikumsleiter Computational Physics  
10/2009 – 02/2010  
10/2011 – 02/2012  
10/2009 – 10/2011            Academic Mentor der Abbe School of Photonics  
10/2012 – 03/2013            Seminarleiter Fundamentals of Modern Optics  
seit 01/2010                  Betreuung von einer Masterarbeit, zwei Bachelorarbeiten, einer  
Diplomarbeit und mehreren Praktikanten

### ***Stipendien und Preise***

06/2008 – 06/2009            Endeavour Europe Award of the Australian Government to  
undertake research in Australia

- 06/2009 Fakultätspreis der Physikalisch-Astronomischen Fakultät für die beste Diplomarbeit
- 06/2011 Heptagon-Sven-Bühling Preis der Physikalisch-Astronomischen Fakultät der Universität Jena

### ***sonstige Aktivitäten***

Wissenschaftlicher und organisatorischer Leiter der DoKDoK Konferenz

Reviewer für Physical Review Letters, Optics Express, Optics Letters, Optics Communications, Journal of Modern Optics, Physics Letters A

### ***soziales Engagement***

- 01/2004 -10/2006 Mitglied des Fachschaftsrats der Physikalisch-Astronomischen Fakultät, seit 01/2005 Vorsitzender
- 04/2006 – 02/2008 Mitglied des Fakultätsrates der Physikalisch-Astronomischen Fakultät
- 01/2011 – 12/2011 Vizepräsident OSA Student Chapter Jena

## **Appendix E: Ehrenwörtliche Erklärung**

Hiermit erkläre ich ehrenwörtlich, dass ich die vorliegende Arbeit selbstständig, ohne unzulässige Hilfe Dritter und ohne Benutzung anderer als der angegebenen Hilfsmittel und Literatur angefertigt habe. Die aus anderen Quellen direkt oder indirekt übernommenen Daten und Konzepte sind unter Angabe der Quellen gekennzeichnet.

Weitere Personen waren an der inhaltlich-materiellen Erstellung der vorliegenden Arbeit nicht beteiligt. Insbesondere habe ich hierfür nicht die entgeltliche Hilfe von Vermittlungs- bzw. Beratungsdiensten (Promotionsberater oder andere Personen) in Anspruch genommen. Niemand hat von mir unmittelbar und mittelbar geldwerte Leistungen für Arbeiten erhalten, die im Zusammenhang mit dem Inhalt der vorgelegten Dissertation stehen.

Weder diese Arbeit noch eine andere wurde bisher im In- oder Ausland in gleicher oder ähnlicher Form einer anderen Prüfungsbehörde vorgelegt.

Die geltende Promotionsordnung der Physikalisch-Astronomischen Fakultät ist mir bekannt.

Ich versichere ehrenwörtlich, dass ich nach bestem Wissen die reine Wahrheit gesagt und nichts verschwiegen habe.

Jena, 13.03.2014

## Appendix F: Symbols

$\tilde{a}_{nm}$	stationary solution of normalized NLSE	$\Delta\omega$	angular frequency bandwidth	$\Lambda$	fiber array pitch (i.e., cell to cell distance)
$A^{(0)}$	pulse peak amplitude	$D$	Diameter	$L$	sample length
$A_0$	WA characteristic amplitude	$\delta$	step height	$\lambda$	vacuum wavelength
$A_{\text{eff}}$	effective mode area of waveguide	$\delta k$	transverse (i.e., angular) wavenumber resolution	$M$	topological charge of a field
$A_{nm}$	amplitude of waveguide mode in waveguide $nm$	$\delta t$	temporal resolution	$\mu, \nu$	transverse Bloch momenta normalized to inverse array pitch
$a_{nm}$	normalized amplitude of waveguide mode in waveguide $nm$	$\delta z$	propagation step size	$n_2$	material nonlinear refractive index
$\alpha_1$	normalized STC coefficient	$\delta\lambda$	spectral resolution	NN	number of nearest neighbors per unit
$A$	filter describing a pulse analysis device	$\delta\omega$	angular frequency resolution	$n$	refractive index
$b_{\text{crit}}$	smallest nonlinear phase shift for semistable VLBs	$E^{(0)}$	input pulse amplitude	$\mathcal{N}$	nonlinear part of propagation equation
$b_{\text{min}}$	smallest nonlinear phase shift for particular LB family	$E_0$	WA characteristic pulse energy	$\rho^{(0)}$	input pulse peak power
$b_{\text{thresh}}$	nonlinear phase shift at $E_{\text{thresh}}$	$E_{\text{out}}$	output pulse amplitude	$P_0$	WA characteristic power
$\beta_i$	$i^{\text{th}}$ Taylor coefficient of $\beta$ at carrier frequency $\omega_0$	$E_{\text{thresh}}$	minimum energy for particular LB family	$P_{nm}^{\text{NL}}$	nonlinear polarization in waveguide $nm$
$B$	filter describing the ST experiment	$E_{nm}$	real amplitude of mode in waveguide $nm$	$nm$	waveguide index
$b$	normalized nonlinear phase shift	$E$	pulse energy	$r$	fiber core radius
$\beta$	longitudinal wavenumber of isolated waveguide	$\varepsilon$	fiber array core scaling factor	$S$	filter describing a pulse shaping device
$C_{nm}^{nm'}$	coupling matrix, modeling particular WA geometry	$\varepsilon$	deviation of solution from initial state	$\langle T_c \rangle$	temporal center of gravity of the central waveguide
$c^{(i)}$	waveguide coupling coefficients	$\Phi_i^{(A/B)}$	phase shift applied on the $i^{\text{th}}$ pixel of display A/B of SLM	$\langle T_o \rangle$	temporal center of gravity of all other waveguides
$c_{\text{ph}}$	vacuum speed of light	$F^*$	filter finesse	$\langle T \rangle$	pulse center of gravity time, integral of luminality
$c_i$	$i^{\text{th}}$ Taylor coefficient of coupling constant $c$	$\mathcal{F}$	field of waveguide mode	$t^{(0)}$	pulse FWHM duration
$C$	2 <sup>nd</sup> order chirp	$F$	an arbitrary ST linear filter	$t_0$	WA characteristic time
$c$	singular waveguide coupling coefficient	$f$	focal length	$\tau_1, \tau_2$	characteristic time scales of the SRS
$\Delta_{\text{SF}}$	spectral asymmetry measure	$\phi$	the phase of a pulse, i.e., $\phi = \arg(E)$	$t$	temporal transverse coordinate (in a co-propagating frame of reference) or measure of delay
$D_{nm}$	entries for hessian matrix of dispersion relation	$g$	relative strength of non-instantaneous nonlinear response	$\tau$	normalized time coordinate, in co-propagating frame of reference
DoF $_x$	independently measurable quantities along transverse coordinate $X$	$\gamma$	nonlinear coefficient of waveguide	$U_i^{(A/B)}$	voltage applied on the $i^{\text{th}}$ pixel on display A/B of SLM
$\Delta T_{\text{sim}}$	mean time of arrival difference for simulations with or without STC	$h$	Non-instantaneous nonlinear response function	$v_g^{(0)}$	group velocity of isolated waveguide mode
$\Delta T$	mean time of arrival difference between central waveguide pulse and pulses in all other waveguides	$k_{x/y}$	transverse wavenumbers in homogeneous media	$v_g$	group velocity
$\Delta k$	transverse (i.e., angular) wavenumber range	$k$	wavenumber in homogeneous media	$\omega_0$	carrier wave angular frequency
$\Delta n$	refractive index shift	$\langle L_{\text{Diff}} \rangle$	average diffraction length	$w$	beam FWHM diameter
$\Delta t$	duration of a window over which a signal is defined	$\langle L_{\text{Disp}} \rangle$	average dispersion length	$\omega$	angular frequency, mostly as an offset to $\omega_0$
$\Delta\beta$	longitudinal wavenumber shift of the Bloch mode	$L_{\text{Diff}}$	diffraction length	$x, y$	spatial transverse coordinates
$\Delta\lambda$	spectral measurement windows or free spectral range	$L_{\text{Disp}}^{(N)}$	dispersion length of order $N$ , if $N$ omitted then $N = 2$	$\eta$	fiber array overall scaling factor
		$L_{\text{LB/VLB}}$	LB / VLB propagation length	$z_0$	WA characteristic length
		$L_{\text{NL}}$	nonlinear length	$z$	propagation coordinate
		$L_{\text{Raman}}$	Raman and higher order nonlinearity length	$\zeta$	normalized propagation coordinate
		$\lambda_0$	carrier wave vacuum wavelength		
		$\lambda_C$	local carrier wavelength of LB		
		$\mathcal{L}$	linear part of propagation equation		

## Appendix G: Abbreviations

1D .....	one-dimensional
2D .....	two-dimensional
3R.....	Re-amplify, Re-time, and Re-generate
AbC.....	Analysis-by-Control
BBO .....	Beta-Barium-Borate
CCD .....	Coupled Charge Device
CPA .....	Chirped Pulse Amplifier
DFG .....	Difference Frequency Generation
DO.....	Discrete Optical/Optics
DR.....	Dispersion Relation
DSC.....	Direct Space-Time Coupling
FA.....	Fiber Array
FPI.....	Fabry-Pérot Interferometer
FROG.....	Frequency Resolved Optical Gating
FSR .....	Free Spectral Range
FWHM.....	Full Width at Half Maximum of intensity
GPU .....	Graphic Processing Unit
IAP.....	Institute of Applied Physics
ImXFROG .....	Imaging Cross-correlating FROG
iXCorr .....	Imaging Cross-Correlator
LB .....	Light Bullet
MIIPS.....	Multiphoton Intrapulse Interference Phase Scan
NA.....	Numerical Aperture
OAM .....	Orbital Angular Momentum
OL .....	Optical Limiting
OPA.....	Optical Parametric Amplifier
OXFROG .....	fast One dimensional imaging Cross-correlating FROG
PC .....	Photonic Crystal
PCF .....	Photonic Crystal Fiber
SF.....	Sum Frequency
SLM .....	Spectral Light Modulator
SPM .....	Self Phase Modulation
SPS.....	Spectral Pulse Shaper
SRS .....	Stimulated Raman Scattering
ST.....	SpatioTemporal
STC.....	Space-Time Coupling
SVEA .....	Slowly Varying Envelope Approximation
SWA .....	Segmented Waveguide Array
Ti:Sa.....	Titanium Sapphire
TOC .....	Third Order Chirp
UME .....	Unidirectional Maxwell Equations
VLB .....	Vortex Light Bullet
WA.....	Waveguide Array
WG.....	WaveGuide
XFROG.....	Cross-correlating FROG